Experimental and Numerical Study of Primary Consolidation of Soft Clay

By

Attasit Korchaiyapruk

Bachelor of Engineering in Civil Engineering
Chulalongkorn University
Bangkok, Thailand
1998

Master of Science in Civil and Environmental Engineering
Massachusetts Institute of Technology
Cambridge, MA
2000

Submitted to the
Department of Civil and Environmental Engineering
in partial fulfillment of the requirements for the degree of

Doctoral of Philosophy in Civil and Environmental Engineering

At the

MASSACHUSETTS INSTITUTE OF TECHNOLOGY

September, 2007

Signature of Author_____
Department of Civil and Environmental Engineering, June 19, 2007

Certified by_____
John T. Germaine
Senior Research Associate of Civil and Environmental Engineering
Thesis Supervisor

Accepted by_____
Daniele Veneziano
Chairman, Departmental Committee on Graduate Studies

Experimental and Numerical Study of Primary Consolidation of Soft Clay

By

Attasit Korchaiyapruk

Submitted to the Department of Civil and Environmental Engineering on June 19, 2007 in partial fulfillment of the requirements for the degree of Doctoral of Philosophy in the field of Civil and Environmental Engineering

ABSTRACT

This research investigates, experimentally and numerically, the three main factors that differentiate predictions based on Terzaghi's one-dimensional consolidation theory from those observed in the laboratory and field. These factors include 1) the non-uniqueness of the virgin compression line when the same soil specimen is subjected to different strain rates, 2) the effects of hydraulic gradient on consolidation behavior, and 3) the scaling effects based on c_v ratio [$c_v(\sqrt{t})/c_v$(log t)] from oedometer tests with varying drainage heights.

This research is separated into two main parts including the experimental program and the numerical simulation program. The experimental program is set up to test the strain rate sensitivity, effects of hydraulic gradient on the consolidation behavior based on the Gradient-controlled Constant Rate of Strain (GCRS) tests, and the scaling effects on the oedometer tests. The tests are performed on two natural soils, Maine Blue clay (MBC) and San Francisco Bay mud (SBM). The numerical simulation programs focus on the simulation of the GCRS test to simulate the excess pore pressure distribution during the gradient-controlled loading phase and the oedometer tests.

The strain rate sensitivity tests show that while the MBC behavior is essentially strain rate independent for strain rate faster than 1.5 %/hr, the SBM clearly shows strain rate dependent behavior. The GCRS test results together with the predicted average excess pore pressure from the simulation indicate that while high gradients shifts the Virgin Compression Line (VCL) to the left of the normal VCL for both soils, SBM shows more pronounced effects than MBC. The results from a series of oedometer tests with varying drainage heights also show that the c_v ratio based on the MBC tests is independent of the drainage heights. The SBM tests, on the other hand, clearly show that the c_v ratio is dependent on the drainage heights. The representative c_v can also be predicted from the oedometer simulation. A relationship between c_v(rep)/$c_v(\sqrt{t})$ or c_v(rep)/c_v(log t) and the drainage height obtained from the simulation can be used to obtain c_v(rep) based on the $c_v(\sqrt{t})$ or c_v(log t)from an oedometer test for engineering applications.

Thesis Supervisor: John T. Germaine

Title: Senior Research Associate of Civil and Environmental Engineering

Acknowledgements

I would like to express my deepest gratitude and sincere thanks to Dr. Germaine for all the support he provided me throughout my time at the MIT. This has been a long journey for me. Without his support and contributions, I would had never been able to complete my work. His encouragement and advice really helped me to go through several difficult times at MIT especially during the general examination and the last several months of my PhD career at MIT. I have always admired his passionate pursuit of sciences and engineering in the field soil mechanics and the great insight and expertise he possesses in the subject. He is truly one of the greatest educator and mentor I have ever known.

I feel very fortunate to have had the opportunity to work with Professor Ladd. I would like to thank Professor Ladd for his tremendous contributions, support, and guidance throughout my time at MIT.

I would like to thank Professor Sheahan for his continual support and advice throughout the research and especially for the valuable time he spent for me during all the committee meetings. I admire his positive personality toward solving problems and his enthusiasm in the research.

I would like to thank Professor Patrick Jaillet and Patricia Dixon for their continuing support and help throughout my time at MIT as the CEE-NET administrator. I am thankful for their friendship and advice. I would also like to express my gratitude to Professor Louis L. Bucciarelli, Professor Patricia J. Culligan, Professor Eduardo A. Kausel, and especially Dr. Germaine for guidance and advice all the times I assisted them in teaching undergraduate level classes at MIT.

Special thanks to Steven Rudolph for helping with the construction and repairing of test equipments along with all the assistance and friendship he provided me. He is truly an amazing builder and a great friend. I would also like to thank Cynthia Stewart, Jeanette Marchocki, Sheila Fay, Alice Kalemkiarian, Donna Hudson, Patty Glidden, Kris Kipp, and the staff in the department of civil and environmental for all their help, assistance, and friendship.

I would like to thank all my friends at MIT for the support and friendship throughout the years: Yo-Ming Hsieh, Nguyen Q. Hoang (BA), Kartal Nabi Toker, Louis Z. Locsin, Maria – Katerina Nikolinakou, Sangyoon Min, Abdulhadi Naeem, Pei Jianyong, and Matt Chartier.

Throughout my life, there have been many good times and many difficult times, some were especially difficult and truly a test of my strength and conviction. At all times, the support and unconditional love from my parents and family allow me to continue forward in life. I cannot imagine that I could have made it this far in my life without my family' guidance and support.

Finally, I would like to express my deepest gratitude to Chanathip "Nick" Pharino for the support and love she has given me. I came to learn that there is a thing in life more important than fame, more important than wealth, in fact more important than everything else, and this is love, unconditional and true love such as my family and Nick have given me. Only with true love, I find happiness and peace.

Attasit "Pong" Korchaiyapruk

"Through love spring strength and conviction"

Table of Contents

Table of Figures

Table of Tables

Chapter 1: Introduction

The consolidation behavior of soft clays is one of the most important topics in the geotechnical engineering discipline. The behavior can be described in the simplest form using Terzaghi's 1-dimensional consolidation theory that marked the birth of modern soil mechanics. However, in the past decades, laboratory test results and field observations indicate that the actual consolidation behavior differs from that based on Terzaghi's theory. Much effort has been spent to investigate and improve our understanding of this behavior. But there are still many aspects of the behavior that remains uncertain, which can cause significant problems in the interpretation and extrapolation of laboratory results to field applications.

One of the critical aspects of consolidation behavior of clays is the effects caused by strain rate approximately that change in proportion to the drainage height squared. There are significant efforts in the study of the strain rate effects on consolidation behavior of soft clays. However, there are still many debates as what is the actual governing hypothesis for the consolidation behavior with respect to the strain rate issues. There are two opposing hypotheses (designated as hypothesis A and B) concerning this fundamental aspect of clay behavior (Ladd et al., 1977). While hypothesis A, effectively, categorizes the consolidation behavior as strain rate independent, hypothesis B asserts an opposite view that the behavior is strain rate dependent. These contradictory hypotheses can result in large differences in the predicted magnitude of settlements at the end of primary consolidation when extrapolating measured laboratory tests results to field performance.

Another important parameter that affects in the consolidation process is the hydraulic gradient. It is well known that the hydraulic gradient is much larger in laboratory consolidation tests compared to found in the field. However, researchers have not investigated the influence of hydraulic gradient on the consolidation behavior of soft clay. It is hypothesized that the very high flow velocities that occur in laboratory consolidation test cause "hydraulic gradient induced disturbance", resulting in changes of the location of the Virgin Compression Line (VCL). This hydraulic gradient effect can make the laboratory test interpretation difficult and field extrapolation based on the test results more complicated.

The third principle aspect that is very important is the interpretation of the coefficient of consolidation, c_v that governs the rate of consolidation. There are two well-established methods in obtaining the c_v from an incremental loading oedometer test including the $\sqrt{t}$ and log(t) methods. Technical details of these methods can be found in Chapter 2 of this thesis. The c_v obtained from the two methods, based on laboratory tests, generally differ significantly (Lambe and Whitman, 1979). The c_v based on the $\sqrt{t}$ method is

usually larger than that based on the log(t) method. The difference in the c_v from these methods can be expressed by the c_v ratio [$c_v(\sqrt{t})/c_v(\log t)$]. This difference can cause uncertainty as to which c_v is the best representative c_v for predicting the rate of consolidation in the field.

This research program aims to improve our understanding of the consolidation behavior of soft clays by focusing on the three principal problems as outlined above. The research addresses several important issues including the magnitude of strain-rate effects, hydraulic gradient disturbance, and scaling effects. The research introduces a novel testing technique that allows the hydraulic gradient to be controlled independently from the strain rate during a constant rate of strain (CRS) test. There are three main experimental programs.

1) Strain-rate sensitivity tests,
2) Gradient-controlled Constant Rate of Strain (GCRS) tests, and
3) Laboratory incremental oedometer test with varying drainage heights.

These three experimental programs are designed to evaluate the three principal parameters that can significantly affect the consolidation behavior of soft clay. The experimental program focuses on establishing a relatively simple, yet, effective testing procedures and set up to allow for high quality tests with well controlled boundary conditions. Detailed discussion of the experimental program can be found in the Chapter 3.

In addition to the three experimental programs, two numerical simulation programs are developed to aid in the interpretation of the GCRS and oedometer tests. The main objective of the GCRS simulation is to model the consolidation behavior of a soil specimen under the GCRS test with the focus on the prediction of pore pressure distribution inside the soil specimen during the imposed gradient CRS loading phase. The oedometer simulation is created to simulate the consolidation behavior of a specimen subjected to a constant load. Both simulation programs are designed to take into account the large axial strain and variation in material properties occurring during the consolidation process. These programs offer more accurate predictions relative to Terzaghi's one-dimensional consolidation theory which is based on small strains (Lambe and Whitman, 1979).

Chapter 4 provides details of the simulation programs, including the governing assumptions and equations, numerical evaluations of the simulation programs, and basic parametric studies to explore the models' mechanism and behavior. Flowcharts for the program executions are provided to help facilitate the understanding of the mechanics

of the programs. The source codes for both programs are available in the Appendix B along with the list of input parameters and an example of processed output files based on Microsoft Excel ®. The simulation programs are written in C++ programming language for Microsoft Windows ® operating systems including Microsoft Windows ® 98, ME, 2000, and XP. Depending on the version of Microsoft Windows ® operating systems, extra C++ runtime files may be necessary to run the program. These C++ runtime files, if required, can be obtained from the official Microsoft web site (http://www.microsoft.com).

Chapter 5 discusses the analysis and results from the experimental and simulation programs. Due to a large number of experiments performed in this research, one typical test for each experimental program is selected for discussion before evaluating the results for each program. Results from the numerical simulations are also provided in this chapter. The predicted pore pressure distribution and average excess pore pressure from the GCRS simulation are used to help interpreting of the GCRS test results. The results from oedometer simulation are provided with focus on the study of the effects of important parameter, including coefficient of consolidation, hydraulic conductivity, and drainage heights, on the predicted c_v ratio. This chapter also discusses the procedures to obtain the representative c_v based on oedometer simulation for engineering applications. The complete laboratory test results can be found in the Appendix A.

Chapter 6 provides the conclusions and contributions of this research, along with recommended future work. The conclusions are divided into three sections covering all three aspects of the studies of this research. The chapter also lists the main contributions of this research that focuses mainly on the development of the new experiment techniques and set up and applications of the research findings in engineering applications. Several topics of future research are recommended along with detailed discussion of basic concepts, purposed equipment design, and data interpretations.

Chapter 7 contains the lists of references, followed by two sections of Appendixes. The summary tables of all test results, data sheets, and important graphs are presented in the Appendix A. Appendix B documents the source codes for both GCRS and oedometer simulation including the input files and examples of output files.

Chapter 2: Background

The consolidation behavior of clays is a complicated aspect of soil mechanics. Much effort has been spent to investigate and improve our understanding of the behavior. Terzaghi's one-dimensional consolidation theory offers a simple way to predict or simulate the consolidation behavior of soft clays. However, the theory cannot capture the overall behavior quite accurately. Often, the theory yields reasonable results comparing to laboratory test results or field observation. But there are still numbers of issues that need to be studied to ensure that the prediction can more accurately capture the real soil behavior.

A prime example of the difference between the Terzaghi's theory and the observed behavior in the laboratory relates to the calculation of the coefficient of consolidation, c_v. Terzaghi's theory assumes a constant and single value of c_v during primary consolidation. The primary consolidation refers to the deformation of the soil skeleton over time as the excess pore pressure is allowed to dissipate until it reaches zero. The deformation that occurs after the point where excess pore pressure reaches zero, is referred to as secondary compression. Laboratory results indicate that the values of c_v differ significantly based on the interpretation method applied to the data and that c_v also changes considerably during consolidation. This deviation creates a problem facing engineers wishing to apply laboratory consolidation result to field scale c_v (Lambe and Whitman, 1979).

The coefficient of consolidation, c_v, is defined as

$$c_v = \frac{k_v}{m_v \cdot \gamma_w} \tag{2.1}$$

where k_v is the vertical hydraulic conductivity, m_v is the coefficient of volume change, and γ_w is the unit weight of water. m_v is defined as

$$m_v = \frac{d\varepsilon_v}{d\sigma'_{vc}} \tag{2.2}$$

The following sections present the details of several important issues where Terzaghi's theory does not represent the real situation;

1) the non-uniqueness of the virgin compression line when the same soil specimen is subjected to different strain rates or have different drainage height,
2) the theory not taking into account the differences in hydraulic gradient during the loading sequences,
3) the coefficient of consolidation, c_v from square root of time and log time methods obtained from laboratory tests can be significantly different, and
4) large strains that Terzaghi's one-dimensional consolidation theory does not take into account.

These factors cause predictions based on Terzaghi's theory to differ from those observed in the laboratory and field. There are significant amounts of research focusing on these problems but many questions still remain unanswered. The main objectives of this research are to investigate, experimentally and numerically, the above factors which can open a new path leading to a better theory that can be used to better prediction and simulation of consolidation of soft clays.

2.1 Non-uniqueness of The Virgin Compression Line (VCL)

This main controversy is whether the virgin compression line is unique with respect to strain rate and hence drainage height. There are two opposing hypotheses (designated A and B) regarding to this fundamental aspect of clay behavior (Ladd et al., 1977). The hypotheses are based on different concepts of behavior and result in large differences for the predicted time rate and magnitude of final settlement when extrapolating measured laboratory scale results to anticipated field performance.

Hypothesis A separates the deformation process into two independent domains: primary consolidation and secondary compression. Secondary compression occurs after primary consolidation is complete (defined as the point of zero excess pore pressure) and hence implies an unique Virgin Compression Line (VCL) for all specimens having a strain rate equal to or higher than that used to achieve the End of Primary (EOP) curve. On the other hand, Hypothesis B represents the deformation process as an integrated combination of secondary compression and primary consolidation. The assumption that deformations associated with secondary compression occur simultaneously with primary consolidation results in a non-unique VCL. In fact, the relationship between void ratio and consolidation stress will be a function of the strain rate and drainage height used in the consolidation test.

While both Hypothesis A and B describe secondary compression behavior of clays, the results from implementing the Hypotheses are very different. Hypothesis A predicts that a larger specimen (i.e., soil layer in the field) will follow the same consolidation pattern

as a smaller specimen (i.e., laboratory specimen) and hence the VCL obtained from a laboratory test can be used to predict the field consolidation behavior (same $\varepsilon_c = f(H_d)^2$ where ε_c is the consolidation strain and H_d is the drainage height) with differences in time (and strain rate) required to achieve the EOP state.

Hypothesis B predicts a thickness dependent consolidation pattern and yields higher consolidation strain for thicker layers at any given time. The differences in the settlement prediction become larger with increasing time (and hence, increasing soil layer thickness). Figure 2.1 presents an illustration of the differences between hypothesis A and hypothesis B prediction for a large soil layer. The predicted consolidation curve based on hypothesis A is essentially based on the same parameters as those from the laboratory consolidation curve. The predicted hypothesis A curve assumes that secondary compression happens only after the end of primary consolidation. The only difference is the drainage height (100 cm for the predicted field consolidation for both hypothesis A and B and 2 cm for the laboratory consolidation curve). The predicted consolidation curve based on the hypothesis B assumes that the secondary compression occurs throughout the consolidation process. Therefore, the overall predicted deformation (or axial strain) based on the hypothesis B is much larger than that of hypothesis A as illustrated in Figure 2.1. The simulated oedometer consolidation curve in the Figure 2.1 is based on the Taylor expansion of the Terzaghi's one-dimensional consolidation theory (Taylor, 1948). Equation 2.3 and 2.4 presents the solution of the Terzaghi's one dimensional consolidation for uniform initial excess pore pressure.

$$u_e = \sum_{m=0}^{m=\infty} \frac{2u_0}{M} (\sin MZ) e^{-M^2 T} \tag{2.3}$$

The variable M is calculated from

$$M = \frac{\pi}{2}(2m+1) \tag{2.4}$$

where m is a dummy variable taking on values 1,2,3,...

The calculation proceeds until the normalized excess pore pressure becomes extremely small ($\Delta U_e/\sigma'_v < 0.001$). The consolidation is then governed by a constant coefficient of secondary compression, C_α to simulate secondary compression occurring after the end-of-primary. The predicted consolidation curve based on the hypothesis A is calculated using the same method but with drainage height of 100 cm. The predicted hypothesis B consolidation curve is calculated by allowing the secondary compression to occur together with primary consolidation throughout the consolidation. Essentially, the

deformation from secondary compression is added to the deformation from primary consolidation throughout the process.

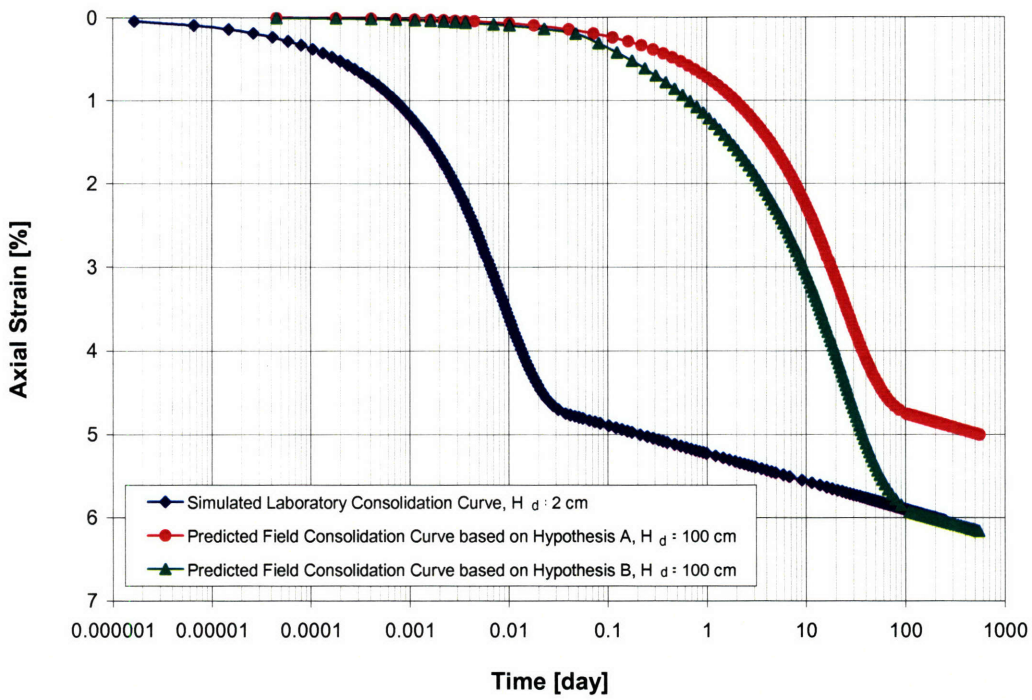

Figure 2.1 Comparison between simulated laboratory consolidation curve and predicted consolidation curve based on hypothesis A and B

There are several noted researches working in this field attempting to answer this important question. Two of the most notable studies are performed by Leroueil et al. (1985), to support hypothesis B, using series of Constant Rate of Strain (CRS) tests and Mesri et al. (1995), to support hypothesis A, using interconnected triaxial specimens.

CRS tests have been performed over a range of strain rates in an attempt to establish the validity of a unique end of primary (EOP) compression curve. Leroueil proposed that during one-dimensional consolidation, the behavior is controlled by a unique effective stress-strain-strain rate (σ'_v, ε_v, $\dot{\varepsilon}_v$) relationship (Leroueil et al., 1985 and Leroueil et al., 1996). Leroueil et al. (1985) also showed that the (σ'_v, ε_v, $\dot{\varepsilon}_v$) relationship can be simply described by two curves, one giving the variation of the preconsolidation pressure (σ'_p) with strain rate [$\sigma'_p = f(\dot{\varepsilon}_v)$] and the other presenting the normalized stress-strain curves [$\sigma'_v/\sigma'_p(\dot{\varepsilon}_v) = g(\varepsilon_v)$]. Figure 2.2 shows the $\sigma'_p/\sigma'_{p(REF)} = f(\dot{\varepsilon}_v)$ curves for Champlain Sea clay and Finish clay (Leroueil, 1996).

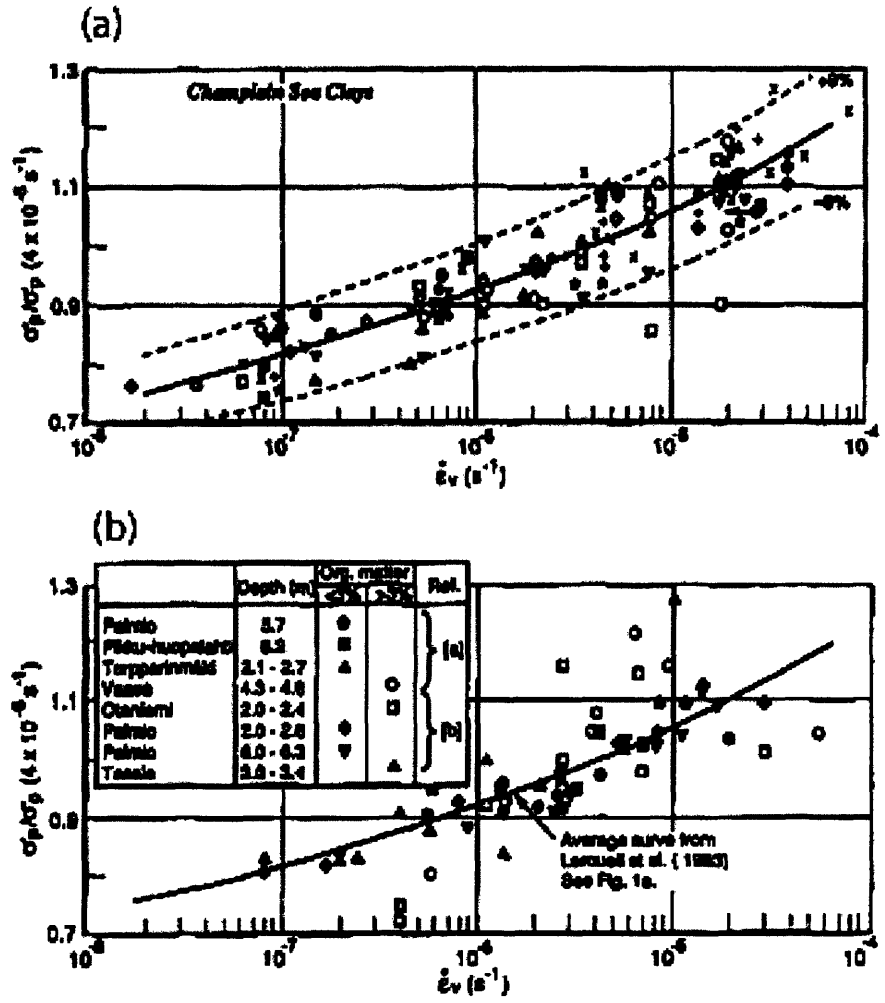

Figure 2.2 Strain-rate effect on preconsolidation pressure (a) Champlain Sea clay; (b) Finnish clays [after Leroueil, 1996]

Imai and Tang (1992) also reported that the strain at the end of primary consolidation increases with the specimen thickness. The model was confirmed by Imai (1995) for the Yokohama Bay mud. Imai (1995) performed a series of consolidation tests on reconstituted soil samples prepared from the Yokohama Bay mud using an interconnected consolidometer to examine the consolidation behavior of clay elements located at different drainage distances (Imai, 1995). Figure 2.3 presents a schematic drawing of basic concept of interconnected consolidation test. Figure 2.4 shows the compression curves obtained from the tests on the Yokohama Bay mud.

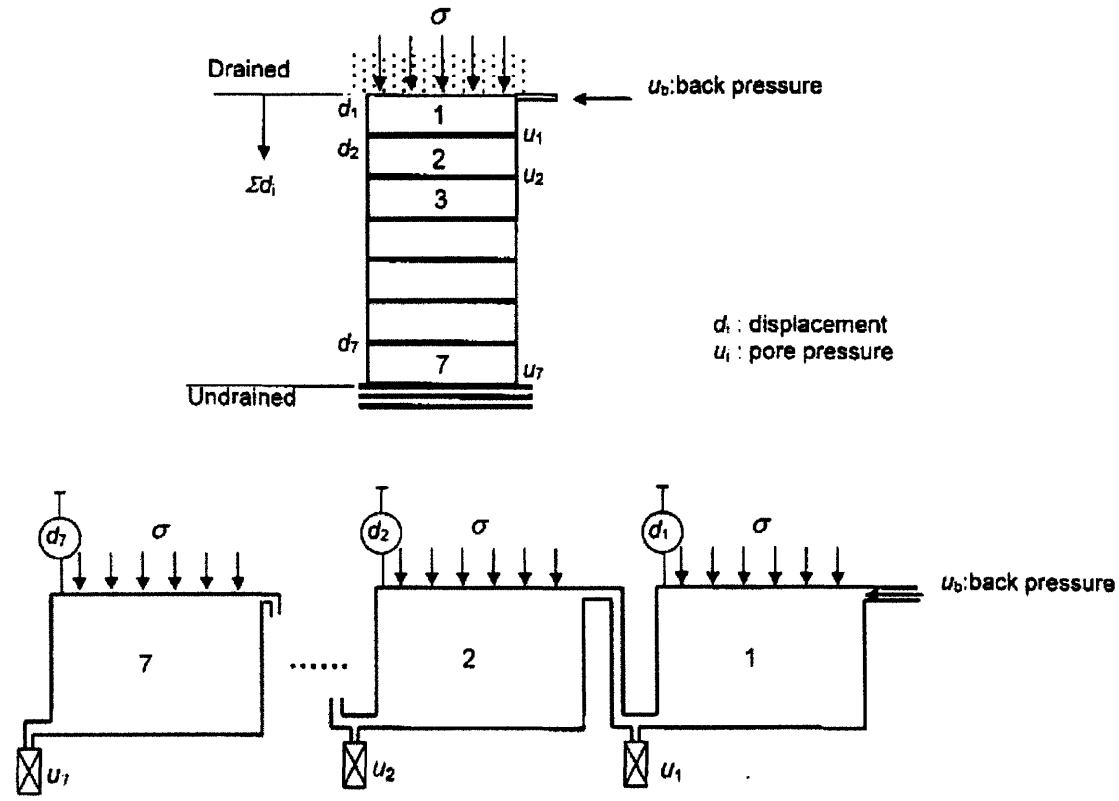

Figure 2.3 Sketch of the interconnected consolidometer used by Imai (after Imai, 1995)

Leroueil et al. (1985) discusses in detail the strain-rate effects on the consolidation behavior. The main evidence used in the discussion is the results from various Constant Rate of Strain (CRS) tests performed at different strain rate. The test results show clear dependent of effective stress on the strain rate used in the tests. However, there are other important factors that remained unstudied and should be properly included into the study of strain rate effects to provide a better understanding of the behavior. The main factor is the hydraulic gradient during the CRS test. Higher strain rate means the hydraulic gradient during consolidation is higher. The authors observe only the overall results from the CRS tests but did not go into a detailed study of effect of hydraulic gradient on the CRS tests.

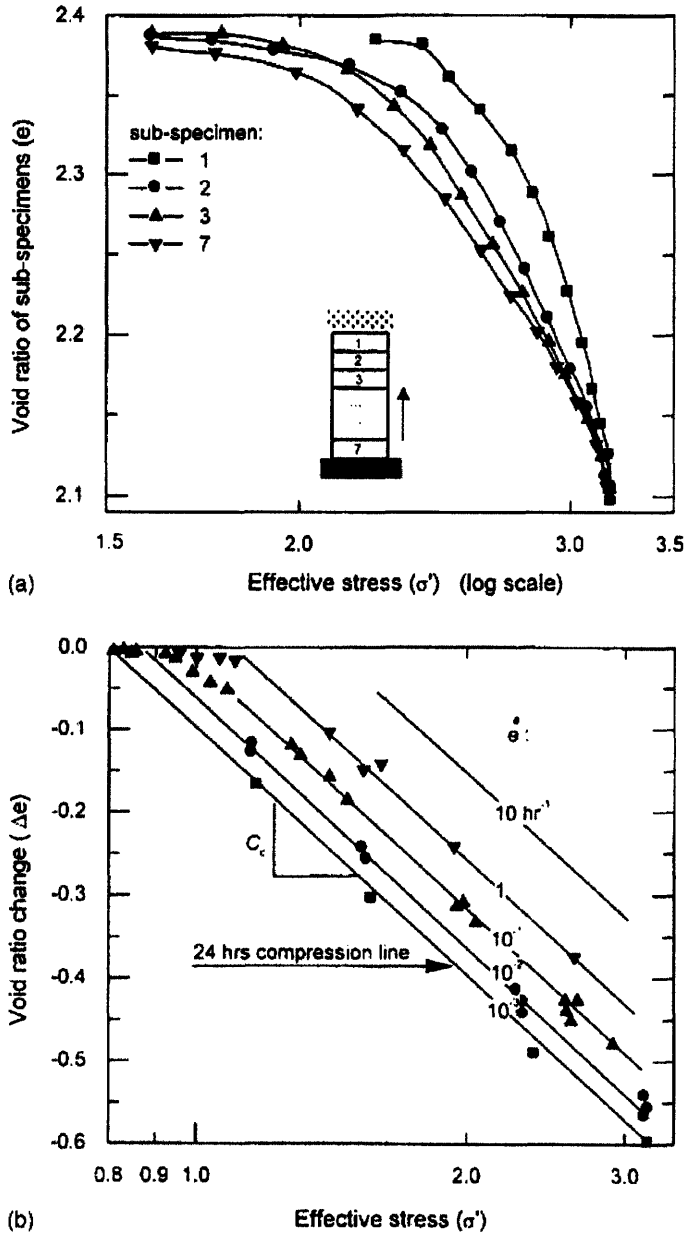

Figure 2.4 Compression curve obtained from the interconnected consolidation test on Yokohama Bay mud (after Imai, 1995)

Mesri and Choi (1985) examined the relationship between the magnitude of End of Primary (EOP) compression and duration of primary consolidation by comparing EOP void ratio versus effective vertical stress relationships of thin and thick specimens of a block sample. The authors achieved this objective by comparing the compression curve (ε_{EOP} versus log σ'_v) of a 125 mm and a 500 mm thick specimen. The 500mm thick specimens were constructed by connecting a series of four 125mm thick specimens.

The materials used in the tests were St. Hilaire clay (Plasticity Index, PI = 22). The specimens are prepared to be as identical as possible by cutting them from an undisturbed sample taken by Laval or Sherbrooke samplers at the same elevation (one for a 125 mm and four for the interconnected 500 mm thick specimen).

These tests effectively increase the specimen thickness and allow measurement of individual layer performance. Mesri performed tests on hydrostatically consolidated specimens in four interconnected triaxial cells. He concluded that for all practical purposes the EOP curve was unique. Figure 2.5 presents the EOP e versus log σ'_v curves of a thin and thick layer of St. Hilaire clay (Mesri et al., 1995). The curves clearly show that, despite the 4 times difference in the drainage height, there is no observable differences in the VCLs.

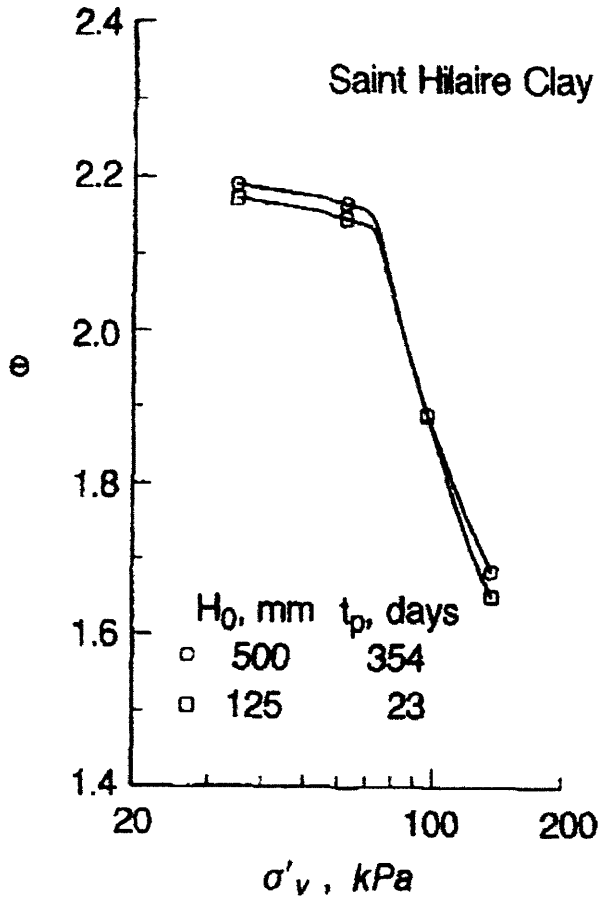

Figure 2.5 Compression curves for 500 and 125 mm equivalent drainage height (after Mesri, 1985)

In addition, Sheahan (1997) measured pore pressures within the specimen during CRS tests on Resedimented Boston Blue Clay (RBBC) and reports a unique EOP relationship provided that a non-linear soil model is used with the measured pore pressure distribution.

Another interesting observation can be obtained from a large batch consolidation test. At MIT, Resedimented Boston Blue Clay (RBBC) is routinely consolidated from a slurry using a 30 cm diameter by 14 cm tall batching oedometer. Figure 2.6 presents the strain during the increment versus log time results of one typical stress increment from 50 to 100 kPa. A time curve from a 2 cm tall oedometer specimen of RBBC loaded from 200 to 400 kPa is also included for comparison (Germaine, 2002). Both increments are in the normally consolidated range of the soil. The stress increments are different because the small oedometer test is performed on soil prepared in the tall batching oedometer.

As a preliminary result, the data suggest that RBBC tends to behave according to Hypothesis B. However, there are several problematic features about these data.

- The early portions of the two curves are not geometrically similar as would be expected with either Hypothesis A or B. In fact, one might expect a steeper slope for the consolidation curve of the large specimen based on the Hypothesis B.
- The end of primary consolidation is poorly defined (as typical of other soils) in the thin oedometer that does not support either Hypothesis A or B.
- The c_v is independent of the method of calculation (Taylor or Casagrande) for the large oedometer and equal to CRS values which is consistent with Hypothesis A. Additional discussion about coefficient of consolidation can be found in the section 2.3 of this chapter.
- The c_v Taylor to c_v Casagrande ratio is about 1.7 for the thin oedometer and about 60% of the CRS values, which is consistent with reported trends used in support of Hypothesis B.

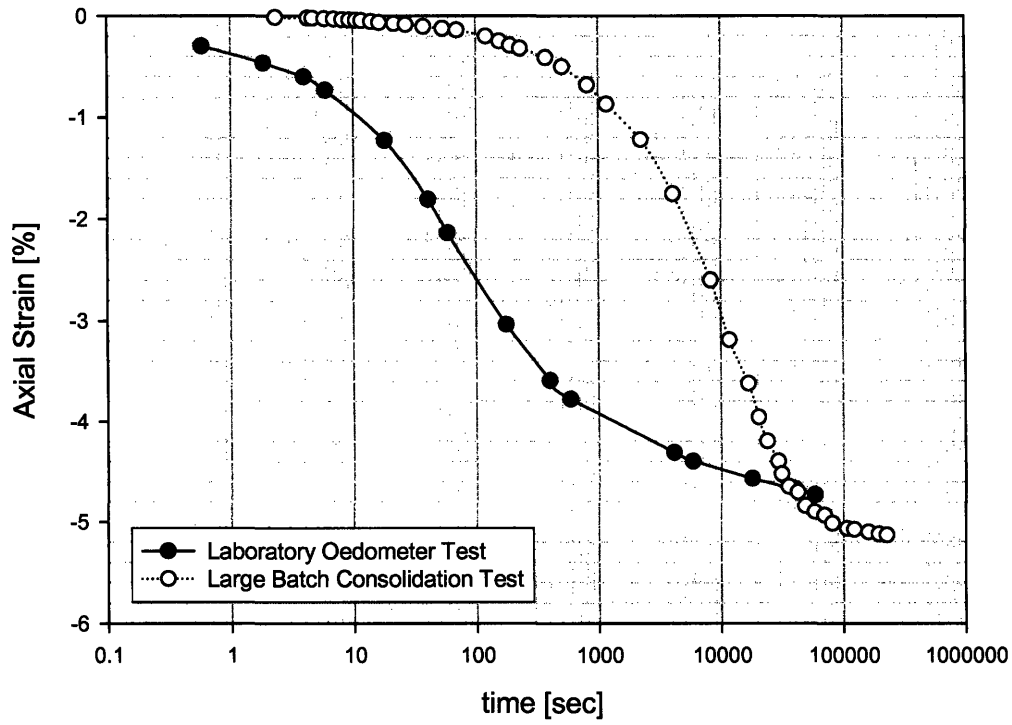

Figure 2.6 Comparison between consolidation curves from laboratory oedometer test and large batch consolidation test for RBBC [after Germaine, 2002]

The cause of these conflicting observations is highlighted in Figures 2.7 and 2.8 which plot double normalized settlement time curves. Figure 2.7 is obtained by normalizing the theoretical values presented in Figure 2.1 by the strain and time at the EOP as determined by the Casagrande method. This essentially collapses the two Hypothesis A curves and the Hypothesis B thin layer curve to one. The Hypothesis B thick layer curve is noticeably lower at early times. Figure 2.8 presents results of the same calculation performed on the measured RBBC data of Figure 2.6. At early normalized times the thick specimen undergoes less settlement than the thin specimen. This trend is opposite to the theoretical prediction and clearly shows that the observed scale effect is not solely an issue of secondary compression. In addition, the transition between primary consolidation and secondary compression is more definitive for the large specimen. The small specimen has a poorly defined transition and a continuously decreasing rate of secondary compression.

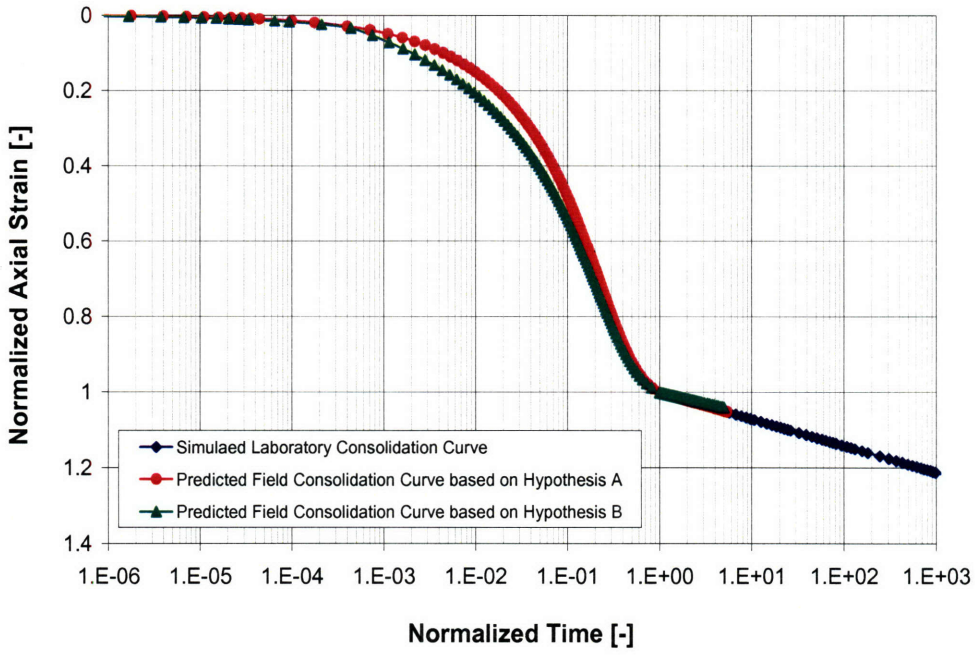

Figure 2.7 Normalized consolidation curve comparing the simulated laboratory oedometer curve with the predicted field consolidation curves based on the Hypothesis A and B

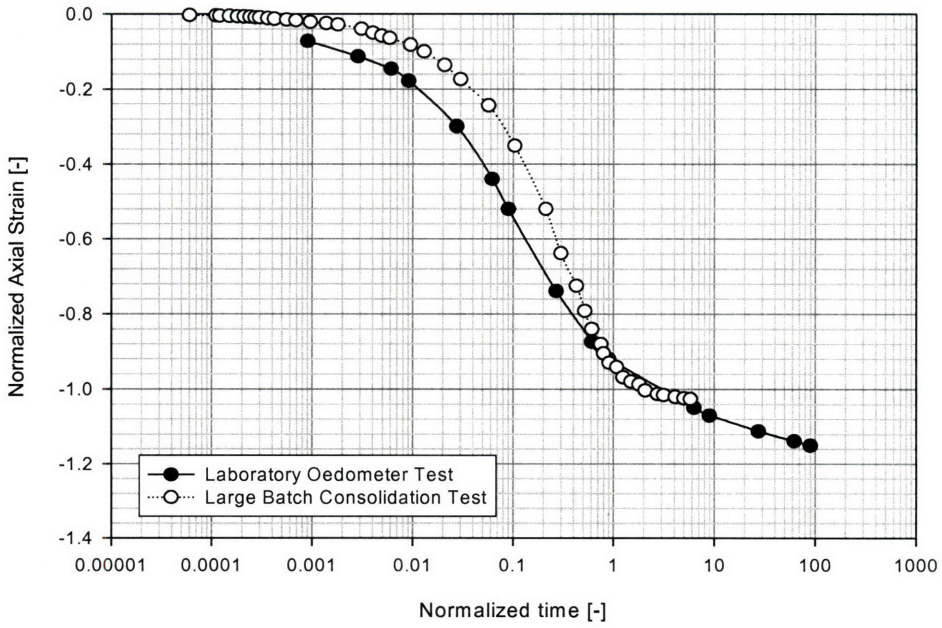

Figure 2.8 Comparison between normalized consolidation curves from laboratory oedometer test and large batch consolidation test for RBBC

2.2 Hydraulic Gradient During Loading Sequence

The interpretation of the consolidation test is complicated by the fact that it involves highly nonuniform effective stress, strain, strain rate, and hydraulic gradients. While there have been significant efforts spent on the study of strain rate effects on consolidation behavior of soft clays, apparently no one has tried to decouple the effect of strain rate and gradient during the constant rate of strain test. This is important because without knowledge of how gradient play a role in the overall behavior, we cannot fully understand the behavior.

Additionally, in another test, a two-way drainage oedometer test of a 2 cm specimen under a 1 kg/cm^2 pressure increment experiences a gradient above 1000 for a significant portion of the increment based on Terzaghi's theory. Figure 2.9 presents the predicted hydraulic gradient during an oedometer test at the Z equal to 0.2. Z is a nondimensional variable refers the relative location of the interested point in a soil specimen. Z is defined as

$$Z = \frac{z}{H} \tag{2.5}$$

where z is the distance measured from the top of the specimen and H is the total height of the specimen.

Given that strain rates used in a CRS test can vary from very low (0.1%/hr) to extremely high (>3%/hr), this can become a big issues. Hydraulic gradients vary significantly and can greatly affect the interpreted behavior.

This hydraulic gradient is 30 times larger than maximum gradients set by ASTM (D5084) for hydraulic conductivity measurements. While others have noted the fact that gradients are quite large in the oedometer test (Imai, 1997), no one has conducted a systematic study to isolate its importance on deformation.

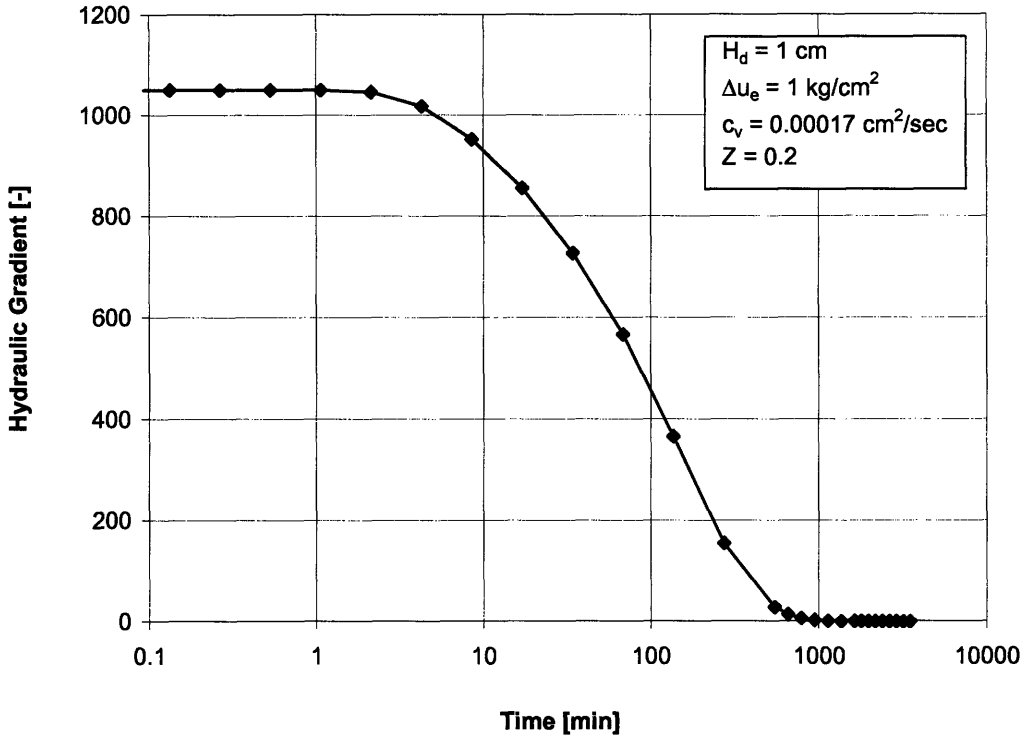

Figure 2.9 Hydraulic gradient versus time (in logarithm scale) for a 2 cm oedometer specimen at Z = 0.2.

Another important question is whether the hydraulic conductivity is affected by the hydraulic gradient and if so what is the magnitude of the effects. Imai and Tang (1992) presented results from the interconnected consolidation tests showing that the hydraulic gradient is a constant at a given void ratio regardless of the hydraulic gradient occurred during the test. Figure 2.10(a) presents the relation of flow velocity and hydraulic gradient for constant void ratio for the Yokohama Bay mud. Figure 2.10(b) shows the relationship between void ratio and hydraulic conductivity.

However, other research conducted in recent years indicates that large hydraulic gradients applied during hydraulic conductivity testing can cause reductions in measured hydraulic conductivity (Fox, 1996). He further concludes that the magnitude of the effects is expected to be more important for normally consolidated soils with high compressibility, such as soft clays (Fox, 1996). Mitchell (1993) also suggested that the failure to account for seepage-induced consolidation in laboratory tests can cause significant errors in time rate of settlement calculations for highly compressible soils (Fox, 1996).

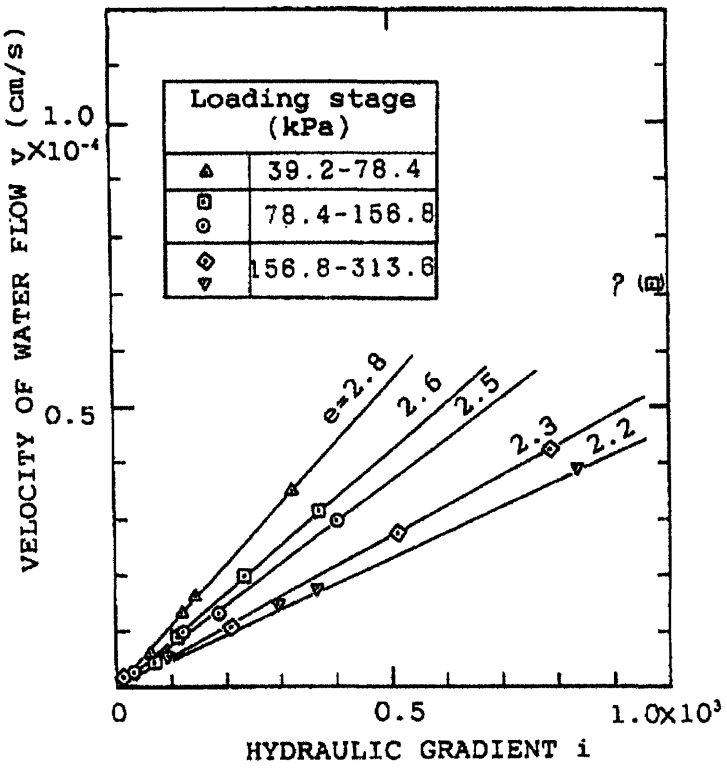

Figure 2.10(a) Relationship of flow velocity and hydraulic gradient at constant void ratio for the Yokohama Bay mud (after Imai and Tang, 1992)

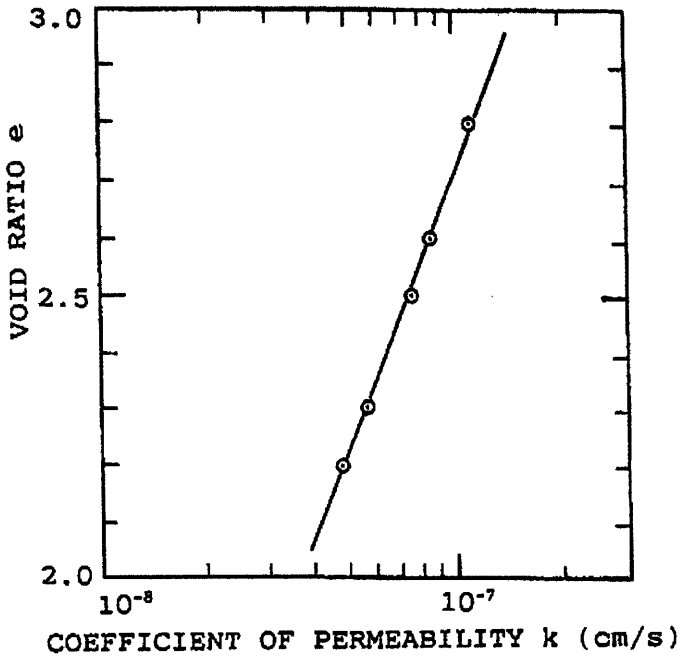

Figure 2.10(b) Relationship between void ratio and hydraulic conductivity (after Imai and Tang, 1992)

2.3 Differences in Coefficient of Consolidation, c_v, From Square Root of Time and Log Time Methods

The coefficient of consolidation is a parameter that combines two material properties hydraulic conductivity and soil compressibility. It is the main variable used in the Terzaghi's theory in the prediction of consolidation behavior. The theory assumes that the coefficient of consolidation is a constant and there is one value representing the soil under specific condition throughout the load increment. In reality, the values of c_v can vary during consolidation and multiple values can be obtained based on different interpretation techniques.

The coefficient of consolidation, c_v, can be obtained from an oedometer test result using two main methods: 1) square root of time; and 2) log time method. Other methods are also available for the interpretation of c_v but the above two methods are the most well-known methods which will be used throughout this research for the interpretation of c_v.

2.3.1 Square Root of Time Method

Taylor (1948) developed a method for evaluating c_v using the square root of time method. The method is based on the similarity between the shapes of the theoretical and experimental curves when deformation, ΔH, is plotted versus the square root of time. Figure 2.11 shows an example of consolidation curve plotted on strain [%] and square root of time [$s^{1/2}$or $m^{1/2}$] scale. In theory the curve is a straight line to U ~ 60%. Taylor computed that the abscissa of the curve at 90% consolidation was 15% larger than the abscissa of the extension of the initial straight line. This is the point of 90% consolidation on a laboratory time curve.

Using this method, c_v is calculated from

$$c_v = \frac{0.848(H_d)^2}{t_{90}} \tag{2.6}$$

where H_d is the drainage height at t_{50} and t_{90} is the time to 90% consolidation.

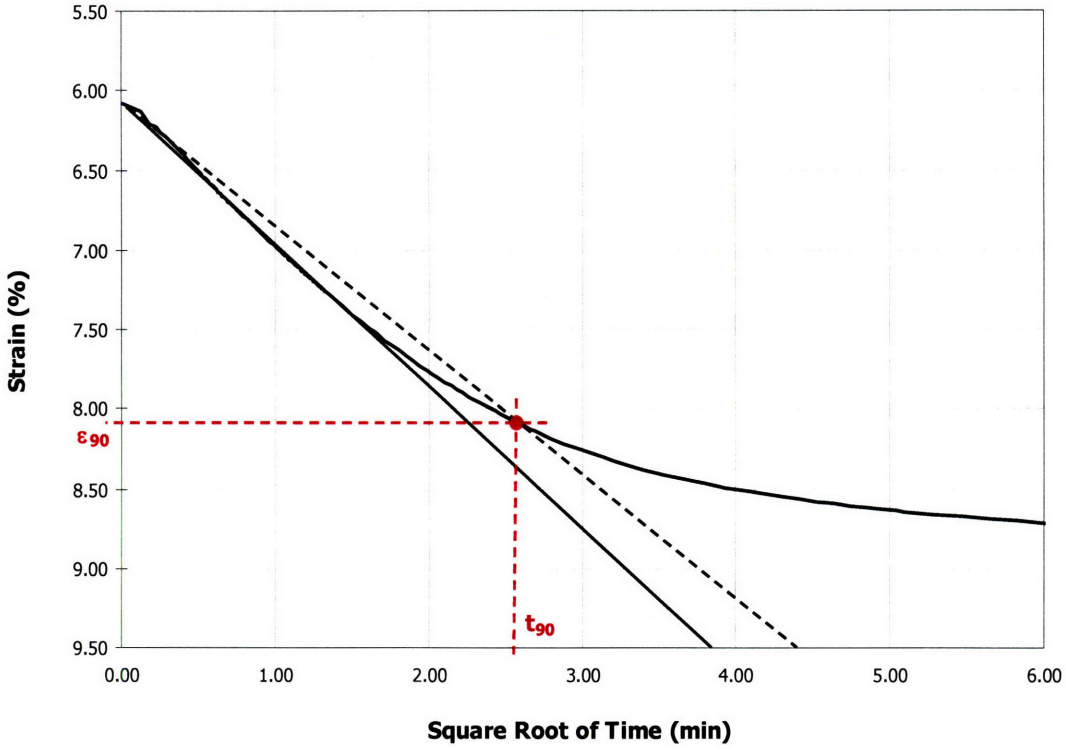

Figure 2.11 c_v from square root of time method

2.3.2 Log Time Method

The other most frequently used method to obtain the coefficient of consolidation is the log time method (Casagrande, ???). In this method, the consolidation curve is plotted on the deformation, ΔH, or strain, ε_a, versus the logarithm of time. Figure 2.12 shows an example of the consolidation curve plotted in such space. Based on the plot, we can draw two straight lines, one representing the steepest linear portion of the curve (shown as line A in the Figure 2.12) and another representing the linear portion of the secondary compression line (shown as line B in the Figure 2.12).

The intersection of these lines indicates the end-of-primary consolidation (EOP) of the step. From the point, we can obtain the strain and time at EOP (ε_{EOP} and t_{EOP}, respectively). Based on the known starting height of the specimen, we can obtain e_0. With the known e_0 and ε_{EOP}, we can find the point of 50% consolidation (ε_{50}). The coefficient of consolidation, then can be calculated from

$$c_v = \frac{0.197(H_d)^2}{t_{50}} \tag{2.7}$$

where H_d is the drainage height at t_{50} during the increment and t_{50} is the time to 50% consolidation.

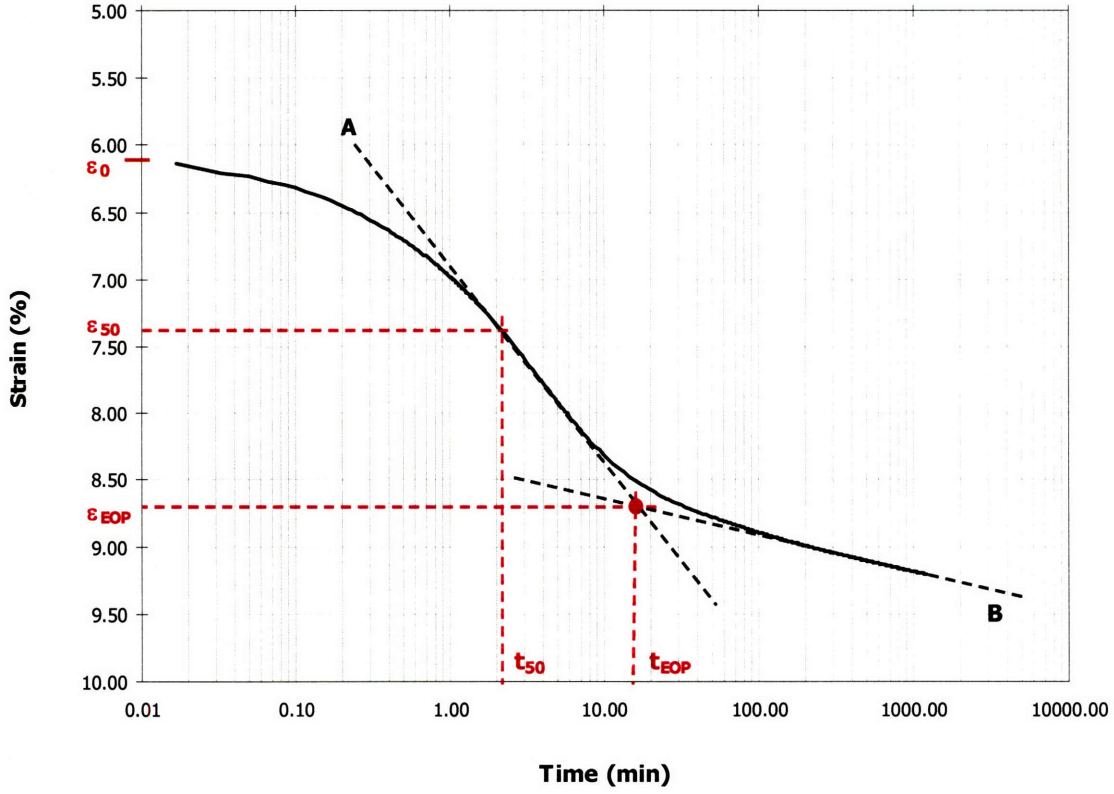

Figure 2.12 c_v from log time method

It is well documented that the coefficient of consolidation, c_v, obtained from the square root of time and log time methods can differ significantly for soft clays (Lambe and Whitman, 1979). This is one of the most notable differences between the assumption used in the Terzaghi's 1-D consolidation theory and the observed results from laboratory. The differences in c_v leads to uncertainty in selecting the values for uses in the field design and analysis.

2.4 Large Strain Consolidation

One of the main assumptions involved in the derivation of the Terzaghi's theory is a limitation to small strains (Lambe and Whitman, 1979). In a laboratory testing or field observation, the strains from consolidation can be quite large. To accurately predict the consolidation behavior, a more sophisticated model or simulation that accounted for the large strain deformation should be considered.

Chapter 3: Experimental Technologies

This chapter presents the experimental technologies used in this research. There are three main experimental programs.

1) Constant Rate of Strain (CRS) tests with varying strain rate, $\dot{\varepsilon}$.
2) Gradient-controlled CRS (GCRS) tests.
3) Incremental oedometer tests with varying drainage height.

All experiments are performed on two soil types, San Francisco Bay mud (SBM) and Maine Blue clay (MBC). The following sections explain in detail the basic material properties and the experimental technologies used in this research.

3.1 Materials and Specimen Preparation

Two soils are selected for the experimental program in this research including 1) San Francisco Bay mud (SBM) and Maine Blue clay (MBC). The two soils are selected for the experiments because of significant differences of their basic behaviors and the availability of good quality tube samples. With natural soils, we can perform the test with soil structure as close to those in the field condition as possible with well controlled boundary conditions. It should be noted, however, that there is the specimen to specimen variation for natural soil samples that are obtained from different location and elevation.

3.1.1 San Francisco Bay mud

San Francisco Bay mud is a highly plastic, organic clay (CH-OH), with high compressibility, low undrained shear strength, and generally low permeability. SBM has average liquid limit (LL) of 109.8 and average plastic index (I_P) of 62.6. The average liquidity index (I_L) is 0.75. The average compression ratio (CR) and ratio of $C_{\alpha\varepsilon}$/CR of SBM specimens are 22.9 and 0.0341, respectively. Table 3.1 presents the summary of basic soil properties for SBM and MBC. Figure 3.1 presents a plasticity chart with a typical SBM Atterberg limit. All SBM specimens are obtained from 3" tube samples.

3.1.2 Maine Blue clay

Maine Blue clay is a low plasticity silty clay (CL). The average liquid limit (LL) of MBC is 30. The average plasticity index (I_P) and liquidity index (I_L) are 10 and 1.2, respectively. The average Compression Ratio (CR) and the ratio f $C_{\alpha\varepsilon}$/CR of MBC specimens are 10.3 and 0.0323, respectively. All MBC specimens are also obtained from 3" tube samples.

Material Properties	Maine Blue Clay (MBC)	San Francisco Bay Mud (SBM)
Initial Void Ratio, e_0	0.909 ± 0.0391	2.493 ± 0.25
Natural Water Content, w_n [%]	31.73 ± 1.44	83.34 ± 10.48
Liquidity Limit, w_L [%]*	30 ± 2.5	109.8
Plastic Index, I_P*	10 ± 2	62.6
Liquid Index, I_L*	1.2 ± 0.2	0.67 ± 0.12
Compresison Ratio, CR	10.3 ± 1.4	22.9 ± 4.6
$C\alpha\varepsilon/CR$	0.0323 ± 0.0073	0.0341 ± 0.0046

* The Atterberg limits data of MBC and SBM are obtained from Germaine, 2007

Table 3.1 Summary of basic soil properties of MBC and SBM

3.1.3 Specimen Preparation

Specimen selection within each tube was based on x-ray photographs of the sample tube to obtain the best possible quality specimen. X-ray photograph is very helpful in sample selection since it shows the layering of soil and degree of disturbance that occurred from the sampling processes. The sample tube is cut into small section approximately 2 - 2.5" long. A small wire is used to cut through the circumference of the tube to eliminate the bond between the soil and the side of the tube. The soil is then normally extruded from the tube. To obtain the best possible quality soil, the specimen is obtained from the location as near the middle of the tube as possible using trimming process. The final trimming of the specimen surface is performed using very sharp straight edge hold at 45 degree angle. The specimen is also subjected to a recess tool to create a recess at the top of the consolidation ring to allow the porous stone to sit accurately on the specimen.

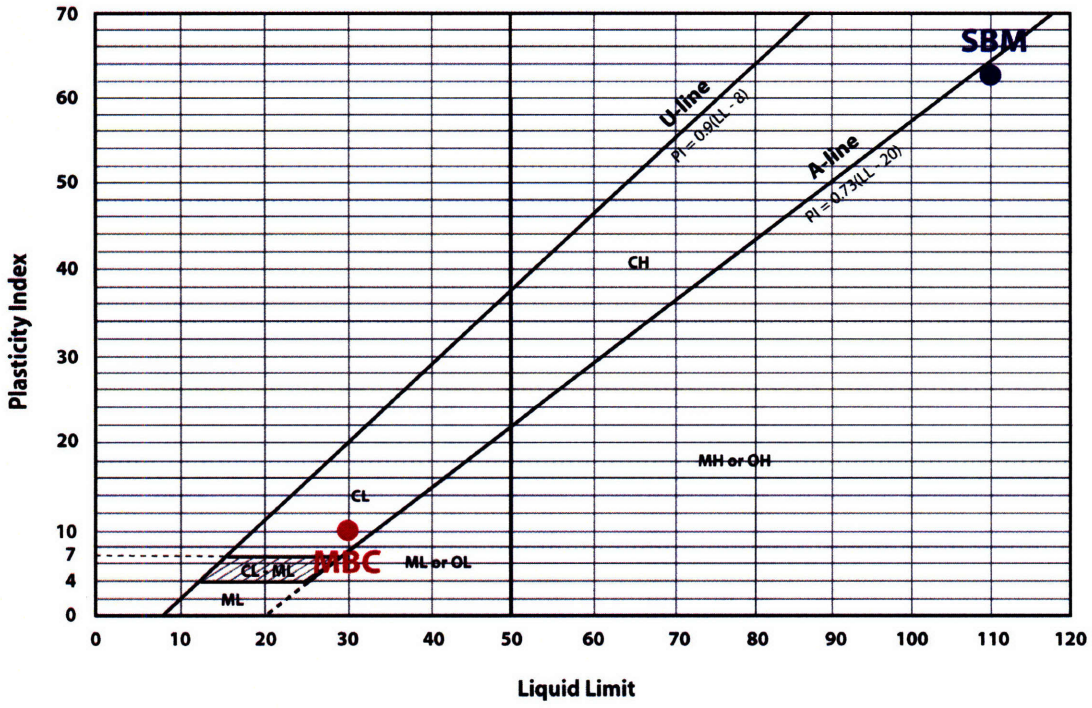

Figure 3.1 Plasticity chart identify Maine Blue clay (MBC) and San Francisco Bay mud (SBM)

3.2 Constant Rate of Strain (CRS) Test with Varying Strain Rate, $\dot{\varepsilon}$

Constant rate of strain (CRS) test is a relatively simple and popular test for obtaining the consolidation behavior of soft clays. The concept of CRS test is to apply a constant strain rate, $\dot{\varepsilon}$, to a soil specimen under 1-dimensional consolidation. The specimen is deformed at constant rate and the deformation and reactions are measured.

3.2.1 Equipments

Several transducers and measurements are performed during each test including

1) Vertical load (F)
2) Vertical deformation (ΔH)
3) Cell pressure (CP)
4) Base pore pressure (BP)

The system is computerized to ensure good precision and continuous control. All data from the transducers are collected through the central data acquisition system. Figure 3.2 shows the standard set up of a CRS test using Trautwein cell.

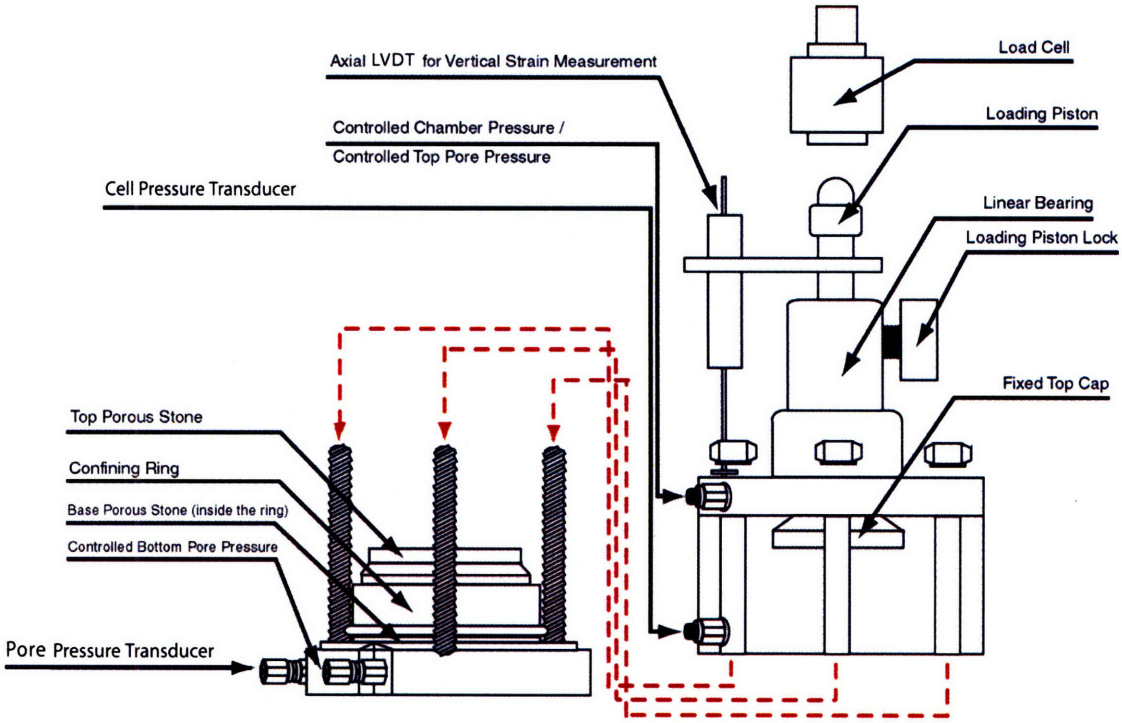

Figure 3.2 Trautwein CRS cell

The standard sample preparation process includes the cutting of the soil tubes, special sample extraction, and specimen trimming. The CRS ring is used both as the final cutting tool and as the consolidation ring. One 5μm mono filament nylon filter fabric, each, is used on the top and bottom of the specimen.

A standard CRS test begins with back pressuring of the specimen inside the cell to at minimum of 2 kg/cm^2. This is to ensure that the specimen and pore pressure system are fully saturated before the 1st consolidation stage. Once the specimen is fully saturated, the bottom drainage line is closed and it is consolidated at constant rate of strain. The base pore pressure, cell pressure and vertical total stress are measured along with vertical deformation. The strain rate used in the test can vary from very slow (< 0.1%/hr) to very fast (> 3%/hr).

3.2.2 Test Processes

For a CRS test with varying strain rate, the steps are more complicated and involve several sequences. The experimental process is developed to ensure that the test results can be interpreted without ambiguity. The standard CRS test procedures are modified to

allow the test to cycle through three different strain rates in the way that each strain rate produces at least two well-defined sections of Virgin Compression Line (VCL) sections. The processes allow for easier and more accurate interpretation and comparison by connecting the two sections together to form a representative VCL for each strain rate. The processes are especially critical in the case that the VCL of a soil is not perfectly linear. Figure 3.3 illustrates a schematic drawing representing CRS test with varying strain rate.

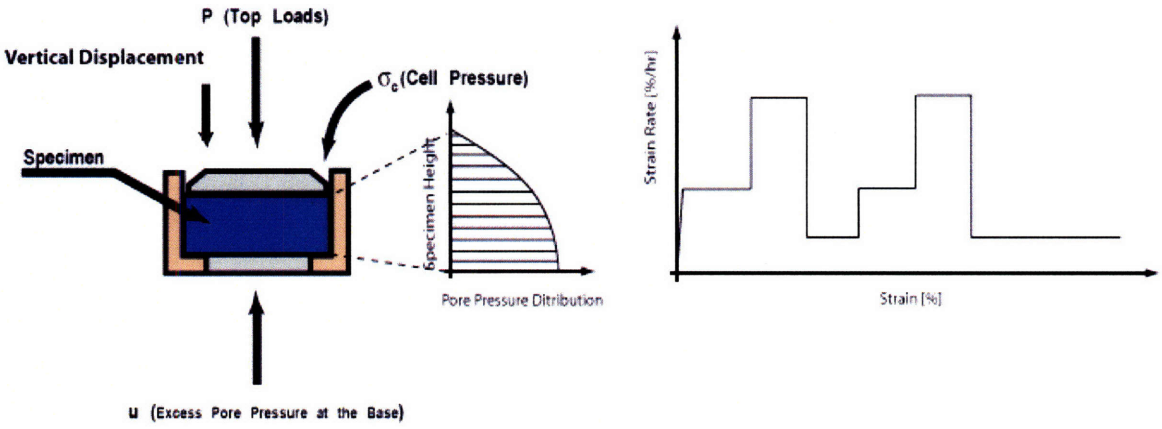

Figure 3.3 Schematic drawing illustrating the strain rate sensitivity test

The following section provides details of the procedures used in a CRS test with varying strain rate.

1) The specimen is consolidated with a medium strain rate beyond the preconsolidation pressure, σ'_p, to speed up the test since we are always interested in the virgin compression range.
2) Once a well-defined section in the virgin compression range (approximately 7% ε_a, dependent on soil type) is established, the strain rate is changed to the higher bound (or lower depending on the test).
3) Maintain this strain rate until a linear compression line is significant enough for the interpretation (approximately 2-3% ε_a).
4) Reduce the strain rate to the lowest ε_a for the test and keep the consolidation process until a well-defined portion of VCL is large enough (again, approximately 2-3% ε_a).
5) Adjust the strain rate back to the medium ε_a and repeat step 2 to 4.

For each test, this yields three pair of interpreted VCLs representing the virgin compression lines at each strain rate.

3.2.3 Calculations

Based on the collected data, the vertical effective stress can be calculated using the linear theory presented by Wissa et al. (1971). The total vertical stress can be obtained from

$$\sigma_v = \frac{F}{A} \tag{3.1}$$

where σ_v is the total vertical stress, F is the vertical load, and A is the cross-sectional area of the specimen.

The average pore pressure and the average vertical effective stress based on the Wissa linear theory are calculated from

$$\Delta u_{avg} = \frac{2}{3}\Delta u_b \tag{3.2}$$

$$\sigma_v' = \sigma_v - \Delta u_{avg} = \sigma_v - \frac{2}{3}\Delta u_b \tag{3.3}$$

where Δu_{avg} is the average pore pressure and Δu_b is the base excess pore pressure. σ'_v is the average vertical effective stress of the specimen.

Wissa et al. (1971) also formulated a nonlinear theory based on an assumption of a constant cv. The hydraulic conductivity, k, and coefficient of volume change, m_v, can, however, change during consolidation. For the nonlinear theory, a dimensionless variable T is derived to indicate the degree of transience in the specimen strain distribution.

$$T = 4.78(F_3)^3 - 3.21(F_3)^2 + 1.65(F_3) + 0.0356 \tag{3.4}$$

where F_3 is defined as

$$F_3 = \frac{log(\sigma_v - \Delta u_b) - log(\sigma_{v(t=0)})}{log(\sigma_v) - log(\sigma_{v(t=0)})} \tag{3.5}$$

where σ_v is the total vertical stress, Δu_b is the base excess pore pressure.

Steady-state conditions can be defined as when T is greater than 0.5. ASTM D4186 provides the stead-state solution for the nonlinear theory of Wissa et al. (1971). The

ASTM D4186 also restricts the base excess pore pressure to 30% of the total vertical stress.

For a steady-state condition (T > 0.5), the average vertical effective stress, σ'_v, is defined as

$$\sigma_v^{'} = \left(\sigma_v^3 + 2\sigma_v^2 \Delta u_b + \sigma_v \Delta u_b^2\right)^{1/3} \tag{3.6}$$

The coefficient of consolidation, c_v, and the vertical hydraulic conductivity, k_v, are defined as

$$c_v = \frac{-H^2 \log\left(\frac{\sigma_{v2}}{\sigma_{v1}}\right)}{2\Delta t \log\left(1 - \frac{\Delta u_b}{\sigma_v}\right)} \tag{3.7}$$

$$k_v = \frac{-0.434 \dot{\varepsilon} H^2 \gamma_w}{2\sigma_v^{'} \log\left(\frac{\sigma_v - \Delta u_b}{\sigma_v}\right)} \tag{3.8}$$

where H is the current specimen height, $\dot{\varepsilon}$ is the strain rate at which loading occurs, γ_w is the unit weight of water, σ_{v1} and σ_{v2} are total vertical stresses (subtract any back pressure applied at top surface) at two times of difference Δt.

3.2.4 Test Interpretations

The linear theory is used for all data reductions for all tests with normalized excess pore pressure ($\Delta U_e/\sigma'_v$) less than 20%. Gonzalez (2000) showed that the differences of the vertical effective stresses obtained, hydraulic conductivity, and coefficient of consolidation from the linear and nonlinear theory are less than 1%, 12.5%, and 12.5%, respectively, when $\Delta U_e/\sigma'_v$ is less than 20%. For all tests with $\Delta U_e/\sigma'_v$ more than 20%, the differences increase significantly and the nonlinear theory is used for the data reduction. Based on the calculated effective vertical stress and measured vertical strain, the compression curve is plotted.

If a soil follows hypothesis A, and assuming that the strain rate is high enough to generate excess pore pressure, the three pairs for each ε_a should connect to form a unique line. This shows that the strain rate has no effect on the consolidation behavior of the soil. However, if the three pairs form three different VCLs (supposedly parallel to each other), then the soil exhibits strain rate dependent consolidation behavior. Figure

3.4 shows an illustration of the compression curve of a strain rate dependent soil with constant compression ratio, CR. Figure 3.5 presents an illustration of the compression curve of a strain rate independent soil with constant compression ratio, CR. The compression ratio is defined as

$$CR = \frac{d\varepsilon_a}{d\,log\left(\sigma_v^{'}\right)} \qquad (???)$$

where CR is the compression ratio, ε_a is the axial strain and σ'_v is the vertical effective stress.

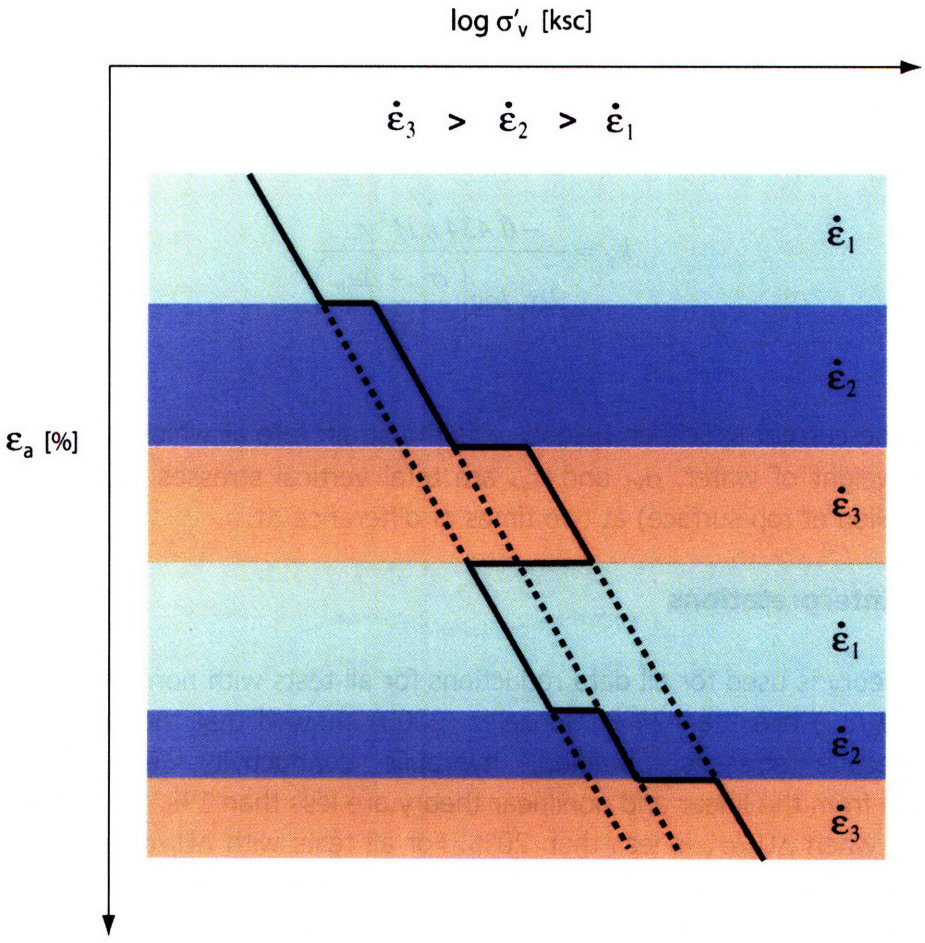

Figure 3.4 Compression curve illustrates the consolidation behavior of strain rate dependent soil with constant CR

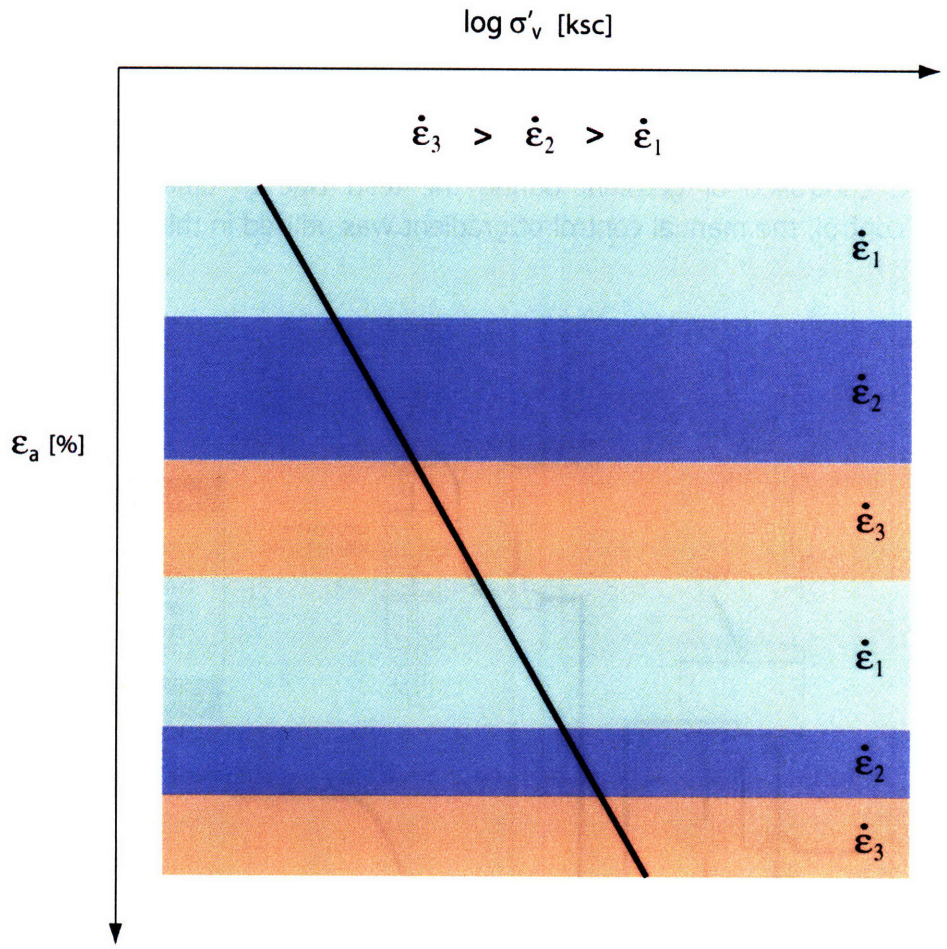

Figure 3.5 Compression curve illustrates the consolidation behavior of strain rate independent soil with constant CR

The interpretation of strain rate sensitivity is relatively simple using the Wissa et al. CRS theory. The average pore pressure and vertical effective stress can be calculated using the equation 3.1 to 3.3.

A series of strain rate sensitivity tests for MBC and SBM are performed in this research covering strain rates of 0.1%/hr (low) to 3%/hr (high) for SBM and 1%/hr to 8%/hr (very high) for MBC. The results from the tests will be discussed in detail in Chapter 5.

3.3 Gradient-controlled CRS (GCRS) Test

To decouple the effects of hydraulic gradient from the compressibility of a soil, a special test is developed based on the CRS test concept. The test set up is more complicated than a normal CRS test because it involves decoupling of hydraulic gradient from the consolidation behavior. However, it is still relatively easy to perform and offers insight into a fundamental aspect of soil behavior, i.e., the effects of hydraulic gradient.

3.3.1 Equipments

Figure 3.6 shows a GCRS test set up. The test can be set up with manual or computerized controlled of gradient during the test. Due to time constraint and to simplify the control, the manual control of gradient was utilized in this research.

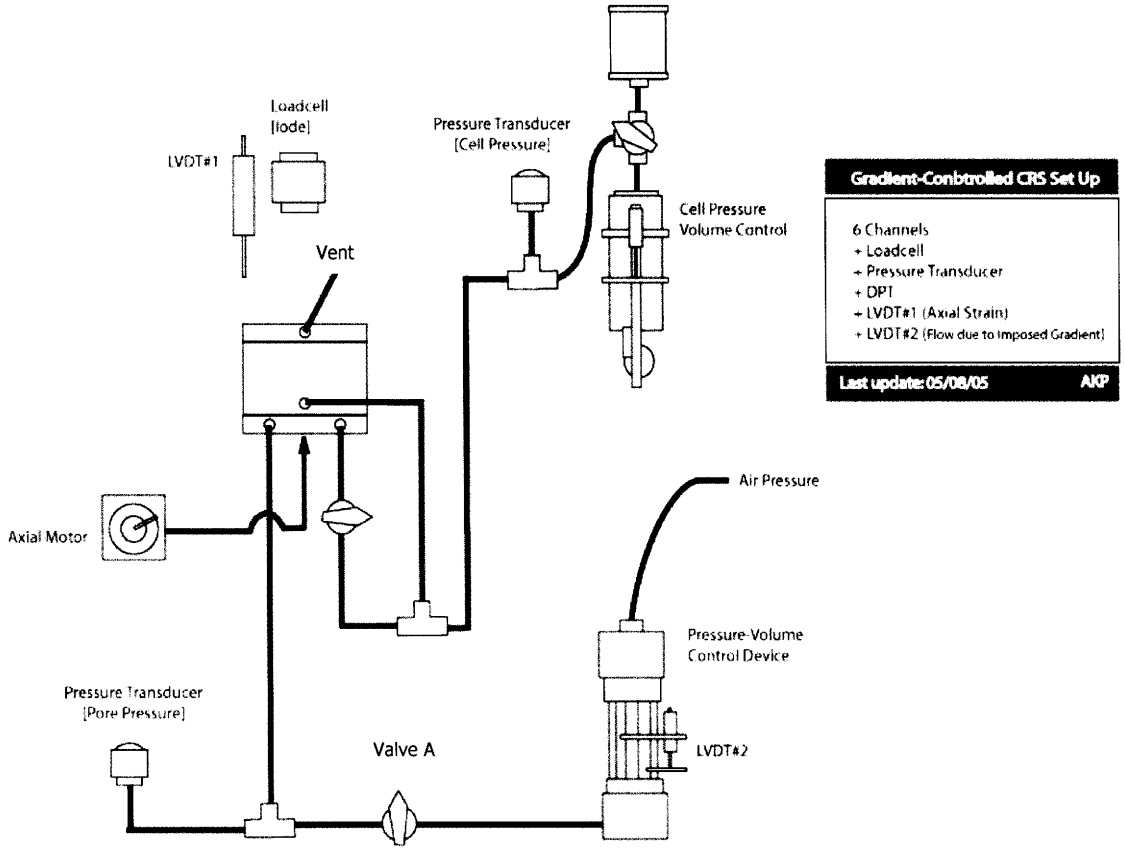

Figure 3.6 Schematic drawing of the GCRS set up

An extra pressure-volume control device is added to the CRS set up with an additional LVDT for the control of pore water pressure at the base of the specimen and measurement of the flow rate.

3.3.2 Test Processes

The steps involve in a GCRS test consist of

1) Specimen preparation (the same as a CRS test).
2) Back pressure of the specimen (to a minimum of 2 ksc).

3) The 1st phase of the consolidation at constant strain rate. This phase of consolidation usually runs until the soil establishes a well-defined section of the virgin compression line (usually 7% or more ε_a). In this phase, if the target strain rate for the test is low or very low, a faster strain rate is used at the beginning to speed up the test until the compression passes the preconsolidation pressure (σ'_p) before the strain rate is reduced to the planned strain rate for the test.
4) The specimen is then subjected to an imposed controlled gradient from the pressure-volume control device by maintain a constant pore water pressure, u, at the base of test specimen. The soil will undergo a transient state during the first 5-10 min before entering a steady state. It is important to note that during all steps, the axial deformation is maintained at the same rate. This is the beginning of the 2nd phase of consolidation or the GCRS phase.
5) The specimen continues to consolidate at the same rate until it establishes a well-defined virgin compression line (usually for $\Delta\varepsilon_a \sim 5\%$ or more).
6) The imposed hydraulic gradient is removed (end of the 2nd phase of consolidation) by closing the valve connecting the specimen to the pressure-volume control device (valve A in the Figure 3.6).
7) The 3rd phase of consolidation, then, begins. This phase of consolidation continues for at minimum 5% ε_a or until a well-defined virgin compression line can be established from the test or the maximum stress is reached for the test set up.

Figure 3.7 presents a schematic drawing of a GCRS test. The test can be performed at different strain rates to study the effect of strain rate on the GCRS section. It is important to note that for a GCRS test with very slow strain rate, it is generally more efficient to start the test with a higher strain rate to speed up the consolidation process until the specimen is into the Virgin Compression Range (VCR). Then, the strain rate is reduced to the planned value and the consolidation process continues until the beginning of the 2nd phase consolidation. It should be noted that the consideration of strain rate at the initial phase should be based on prior experience or test data to ensure appropriate strain rate is selected for the soil. Figure 3.8 presents an example of a compression curve of a GCRS test.

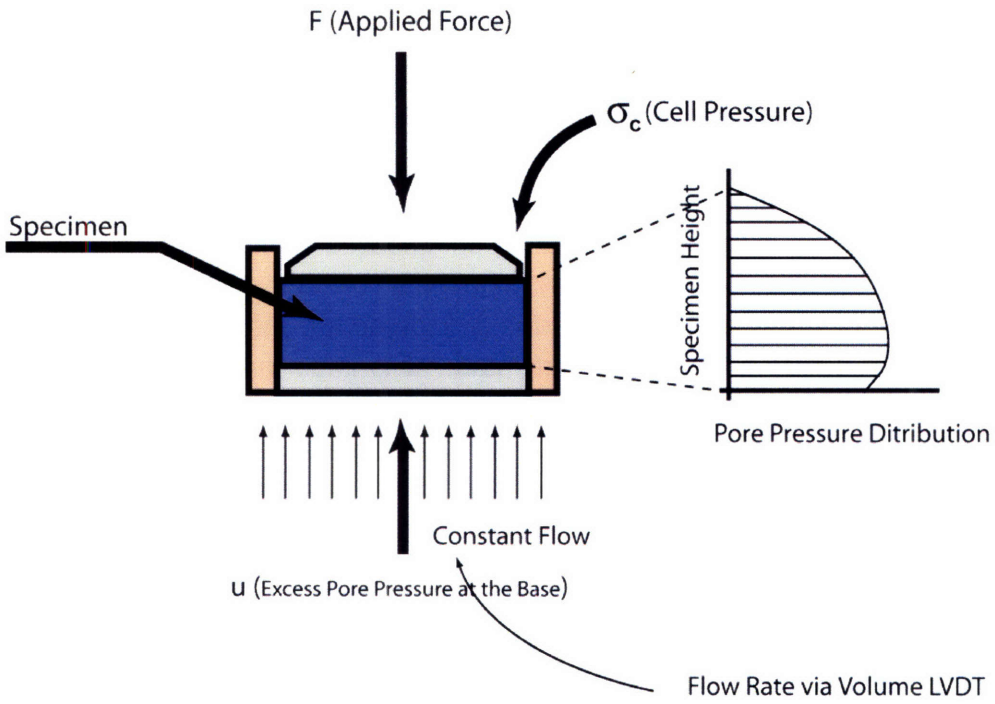

Figure 3.7 Schematic drawing of a GCRS test

Due to the time involved in developing and testing an additional automated control program for the imposed gradient, a manual control set up is used in this research. The control is relatively simple to implement. Air pressure is applied to the top of the pressure-volume control device which, in turn, forces the water to flow through the base of the specimen. A transducer at the base of the specimen is used to monitor the imposed base excess pore pressure. A LVDT is installed on the pressure-volume control device to monitor the amounts of water flow through the specimen during the GCRS phase.

The tests cover a wide range of strain rate as well as imposed gradient at the base. The strain rates used in this experimental program range from 0.1%/hr (very slow) to 3%/hr (very fast). The normalized imposed gradients ($\Delta u_b/\sigma'_v$) range from 5% to 65%. The test usually takes approximately 2 - 3 days for a high strain rate test and approximately 6 - 7 days for a low strain rate test.

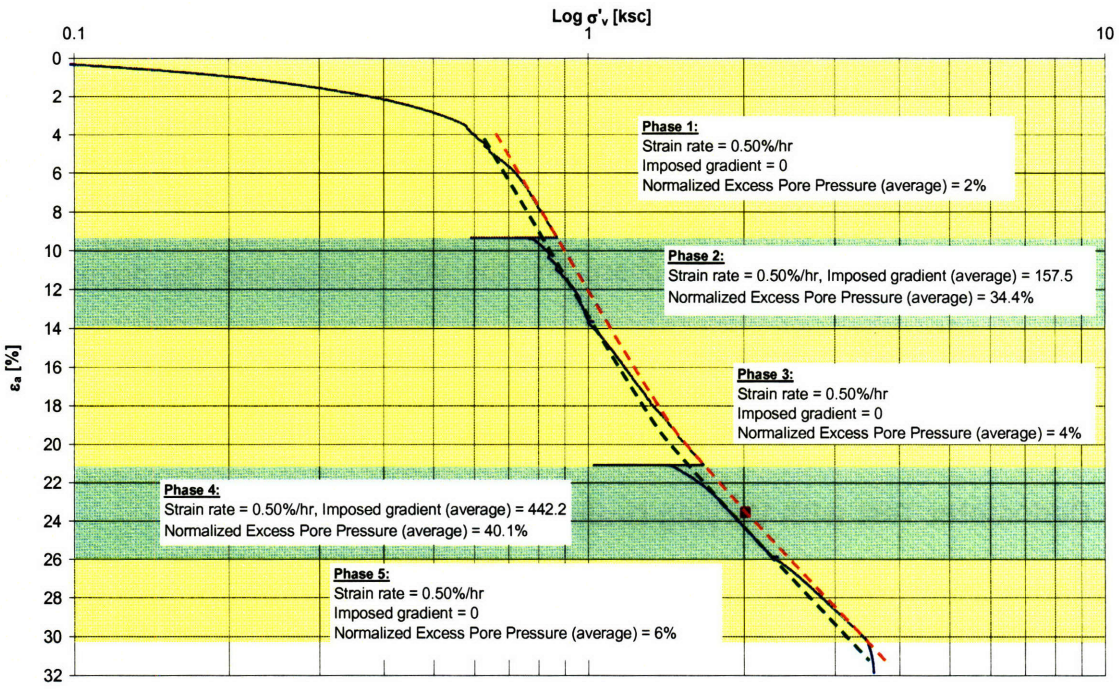

Figure 3.8 Compression curve from a Gradient-controlled CRS test indicating two consolidation sections with average imposed gradient of 157.5 and 442.2 (CRS680)

3.3.3 Calculations

The average excess pore pressure (Δu_{avg}) and vertical effective stress ($\sigma'_{v(AVG)}$) during the normal CRS loading phase is obtained from the Wissa et al. linear CRS theory as shown in the equation 3.2 and 3.3.

During the gradient-controlled CRS loading phase, the internal excess pore pressure is a combination of the excess pore pressure caused by the consolidation and that of the upward flow. The determination of the excess pore pressure distribution requires a simulation (details of the GCRS simulation can be found in Chapter 4). Based on the predicted excess pore pressure distribution, the average excess pore pressure can be calculated and used to calculate the average vertical effective stress. It should be noted that the simulation assume a steady-state condition. Therefore, the transient phase is not considered in this research.

3.3.4 Test Interpretations

The interpretation of a GCRS test is quite complicated during the GCRS consolidation phase. The vertical effective stress, σ'_v during a normal CRS phase (the 1st and 3rd phase

can be determined using linear CRS theory (equation 3.1 to 3.3). During the GCRS phase, the pore pressure distribution no longer has a parabolic form. This is due to the imposed gradient at the base of the specimen. A simulation program was developed to model the pore pressure distribution during this phase.

The focus of the test interpretation is on the shift of the VCL during the gradient-controlled CRS phase. The amounts of the VCL shift is defined as $\Delta\sigma'_v$ which is, essentially, the difference between the average vertical effective stress based on the VCL during the gradient-controlled phase and the VCL representing the normal CRS loading.

Chapter 4 explains this simulation program in detail. Chapter 5 discusses in detail the analysis and experimental results of GCRS test series.

3.4 Oedometer Test with Varying Drainage Height

The incremental oedometer test is a basic laboratory consolidation test used in geotechnical engineering. The test is simple to perform and requires minimum supervising other than careful loading technique and selection of the appropriate loading sequence.

For this research, oedometer test program is set up to investigate the effects of drainage height and the amount of secondary compression on the differences in the coefficient of consolidation (c_v) obtained from the square root of time ($\sqrt{t}$) and logarithm of time (log t) methods.

Due to the large amount of time required for a large batch consolidation test (can take upto 1 - 2 months per increment), a new strategy was developed to study the effects of drainage height in the opposite direction. Basically, instead of performing a series of oedometer tests on large specimens which take significant amounts of time and expenses, the key idea was to perform a series of oedometer tests with three small drainage heights (2.35 cm, 1.18 cm, and 0.6 cm). This program allows more numbers of tests to be performed in the same time period. However, for a single drainage test with the largest drainage height, each load increment still requires approximately 1 days for MBC and SBM to ensure good secondary compression portion at the end of each increment.

Another important consideration is the amount of time of secondary compression (t_{SEC}) of each increment. This becomes an issue because it is unclear how much the time to secondary compression of an increment will have effects on the next increment consolidation behavior. It is, therefore, included in this experimental program. Several tests are performed in the fashion that alternate the time to secondary compression between each increment.

To summarize, the main components of this experimental program are

1) laboratory oedometer tests with three different initial drainage heights (approximately 2.35, 1.18, and 0.6 cm, respectively),
2) alternating time of secondary compression (t_{SEC}) between each increment of the same tests to study the effects of the t_{SEC} on consolidation behaviors,
3) maintain the same aspect ratio (D/H) for each test,
4) a modified oedometer cell for a single drainage test to ensure no water drainage at the base.

3.4.1 Equipments

The oedometer cell, for a single drainage test, is modified to ensure that no water can drain from the base. The saturation of the base porous stone is also a problem since if the porous stone is not fully saturated (which is difficult without significant amount of back pressure to the system), water can drain from the specimen into the stone. The water draining at the base, where it should not occur, cause significant problems in the interpretation of the test results.

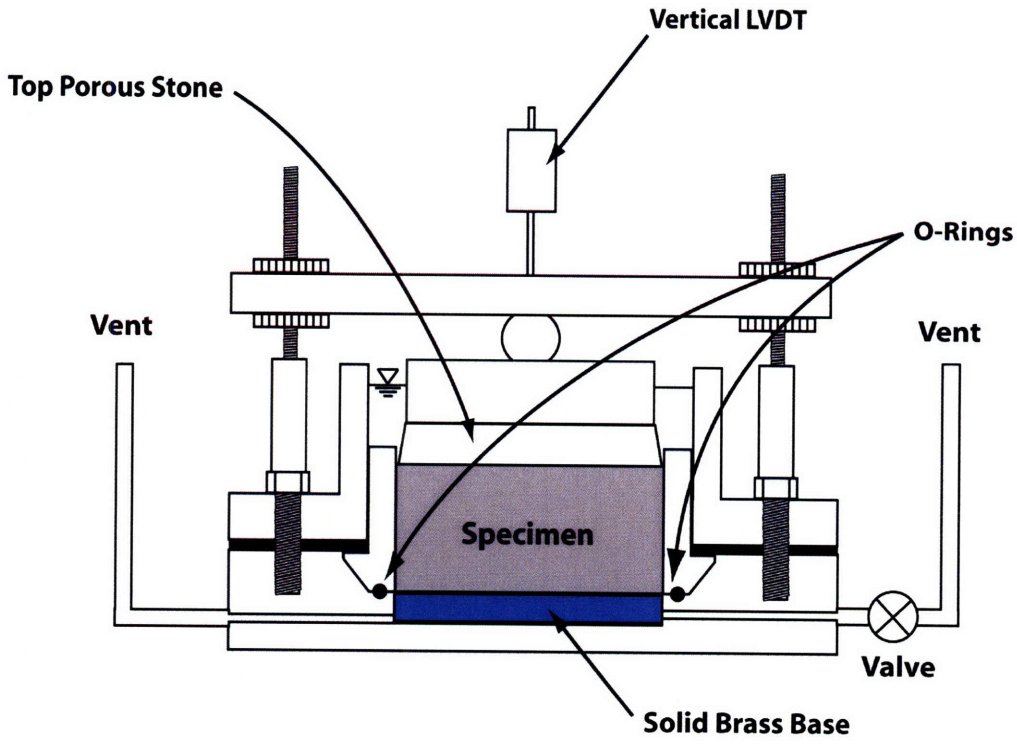

Figure 3.9 Modified oedometer set up for single drainage test

To solve this issue, the base of the oedometer cell is modified by using a solid brass base instead of the porous stone. The solid brass base eliminates the possibility of water draining at the base. Figure 3.9 shows a sketch of the modified oedometer cell for a single drainage test. Figure 3.10 shows an illustration of the oedometer tests with three different drainage heights.

Same oedometer cell was used for the 2.35 and 1.18 cm drainage height. The 2.35 cm drainage height is a single drainage test while the 1.18 cm drainage height is a double drainage height. For the smaller drainage height (0.6 cm), a special oedometer cell was made to allow for the usage of smaller specimen while maintain the same aspect ratio of that used in the larger specimen tests.

Another important factor in this experimental program is the back pressure saturation of the system. To study the effect of back pressure saturation issues, the standard oedometer cell was replaced with a modified Trautwein CRS cell connected to pressure-volume control device. This allows the back pressure saturation of the system at any pressure compared to the atmospheric pressure used in the normal oedometer test. Figure 3.11 shows a sketch of the modified Trautwein cell used in this study.

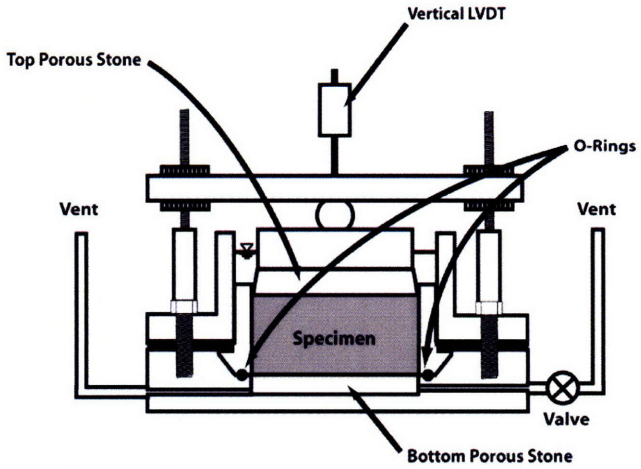

(a) Double Drainage Test Set Up

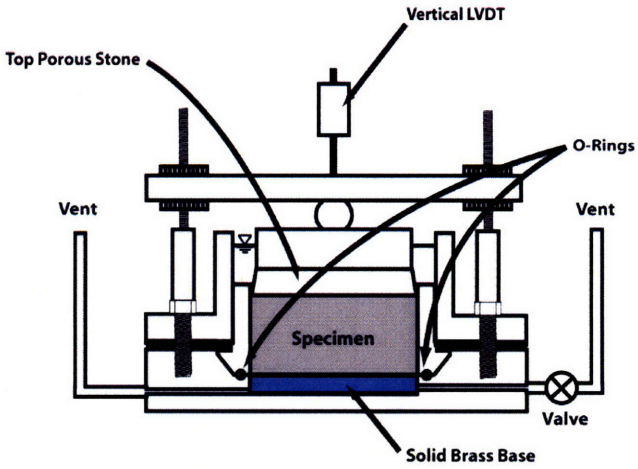

(b) Single Drainage Test Set Up

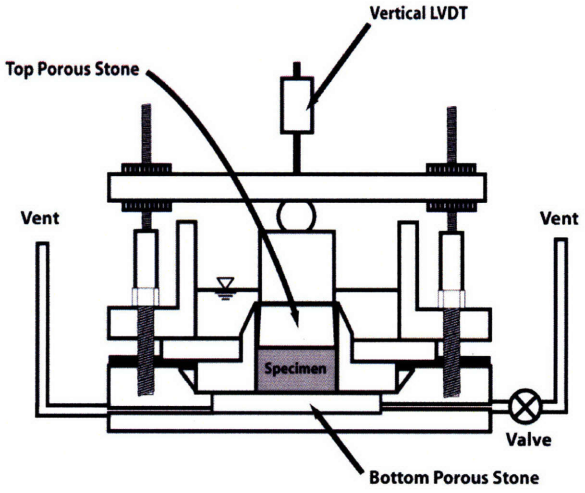

(c) Single Drainage Test with Small Specimen Set Up

Figure 3.10 A schematic drawing of the oedometer test set up with three different drainage heights, H_d = 2.35, 1.18, and 0.6 cm, respective.

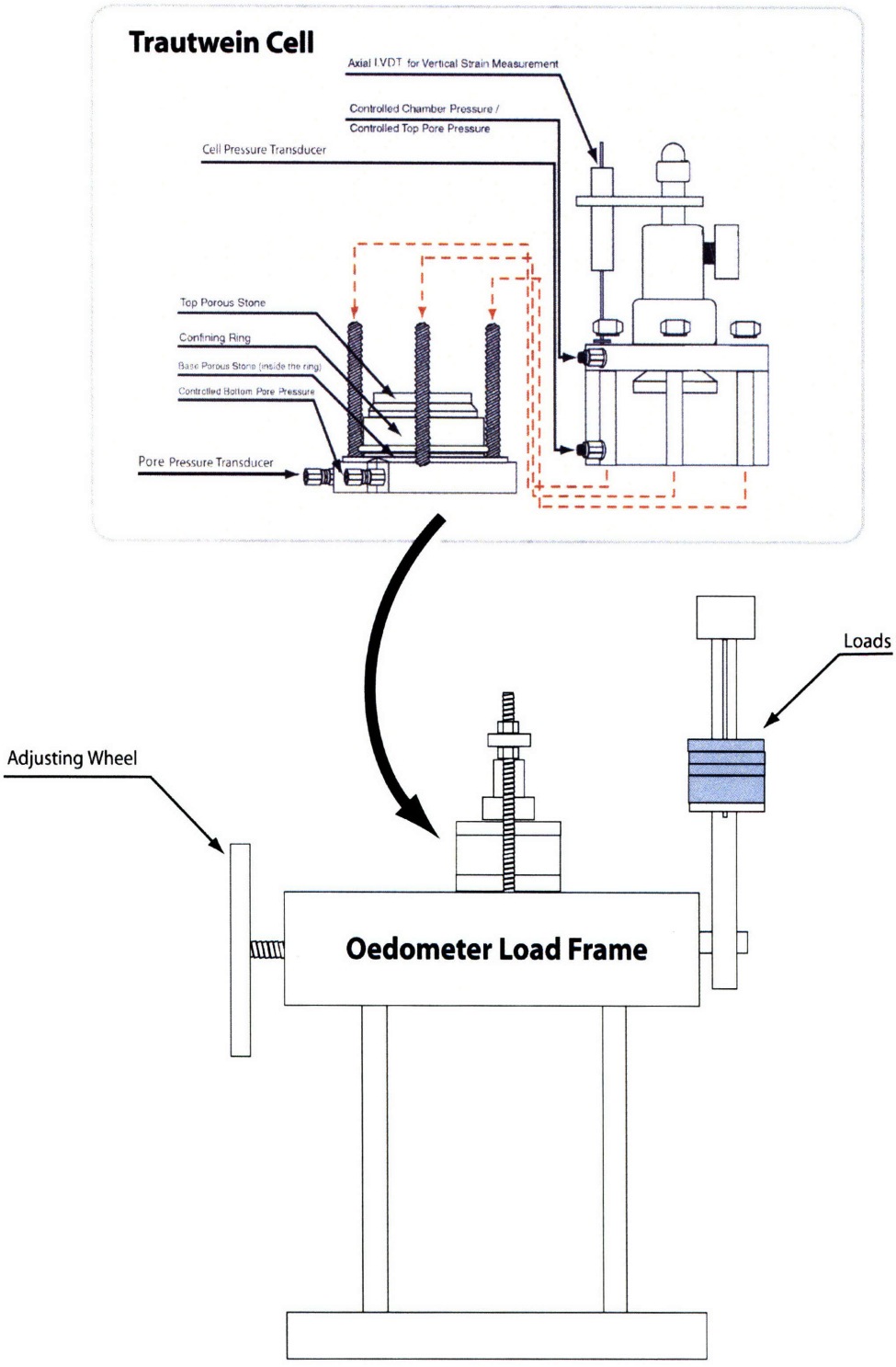

Figure 3.11 Trautwein cell with oedometer load frame

3.4.2 Test Processes

In a standard oedometer test (ASTM D2435), a soil specimen is cut into a rigid ring with minimum diameter of 5 cm and minimum height of 1.2 cm. The minimum specimen diameter-to-height ratio is 2.5. The ring prevents any lateral expansion. The specimen is then assembled into a load frame. Load increments are selected such that the Load Increment Ratio (LIR) is between 0.5 and 1.0. LIR of 1.0 is the most common. Each load is applied instantaneously (as fast as possible) and hold constant while axial displacement is recorded over time. Figure 3.12 shows a sketch of an oedometer test.

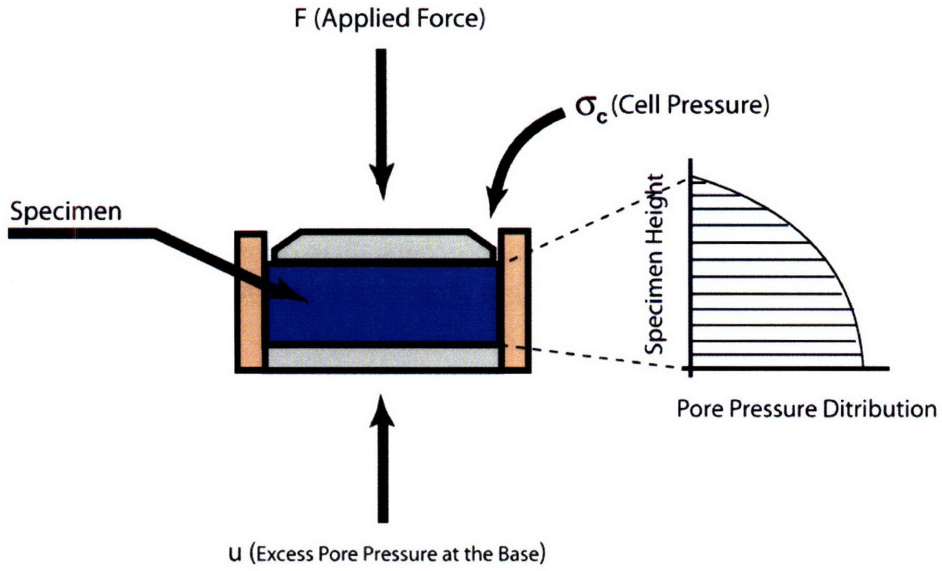

Figure 3.12 Schematic drawing of a laboratory oedometer test

3.4.3 Calculations

Section 2.3.1 and 2.3.2 discusses the square root of time ($\sqrt{t}$) and logarithm of time (log t) methods for c_v calculation in detail. The c_v is calculated for each loading step but the focus is on the load increments during the virgin compression range. The c_v based on square root of time ($\sqrt{t}$) and logarithm of time (log t) methods and c_v ratio are defined as

$$c_v\left(\sqrt{t}\right) = \frac{0.848\left(H_d\right)^2}{t_{90}} \qquad (???)$$

$$c_v\left(\log t\right) = \frac{0.197\left(H_d\right)^2}{t_{50}} \qquad (???)$$

$$c_v\ Ratio = \frac{c_v(\sqrt{t})}{c_v(\log t)} \qquad (???)$$

where H_d is the drainage height at t_{50}, t_{50} is the time to 50% consolidation, and t_{90} is the time to 90% consolidation.

3.4.4 Test Interpretations

The interpretation of c_v based on the two methods must be carefully performed to ensure that the interpretation is accurate. For the square root of time ($\sqrt{t}$) method, the line A (as shown in Figure 3.13) should represent the initial straight line of the consolidation curve. However, this initial straight line portion is often difficult to determine especially for a small drainage height test. This is due to the fact that the consolidation happens very fast for a test with small drainage height. The smaller the drainage height, the faster the consolidation occurs. It is often problematic and difficult to obtain an accurate consolidation curve for the first few seconds of each load increment.

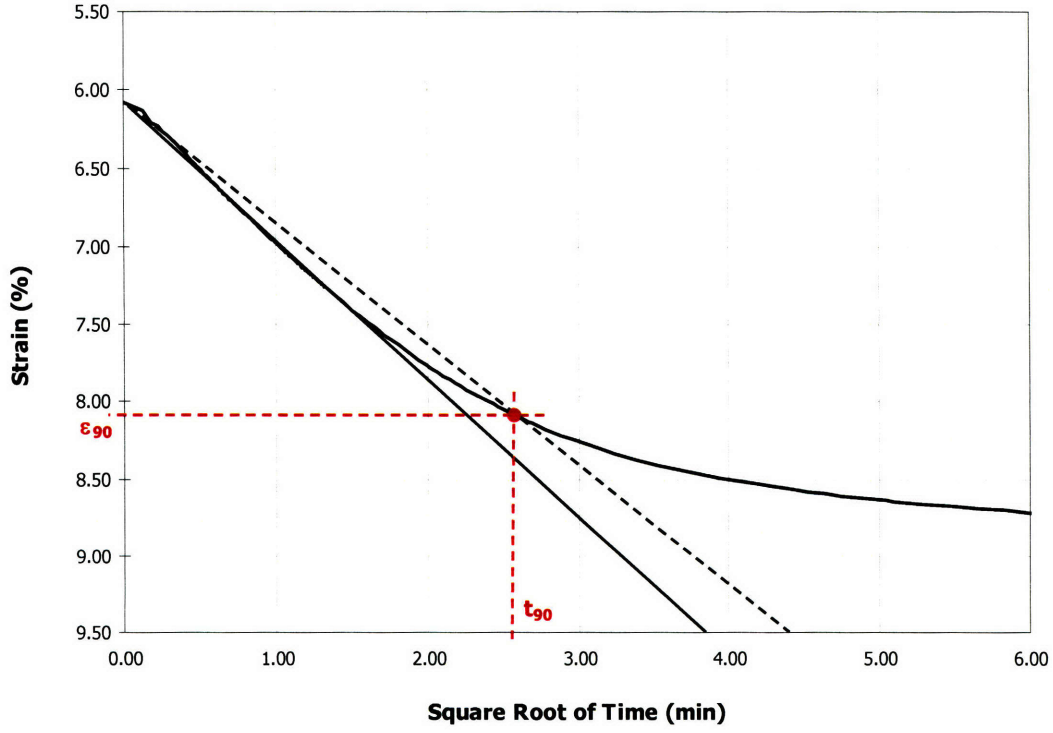

Figure 3.13 Consolidation curve in logarithm of time space

For the log time method, the first straight line (line A in Figure 3.14) must represent the steepest linear portion of the curve. The second straight line (line B in Figure 3.14) should represent at least 1 logarithm cycle of the secondary compression of the load increment. The intersection of the two lines represents the end-of-primary consolidation (EOP).

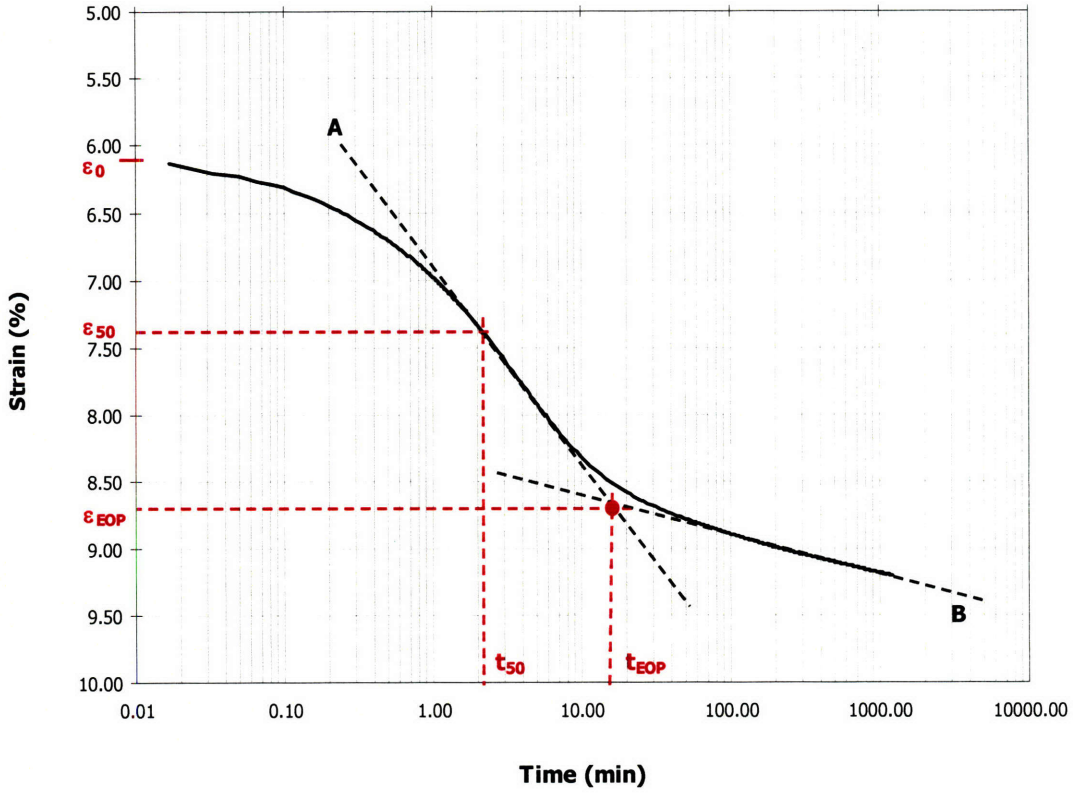

Figure 3.14 Consolidation curve in the $\sqrt{t}$ space

Based on the interpreted axial strain or vertical deformation at EOP and that of starting of the test, we can obtain the axial strain or vertical deformation and time at 50% consolidation. The t_{50} is, then, used in the calculation of c_v(log t).

Based on the incremental oedometer test results, the c_v ratio obtained from the three different drainage heights can be compared to evaluate the scaling effects on both MBC and SBM. The effects of amounts of secondary compression of the previous step are also studied in this research. Detailed discussion of the analysis and results of laboratory tests and numerical simulation can be found in Chapter 5.

Chapter 4: Numerical Simulations

This chapter presents the formulation and evaluation of the numerical simulations used in this research. The simulation programs are created to compliment the experimental programs and help with data interpretation. There are two main simulation programs to model:

1) The gradient-controlled Constant Rate of Strain (GCRS) simulation, and
2) The laboratory incremental oedometer simulation.

The simulation models are based on finite difference method that accounts for finite deformation and allows for independent relationship between void ratio and hydraulic conductivity and void ratio and vertical effective stress. The models are developed with aims to account for more realistic soil behavior and to allow for both linear (constant m_v) and nonlinear (constant C_c) compressibility simulation. It is also important to note that the models are designed for normally consolidated soils only and no secondary compression component is included into the two models.

Each simulation program has its own set of principles and procedures. The basic concepts are quite similar, but the actual calculation procedures and methods used are quite different. The next sections discuss the principles and concepts used in each simulation.

4.1 Gradient-controlled Constant Rate of Strain (GCRS) Simulation

The GCRS simulation code is developed for the interpretation of the GCRS test results. The GCRS test involves flow of water through the base of specimen controlled by a pressure-volume control device where base pore pressure is constant. This causes the pore pressure distribution within the specimen to deviate from the distribution of the linear CRS theory. In addition, the pore pressure is imposed and we do not have a measurement of the CRS induced component of the excess pore pressure. In the linear CRS theory, the pore pressure distribution inside a specimen under 1-D CRS loading is a parabolic form. Therefore, the average pore pressure is obtained from

$$\Delta u_{avg} = \frac{2}{3}\Delta u_b \tag{4.1}$$

where Δu_{avg} is the average excess pore pressure and Δu_b is the base excess pore pressure.

The average vertical effective stress is, then, calculated from

$$\sigma_v^{'} = \sigma_v - \Delta u_{avg} = \sigma_v - \frac{2}{3}\Delta u_b \qquad (4.2)$$

where σ'_v and σ_v are the vertical effective stress and vertical total stress, respectively.

These calculations allow for relatively simple data reduction and interpretation of a CRS test. However, for a GCRS test, the determination of the Δu_{avg} is more complicated. The pore pressure distribution should resemble a combination of the parabolic shape from the standard CRS tests and the linear pore pressure distribution, for a simple case of the constant pressure hydraulic conductivity test.

4.1.1 Basic Concepts and Procedures

The GCRS simulation is based on the concept that

1) Water can flow to both the top and bottom boundaries. Both top and bottom boundary are pressure controlled boundaries.
2) The amount of water that flows out of the specimen must be equal to the amount of water that flows in plus the volume change of the specimen due to consolidation (equilibrium of flow).
3) The consolidation of the soil (compression due to loading and flow of water out of specimen) must obey d'Arcy's law for flow and the compressibility relationship of the soil.
4) The total deformation at any time (Δt) must agree with the predetermined values based on the strain rate ($\Delta H = \Delta t * \dot{\varepsilon}$).
5) The void ratio and hydraulic conductivity relationship (e versus log k) is maintained throughout the simulation.

In summary, the pore pressure distribution from a GCRS test is a combination of that from a standard CRS test and that caused by the imposed gradient. The water can flow up and down within the specimen depending on the strain rate and imposed base pressure used in the test. To simulate this effect, the specimen is divided into two large sections designated as top and bottom. The dividing line is called the neutral axis of the specimen. Each section is, then, further divided into many small layers (usually 20 or more). Figure 4.1 shows a sketch of a layered specimen used in the simulation. For this simulation, the input parameters such as specimen height, strain rate, time increment, etc. are recorded in an input file ("input.dat"). Table 4.1 (on page ???) presents the list of input parameters required for the GCRS simulation. The input parameters are transferred to the simulation programs at the beginning of the simulation. Figure 4.2 shows a schematic drawing illustrate GCRS simulation processes.

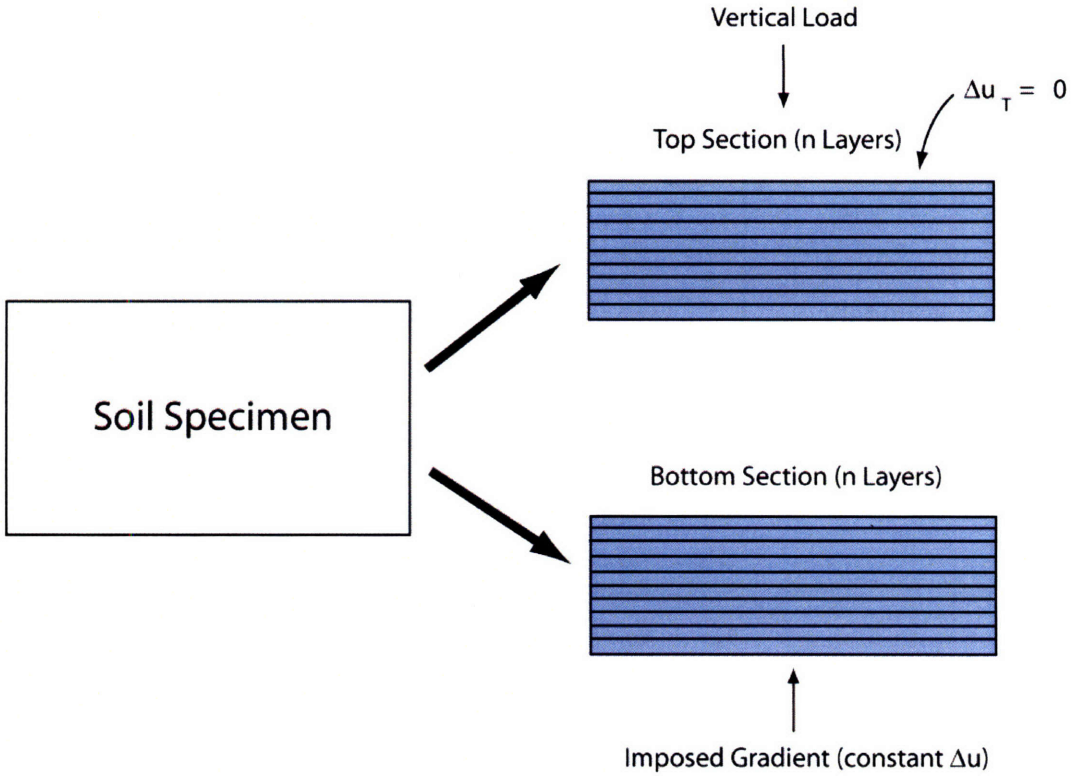

Figure 4.1 Sketch of soil specimen divided into two sections

Figure 4.2 presents a sketch of a single layer for the GCRS simulation. e_{avg}, k_{avg}, and $\sigma'_{v(avg)}$ are the average void ratio, average hydraulic conductivity, and average vertical effective stress of the layer, respectively. H_{TLi} and ΔH_{TL} are the total initial layer height and total deformation of the layer. e_T, e_B, Δu_T, and Δu_B are the void ratio at the top boundary, void ratio at the bottom boundary, excess pore pressure at the top boundary and excess pore pressure at the bottom boundary, respectively.

At the start of a GCRS simulation, the neutral axis is assumed to be at the center of the specimen.

$$\left(NA\ Location\right)_{initial} = \frac{H_0}{2} \tag{4.3}$$

$$H_{Ti} = H_{Bi} = \frac{H_0}{2} \tag{4.4}$$

where H_{Ti} and H_{Bi} are the initial total heights of the top and bottom sections of the specimen, respectively.

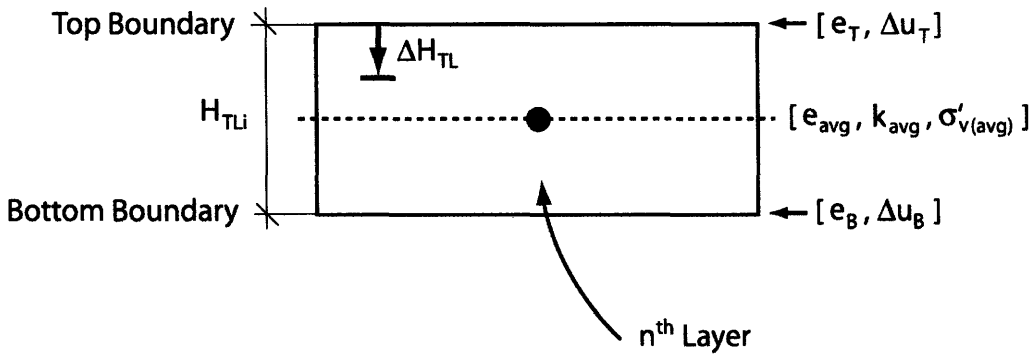

H_{TLi} = Initial total height of the layer
ΔH_{TL} = Total deformation of the layer
e_T = Void Ratio at the top boundary
e_B = Void Ratio at the bottom boundary
e_{avg} = Average Void Ratio of the layer
Δu_T = Excess pore pressure at the top boundary
Δu_B = Excess pore pressure at the bottom boundary
k_{avg} = Average hydraulic conductivity of the layer
$\sigma'_{v(avg)}$ = Average vertical effective stress of the layer

Figure 4.2 Sketch of a single layer for the GCRS simulation

The top and bottom section is divided into n small layers

$$H_{TLi} = H_{TBi} = \frac{H_{Ti}}{n} = \frac{H_{Bi}}{n} \tag{4.5}$$

where H_{TLi} and H_{TBi} are the initial heights of each sublayer of the top and bottom sections of the specimen and n is the number of sublayers for each section.

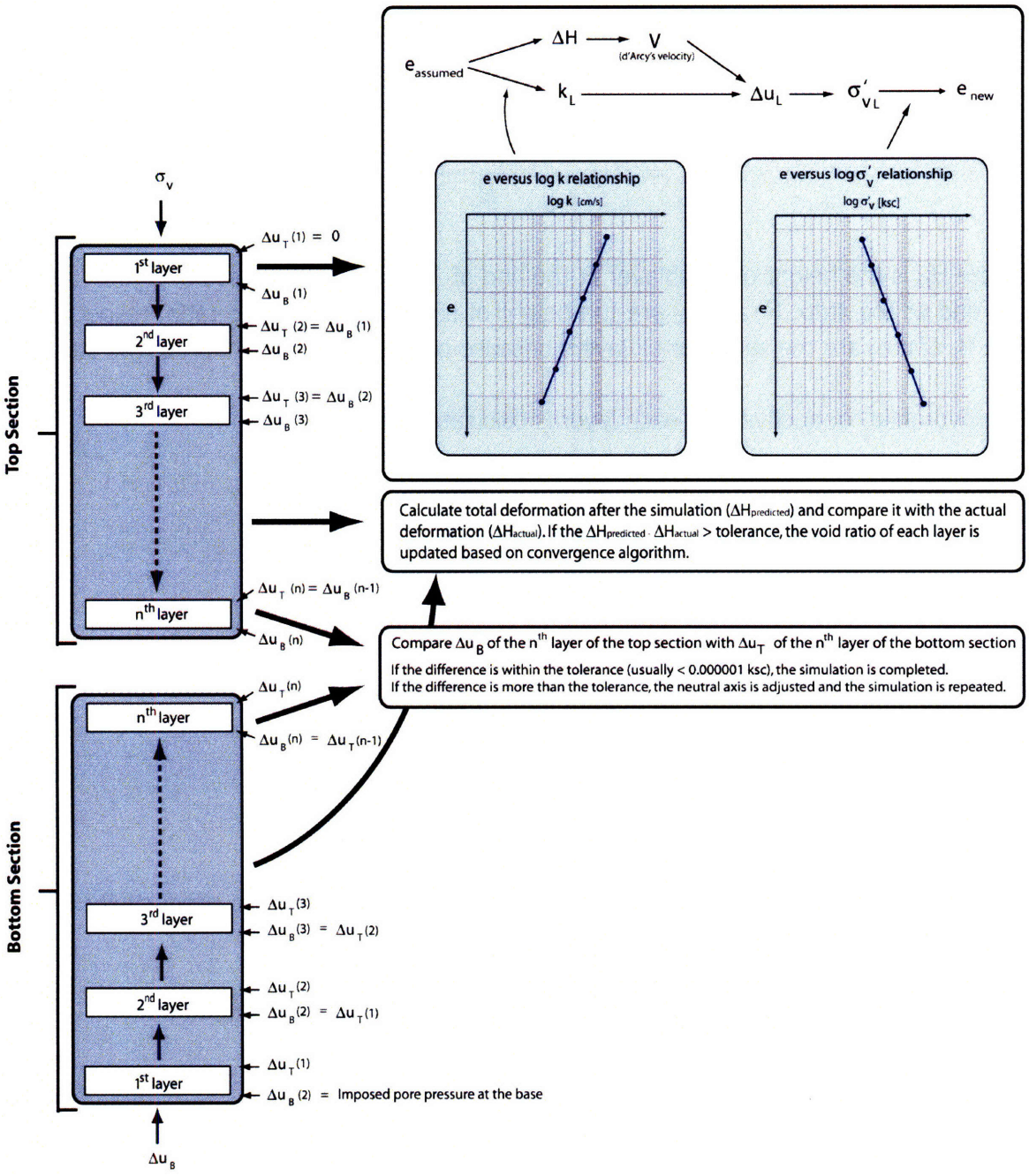

Figure 4.2 Schematic drawing illustrates the GCRS simulation concepts

At the start of the simulation, a void ratio at the end of a step is assumed for each layer. This void ratio will then be updated based on the convergence algorithm (shown later in this chapter as equation 4.27) to ensure that the total deformation is maintained throughout the simulation. Based on this assumed void ratio, the height of each layer after the consolidation can be calculated by

$$H_s = \frac{H_T}{(1+e_0)\cdot n} = \frac{H_{TLi}}{(1+e_0)} \tag{4.6}$$

$$H_{Lf} = H_{Li} - \left[\frac{(H_{Li} - H_s)}{H_s} - e_{fa}\right]\cdot H_s \tag{4.7}$$

where H_{Lf} is the height of a sublayer at the end of Δt and e_{fa} is the assumed void ratio at the end of the step. H_s and e_0 are the height of solid and initial void ratio, respectively. The H_s and e_0 are the same for all layers because of equal layer thickness at the start.

The hydraulic conductivity for each layer is calculated from

$$C_k = \frac{\Delta e}{\Delta log(k)} = \frac{e_{fa} - e_i}{[log(k_L) - log(k_0)]} \tag{4.8}$$

$$C_k[log(k_L) - log(k_0)] = e_{fa} - e_i \tag{4.9}$$

$$log(k_L) = \frac{[e_{fa} - e_i + C_k\, log(k_0)]}{C_k} \tag{4.10}$$

$$k_L = 10^{\left[\frac{e_{fa} - e_i + C_k\, log(k_0)}{C_k}\right]} \tag{4.11}$$

where C_k is the slope of the e versus log k curve, k_L is the hydraulic conductivity of the layer, and k_0 is the initial hydraulic conductivity.

Based on the deformation of each layer, the d'Arcy's velocity is calculated from

$$V_d = \frac{q}{A} \tag{4.12}$$

$$V_d = \frac{\Delta Volume}{\Delta t \cdot A} = \frac{\Delta H \cdot A}{\Delta t \cdot A} = \frac{\Delta H}{\Delta t} \tag{4.13}$$

where V_d is the d'Arcy's velocity associated with the deformation of each layer, q is the flow, A is the cross-sectional area of the specimen, and Δt is the time increment.

There is another component of the flow caused by the imposed hydraulic gradient applied at the base of the specimen. This d'Arcy's velocity (V_i) can be calculated from

$$i = \frac{\Delta u_b}{H} \cdot \frac{1}{\gamma_w} \tag{4.14}$$

$$V_i = k \cdot i \tag{4.15}$$

$$V_i = k_L \cdot \left(\frac{\Delta u_b}{H} \cdot \frac{1}{\gamma_w} \right) \tag{4.16}$$

where Δu_b is the imposed excess pore pressure at the base and γ_w is the unit weight of water.

The total d'Arcy's velocity is obtained from

$$V = V_d + V_i \tag{4.17}$$

The average excess pore pressure across each layer can be calculated based on the hydraulic gradient and the d'Arcy's velocity.

$$V = k \cdot i \tag{4.18}$$

$$V = k_L \cdot \left(\frac{\Delta u_L}{\Delta H_L} \right) \cdot \frac{1}{\gamma_w} \tag{4.19}$$

$$\Delta u_L = \frac{V \cdot \Delta H_L \cdot \gamma_w}{k_L} \tag{4.20}$$

where Δu_L is the excess pore pressure of a layer.

The average vertical effective stress across each layer is calculated from

$$\sigma'_{vL(avg)} = \sigma_v - \Delta u_L \tag{4.21}$$

$$\sigma'_{vL(avg)} = \sigma_v - \frac{V \cdot \Delta H_L \cdot \gamma_w}{k_L} \tag{4.22}$$

where $\sigma'_{vL(avg)}$ and σ_v is the average vertical effective stress and total stress of a layer, respectively.

The new void ratio for the layer is calculated from

$$C_c = \frac{\Delta e}{\Delta \log(\sigma'_v)} \tag{4.23}$$

$$C_c \cdot \left[log(\sigma'_{vL(avg)}) - log(\sigma'_{v0(avg)})\right] = e_n - e_i \tag{4.24}$$

$$e_n = e_i + C_c\left[log(\sigma'_{vL(avg)}) - log(\sigma'_{v0(avg)})\right] \tag{4.25}$$

where C_c is the coefficient of compression, $\sigma'_{v0(avg)}$ is the average initial vertical effective stress, and e_n is the new void ratio of the layer.

Based on the new void ratio, the deformation for the layer can be calculated. The simulation continues to the next layer until it reaches the bottom layer of the top section.

The simulation for the bottom section is similar to the top section. The only notable difference is that the simulation for the bottom section is performed upward from the base of the specimen to the top layer of the section. Once the calculations are done for each layer of both top and bottom sections, the final specimen height for the time step (Δt) can be calculated from

$$H_f = H_{Tf} + H_{Bf} \tag{4.26}$$

The predicted specimen height after consolidation is, then, compared with the expected specimen height (based on the input strain rate and time increment). If the difference between the predicted deformation and the expected deformation is larger than the tolerance, it means that the assumed void ratio is not a correct value. The void ratio for the end of the time step is then updated and the simulation is repeated again until the predicted deformation matches the expected deformation. The void ratio is updated based on a convergence algorithm as shown in the equation 4.27.

$$e_{update} = \frac{e_a}{\left[\frac{H_{f(predicted)}}{H_{f(expected)}}\right]} \tag{4.27}$$

Once the deformation condition is satisfied, the excess pore pressures at the boundaries must also be satisfied including the excess pore pressure at the top of the specimen (Δu_t), excess pore pressure at the bottom of the specimen (Δu_b), and the excess pore pressure at the boundary between the top and bottom section ($\Delta u_{NA(t)}$ and $\Delta u_{NA(b)}$). If the $\Delta u_{NA(t)}$ and $\Delta u_{NA(b)}$ are not the same, the assumed neutral axis (NA) is not correct and must be moved. If the predicted $\Delta u_{NA(t)}$ is larger than the predicted $\Delta u_{NA(b)}$, the neutral axis is set at too low elevation and must be moved upward. If the predicted

$\Delta u_{NA(t)}$ is smaller than the predicted $\Delta u_{NA(b)}$, the neutral axis is set at too high elevation and must be moved downward. The change in the neutral axis location is described by

$$\Delta(NA) = NA_i \pm \frac{H_t}{m} \tag{4.28}$$

where Δ(NA) is the change in the neutral axis location, NA_i is the initial location of the neutral axis, H_t is the total height of the specimen, and m is incremental movement of the neutral axis. The neutral axis is allowed to move freely inside the specimen. The minimum allowable movement of the neutral axis is controlled by the factor m in the equation 4.28. Therefore, the n factor should be relatively high (100 or more) to allow a finer change in the neutral axis location. Once the new neutral axis is obtained, the top and bottom sections are divided into n sublayers again before the new simulation step is started.

Once both the specimen deformation and excess pore pressure at the boundaries are satisfied, the simulation is complete for this time increment. The simulation results are, then output to a text file "results.dat". Figure 4.3 shows the flowchart for the GCRS simulation. Table 4.1 presents the summary of input parameters for the GCRS simulation.

Input Parameters	Descriptions
H_0	Initial total specimen height
c_v	Input coefficient of consolidation
$\dot{\varepsilon}$	Strain rate
e_0	Initial void ratio
k_0	Initial hydraulic conductivity
C_k	Slope between e versus log(k)
C_c	Compression index
Δu_b	Imposed base excess pore pressure
Δt	Time increment for the simulation

Table 4.1 Summary of input parameters for GCRS simulation

The source code for the GCRS simulation including the sample input file and output file can be found in the appendix A. The simulation program is written in C++ programming language for Microsoft Windows ® operating systems including Microsoft Windows ® 98, ME, 2000, and XP. Depending on the version of Microsoft Windows ® operating systems, extra C++ runtime files may be necessary to run the program. These C++ runtime files, if required, can be obtained from the official Microsoft web site (http://www.microsoft.com).

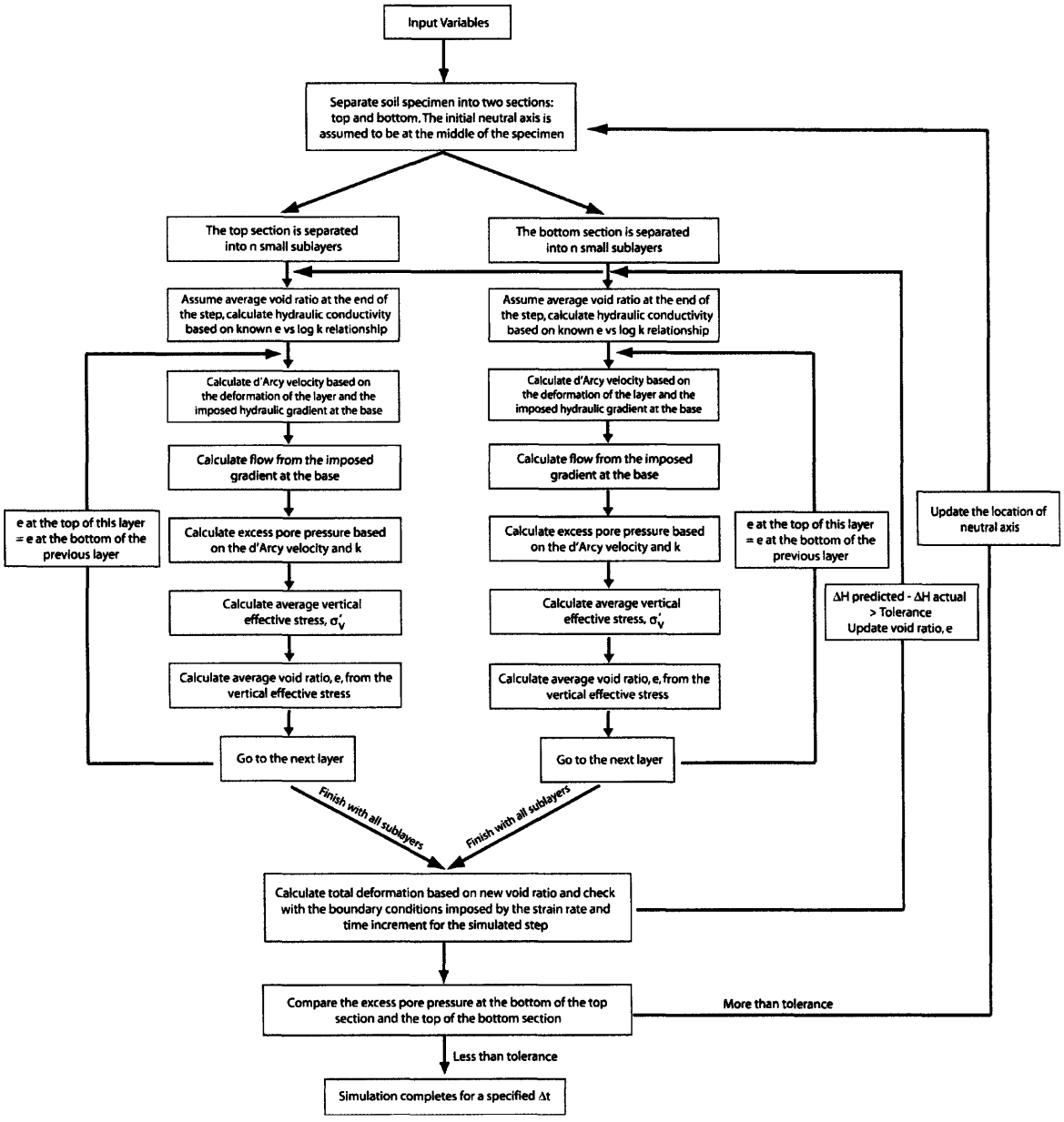

Figure 4.3 GCRS simulation flowchart

4.1.2 Interpretation of the Pore Pressure Distribution

The GCRS simulation yields pore pressure distributions within the specimen for the gradient phase of a test. which allows one to accurately calculate the average vertical effective stress. There are several methods that can be used to calculate the $\sigma'_{v(AVG)}$ including calculate the average ΔU based on individual simulation results and calculate the differences of pore pressure from the GCRS simulation and that calculated based on the linear pore pressure distribution or Wissa linear or nonlinear (depending on the $\Delta u_e/\sigma'_v$) CRS theory or a combination of both. The differences, then, can be applied to obtain a correct $\sigma'_{v(AVG)}$. The latter method can be applied more efficiently for a soil type covering a wide range of strain rate and base pore pressure (Δu_b) as described below.

The basic concept of interpretation of a GCRS test can be outlined as follow:

1) Perform the CRS data reduction as normal using Wissa linear CRS theory ($\Delta u_{AVG} = 2/3\Delta u_b$ for the normal CRS consolidation phase. For the GCRS phase, the average excess pore pressure is initially calculated from

$$\Delta U_{avg} = \frac{1}{2}\left(\Delta U_{imposed\ flow}\right) + \frac{2}{3}\left(\Delta U_{consolidation}\right) \tag{4.29}$$

   where ΔU_{avg} is the average excess pore pressure, $\Delta U_{(imposed\ flow)}$ is the excess pore pressure at the base of the specimen caused by the imposed gradient (linear pore pressure distribution), and $\Delta U_{consolidation}$ is the excess pore pressure at the base of the specimen caused by the CRS consolidation process. Other methods for calculating the ΔU_{avg} can be used as well such as using solution from the Wissa linear CRS theory. In this research, the strain rate is relatively low so that the imposed gradient at the base is the main source of the excess pore pressure and, therefore, the pore pressure distribution is closer to the linear distribution than the parabolic distribution form.

2) For a soil type, perform a series of GCRS simulations covering the range of tested strain rates and imposed base excess pore pressure and construct a correlation between %Difference between Δu_{AVG} from GCRS simulation and ΔU_{avg} and strain rate (GCRS correlation graph).

3) Based on the correlation, a correction factor can be applied to the initial average excess pore pressure to obtain a correct $\sigma'_{v(AVG)}$ for the specimen throughout the test.

With the correction factors, a GCRS test at any strain rate can be interpreted effectively and accurately. Figure 4.4 shows the pore pressure distribution curve from the

simulation of CRS662 for San Francisco Bay mud. It should be noted that the predicted pore pressure distribution in Figure 4.4 only applies to the initial hydraulic conductivity and normalized excess pore pressure of the CRS662. Ideally, a GCRS simulation should be performed with appropriate input parameters for each GCRS test. However, a series of GCRS simulation can be performed to cover the strain rate used in the GCRS tests for the same soils with similar normalized excess pore pressure. The simulation results should provide good approximated predicted pore pressure distribution for the tests. Figure 4.5 shows an example of the GCRS correction graph for San Francisco Bay mud.

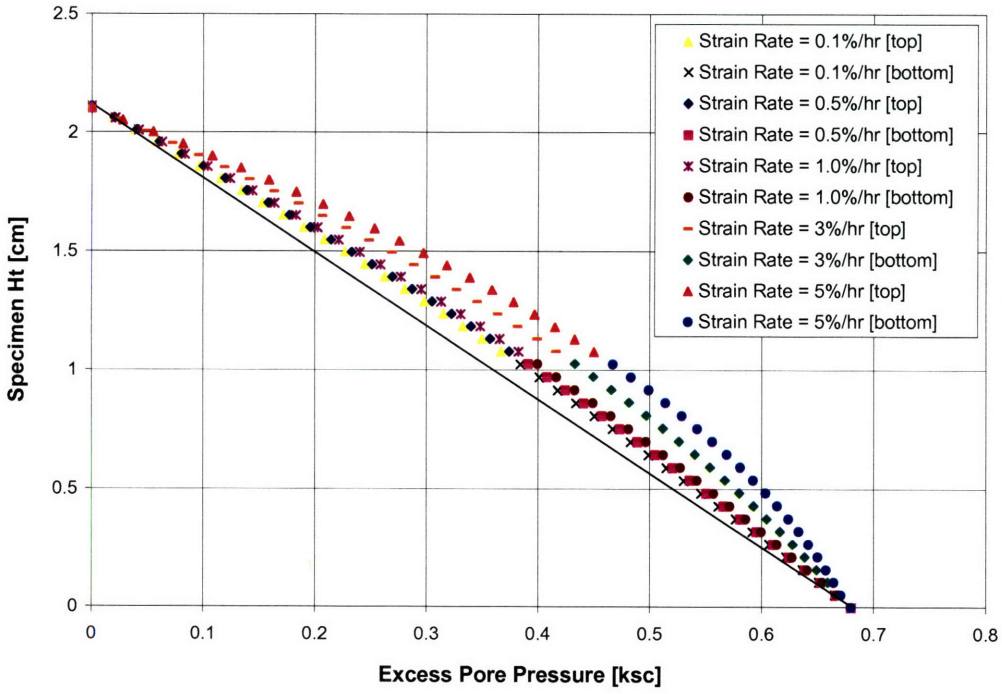

Figure 4.4 Predicted Pore pressure distribution curve for SBM (CRS662)

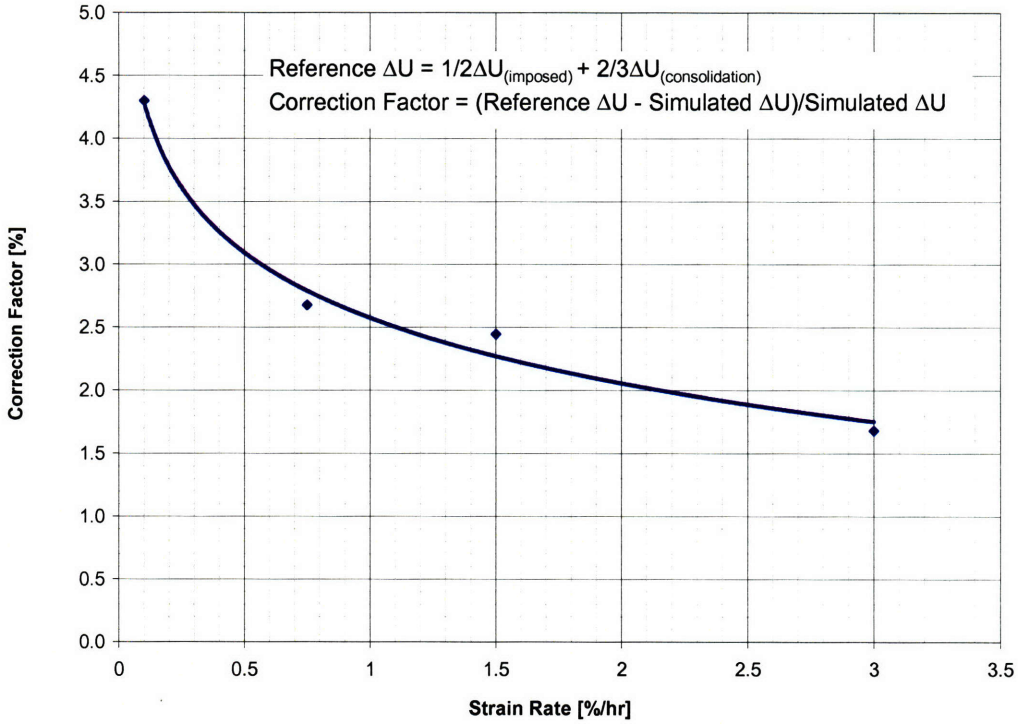

Figure 4.5 GCRS correction graph for San Francisco Bay mud

4.1.3 Evaluation of the GCRS Simulation

To evaluate the GCRS simulation, a numerical simulation is performed to compare with the pore pressure distribution predicted based on Wissa linear CRS theory. Figure 4.6 presents the comparison between the predicted pore pressure distributions. The GCRS simulation is based on the strain rate of 0.2%/hr. The pore pressure distribution based on Wissa linear CRS theory can be obtained from the maximum excess pore pressure.

Since there is no imposed excess pore pressure at the base for this simulation, the GCRS simulation proceeds as from the top of the specimen downward.

Figure 4.6 clearly shows that the simulation program yields accurate pore pressure distributions compared to the prediction based on the Wissa linear CRS theory. This proves that the simulation program is numerically correct and can simulate normal CRS process accurately. The main differences between the GCRS simulation and the pore pressure distribution predicted based on Wissa linear CRS theory is the strain. While Wissa linear CRS theory is based on a small strain assumption, the GCRS simulation requires deformation for the convergence calculation and will predict the pore pressure distribution for large strain deformation problem.

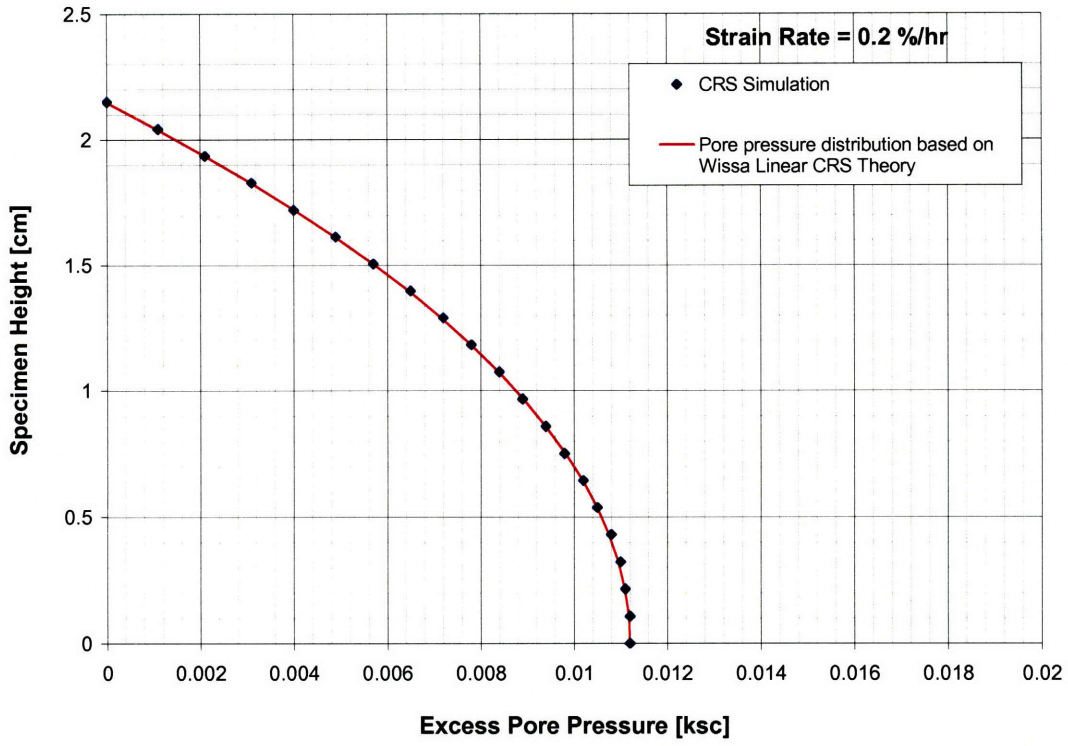

Figure 4.6 Comparison of pore pressure distribution for MBC

The simulation result, even tough, is based on the nonlinear compressibility, can be compared to the predicted pore pressure distribution based on the Wissa linear CRS theory. This is because the differences between the predicted pore pressure based on Wissa linear and nonlinear theory is less than 1% when $\Delta u_b/\sigma'_v$ less than 20%.

4.2 Laboratory Oedometer Simulation

From the experimental programs, the effects of the drainage heights on c_v can be observed but it is important to confirm analytically and also to investigate how to quantify the effects for practical applications. The simulation programs focus on simulating the consolidation behavior following basic d'Arcy law with finite difference calculation. The model allows for finite deformation and follows the relationship between void ratio and logarithm of hydraulic conductivity.

4.2.1 Simulation Concepts and Procedures

The concept of the oedometer simulation is fairly straight forward. It is based on the assumption that the deformation of a specimen under 1-dimensional consolidation is controlled by the flow of pore water out of the specimen and the compressibility of the soil. Therefore, the specimen is divided into n small layers (n = 50 or more) to ensure

good accuracy in the prediction. Figure 4.7 presents a sketch of a specimen divided into layers for an oedometer simulation.

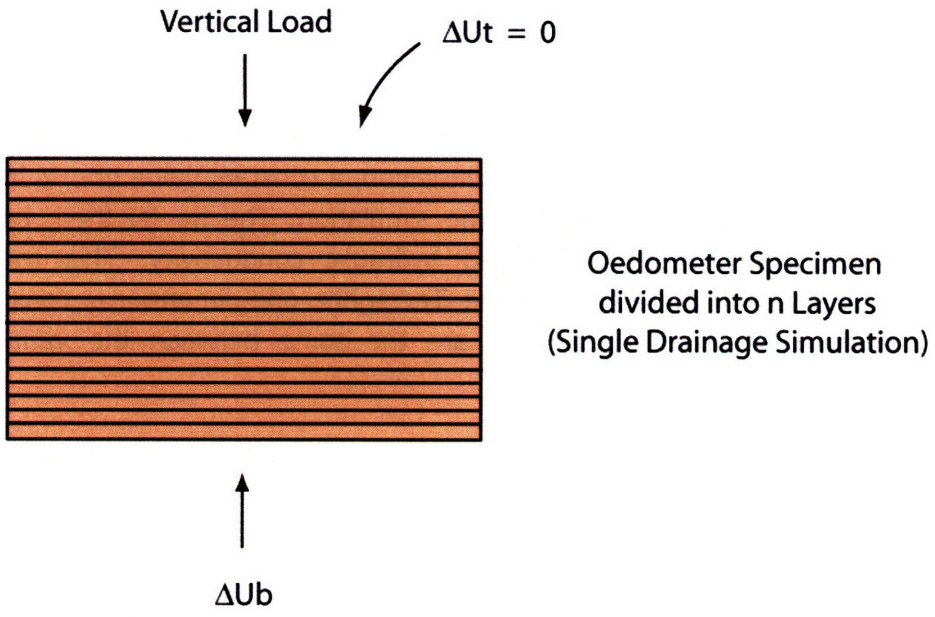

Figure 4.7 Sketch of a specimen divided into layers for an oedometer simulation

The oedometer simulation is different from the GCRS simulation in two vital aspects. The oedometer simulation goal is to simulation soil behavior under constant load for a period of time. The GCRS simulation simulates soil behavior under constant strain rate with an imposed gradient. And there is no imposed hydraulic gradient for oedometer simulation.

For the oedometer simulation, the simulation must cover sufficient time (usually larger than 2 hr). This time is required for the specimen to reach the end-of-primary. The time is divided into many small steps. The time steps are set at 200 or higher. The number of time steps can be increased to achieve a higher level of accuracy. However, increasing the number of time steps will result in a larger computer memory required for the simulation and storage space for post simulation calculations. The time step at the beginning of the simulation is very small (usually between 0.1 sec and 1 sec). The time step is increased to a larger value (usually between 10 sec and 10000 sec) toward the end of the simulation. The time step at the beginning must be small because consolidation happens very fast at the beginning and slow down significantly toward the end of consolidation. It is important to note that the decision on choosing time step size is very important since it affect the accuracy of the results. The time step size should be selected based on the layer thickness and c_v in order to obtain an accurate simulation while allowing the simulation to continue until the end-of-primary consolidation. The smaller the layer thickness is, the faster the consolidation occurs. Therefore, we must ensure that the time step size in this case is small enough so that the simulation can

model the beginning portion of the consolidation. Also a large time step will result in increase in errors from linearization of the model. For a larger layer thickness, the time step size can be larger to allow for faster simulation process.

The simulation can be a variable c_v or a constant c_v simulation. In a variable c_v simulation, the soil behavior is controlled by hydraulic conductivity, k, and compressibility, m_v (or C_c). The hydraulic conductivity is represented by a void ratio (e) versus log(k) relationship. In a constant c_v simulation, a constant value of c_v is input into the program and maintained throughout the simulation. The m_v is, then, calculated based on the constant c_v and calculated hydraulic conductivity. This concept is essentially a large strain equivalent to the Terzaghi's one-dimensional consolidation solution. Otherwise, the overall concepts are the same between the variable and constant c_v simulation.

The simulation starts, as mentioned above, with dividing the specimen into n small layers (usually 50 or more)

$$H_L = \frac{H_0}{n} \tag{4.30}$$

where H_L, H_0, and n are the height of the layer, original height of the specimen, and numbers of layer, respectively.

For the first time step, the void ratio of each layer, e_L, is equal to the initial void ratio, e_0, at the start of the simulation. Since the vertical effective stress at the end of each time step, σ'_{vL}, is unknown, the effective stress at the end of the first time step is assumed to be the initial effective stress, σ'_{v0}. This vertical effective stress will be updated later in the simulation for each time step. The void ratio at the top and bottom boundary of each layer is, then, calculated from

$$e_{L(top)} = e_0 - \left[log\left(\sigma'_{vL(T)}\right) - log\left(\sigma'_{v0}\right)\right] \cdot C_c \tag{4.31a}$$

$$e_{L(bottom)} = e_0 - \left[log\left(\sigma'_{vL(B)}\right) - log\left(\sigma'_{v0}\right)\right] \cdot C_c \tag{4.31b}$$

where $\sigma'_{vL(T)}$, $\sigma'_{vL(B)}$, σ'_{v0}, and C_c are the vertical effective stress at the top of the layer, effective stress at the bottom of the layer, initial vertical effective stress, and the coefficient of compression of the soil. $e_{L(top)}$ is the void ratio at the top of the layer and $e_{L(bottom)}$ is the void ratio at the bottom of the layer

The assumed vertical effective stress at the end of each time step will be compared with the expected σ'_v based on the flow of water out of the specimen later in the simulation.

The void ratio at the top and bottom of each layer is calculated using equation 4.31a and 4.31b.

The hydraulic conductivity for each layer is calculated from the void ratio using

$$k_L = 10^{\left[\log(k_0)-\left(\frac{e_0 - e_{L(avg)}}{C_k}\right)\right]} \tag{4.32}$$

The k_L is the average hydraulic conductivity for each layer. It is based on the relationship between the e and log(k). The current void ratio of the layer is the average of the void ratio at the top and bottom of the layer.

$$e_{L(avg)} = \frac{e_{L(top)} + e_{L(bottom)}}{2} \tag{4.33}$$

where $e_{L(avg)}$ is the average void ratio of the layer.

Based on the change in void ratio, the flow of each layer is calculated from the bottom upward to the top of the specimen.

$$q = \frac{\Delta e}{(1+e_0)} \cdot H_L \tag{4.34}$$

$$\Delta e = e_0 - e_{L(avg)} \tag{4.35}$$

where q and Δe are the flow and the changes in void ratio.

The total flow of each layer is the summation of the flow of the current layer and the flow from the layers below.

$$q_{i(total)} = q_i + \sum_{m=n}^{m=i+1} q \tag{4.36}$$

where $q_{i(total)}$ and q_i are the total flow of the current layer and the flow of the current layer based on the deformation of the layer (equation 4.34).

Based on the flow and hydraulic conductivity, the excess pore pressure of each layer can be calculated from

$$\Delta u_L = \frac{q}{\Delta t \cdot k} \cdot \frac{H_L}{1000} \tag{4.37}$$

where Δt is the time step (start at 1s and increase to 300 – 500s toward the end of the simulation). Based on the excess pores pressure obtained from equation 4.37, the vertical effective stress can be calculated from

$$\sigma'_{vN} = \sigma_v - \Delta u_L \tag{4.38}$$

where σ_v is the total vertical stress which can be obtained from

$$\sigma_v = \sigma'_{vo} + \Delta u_0 \tag{4.39}$$

This vertical effective stress can be compared with the assumed σ'_v at the beginning of the simulation time step. The difference between the assumed σ'_v and the calculated σ'_v is the error(E_r).

$$E_r = \sigma'_{vL} - \sigma'_{vN} \tag{4.40}$$

If the error is less then the set tolerance of the simulation ($1x10^{-6}$ kg/cm^2), the simulation for this time step is complete. The next time step simulation, then, begins. However, if the error is larger than the tolerance, the vertical effective stress of each layer is updated based on a convergence criterion. For this simulation, the new vertical effective stress can be obtained from

$$\sigma'_{v(update)} = \sigma'_{vL} - \frac{E_r}{30} \text{ (for each layer)} \tag{4.41}$$

The simulation continues until it reaches the specified time for the oedometer increment. The output is saved as a text file ("results.dat"). Figure 4.8 shows a flowchart summarizing the oedometer simulation steps. Table 4.2 presents the summary of the input parameters for the oedometer simulation.

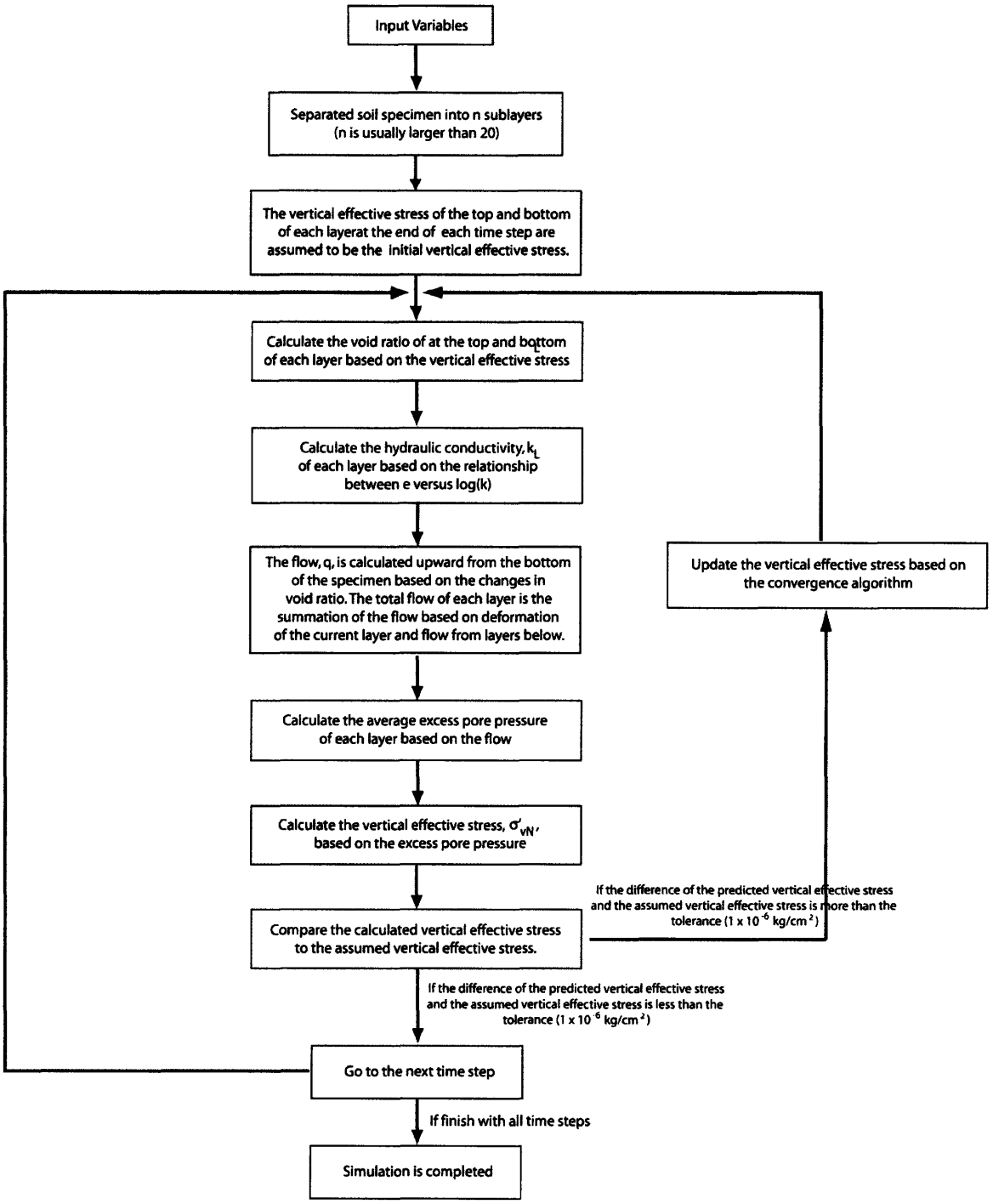

Figure 4.8 Oedometer Simulation Flow Chart

The source code of the oedometer simulation can be found in appendix B of this thesis along with an example of an output file from the simulation. The simulation program is written in C++ programming language for Microsoft Windows ® operating systems including Microsoft Windows ® 98, ME, 2000, and XP. Depending on the version of

Microsoft Windows ® operating systems, extra C++ runtime files may be necessary to run the program. These C++ runtime files, if required, can be obtained from the official Microsoft web site (http://www.microsoft.com).

Input Parameters	Descriptions
H_d	Initial drainage height
c_v	Input coefficient of consolidation
e_0	Initial void ratio
k_0	Initial hydraulic conductivity
C_k	Slope between e versus log(k) graph
C_c	Compression index
Δt	Time increment for the simulation
σ_v	Total vertical stress at the beginning of the load increment
$\Delta\sigma_v$	Total vertical stress increment for the current load increment

Table 4.2 Summary of the input parameters for the oedometer simulation

4.2.2 Interpretation of the Oedometer Simulation

The result from an oedometer simulation can be interpreted in a similar manner to that of a laboratory oedometer test. Based on the deformation and time, the consolidation curve can be plotted for both $\sqrt{t}$ and log(t) time space. The coefficient of consolidation, c_v, based on both methods can be obtained using the construction methods described in chapter 2, section 2.3.1 and section 2.3.2. Figure 4.9 and 4.10 shows an example of the consolidation curves from the simulation of San Francisco Bay mud on $\sqrt{t}$ and log(t) time space, respectively

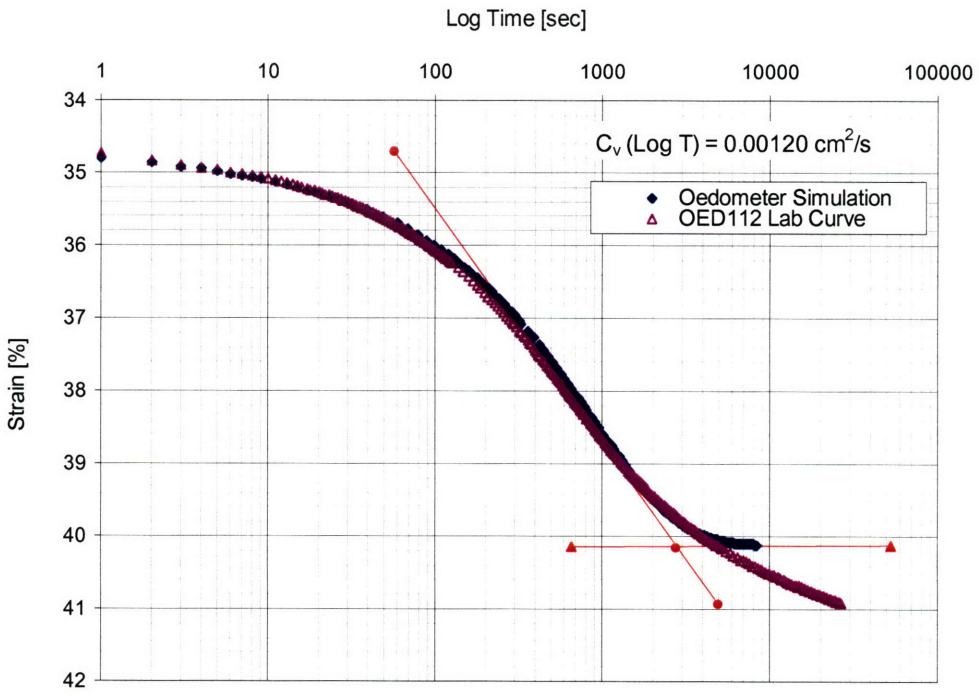

Figure 4.9 Comparison between consolidation curves (log t curve) based on the oedometer simulation and the laboratory curve

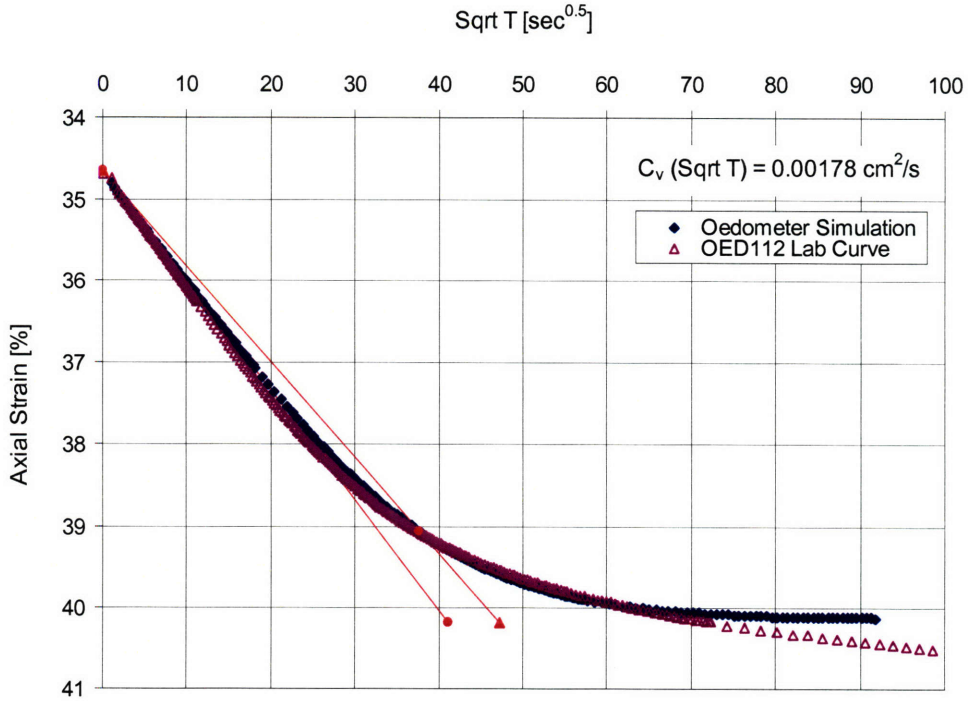

Figure 4.10 Comparison between consolidation curves ($\sqrt{t}$ curve) based on the oedometer simulation and the laboratory curve

4.2.3 Evaluations of the Oedometer Simulation

To evaluate the oedometer simulation, the predicted consolidation curve is compared to the laboratory consolidation curve. The prediction should be very similar to the laboratory curve. There is, however, a limitation of the simulation program. Since the simulation does not take into account the secondary compression, the simulation cannot capture the behavior after the end of primary consolidation accurate. The secondary compression in this case refers to any deformation occurs after the primary consolidation or deformation caused by viscous effect. It should also be noted that the simulation is designed for only normally consolidated soils (OCR = 1).

Figure 4.9 and 4.10 clearly illustrate that the predicted consolidation curve is very closely match the laboratory consolidation curve. The main difference between the prediction and the observed behavior is the secondary compression. Figure 4.9 and 4.10 also show this difference between the prediction and observed behavior in laboratory. After the end of primary consolidation ($t_{EOP} \sim 2900$ sec or $\sqrt{t} \sim 54$ $sec^{0.5}$), the specimen continues to deform in the laboratory as shown in Figure 4.9. The predicted consolidation curve, however, has no deformation after it reaches the end of primary consolidation.

4.3.4 Parametric Studies of the Oedometer Simulation

The development goal of the oedometer simulation is to create a simulation program that can capture the consolidation behavior of soft clays under 1-dimensional consolidation with constant load. The simulation can also be used to study the effects of scaling on the coefficient of consolidation, c_v.

The main idea is to observe whether the scaling have effects on the coefficient of consolidation based on the simulation concept. A series of simulations are performed based on a set of input parameters. The simulations cover the drainage height of 0.5 to 100 cm. The results are plotted in terms of the c_v ratio [$c_v(\sqrt{t})/c_v(\log(t))$] versus drainage height.

Figure 4.11(a) shows a graph between the c_v ratio and drainage height from a series of constant c_v oedometer simulation. Figure 4.11 shows that the c_v ratio decreases with increasing drainage height. The c_v ratio decreases very fast initially when the drainage height is very small. Once the drainage height increases, the c_v ratio continues to decrease but at a slower rate. On a semi-logarithm scale plot, as shown in the figure 4.11(b), the relationship between c_v ratio and the drainage height is approximately linear but still concave upwarded.

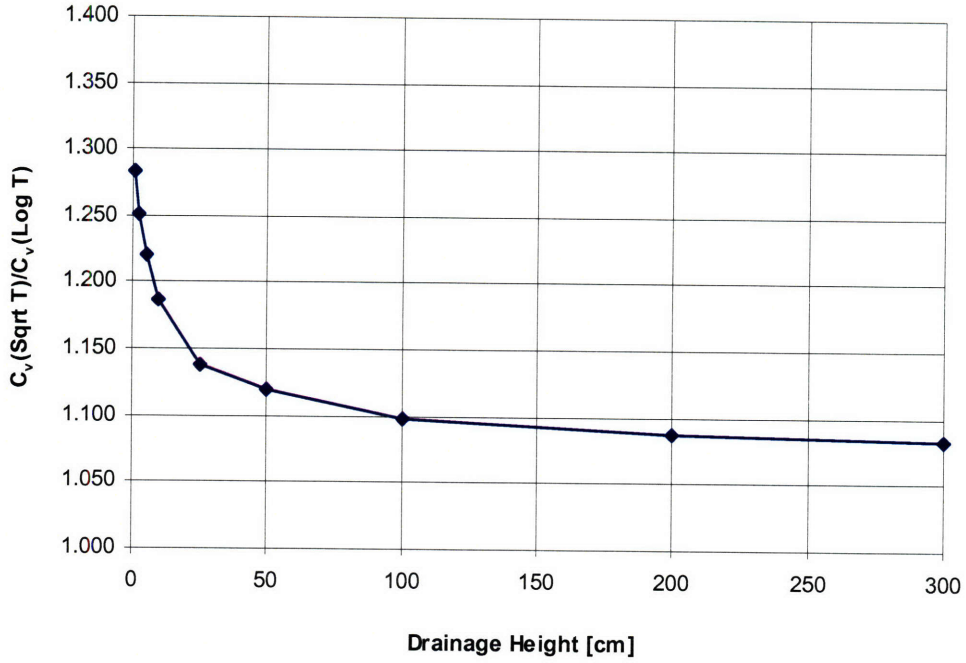

Figure 4.11(a) c_v ratio versus drainage height, constant c_v simulation

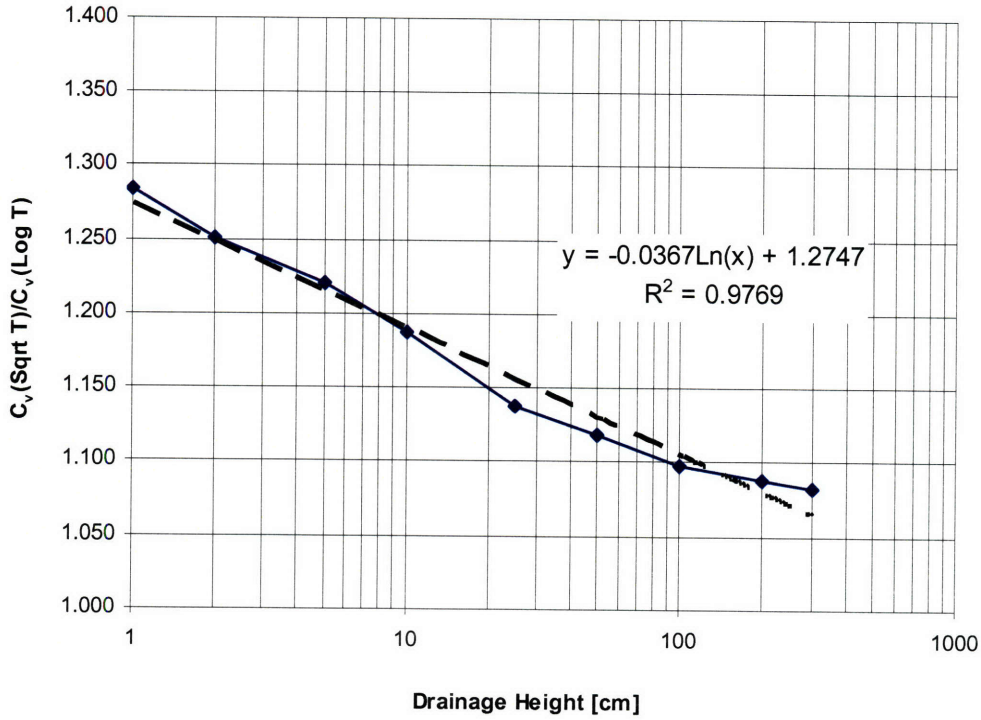

Figure 4.11(b) c_v ratio versus log (H_d), H_d = drainage height, constant c_v simulation

Figure 4.12(a) and 4.12(b) presents the graphs between c_v ratio and drainage height with varying initial hydraulic conductivity (k_0). The simulations cover the initial hydraulic conductivity (k_0) of $1x10^{-6}$ cm/sec to $1x10^{-2}$ cm/sec. The c_v during the simulations is constant and the m_v is calculated based on the k and constant c_v. It is clear from the figures 4.12 that the c_v ratio increases with decreasing k_0.

Figure 4.13(a) and 4.13(b) shows the graph between the c_v ratio and initial hydraulic conductivity (k_0) for a 10cm drainage height. They clearly show that the c_v ratio decreases with increasing hydraulic conductivity. The c_v ratio decreases from 1.205 to 1.125 when the hydraulic conductivity changes from $1x10^{-6}$ cm/sec to $1x10^{-2}$ cm/sec. Based on the figure 4.13(b), the relationship between the c_v ratio and $\log(k_0)$ can be expressed by a linear equation as shown in the figure.

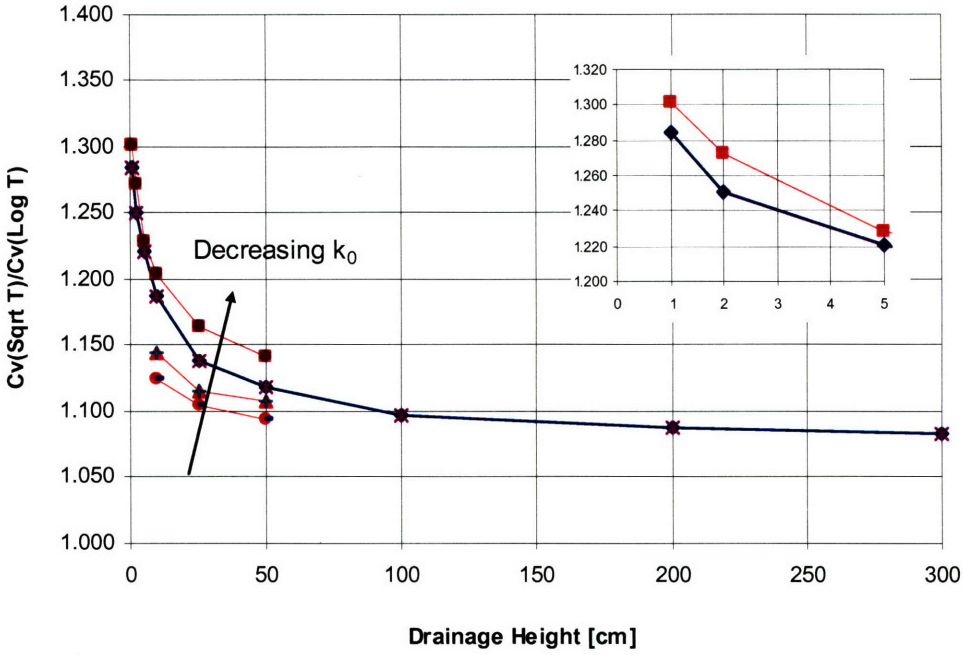

Figure 4.12(a) c_v ratio versus drainage height, varying k_0, constant c_v simulation

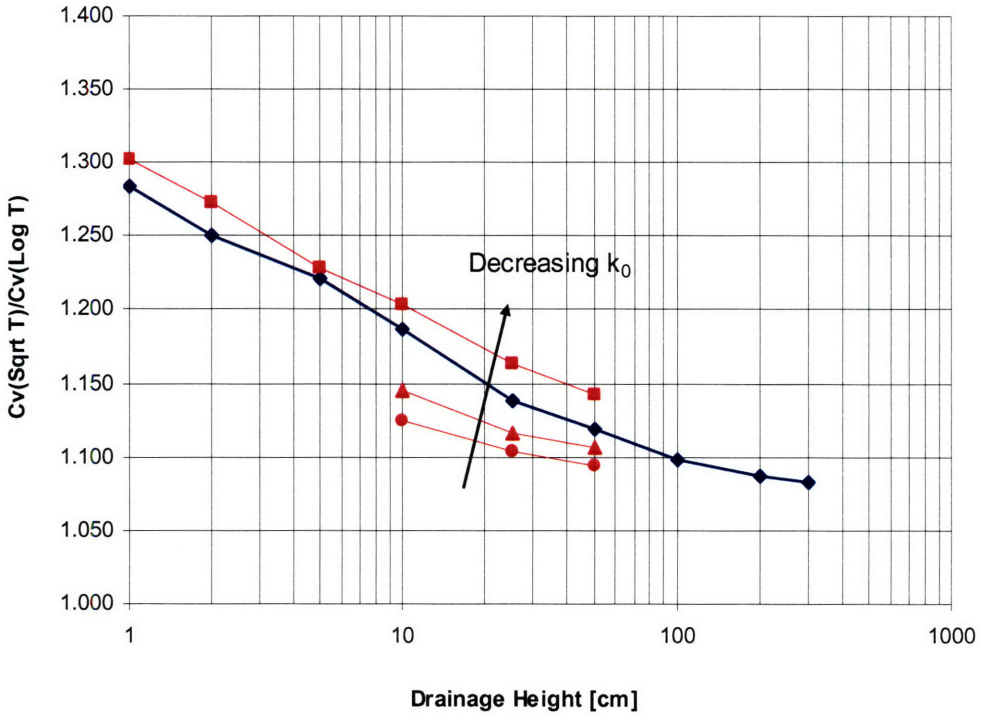

Figure 4.12(b) c_v ratio versus log (H_d), varying k_0, H_d = drainage height, constant c_v simulation

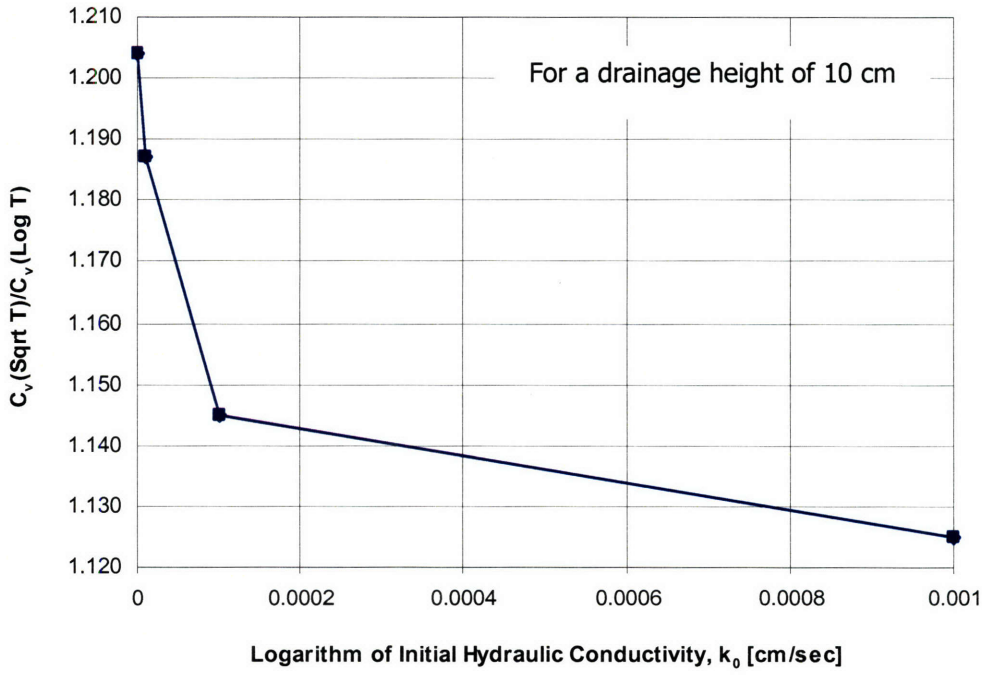

Figure 4.13(a) c_v ratio versus k_0, constant c_v simulation

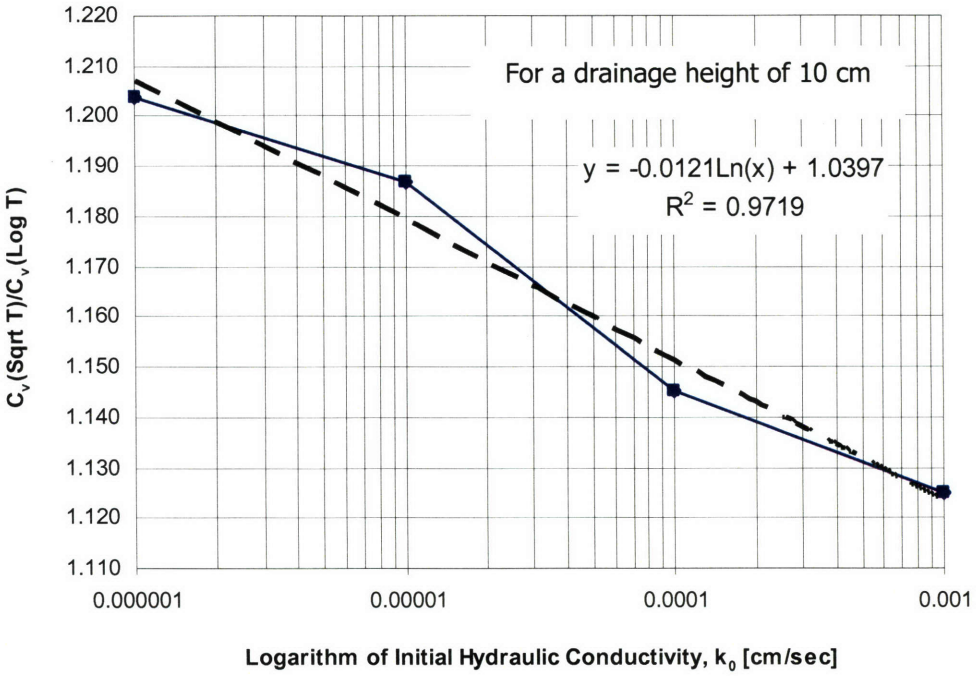

Figure 4.13(b) c_v ratio versus log(k_0), constant c_v simulation

Figure 4.14 presents the comparison between the predicted c_v ratio based on constant c_v and variable c_v simulation. The variable c_v simulation allows the c_v to change based on the relationship between e and log(k) and constant m_v or constant C_c. This allows the c_v of each layer to change during the simulation and to be different from layer to layer.

The difference between predicted c_v ratio from the constant and variable c_v simulations are not very large (less than 2.5% at the maximum). The relationship between the c_v ratio and drainage heights, however, is very similar for both simulation. It should be noted that the variable c_v simulation should yield more accurate predictions since it allows the c_v to change for each layer during the simulation.

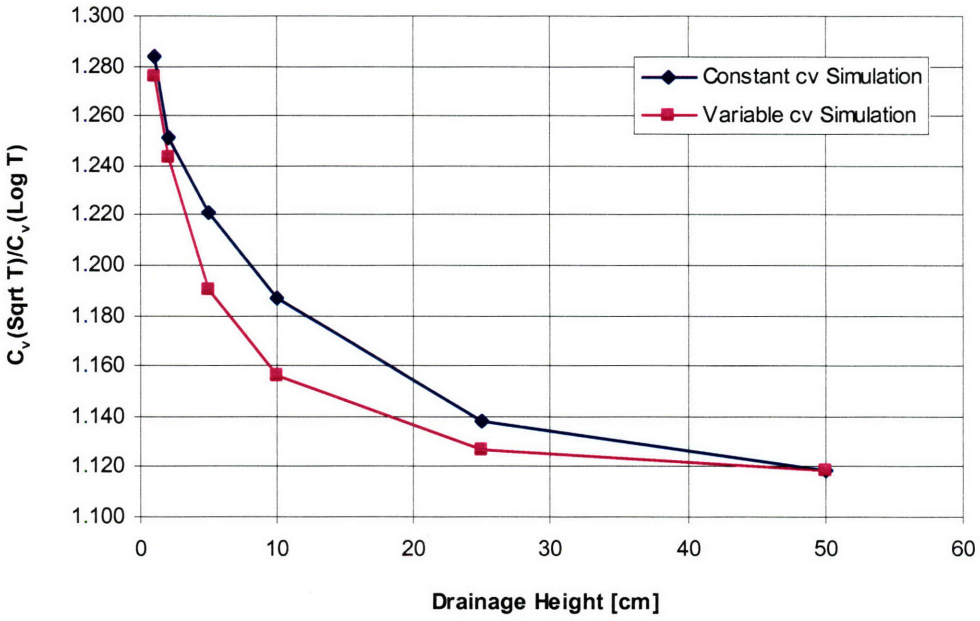

Figure 4.14 Comparison between constant c_v and variable c_v oedometer simulation

Chapter 5: Analysis and Results

This chapter presents the details of analysis methods and results from the research. The focus is on the three main topics including: strain rate sensitivity, effects of hydraulic gradient and scaling effects on the consolidation behavior of San Francisco Bay mud and Maine Blue clay.

The first section of this chapter deals with the analysis and results of the strain rate sensitivity tests. The tests cover strain rate of 0.2%/hr to 8%/hr for Maine Blue clay (data from Germaine, 2007 and Chartier, 2004) and 0.1%/hr to 3%/hr for San Francisco Bay mud. The analysis of the strain rate sensitivity focuses on the observed location of the Virgin Compression Line (VCL) when the strain rate is changed during the test or compares the VCL from tests with different strain rate. Detailed discussions of the experimental technology are provided in section 3.2.

The second section of this chapter provides detailed analysis of the Gradient-controlled Constant Rate of Strain (GCRS) test. The results from the experimental program are combined with the predicted excess pore pressure distribution based on the GCRS simulation to obtain the average vertical effective stress during the imposed gradient CRS loading phase.

The last main section of this chapter presents the results from oedometer tests with varying drainage heights. The focus is on the scaling effects based on the evaluation of the c_v ratio [$c_v(\sqrt{t})/c_v(\log(t))$] from 3 series of tests with different drainage heights. The analysis concepts will be discussed along with the interpreted results of the test. This section also provides the details of analysis and results from oedometer simulation.

5.1 Strain Rate Sensitivity Tests

Strain rate sensitivity is one of the major parameters that can affect consolidation behavior of soft clay. The study of the strain rate effect in this research is performed on San Francisco Bay mud and Maine Blue clay. The test set up is relatively simple and designed to ensure that the results from the experimental program can be interpreted accurately and easily. Chapter 3 presented the experimental methods used for the strain rate sensitivity study. Since the specimens are obtained from tube samples of natural soils, the preconsolidation pressure (σ'_p) is not suitable for this study. The preconsolidation pressure from natural soils differs based on the load history and sample quality of the soil.

The most obvious observation from the strain rate sensitivity study is the shifting of the virgin compression line (VCL) when the strain rate changes. The analysis focuses on the shift in the normally consolidated range. This effect can be presented by two main graphical methods, the compression curve (ε versus log σ'_v) and normalization of differences in the vertical effective stress at the same strain versus strain rate ($\Delta\sigma'_v/\sigma'_v$ versus $\dot{\varepsilon}$). Figure 5.1 shows an example of a compression curve from a CRS test of SBM that clearly shows strain rate dependent behavior. Figure 5.2 presents an example of the normalized differences in vertical effective stress versus strain rate curve. For a strain rate sensitive soil, the VCL changes location when the strain rate is changed as clearly shown in the Figure 5.1. The VCL shifts are more pronounced if the changes in strain rate are larger. This is why the strain rates for each strain rate sensitivity test are carefully selected to ensure that the VCL shifts can be clearly observed on a compression curve.

It is also important to monitor the strain rate during the test to ensure that the proper strain rate is maintained constant throughout each stage of the test. The strain rate graph is a plot of strain rate versus time for a test. Figure 5.3 shows an example of a strain rate graph for a test that had 3 different strain rate (0.1, 0.75 and 1.5%/hr). Figure 5.3 clearly shows that the strain rates during the test remain constant during each phase. The monitoring of excess pore pressure is also important to see the magnitude of excess pore pressure relative to the vertical effective stress. The excess pore pressure during a CRS test should not be too high because it creates high hydraulic gradient which may affect the consolidation behavior of soft clay. Figure 5.4 presents an example of the normalized excess pore pressure graph ($\Delta u/\sigma'_v$ versus ε) from the same test as the strain rate graph in the Figure 5.3. The normalized excess pore pressure graph shows that the $\Delta u/\sigma'_v$ increases with increasing strain rate and it remains relatively constant after reaching the steady state of each phase.

Figure 5.5 presents the graph between coefficient of consolidation, c_v, and axial strain. The c_v decreases significantly during the recompression and becomes relatively linear during the normally consolidated range. Figure 5.6 shows the graph between void ratio and logarithm of hydraulic conductivity, k. The graph shows log linear relationship between the void ratio and hydraulic conductivity. It should be noted that the hydraulic conductivity shows dependency on the strain rates used in the test. The hydraulic conductivity at a higher strain rate is higher than that of the slower strain rate as indicated in Figure 5.6.

The normalized excess pore pressure ($\Delta u/\sigma'_v$) also have tendency to increase within each stage of the test as shown in Figure 5.4. This is more pronounced in the first two stages right after when the stress pass the preconsolidation pressure (σ'_p).

It should also note that the compression curve from two stages of each strain rate is clearly an extrapolation of the same trend line (as shown in the Figure 5.1). This is a clear evidence that the sequence of the strain rate used in the test are not important and does not affect the test result. At the fastest strain rate ($\dot{\varepsilon}$ = 8 %/hr and 3 %/hr for MBC and SBM, respectively), the normalized excess pore pressure is still below the ASTM limit and therefore the interpretation should not be problematic. On the opposite end, at the lowest strain rate, the excess pore pressure is small but still measurable.

The log linear of the compression curve (ε versus log σ'_v) is also an important issue that needs to be considered. Many soils exhibit nonlinear compression curve. The nonlinearity of the compression curve can cause difficulty in the interpretation of the strain rate sensitivity test. To minimize this problem, the tests are performed with two cycles of CRS phases for each strain rate to help establish an accurate compression curve for a particular strain rate.

The shifting of the VCL with strain rate change shows that the soil is strain rate sensitive. The shifting of the compression curve also means that the value of the preconsolidation pressure (σ'_p) of a strain rate sensitivity soil is dependent on the strain rate. Complete test results including all graphs are presented in the appendix C.

5.1.1 Maine Blue Clay (MBC)

The study of strain rate sensitivity of MBC covers the strain rate from 0.1 %/hr to 8 %/hr. These strain rates cover a wide range from slow strain rate to a very fast strain rate based on ASTM standard D4186. If MBC exhibits strain rate dependent behavior, the results from these tests should clearly show a shift in the VCL. Figure 5.7 to 5.9 presents the compression, strain rate and normalized excess pore pressure curves of a typical MBC from a strain rate sensitivity test (CRS594) (data obtained from Chartier, 2004). Figure 5.7 clearly shows that the location of VCL does not change when the strain rates change from 1%/hr to 8%/hr and back to 1%/hr. Generally, the location of the VCL is expected to change if the strain rate changes significantly such as in this test. Since no shift of the VCL is observed, the results conclusively indicate that the MBC exhibit no strain rate dependent behavior.

It should be noted that since MBC is a stiffer soil than SBM, the test cover only one cycle as opposed to multiple cycles used for the SBM. This particular test (CRS594) also has

secondary compression at the end of each strain rate stage but this has no impact on the result. Other strain rate sensitivity tests use continuous loading.

The normalized excess pore pressure clearly decreases as loading continue as shown in Figure 5.9. This trend is different from the SBM. It should also be noted that the $\Delta u/\sigma'_v$ trend is the same for fast and slow strain rate. At the fastest strain rate, the soil generates approximately 18.5% $\Delta u/\sigma'_v$ which is approximately twice as high as the $\Delta u/\sigma'_v$ at the fastest strain rate for SBM. At the slowest strain rate, the $\Delta u/\sigma'_v$ is small but is observable.

Figure 5.10, 5.11, and 5.12 present the MBC compression curves from the strain rate sensitivity test covering the strain rate of 0.1 %/hr and 1 %/hr (CRS862), 0.5 %/hr and 1 %/hr (CRS860), and 1 %/hr and 2 %/hr (CRS861) respectively (data from Germaine, 2007). Based on the compression curves, it is clear that slower strain rates can shift the compression curve to the left. This is particularly obvious on the Figure 5.10 where the difference between the two strain rates used in the test is the largest (0.1 %/hr and 1 %/hr). Based on Figure 5.12, it is also clear that when increasing strain rate from 1 %/hr to 2 %/hr, the amount of shift is very small but observable. Combining these results with the results from the CRS594 discussed earlier, it becomes clear that the MBC exhibit strain rate dependency when the strain rate is lower than approximately 1 to 2 %/hr and becomes strain rate independent at a higher strain rate.

Figure 5.13 presents the graph between coefficient of consolidation, c_v and logarithm of vertical effective stress (σ'_v) from the CRS860. It shows that the coefficient of consolidation increases with increasing vertical effective stress during the normally consolidated range. Figure 5.14 shows the graph between void ratio and logarithm of hydraulic conductivity for the same test. The graph shows that the relationship between the void ratio and hydraulic conductivity can be approximated by a log linear relationship.

5.1.2 San Francisco Bay Mud (SBM)

For SBM, the strain rate sensitivity tests cover strain rates of 0.1%/hr to 3%/hr. The strain rate of 0.1%/hr is very slow and is on the lower end of the recommended strain rate based on ASTM D4186 for CRS tests, while the strain rate of 3%/hr is very fast. This allows the tests to cover wide range of strain rate. Figure 5.15 through 5.17 shows the compression, strain rate and normalized excess pore pressure curves from a typical SBM strain rate sensitivity test (CRS691). Figure 5.15 shows clear shifts in the VCL for the SBM when the strain rate changes. This clearly indicates that the consolidation behavior of SBM is strain rate dependent.

It should also be noted that the excess pore pressure during each constant $\dot{\varepsilon}$ phase increases slightly. The excess pore pressure is also increasing with increasing strain rate. The normalized excess pore pressure, $\Delta u/\sigma'_v$ is approximately 5%, 8-9%, and 15-25% for the strain rate of 0.75%/hr, 1.5%/hr, and 3.0%/hr, respectively. The normalized excess pore pressure is quite high at strain rate of 3.0%/hr. Based on Gonzalez (2000), the high $\Delta u/\sigma'_v$ can cause the calculated σ'_v based on the Wissa linear CRS theory to differ from that of nonlinear theory by approximately 1%. Although the difference in the σ'_v from the linear and nonlinear theory calculation is small, the differences in the hydraulic conductivity and coefficient of consolidation can be up to 12.5%. If the k and c_v are important, the nonlinear CRS theory should be considered in the data reduction. Figure 5.18, 5.19, and 5.20 show the graph between the σ'_v(linear)/σ'_v(nonlinear), k(linear)/k(nonlinear), and c_v(linear)/c_v(nonlinear) versus $\Delta u_b/\sigma'_v$ (Gonzalez, 2000).

Combining the results from the strain rate tests of MBC and SBM shows clearly that the soils exhibits totally different consolidation behavior. Figure 5.21 presents the normalized differences in vertical effective stress versus normalized strain rate curve of MBC and SBM. The strain rate is normalized by the strain rate where normalized base excess pore pressure ($\Delta u_b/\sigma'_v$) is 2%. The normalization strain rate is approximately 1 %/hr and 0.17 %/hr for MBC and SBM, respectively.

Figure 5.21 shows that MBC clearly exhibits hypothesis A behavior when the normalized strain rate is higher than approximately 1.5 (or equivalent to strain rate of 1.5 %/hr). This is especially clear when considering the results from the CRS594 discussed earlier which the strain rate is increased from 1 %/hr to 8 %/hr and no shift of the compression curve is observed. In contrast, the consolidation behavior of SBM can be better described using hypothesis B since the compression behavior is clearly strain rate dependent. The difference is particularly obvious when consider the results from strain rates that produce normalized excess pore pressure larger than 5%. While MBC shows no rate dependency behavior, the shifts of the VCL for SBM is approximately 15% per log cycle of increases in normalized strain rate.

The reasons for difference exhibits from these two soils are beyond scope of this research. However, it is clear that under exactly the same testing condition, the two different materials exhibit very different behavior. It is, therefore, important to understand that different soils can have different strain rate dependent behavior.

5.2 Gradient-controlled Constant Rate of Strain Tests (GCRS)

The gradient-controlled constant rate of strain tests include three main phases. The first phase is a standard CRS loading until passing the preconsolidation stress. The CRS loading in the first phase continues until a well-defined portion of virgin compression line is observed or until the consolidation reaches approximately 5% axial strain. The second phase includes the same CRS loading (with the same $\dot{\varepsilon}$) with an imposed constant base pore pressure which resulting in an upward gradient. The imposed base excess pore pressure is applied to the specimen through a pressure-volume control device and is maintained throughout the entire phase with brief interruptions to recharge the pressure-volume control device when necessary. This phase usually covers approximately 5% axial strain. The strain rate remains constant while the test switches from measuring the ΔU_{base} to control ΔU_{base} during the 2nd phase. Once the 2nd phase finished, the valve connecting the pressure-volume control device to the base of the specimen is closed and the test control returns to measurement of base excess pore pressure (Δu_b). The third phase is essentially another CRS loading phase at the same strain. It should also be noted that there is no interruption in strain rate between phases. Figure 5.22 presents a typical compression curve for a GCRS test.

The interpretation of the test results is straightforward during the phase 1 and 3. However, during phase 2, the pore pressure distribution is complicated because it contains both the element of excess pore pressure from consolidation and the pore pressure from the imposed gradient. The average excess pore pressure obtained using Wissa CRS theory can no longer be used for the phase 2 calculations. Hence, equation (4.1) and (4.2) no longer applies. The pore pressure distribution during phase 2 can be obtained from the GCRS simulation as outlined in section 4.1.

The GCRS test program is also designed to cover wide range of strain rate (from 0.1%/hr to 3%/hr) and imposed hydraulic gradient (from $\Delta u_e/\sigma'_v$ = 2% to 66%). This allows for an extensive study of other important factors that might affect the consolidation behavior. Because the experiments are set up such that the hydraulic gradient can be controlled independently from the strain rate, the tests offer valuable insight into the study of both parameters separately under a controlled environment.

Chapter 3 explains the test set up in details. The study focuses mainly on the comparison between the virgin compression line (VCL) of phase 2 to those of phase 1 and 3. If the hydraulic gradient affects the consolidation behavior of the specimen, the VCL should clearly show the shift. If the hydraulic gradient has no effect on the consolidation behavior, the VCL during phase 2 will simply remain the same as those in phase 1 and phase 3. The following sections present and discuss the results of Maine Blue clay (MBC) and San Francisco Bay mud (SBM) in details.

5.2.1 Pore Pressure Distribution during GCRS Phase

The interpretation of GCRS tests requires prediction of the excess pore pressure distribution during the gradient-controlled phase. Because the excess pore pressure distribution is a combination of the excess pore pressure generated from the consolidation process and the imposed gradient, a simulation is required to predict the excess pore pressure distribution and the average pore pressure. This is used to calculate the average vertical effective stress.

Figure 5.23 presents the compression curve from a typical GCRS test interpreted using Wissa linear CRS theory. Figure 5.24 shows the graph between normalized base excess pore pressure ($\Delta u_b/\sigma'_v$) versus axial strain for the same test. The actual average excess pore pressure during the GCRS phases is small than the $2/3\Delta u_b$ based on the Wissa Linear CRS theory. Therefore, we need to perform GCRS simulations to obtain the average excess pore pressure (based on the predicted pore pressure distribution). We can either directly use the predicted average excess pore pressure to calculate the average vertical effective stress or follow the process outlined in the section 4.1.1.

Based on the distribution, we can calculate the average excess pore pressure and use it to calculate the average vertical effective stress. Figure 5.25 shows the compression curve based on the predicted average excess pore pressure.

The above processes can be used to interpret all GCRS tests. However, this is very time consuming process since the simulation have to be performed for each test covering various imposed excess pore pressure and strain rate used in the tests. Because of time constraint and also many tests are performed at similar normalized excess pore pressure level, it is, therefore, much more efficient to perform analysis of those tests using a typical correction curve.

5.2.2 Maine Blue Clay (MBC)

The GCRS tests for MBC cover wide range of hydraulic gradients (approximately 100 to 1200) or in terms of normalized imposed excess pore pressure ($\Delta u/\sigma'_v$) range from 2 to 40%. The strain rate used in the GCRS tests for MBC is approximately 0.2%/hr. Table 5.1 presents the summary information of the GCRS test for SBM.

For the MBC, the GCRS tests cover only four values of average normalized excess pore pressure. It is, therefore, easier to perform four GCRS simulation to obtain the pore pressure distribution for each normalized excess pore pressure. The average excess pore

pressure can be obtained directly from the predicted pore pressure distribution. It should be noted that the average pore pressure obtained from the simulation represents only the GCRS test with a particular $\Delta u/\sigma'_v$. Since the $\Delta u/\sigma'_v$ changes constantly during a GCRS test, this average excess pore pressure is only accurate for a point in the test. Figure 5.26 shows a pore pressure distribution for MBC with normalized excess pore pressure ($\Delta u_e/\sigma'_v$) of 2% (crs640).

Figure 5.27 presents the compression curve from a typical GCRS test of MBC (CRS652). The first phase of the test is a standard CRS loading phase with strain rate of 0.2 %/hr upto axial strain approximately 8%. The specimen is, then subjected to the CRS unloading. At the end of unloading phase, the gradient of approximately 1140 is imposed at the base of the specimen. The specimen is, then, consolidated at the same strain rate as in the phase 1 until an axial strain of approximately 12.2%. The specimen is, then, unloaded and the imposed gradient is removed before the start of the normal CRS loading in phase 3 (with the same strain rate of 0.2%/hr).

It is clear from the compression curve that hydraulic gradient produces small but observable shifts of VCL of MBC. The VCL shift can be described in the term of the normalized changes in vertical effective stress (obtained by compare the VCL of phase 2 to those of phase 1 and 3) to the current vertical effective stress ($\Delta\sigma'_v/\sigma'_v$) as in the strain rate test.

Figure 5.28 presents the compression curve from the CRS640 (average $\Delta u/\sigma'_v$ of 1.1%). It should be noted that the test sequence for the CRS640 differs from that of CRS652. The specimen is continuously loaded throughout the test without unloading phase. The specimen is subjected to CRS loading with strain rate of 0.2%/hr. This strain rate is maintained constant throughout the test. At approximately axial strain of 7.9% and 12.9%, an imposed hydraulic gradient of 55 and 110, respectively, were applied to the specimen. In the phase 3 of the test, the imposed hydraulic gradient is removed and the specimen continues to consolidate under normal CRS loading. At a low imposed hydraulic gradient as in the CRS640, the hydraulic gradient effect cannot be observed but at the higher hydraulic gradient, the effect becomes distinct. At a higher imposed hydraulic gradient of the CRS652 test ($\Delta u/\sigma'_v$ of 24.2 and 40.3%), the VCL shift becomes quite large with $\Delta\sigma'_v/\sigma'_v$ of 1.7 and 3.2%, respectively.

It is interesting to observe that the imposed hydraulic gradient causes the VCL to shift to the left of the normal VCL (the VCL of a CRS test without the imposed gradient obtained from phase 1 and phase 3). Figure 5.29 presents a typical graph of hydraulic gradient variation during phase 2 of GCRS test. It should be noted that the imposed hydraulic gradient remains relatively constant during phase 2 as shown in the Figure 5.29.

5.2.3 San Francisco Bay Mud (SBM)

Table 5.2 presents the summary information of the GCRS test for SBM. Based on the preliminary GCRS test results of MBC in the earlier phase of research, the GCRS test program for SBM is set up specifically to study the hydraulic gradient effects at higher level of imposed hydraulic gradient. For the SBM, the experimental program also includes the GCRS tests at higher strain rate. This is to see whether the effects from hydraulic gradient are the same for varying strain rates.

The GCRS test program for SBM covers wide range of hydraulic gradient (in term of normalized excess pore pressure, $\Delta u_e/\sigma'_{v(AVG)}$ of 35 to 65%) and strain rate (0.1%/hr to 3%/hr). Figure 5.30 presents the correction curve for a typical SBM test representing the GCRS simulation with normalized excess pore pressure ($\Delta u_e/\sigma'_v$) of 40%. The correction factor decreases with increasing strain rate because at a higher strain rate, the excess pore pressure from the consolidation becomes more prominent. Figure 5.31 shows the compression curve of a typical GCRS tests for SBM (CRS674)

The analysis of the GCRS tests for SBM can be separated into two sections. The first section includes the GCRS tests with the slow strain rate (0.1%/hr) but with varying imposed hydraulic gradient. The second section includes the GCRS tests with varying strain rate but with approximately the same imposed hydraulic gradient.

5.2.3.1 GCRS Tests with Strain Rate of 0.1%/hr

A series of GCRS tests for SBM are performed at strain rate of 0.1%/hr. This strain rate is selected based on prior experiences to be as slow as possible without causing the secondary compression to interfere with the test. Also at a low strain rate such as 0.1%/hr, the normalized excess pore pressure is relatively low (less than 2% for SBM) and will allow us to observe the effects of imposed gradient with less uncertainty and make interpretation easier.

Figure 5.32 presents the compression curve of the CRS656. The test starts with strain rate of 0.75%/hr until it reaches ε_a of approximately 7.7%. This is done to speed up the test. After the initial loading phase, the strain rate is reduced to 0.1%/hr and is kept constant for approximately 9.5% to establish a well-defined VCL for the strain rate. Then, the gradient is imposed at the base of the specimen. The average normalized excess pore pressure at the base ($\Delta u_b/\sigma'_v$) is approximately 42.4%. During this phase, the strain rate is maintained constant. The GCRS phase continues for approximately

4.5% axial strain. After the GCRS phase, the imposed gradient is removed (base valve is closed) and the test continue as a normal CRS loading with the same strain rate (as shown in the strain rate graph in Figure 5.33).

The compression curve clearly shows that the VCL shifts to the left of the normal VCL (identified as the VCL connecting the VCL from the normal CRS loading phases at 0.1%/hr). The average normalized shift of the VCL ($\Delta\sigma'_v/\sigma'_v$) is approximately 3.6%.

Figure 5.33 presents the strain rate graph for the test. The graph shows that the strain rate is relatively constant through out each phase. Figure 5.34 shows the gradient measured by base pore pressure transducer. The average imposed gradient during phase 2 is approximately 585. The imposed gradient is relatively constant with the maximum gradient of 605 and minimum of 567. Figure 5.35 presents the normalized excess pore pressure graph for the CRS656. The normalized excess pore pressure remains relatively constant for the normal CRS loading phase (5% and 1% for the CRS loading with strain rate of 0.75%/hr and 0.1%/hr, respectively). The normalized excess pore pressure during the GCRS phase starts at approximately 55% and reduces to 34% at the end of the GCRS loading. The average normalized excess pore pressure ($\Delta u/\sigma'_v$) during the GCRS loading is 42.4%. The normalized excess pore pressure is not constant because the test uses manual control hydraulic gradient which keeps the base pore pressure constant throughout the phase.

The results from the GCRS tests are summarized in a graph between the shifts of the VCL ($\Delta\sigma'_v/\sigma'_v$) and the normalized base excess pore pressure ($\Delta u/\sigma'_v$). Figure 5.36 presents the graph from the GCRS tests with strain rate of 0.1%/hr for SBM and 0.2%/hr for MBC. Table 5.3 presents a summary of the GCRS test results with strain rate of 0.1%/hr. The compression curves clearly show that the VCLs shift significantly to the left. The shift increases with increasing imposed hydraulic gradient or normalized base excess pore pressure. The shifts ($\Delta\sigma'_v/\sigma'_v$) range from 5% to 11% when the normalized base excess pore pressures ($\Delta u/\sigma'_v$) increase from 37% to 65%.

5.2.3.2 GCRS Tests with Varying Strain Rate (0.1%/hr to 3%/hr)

A series of GCRS tests are performed with varying strain rate covering strain rate of 0.1%/hr to 3%/hr. The aim is to observe the effect of strain rate on the GCRS tests at comparable imposed hydraulic gradient or normalized base excess pore pressure. The average normalized base excess pore pressure of GCRS tests in this program is approximately 39%. Table 5.4 presents a summary of the GCRS test results with varying strain rate. Based on Table 5.4, it is interesting to see that the VCL shift decreases with increasing strain rate. At strain rate equal to or higher than approximately 1.5%/hr

(based on the interpretation in Figure 5.37), the VCLs are no longer shift relative to the VCL obtained from the standard CRS loading phase.

Figure 5.37 presents a graph between normalized shift of the VCL to the base excess pore pressure ($\Delta\sigma'_v/\Delta u_b$) and strain rate. The normalized shift of the VCL indicates the relative amount of VCL shift ($\Delta\sigma'_v$) to the base excess pore pressure (Δu_b) imposed on the specimen. This normalization helps to generalize the test results for comparison among GCRS tests with different strain rate.

The figure clearly shows that the VCL shift reduces with increasing strain rate. The test results while limited can be described using a linear line for strain rate between 0.1%/hr to 1.5%/hr ($\Delta\sigma'_v/\Delta u = 0$ at $\dot{\varepsilon}$ =1.5%/hr).

5.3 Scaling Effects Study from Oedometer Tests

A series of oedometer tests are performed to study the scaling effects on consolidation behavior of MBC and SBM. The focus of the study is on the differences between the coefficients of consolidation, c_v, obtained using $\sqrt{t}$ and log(t) methods. It is well known that the c_v from $\sqrt{t}$ method is usually much higher than that obtained from the log(t) method. The ratio between c_v from $\sqrt{t}$ method and c_v from log(t) method is usually 1.5±0.5. This observation results in difficulty in selecting the c_v for use in engineering applications. It also equally important indicates a shortcoming in our understanding of the process.

This experimental program aims to investigate the factors that affect the c_v ratio. It should be noted that the time required for each test quadruples with a doubling of drainage height. Therefore, it is not practical to perform tests with very large drainage heights. Instead, the tests are designed to cover drainage heights of 0.6 to 2.35cm (approximately 4 time differences). This allows for higher numbers of tests that can be performed in the same period. Chapter 3 explains the experimental program in detail including important factors that needed to be considered for the tests.

There are three main variables in the tests: 1) drainage heights (H_d), 2) time of secondary compression of the previous step (t_{sec}), and 3) soil types. Specimen saturation is also another concern in this research. A few tests in the series utilize a modified Trautwein CRS cell to back pressure saturation of the specimen to 4 kg/cm^2. It is found that back pressure using Trautwein CRS cell does not have any impact on the test results.

The following sections explain the oedometer test results in detail. The interpretation of the oedometer tests follow standard procedures used at MIT. Based on the measured vertical deformation and recorded loading time, graphs between the vertical strain (or specimen height) and $\sqrt{t}$ and a graph between vertical deformation (or specimen height) and log(t) can be created. The $c_v(\sqrt{t})$ and c_v(log t) can be obtained from the graph using the graphical methods presented in section 2.3.1 and 2.3.2.

5.3.1 Maine Blue Clay (MBC)

There are seven oedometer tests for MBC. Table 5.5 presents the summary of the overview of the oedometer test for MBC.

The Oed111 serves as a base line case for other oedometer tests. The test results are plotted in two main graph including 1) compression curve and 2) c_v analysis graph. The compression curve plot is used to compare the consolidation behavior of each specimen. The c_v analysis graph is the graph between c_v ratio $[c_v(\sqrt{t})/c_v(\log(t))]$ and time of secondary compression of the previous step (t_{sec}). The $c_v(\sqrt{t})$ and c_v(log t) for each load increment are obtained based on the square root of time and logarithm of time methods as outlined in the chapter 2.

Figure 5.38 presents the compression curve for the Oed111. The test consists of 8 load increments as shown in the Table 5.6. The specimen is loaded with load increment ratio (LIR) of 1. The load is maintained for approximately 24 hr or until the primary consolidation process is completed and a large enough portion of secondary compression is established. It is necessary to leave the specimen under load for a period of time after the end-of-primary for the interpretation of c_v based on log(t) method. The research focuses on the normally consolidated range, therefore, each oedometer test can yield only 3 or 4 useable loading increments.

Figure 5.39 presents the consolidation curve for the Oed111 with load increment of 2-4 ksc in the axial strain (ε_a) versus log(t) space. The time to end-of-primary (t_{EOP}) and specimen height at the end-of-primary (H_{EOP}) are obtained from the intersection of the two lines (line A and B) as shown in the Figure 5.39. The H_{EOP} is especially important since it is required in order to determine the specimen height at 50% consolidation (H_{50}) for the calculation of c_v based on logarithm of time method. The c_v based on the square root of time method is obtained from the consolidation curve plotted in the specimen height and $\sqrt{t}$ space as shown in the Figure 5.40. The calculation of the $c_v(\sqrt{t})$ and c_v(log t) are obtained from the equation 2.1 and 2.2 in the chapter 2, respectively.

Figure 5.41 presents the summary end-of-primary (EOP) compression curves of the MBC oedometer tests. It shows that the compression curves of the tests are in the same approximate region. The preconsolidation stresses are slightly different from specimen to specimen. The compression ratios are very similar for all tests (±15%).

The analysis of c_v ratio can be performed using the c_v analysis graph as shown in the Figure 5.42. There are two important things that can be interpreted from the graph. First, if the consolidation behavior of soil, mainly the c_v ratio, is dependent on the time of secondary compression of the previous step, the effect should be clearly shown on the graph. Second, the graph can clearly show whether the c_v ratio is dependent on the drainage heights provided that the drainage height of each test is clearly marked. Table 5.6 presents the summary of the oedometer test results for MBC.

Based on the Figure 5.42, it is clear that the time of secondary compression of the previous step has no effect on the c_v ratio for MBC. The c_v ratio remains relatively constant even when comparing the results with t_{sec} of 4 hr to 51 hr from comparable tests. The c_v ratios from the seven tests range from 1.22 to 1.50. The results show that the c_v ratio are not dependent on the drainage heights. A clear example can be obtained by comparing the results from Oed 118 (H_d = 2.35 cm) and Oed 120 (H_d = 0.6 cm). The c_v ratio from both tests are comparable (approximately 1.37 and 1.27 for Oed 118 and Oed 120, respectively).

5.3.2 San Francisco Bay Mud (SBM)

The oedometer tests for SBM consist of five tests covering drainage heights of 0.6 cm, 1.18 cm, and 2.35 cm. Table 5.7 presents the summary of the oedometer tests. Figure 5.33 presents the summary of compression curves from SBM oedometer tests. It shows that the compression curves of the tests are in the same approximate region. It is also interesting to see that the SBM compression curves are concave up at higher effective stress level, i.e., Compression Ratio (CR) decreases with increasing σ'_v. Figure 5.43 also shows that the SBM is much more compressible than the MBC (SBM $\varepsilon_{a(max)} \sim 47\%$ compare to MBC $\varepsilon_{a(max)} \sim 13\%$). The average axial strain at σ'_v of 12 kg/cm^2 of SBM is approximately 44%. This is much larger than the average axial strain of MBC at the same vertical effective stress (11%).

It should also be noted that the c_v from different drainage height tests differ significantly for some specimens. This is most likely caused by the variation in soil specimens obtained from different tube samples. The c_v of the specimen obtained from the same tube sample is expected to be similar while the c_v of the specimens from different

sample tube can be significantly different. It is also possible that there are other factors affecting the c_v values. However, that is beyond the scope of this research.

Figure 5.44 shows the c_v analysis graph for SBM. It is clear from Figure 5.44 that the time of secondary compression of the previous step has no effect on the c_v ratio of SBM. Even with the t_{sec} of 6 time differences (8 hr versus 48hr), there is no observable difference in c_v ratio from the test.

The c_v ratio, however, shows a clear dependence on the drainage height. The Figure 5.44 can be separated into three zones representing the results from specimens with drainage height of 0.6, 1.18 and 2.35 cm, respectively. The average c_v ratio from SBM oedometer tests can be summarized as follow.

1) The c_v ratios from the tests with the largest drainage height (H_d = 2.35 cm) range from 1.20 to 1.44 with the average c_v ratio of approximately 1.32.
2) The c_v ratios from the tests with the middle drainage height (H_d = 1.18 cm) range from 1.53 to 1.65 with the average c_v ratio of approximately 1.59.
3) Finally, The c_v ratios from the tests with the middle drainage height (H_d = 0.6 cm) range from 1.72 to 1.95 with the average c_v ratio of approximately 1.84.

It is clear that the c_v ratio increases with decreasing drainage heights. It is very interesting that the c_v ratio can be separated into three zone clearly based on only the drainage height. The tests offer vital insight into the relationship between c_v ratio and drainage height. Comparing the results from SBM and MBC tests, it is also very apparent that the soils behave drastically different. While SBM exhibit obvious drainage height dependent behavior (in term of c_v ratio), the MBC show no dependency on the drainage height at all. Table 5.8 presents the summary of the oedometer test results for SBM. It is also clear that the secondary compression is not the cause of the c_v ratio.

5.4 Oedometer Simulations

The oedometer simulations are performed on both MBC and SBM covering a typical behavior for each soil. The simulation program focuses on theoretical study of scaling effects, i.e., varying H_d, on c_v ratio. The program offers an effective and relatively simple analytical tool to study the scaling effects. Chapter 4 presents the detailed implementation of the program.

5.4.1 Summary of the Simulation Program

There are two main parts of the simulation program including

1) Parametric studies of drainage height (H_d), coefficient of consolidation (c_v), Hydraulic Conductivity (k).
2) Simulation of oedometer tests for MBC and SBM.

The parametric studies are performed, in part, to test the program mechanisms and to see the effects of each parameters on the predicted c_v ratio. Figure 5.45 to 5.47 present typical simulation results for parametric studies of H_d, c_v, and k respectively. Table 5.9 presents the summary of input parameters of oedometer simulation for the parametric studies.

The most interesting results of the parametric studies are the H_d simulations. The results, shown in the Figure 5.45(a), clearly show that the c_v ratio decreasing with increasing drainage height. This trend is consistent with the oedometer test program presented in the section 5.3. Figure 5.45(b) presents the same result plotted in the semi-logarithm scale (c_v ratio versus log(H_d). The figure indicates that the relationship between the c_v ratio and log(H_d) can be approximated by a linear equation as shown in the Figure 5.45(b).

Figure 5.46 presents the c_v ratio plot with three input c_v values. The figure shows that increasing input c_v leads to increasing in the predicted c_v ratio. Figure 5.47 presents the c_v ratio graph with three different initial hydraulic conductivity (k_0). It clearly shows that the c_v ratio is increasing with decreasing k_0.

Figure 5.48 and 5.49 present the comparison of consolidation curves, in $\sqrt{t}$ and log(t) space, respectively, between the Oed112 test (SBM) result and the simulation result. The figures clearly show that the shapes of the simulated consolidation curve very closely match that of the Oed112. The most notable differences are 1) the simulated curves are above the laboratory curves and 2) the simulated curves cannot capture the secondary compression portion of the curve (the simulation does not include the secondary compression). It is remarkable that a relatively simple simulation program can accurately and effectively capture the consolidation behavior of soft clays under an oedometer test. The predicted $c_v(\sqrt{t})$ is also higher than the predicted c_v(log t) which is consistent to the test results. The predicted $c_v(\sqrt{t})$ is 0.00178 cm^2/s compare to the $c_v(\sqrt{t})$ of 0.00182 cm^2/s from the Oed112 test. The predicted c_v(log t) is 0.00120 cm^2/s compare to the c_v(log t) of 0.00113 cm^2/s from the Oed112 test.

5.4.2 Representative Coefficient of Consolidation

The oedometer simulation can be used to obtain a representative coefficient of consolidation (c_v(rep)). The results from an oedometer test yields two different c_v based on the $\sqrt{t}$ and log(t) methods. Instead of choosing a c_v from either one of the method or using an average values, a representative c_v can be objectively obtained based on the simulation. This section explains the concept and methodology on obtaining $c_{v(rep)}$ for a soil.

To objectively obtain a representative c_v, a simulation can be performed with an input c_v for a drainage height (H_d). This input c_v is the representative c_v for this simulation. The simulation also yields $c_v(\sqrt{t})$ and c_v(log(t) based on the square root of time and logarithm of time methods. A series of oedometer simulations is performed with a set of input parameters (see Table 5.10) for the summary of the input parameters) covering drainage height of 0.1 to 100 cm. The simulation results can be studied based on the ratio of c_v(rep)/c_v(log t)) c_v(rep)/$c_v(\sqrt{t})$, and finally $c_v(\sqrt{t})/c_v$(log t) versus drainage height.

Based on the simulation results, a ratio between c_v(rep)/c_v(log t) can be plotted versus drainage height. Figure 5.50 presents the graph between c_v(rep)/c_v(log t) and drainage height. Figure 5.51 shows the same graph plotted in a semi-logarithm scale [c_v(rep)/c_v(log t) versus log(H_d)]

Figure 5.50 shows that at the drainage height of 0.1cm, the c_v(rep)/c_v(log t) ratio is approximately 1.1. This c_v(rep)/c_v(log t) ratio decreases to approximately 1.03 at Hd equal to 100cm. the ratio of c_v(rep)/c_v(log t) decreases rapidly with increasing drainage height at the initial and slow down once the drainage height is above 2 cm. Base on the Figure 5.51, the relationship between c_v(rep)/c_v(log t) and log(H_d) can be represented by a linear relationship.

Figure 5.52 presents a graph between c_v(rep)/$c_v(\sqrt{t})$ versus H_d. Figure 5.53 shows the same graph in a semi-logarithm scale [c_v(rep)/$c_v(\sqrt{t})$ versus log(H_d)). The c_v(rep)/$c_v(\sqrt{t})$ is 0.83 at the drainage height of 0.1 cm. This ratio increases to 0.9 at the drainage height of 100 cm. The results from the ratio of c_v(rep)/c_v(log t) and c_v(rep)/$c_v(\sqrt{t})$ confirmed that the differences between the $c_v(\sqrt{t})$ and c_v(log t) decrease with increasing drainage heights. Essentially, these simulation results indicate that the ratio of $c_v(\sqrt{t})/c_v$(log t) is approaching 1.0 when the drainage height becomes very large. This is confirmed by the Figure 5.54 presenting the graph between $c_v(\sqrt{t})/c_v$(log t) and drainage height. At the drainage height of 0.1cm, the $c_v(\sqrt{t})/c_v$(log t) is 1.33. This ratio decreases with increasing drainage height to approximately 1.12 at the drainage height of 100cm. Figure 5.55 presents the graph between the c_v ratio

[$c_v(\sqrt{t}\,)/c_v$(log t)] and the log(H_d). The relationship can be approximated by a linear equation as shown in the figure.

Based on the graph between c_v(rep)/c_v(log t) versus drainage heights, we can obtain a c_v(rep) objectively based on a laboratory test results. With a known c_v(log t) and H_d, the c_v(rep) can be obtained and used for consolidation calculation. This c_v(rep) is a better representative c_v than choosing c_v from either $c_v(\sqrt{t}\,)$, c_v(log t), or the average of the $c_v(\sqrt{t}\,)$ and c_v(log t).

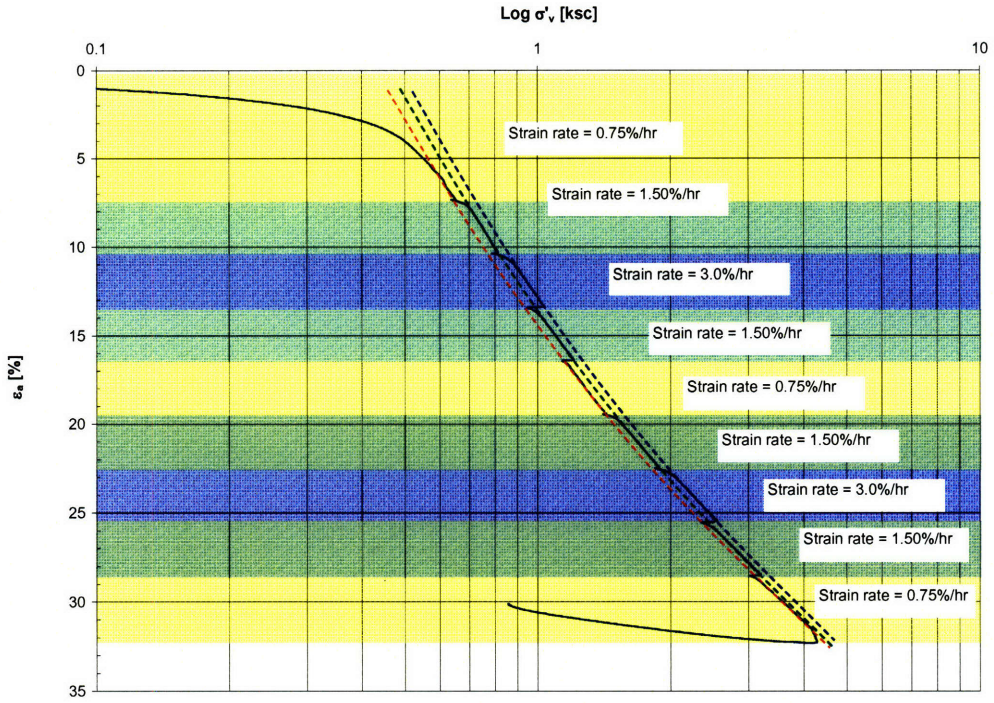

Figure 5.1 Compression curve from a strain rate sensitivity test (CRS691) for SBM covering strain rate of 0.75%/hr, 1.5%/hr, and 3%/hr

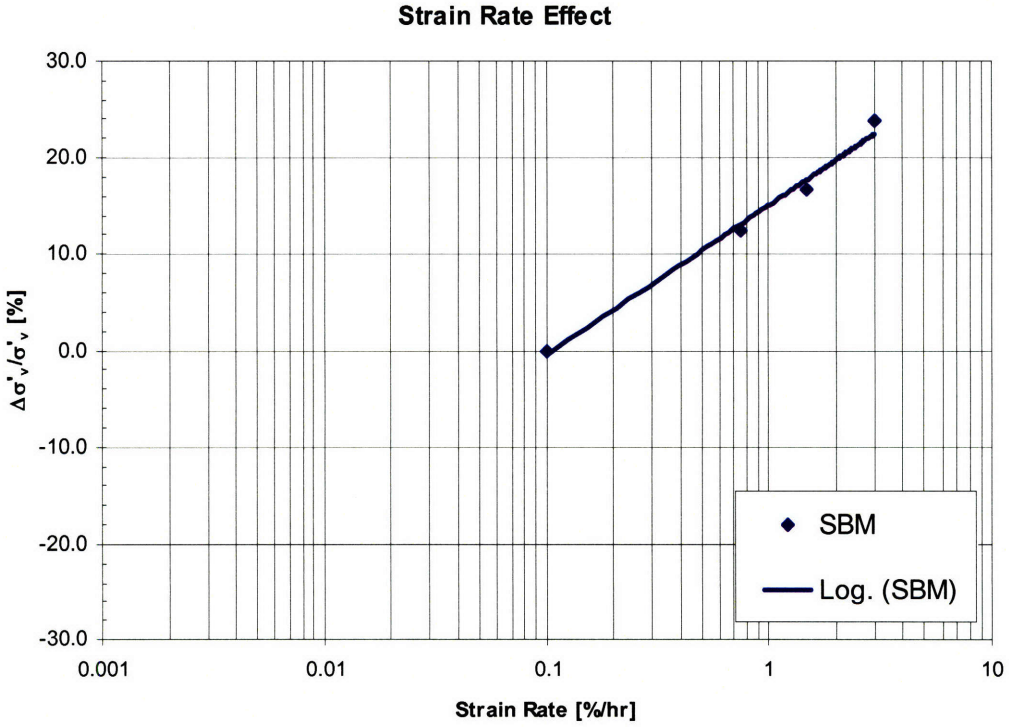

Figure 5.2 Graph between the shifts in the VCL ($\Delta\sigma'_v/\sigma'_v$) and strain rate for SBM

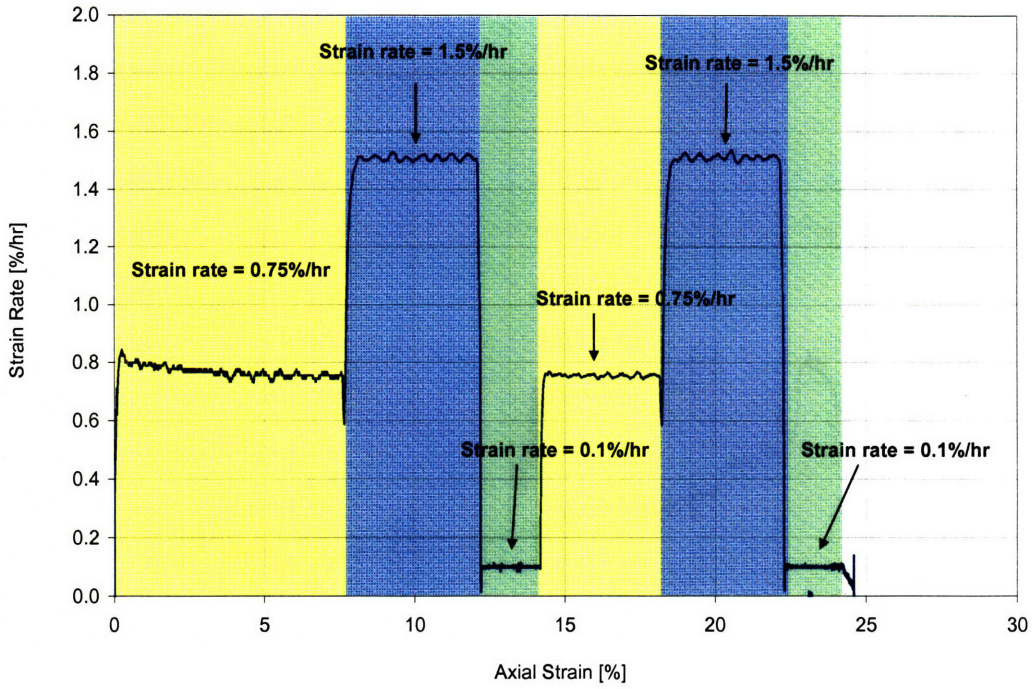

Figure 5.3 Compression curve from a strain rate sensitivity test (CRS672) for SBM covering strain rate of 0.1%/hr, 0.75%/hr, and 1.5%/hr

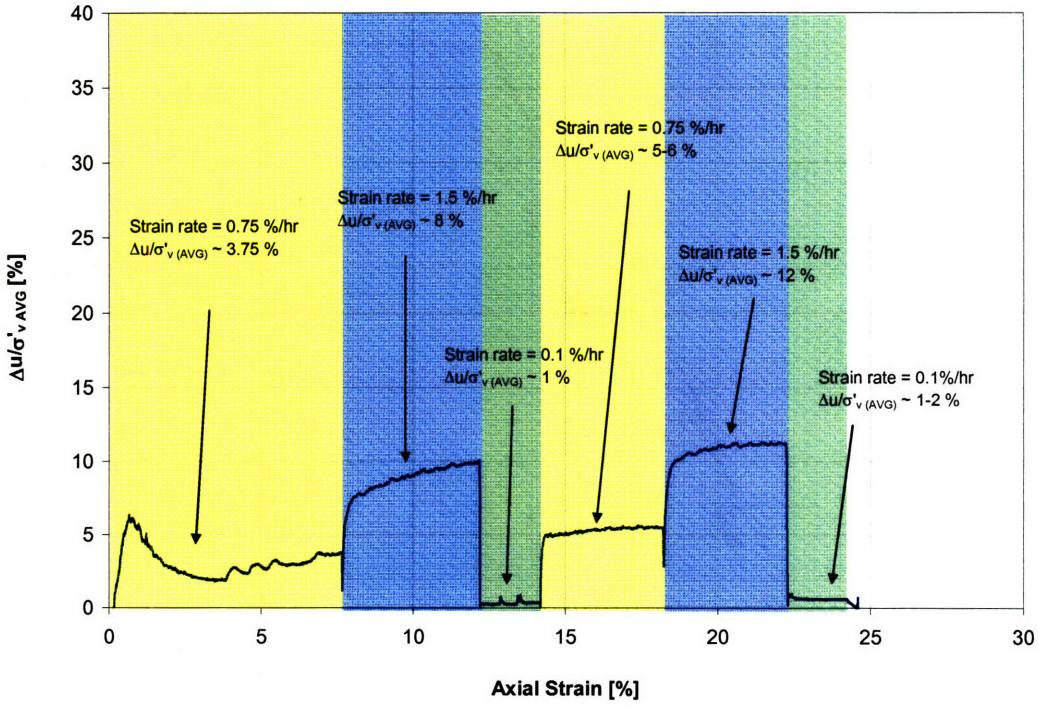

Figure 5.4 Normalized excess pore pressure ($\Delta u_e/\sigma'_v$) versus axial strain for CRS672

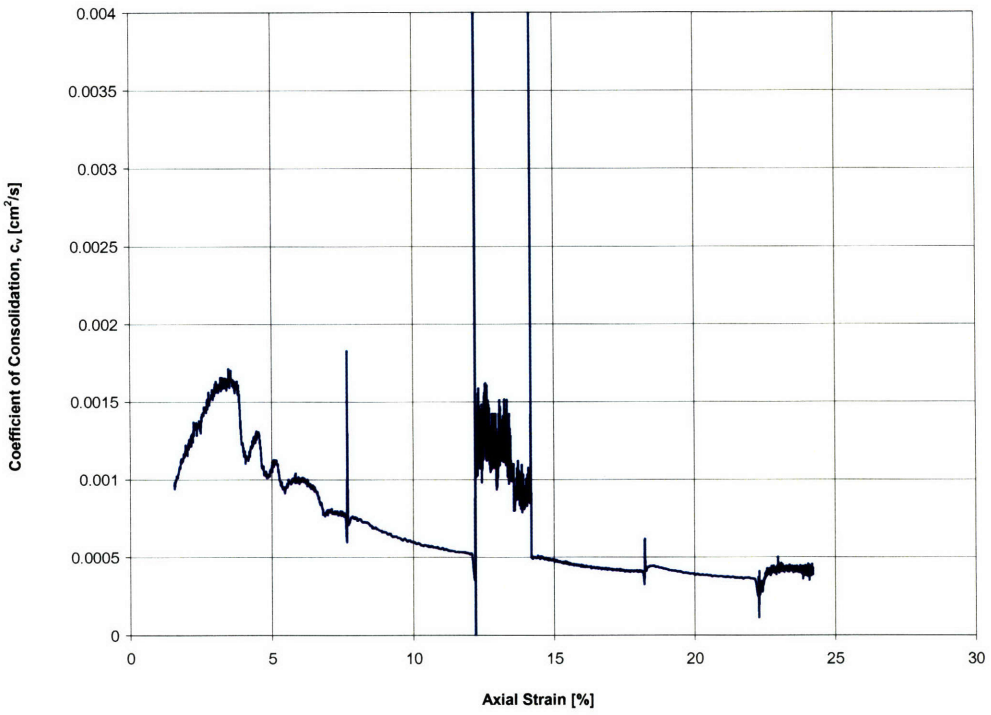

Figure 5.5 Graph between c_v and axial strain for CRS672

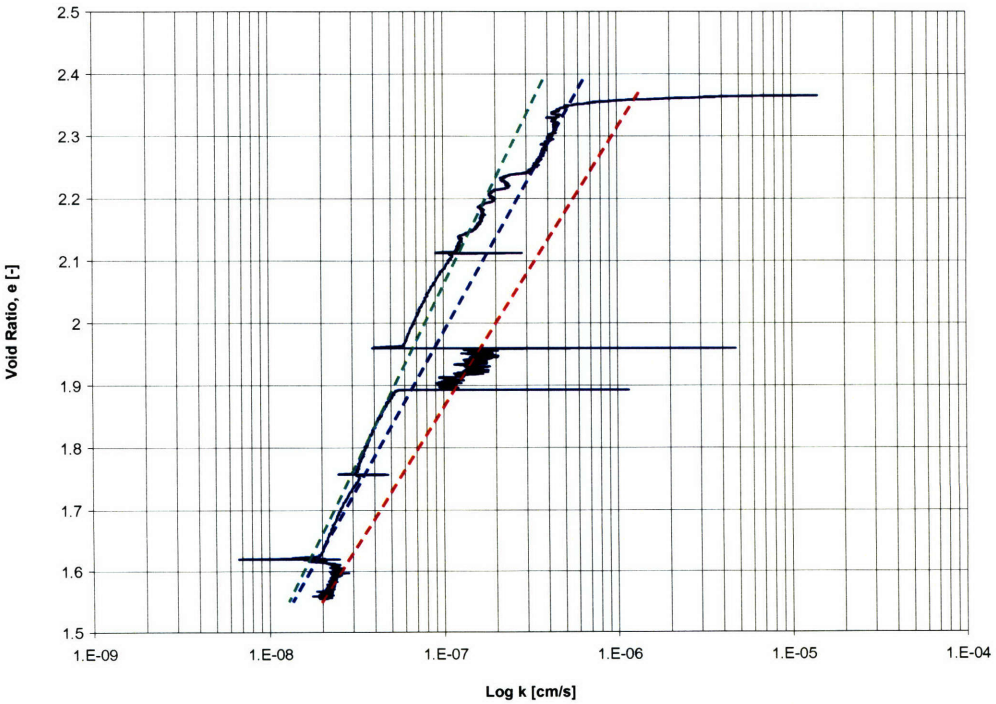

Figure 5.6 Graph between e and log k for CRS672

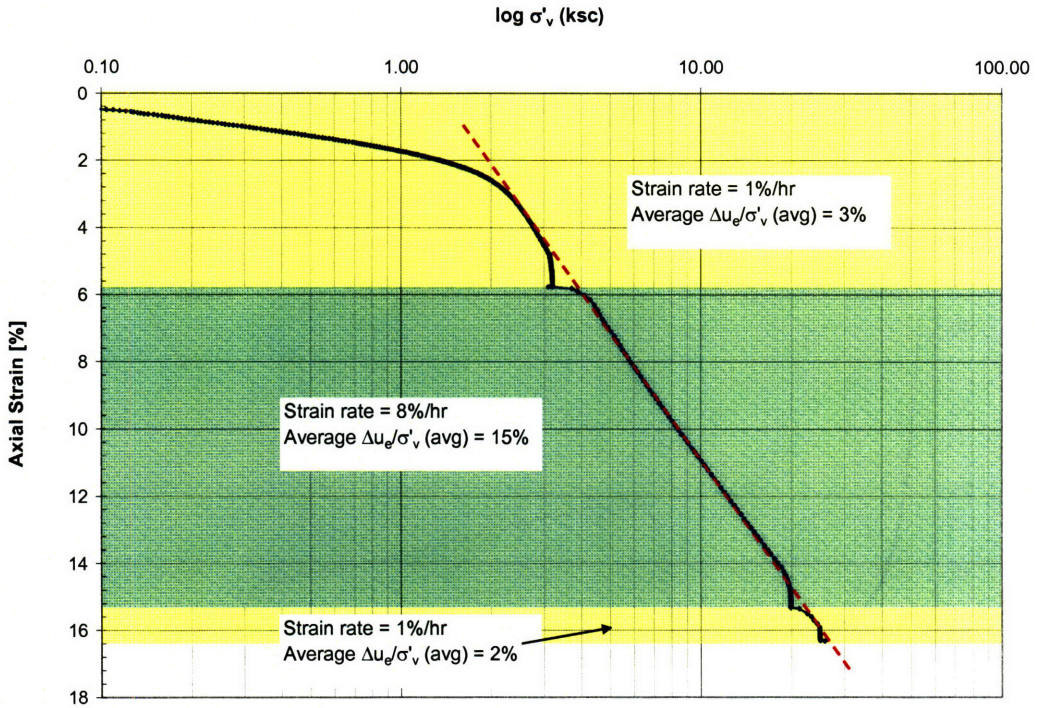

Figure 5.7 MBC compression curve from a strain rate sensitivity test (CRS594) covers strain rate of 1%/hr and 8%/hr (data from Chartier, 2004)

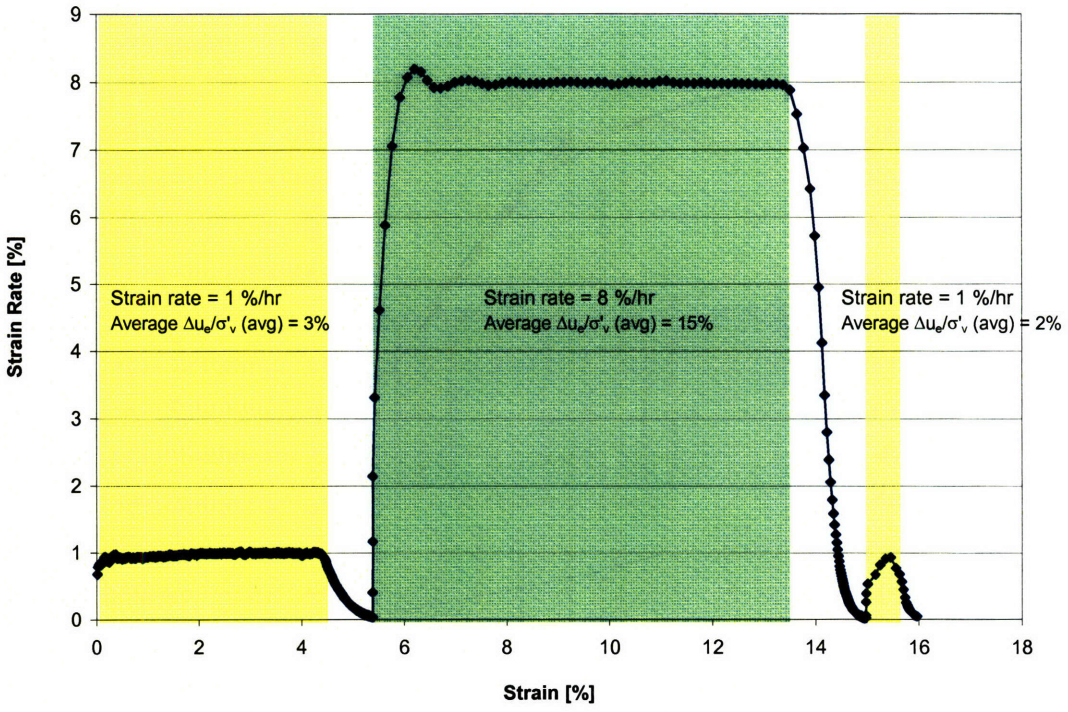

Figure 5.8 Strain rate curve from MBC strain rate sensitivity test, CRS594 (data from Chartier, 2004)

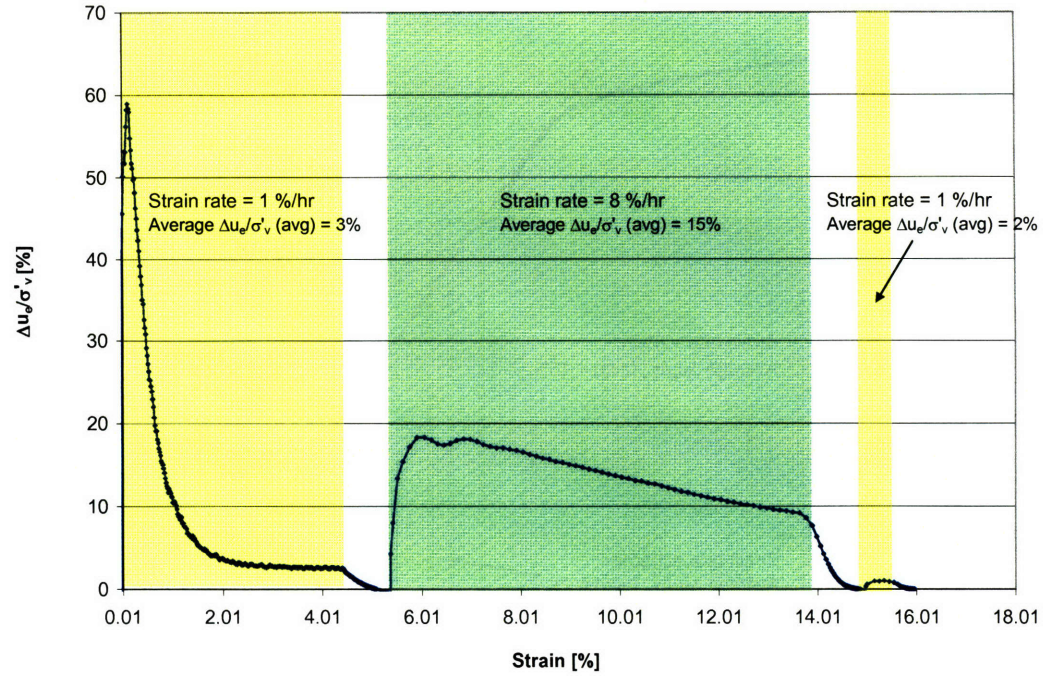

Figure 5.9 Normalized excess pore pressure graph for MBC strain rate sensitivity test, CRS594 (data from Chartier, 2004)

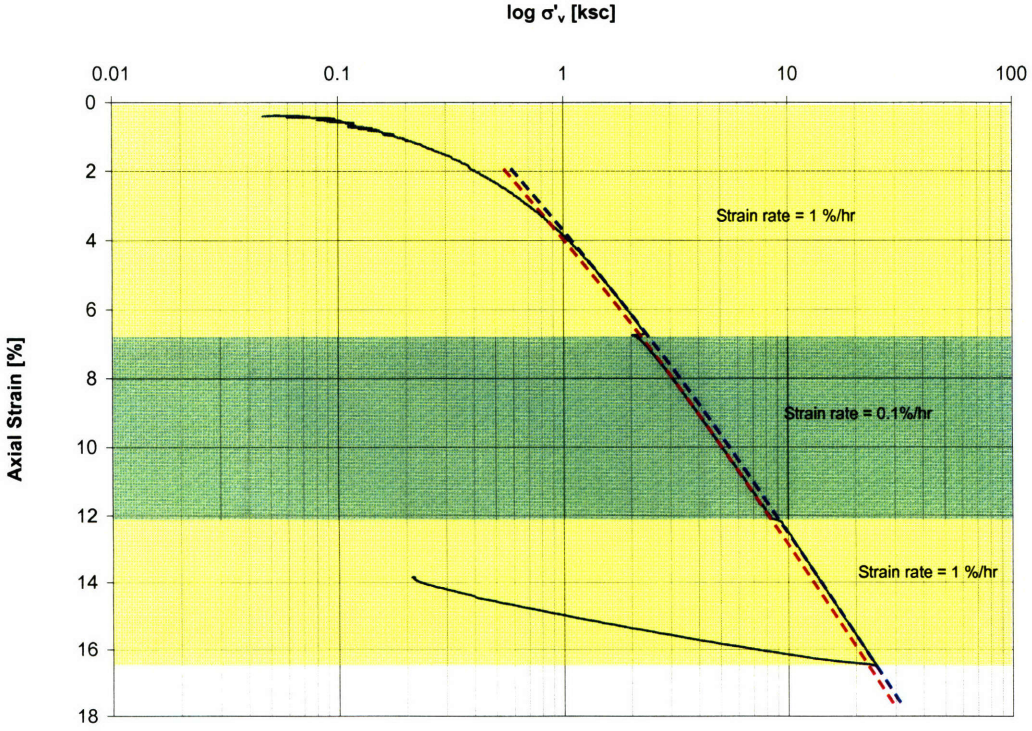

Figure 5.10 Compression curve from CRS862

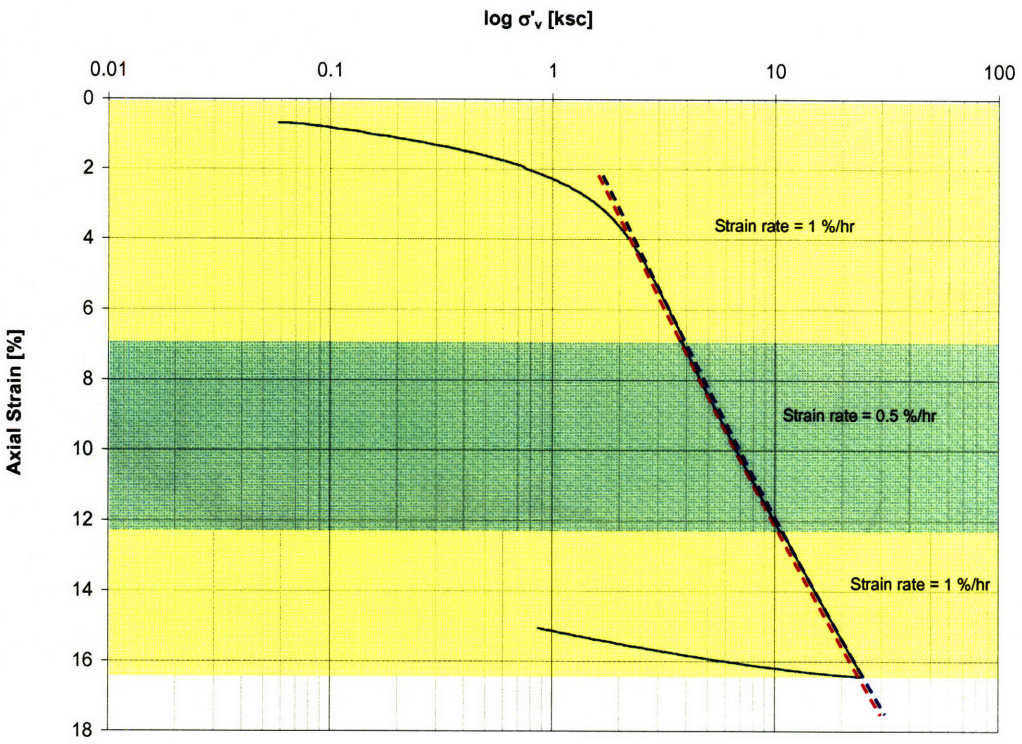

Figure 5.11 Compression curve for CRS860

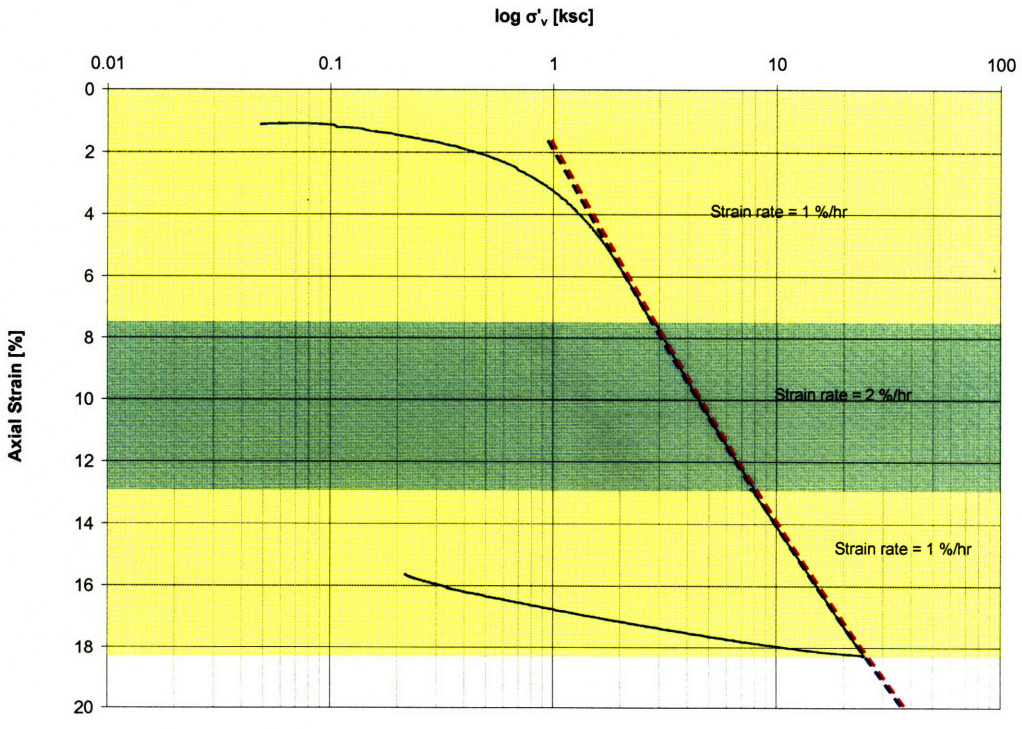

Figure 5.12 Compression curve for CRS861

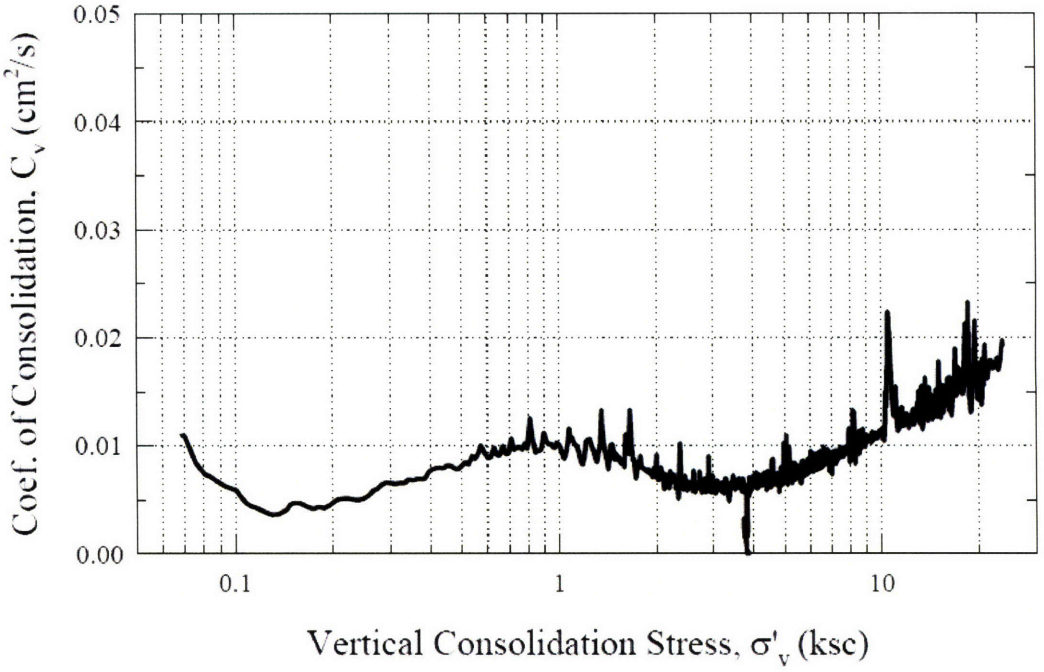

Figure 5.13 Graph of c_v versus log σ'_v (after Germaine, 2007)

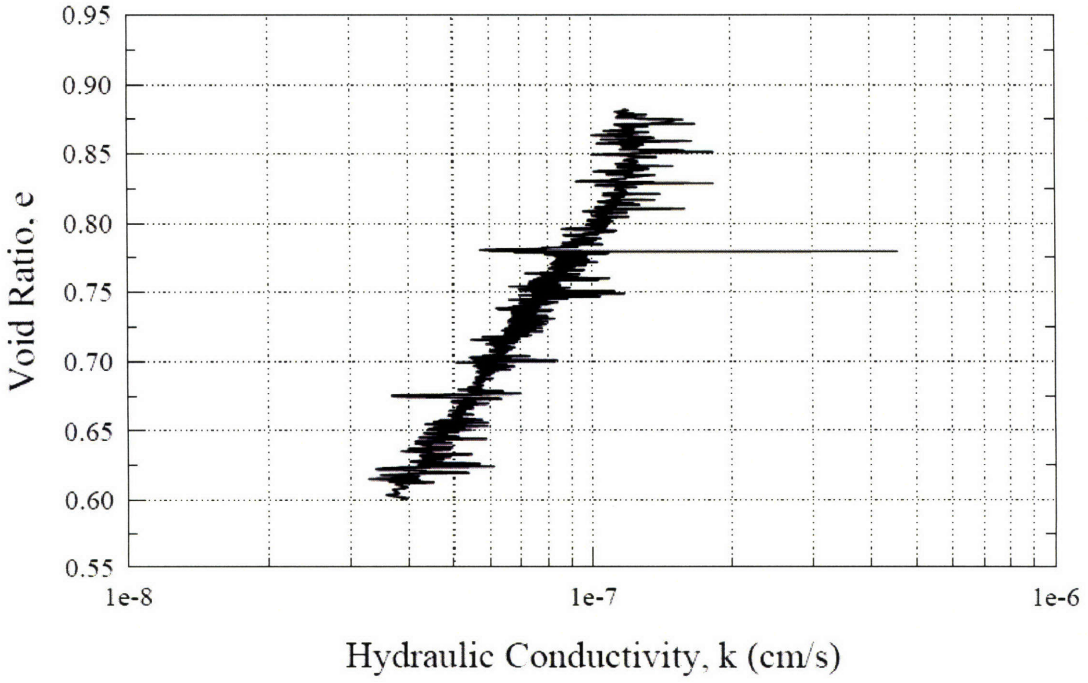

Figure 5.14 Graph between e and log k (after Germaine, 2007)

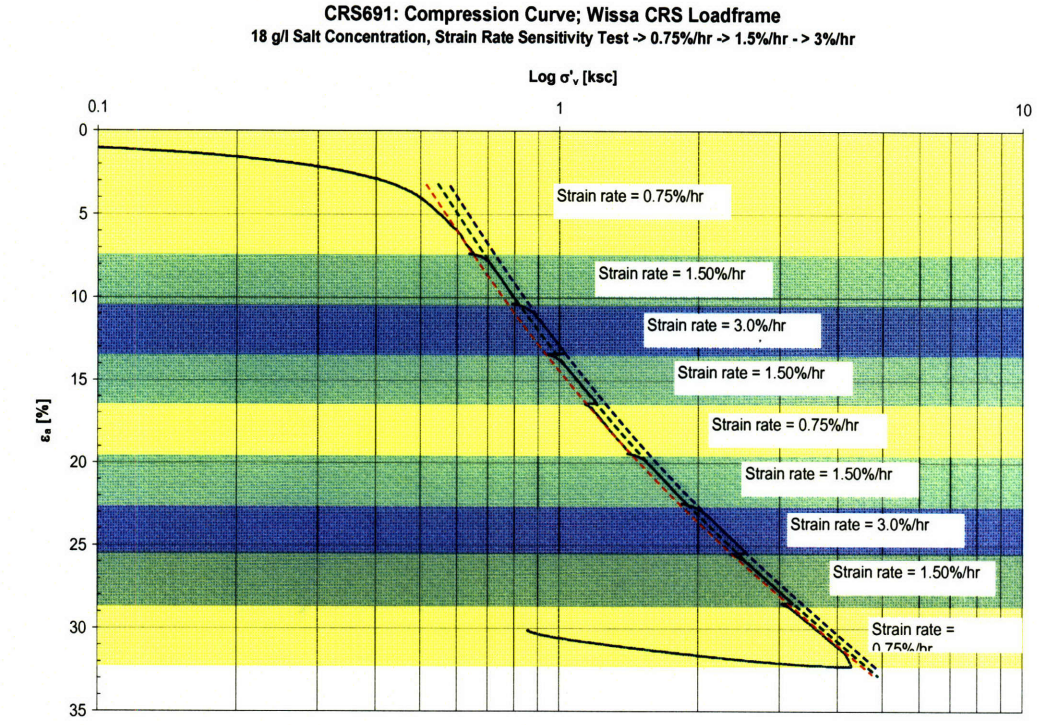

Figure 5.15 Compression curve from a strain rate sensitivity test (CRS691) for SBM covering strain rate of 0.75%/hr, 1.5%/hr, and 3%/hr

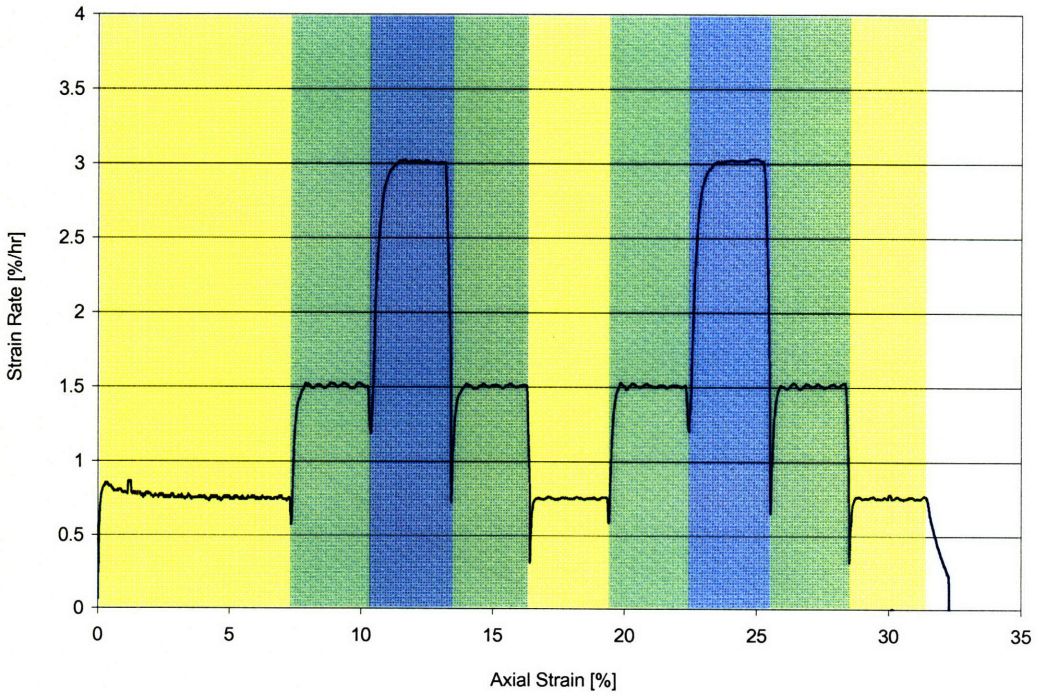

Figure 5.16 Strain rate graph from a strain rate sensitivity test (CRS691) for SBM covering strain rate of 0.75%/hr, 1.5%/hr, and 3%/hr

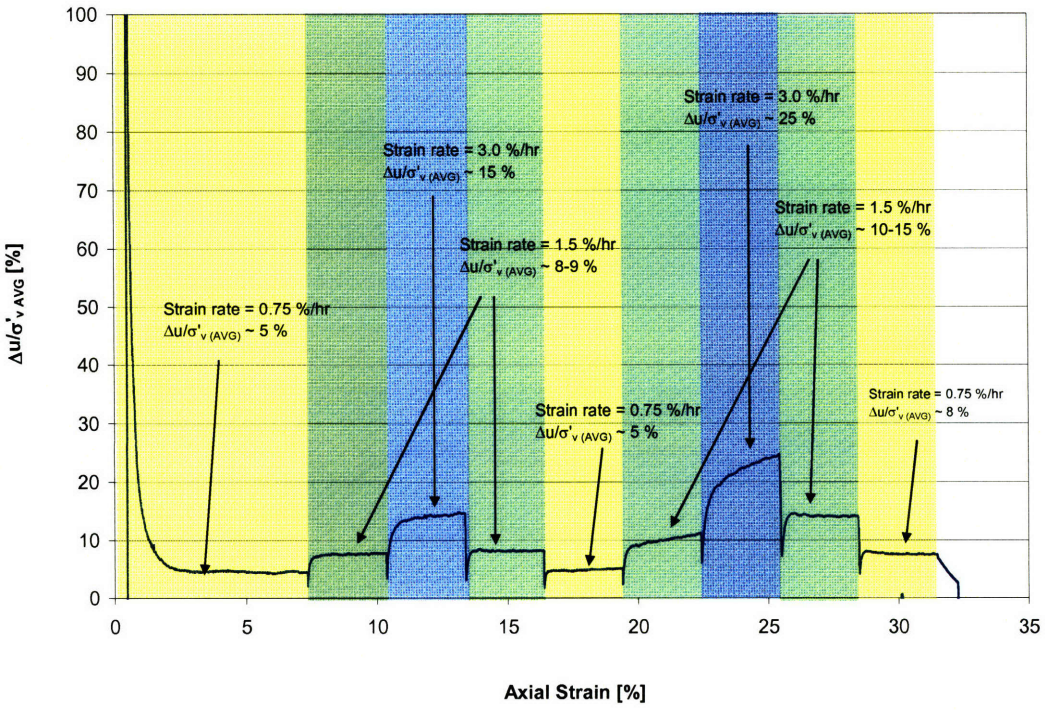

Figure 5.17 Normalized excess pore pressure graph from a strain rate sensitivity test (CRS691) for SBM covering strain rate of 0.75%/hr, 1.5%/hr, and 3%/hr

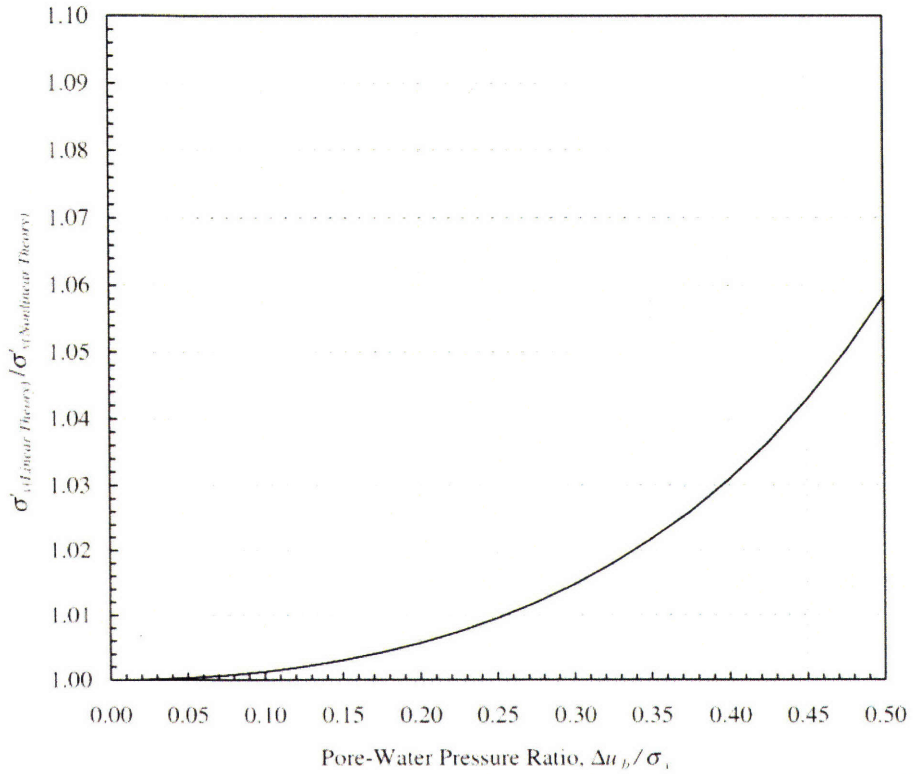

Figure 5.18 Graph between σ'_v(linear)/σ'_v(nonlinear) and $\Delta u_b/\sigma'_v$ (after Gonzalez, 2000).

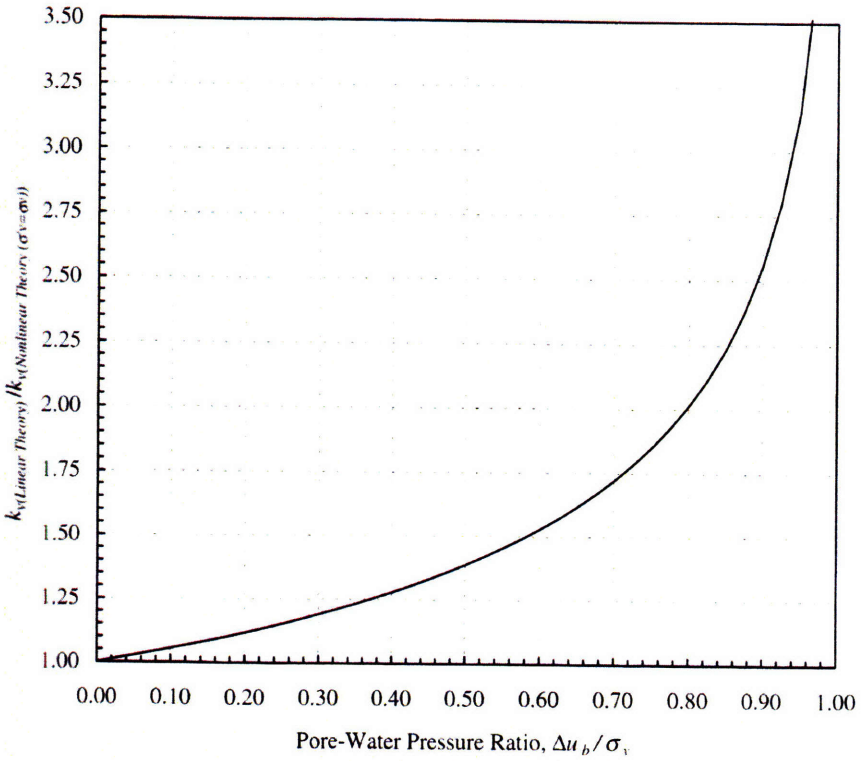

Figure 5.19 Graph between k(linear)/k(nonlinear) and $\Delta u_b/\sigma'_v$ (after Gonzalez, 2000)

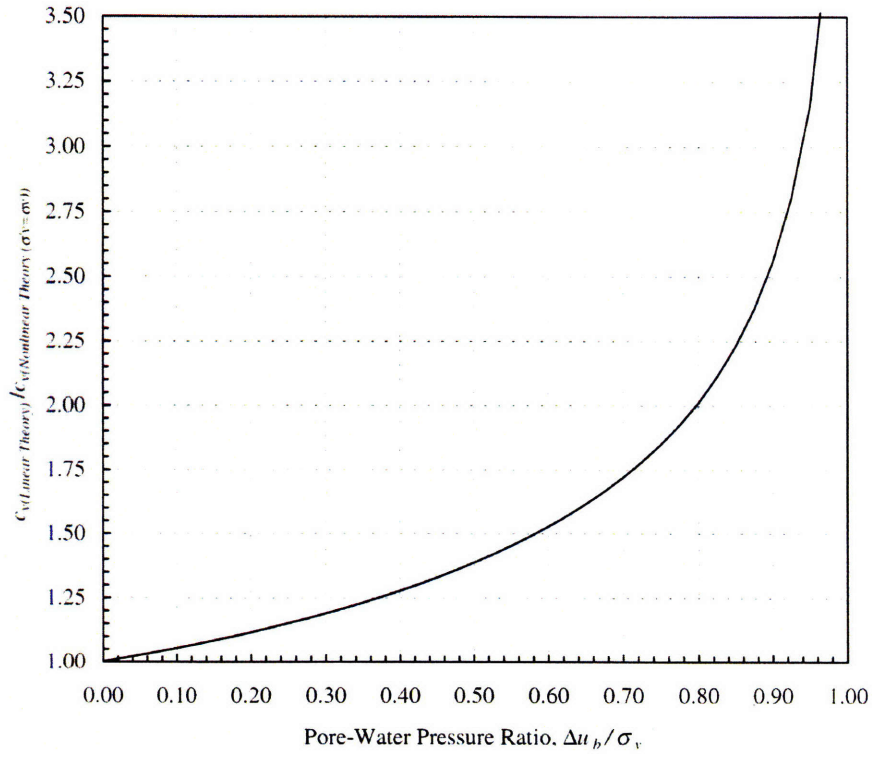

Figure 5.20 Graph between c_v(linear)/c_v(nonlinear) and $\Delta u_b/\sigma'_v$ (after Gonzalez, 2000)

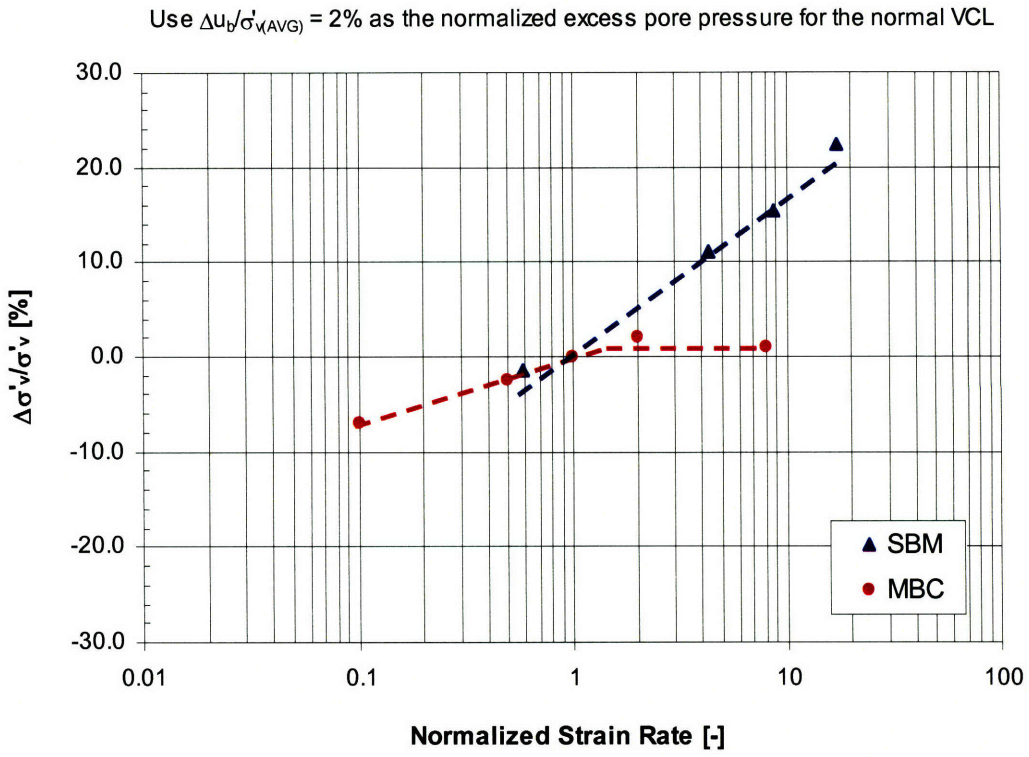

Figure 5.21 Strain rate sensitivity graph for SBM and MBC

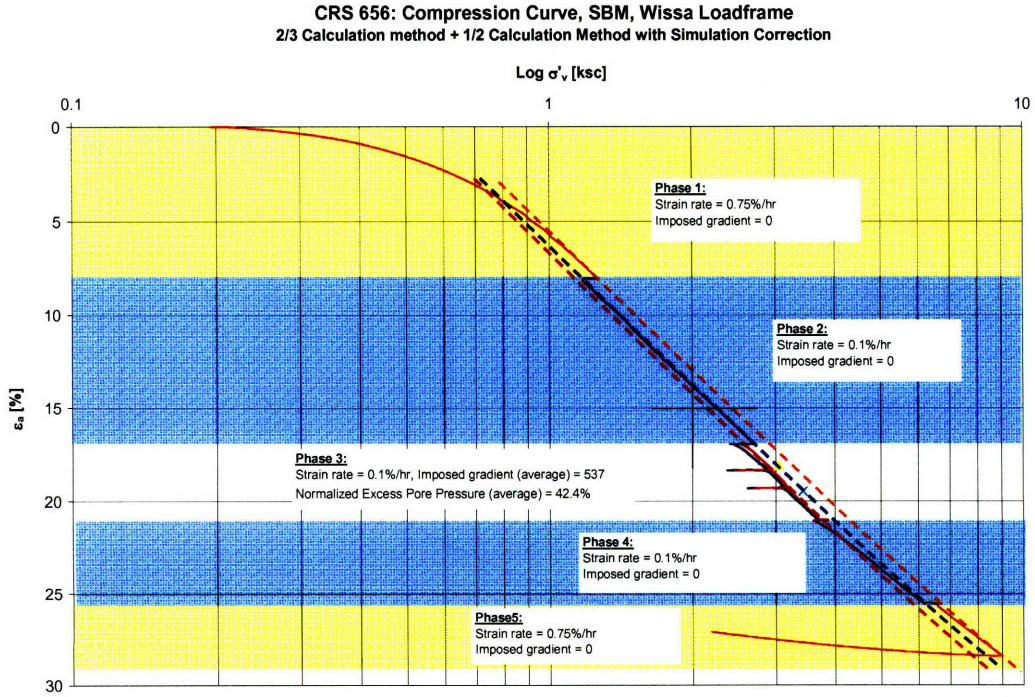

Figure 5.22 Compression curve from GCRS test with strain rate of 0.1%/hr for SBM (CRS656)

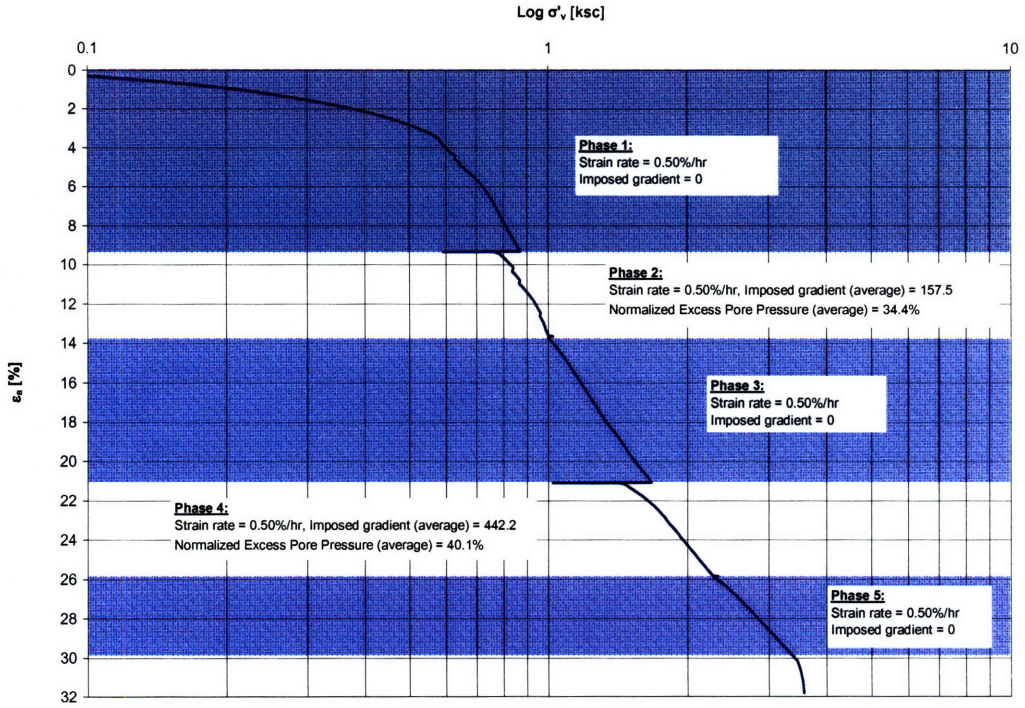

Figure 5.23 Compression curve based on Wissa linear CRS theory (CRS680)

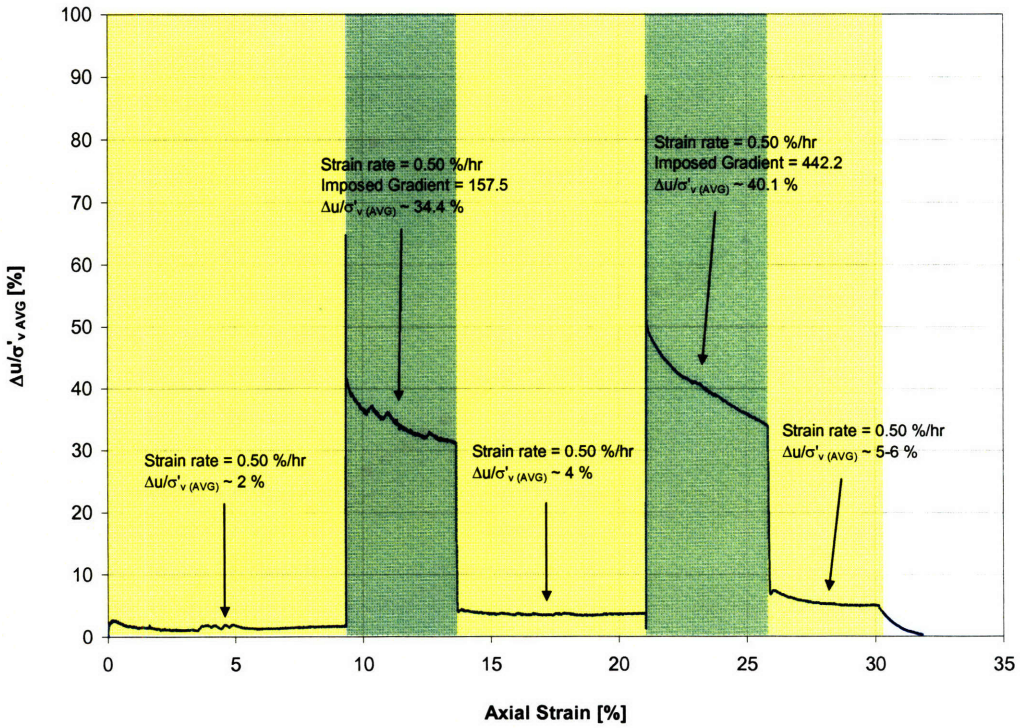

Figure 5.24 Normalized base excess pore pressure versus axial strain

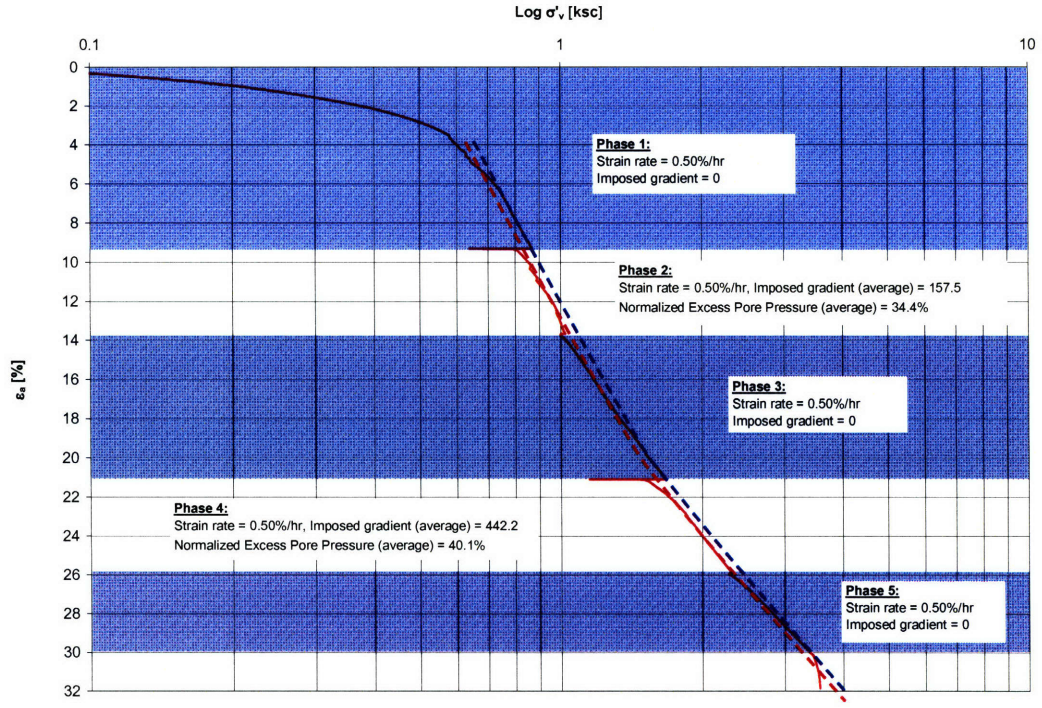

Figure 5.25 Compression curve based on the predicted average excess pore pressure from GCRS simulation (CRS680)

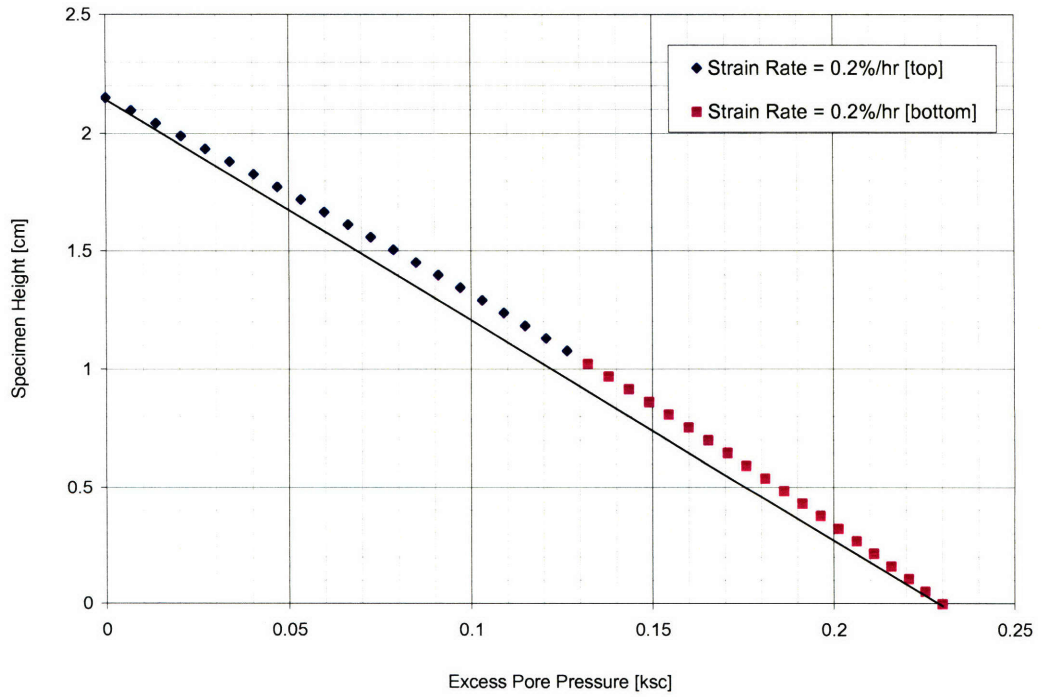

Figure 5.26 Predicted pore pressure distribution for MBC with strain rate of 0.2%/hr and normalized excess pore pressure ($\Delta u_e/\sigma'_v$) of 2%

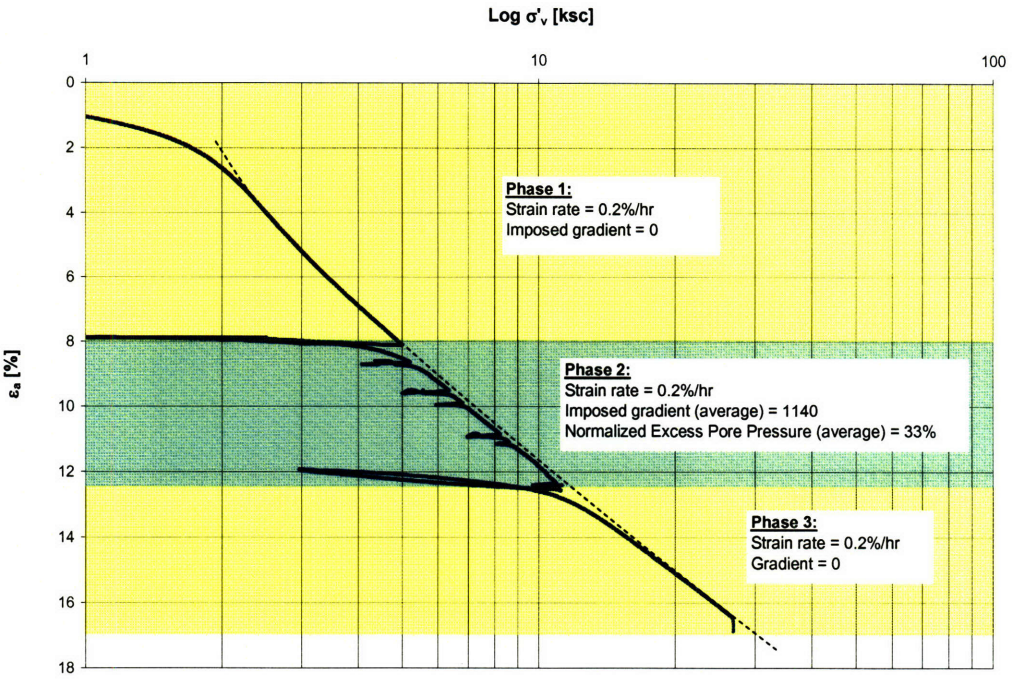

Figure 5.27 Compression curve from CRS652 showing the effect of hydraulic gradient on the consolidation behavior of MBC

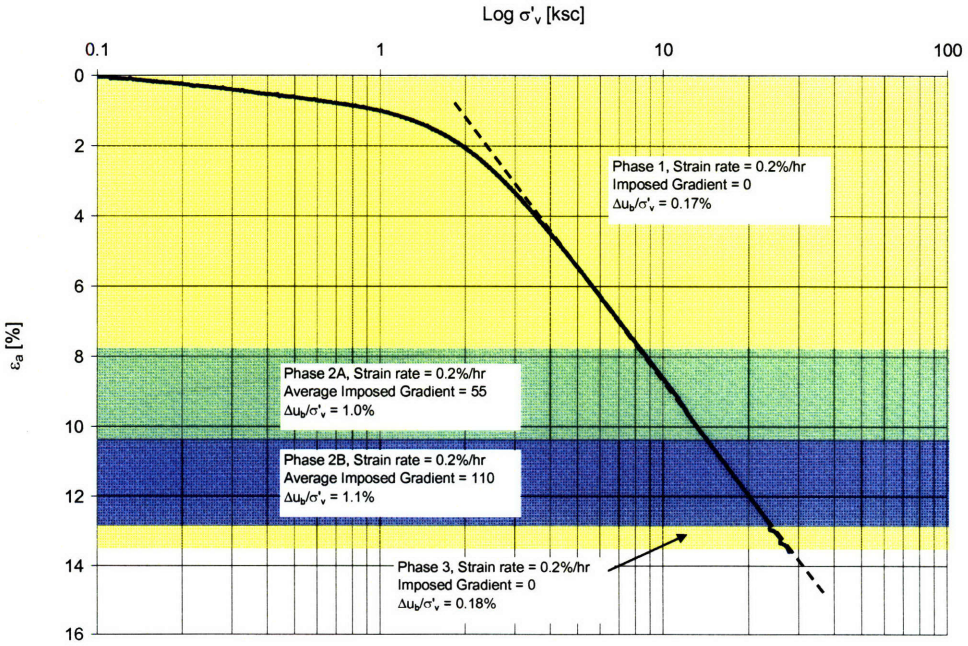

Figure 5.28 Compression curve from GCRS test with strain rate of 0.2%/hr for MBC (CRS640)

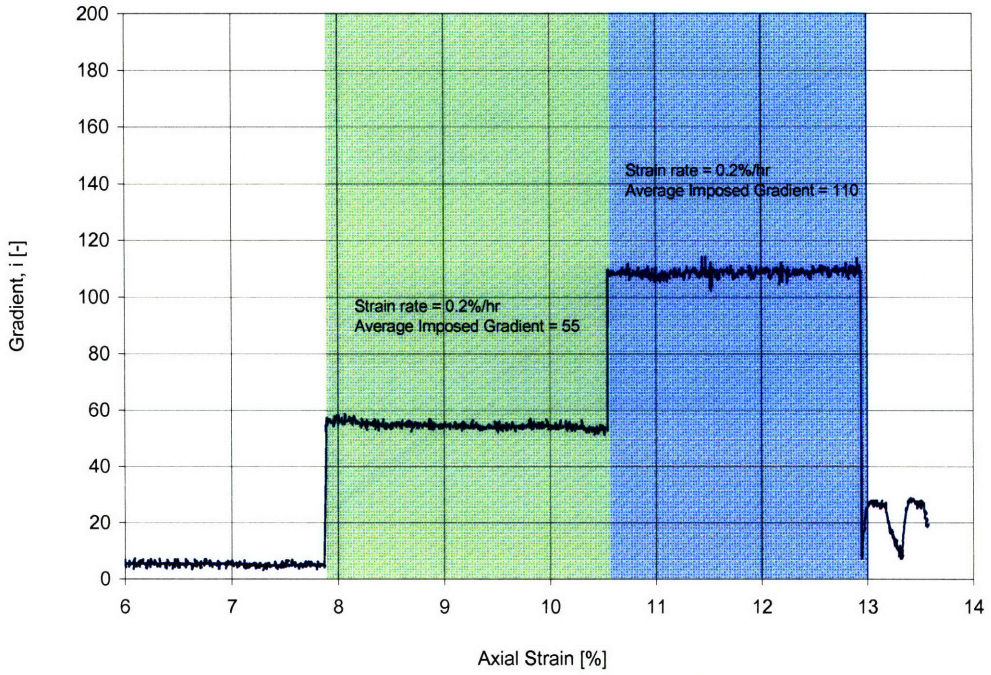

Figure 5.29 Hydraulic gradient versus axial strain during the imposed gradient CRS phase of the CRS640 (MBC)

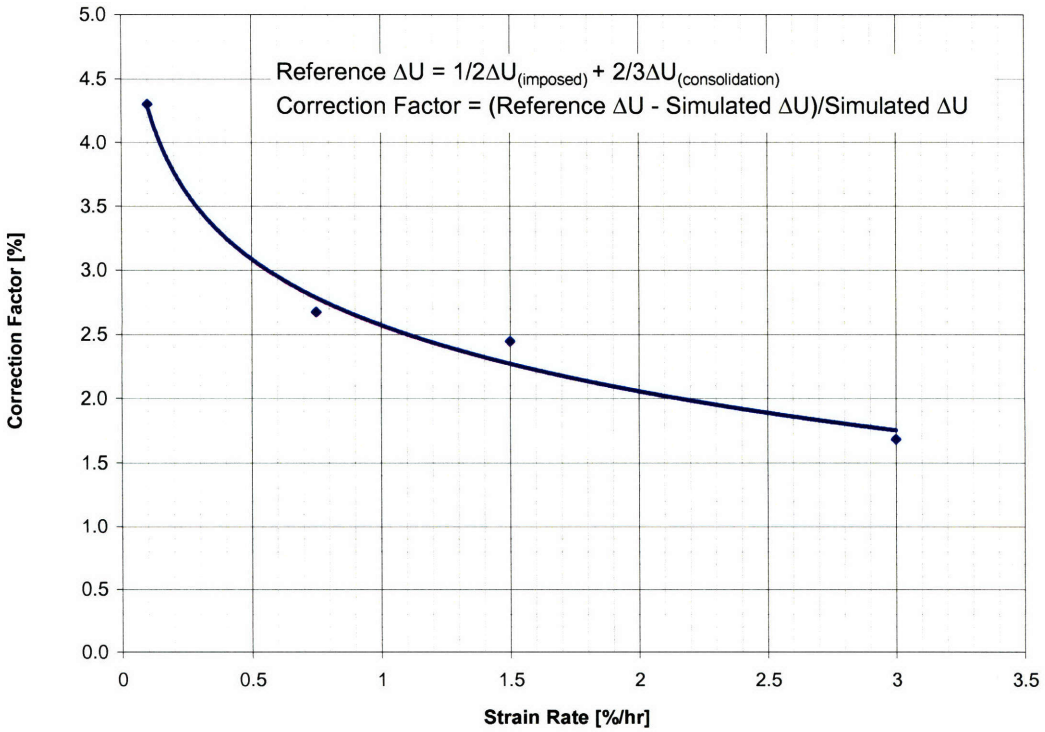

Figure 5.30 Correction factor graph for a typical SBM with normalized excess pore pressure ($\Delta u_e/\sigma'_{v(AVG)}$) of 40%

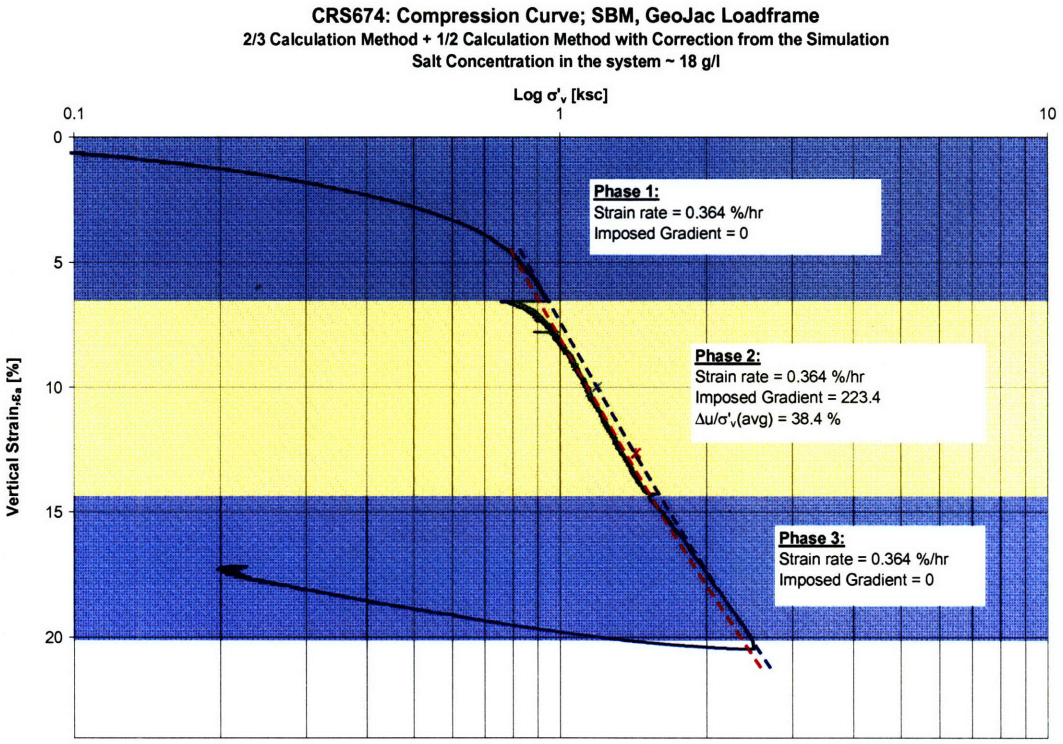

Figure 5.31 Compression curve (CRS674)

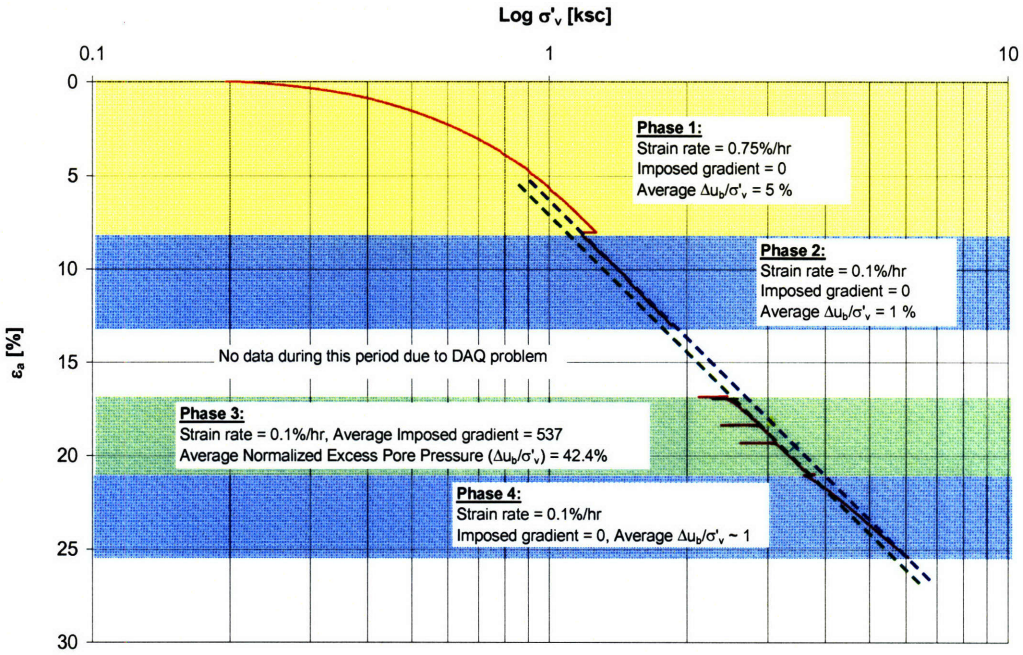

Figure 5.32 Compression curve CRS656

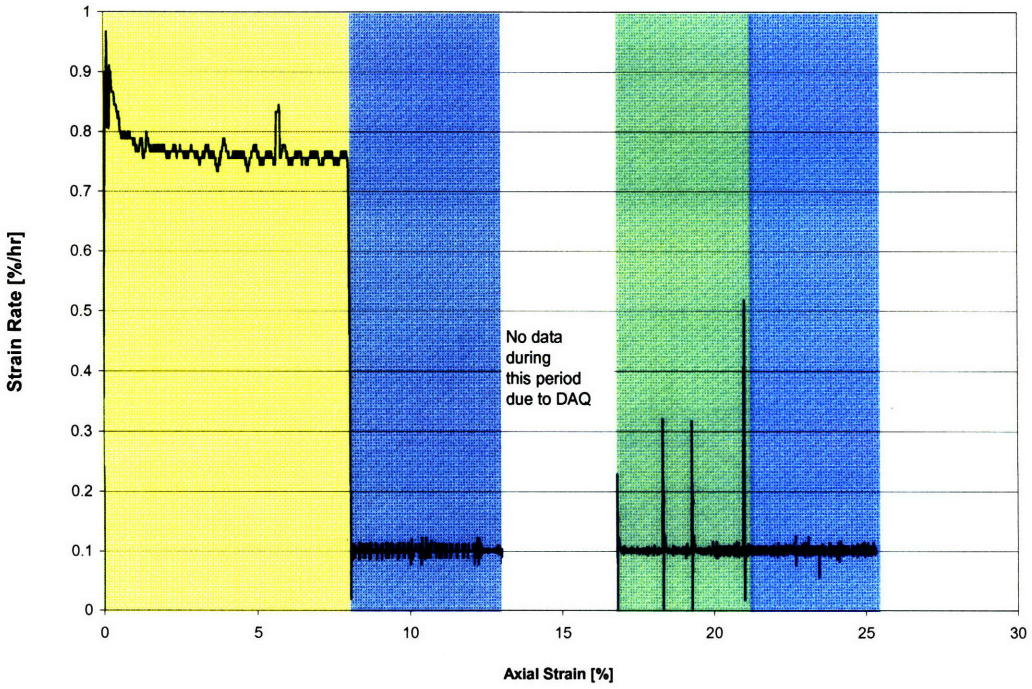

Figure 5.33 Strain rate graph CRS656

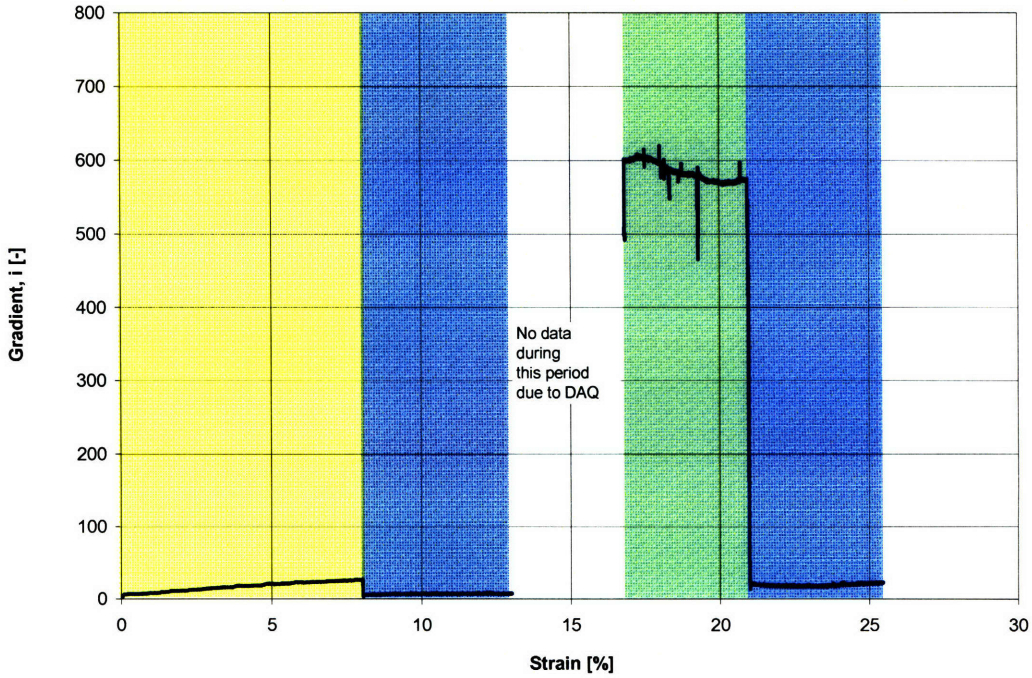

Figure 5.34 Imposed hydraulic gradient during the GCRS loading phase

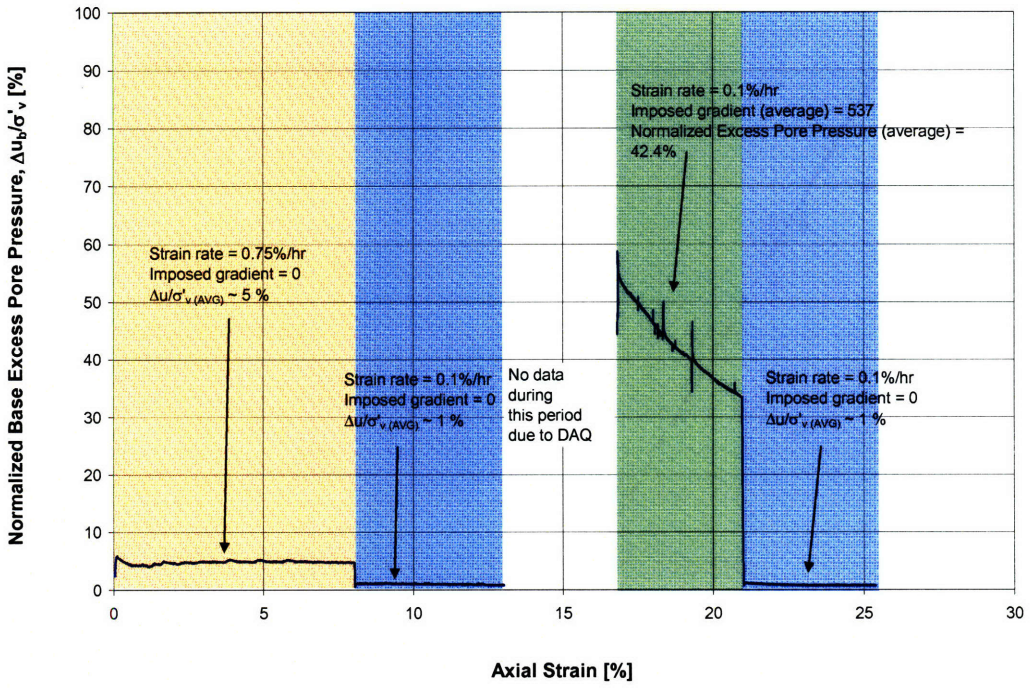

Figure 5.35 $\Delta u_e/\sigma'_v$ versus axial strain

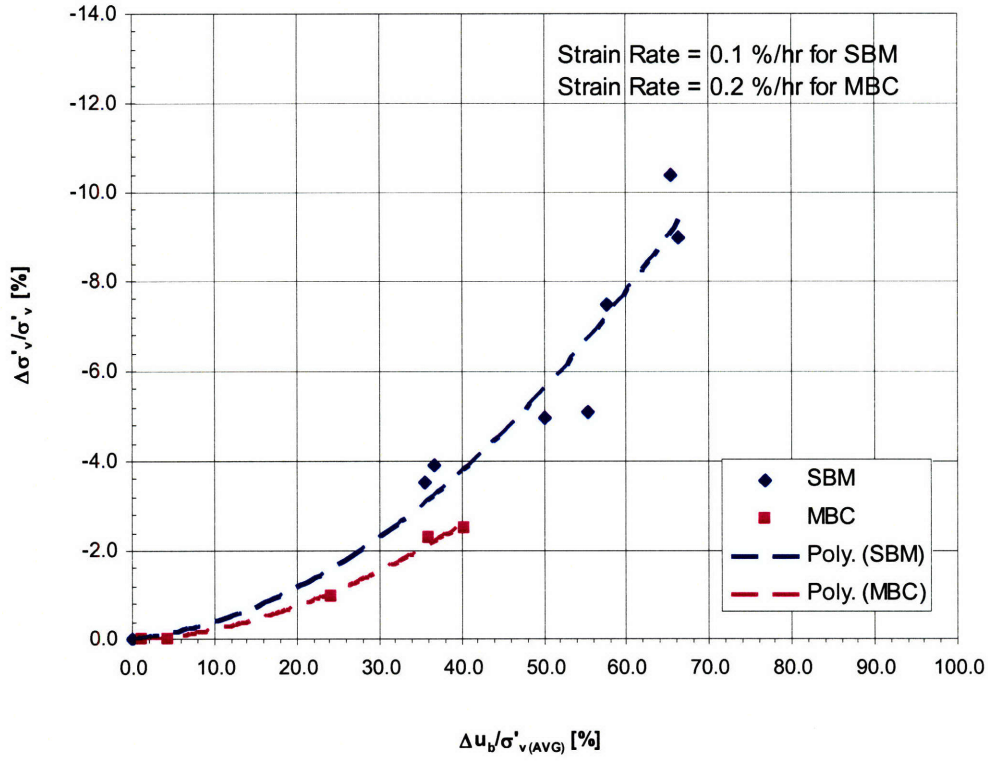

Figure 5.36 $\Delta\sigma'_v/\sigma'_v$ versus $\Delta u_b/\sigma'_{v(AVG)}$

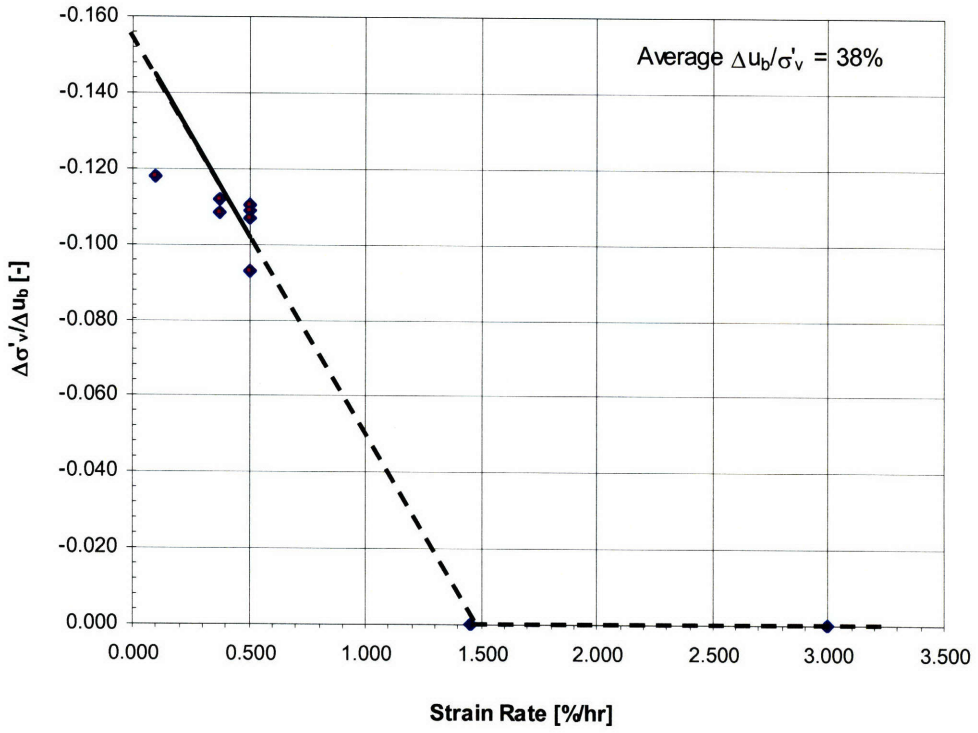

Figure 5.37 $\Delta\sigma'_v/\Delta u_b$ versus strain rate

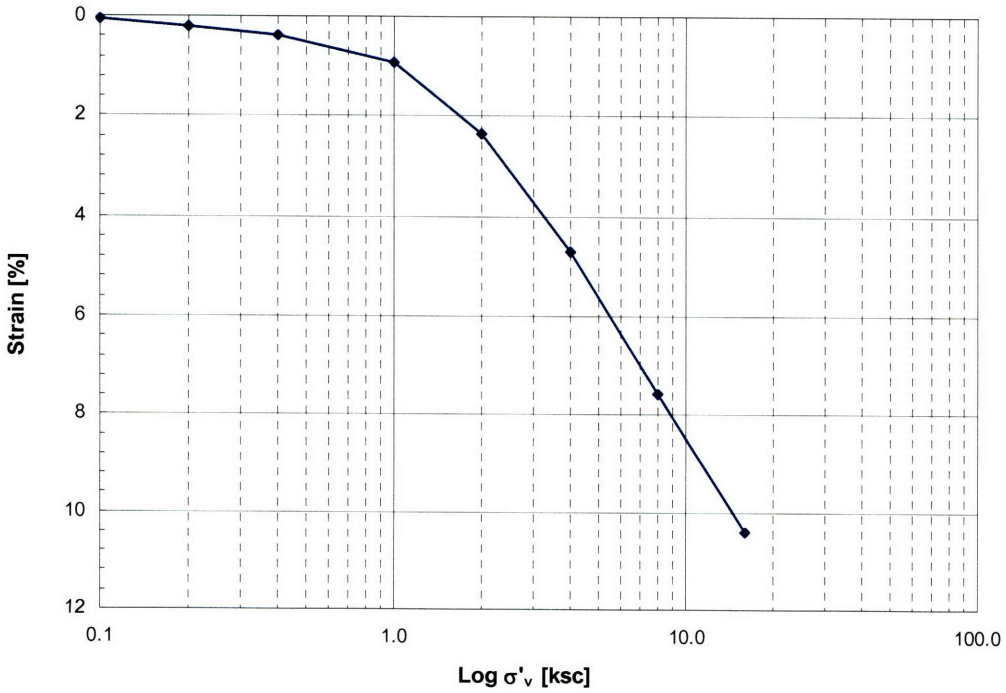

Figure 5.38 End-of-Primary (EOP) compression curve of oed111

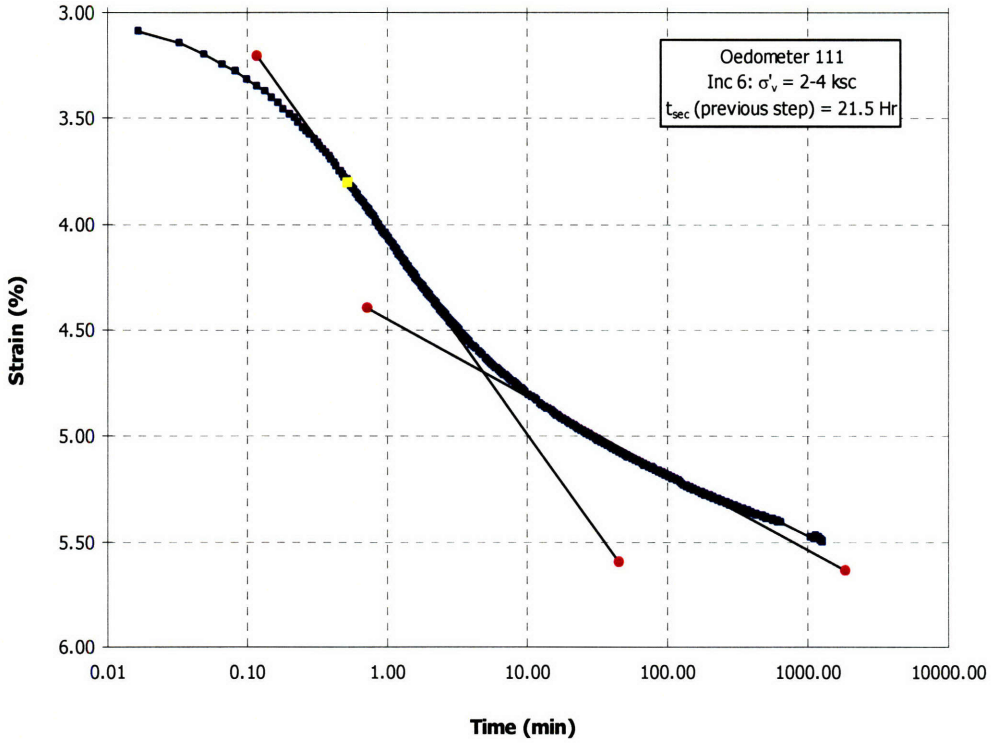

Figure 5.39 Consolidation curve of oed111 step 2-4ksc in the semi-LOG space

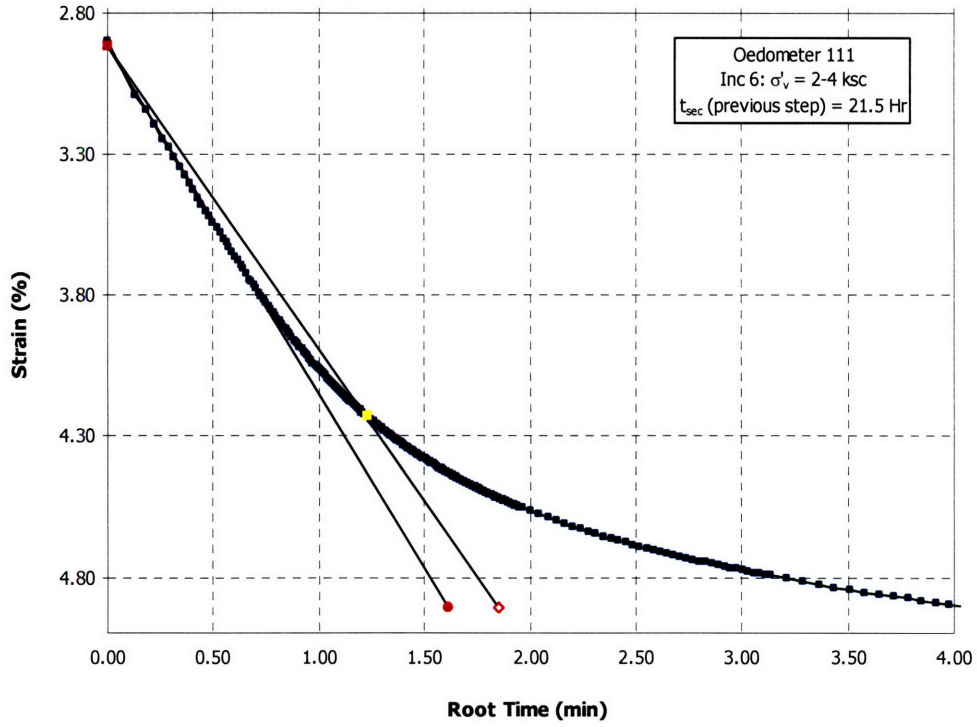

Figure 5.40 Consolidation curve of oed111 step 2-4 ksc in the SQRT space

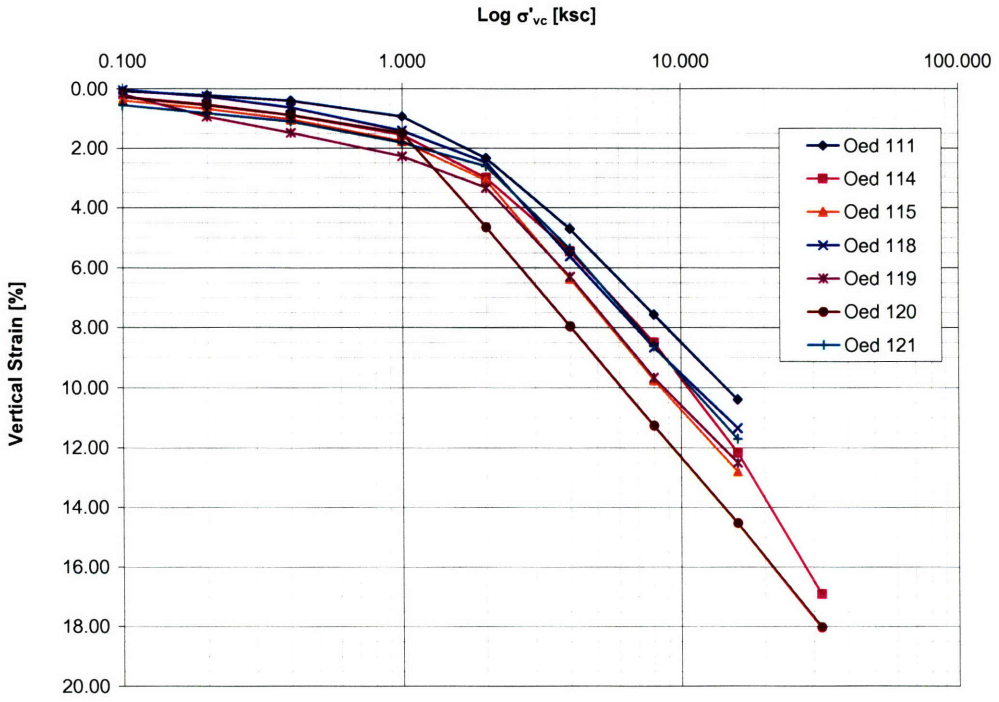

Figure 5.41 Summary of compression curves from the oedometer test for MBC

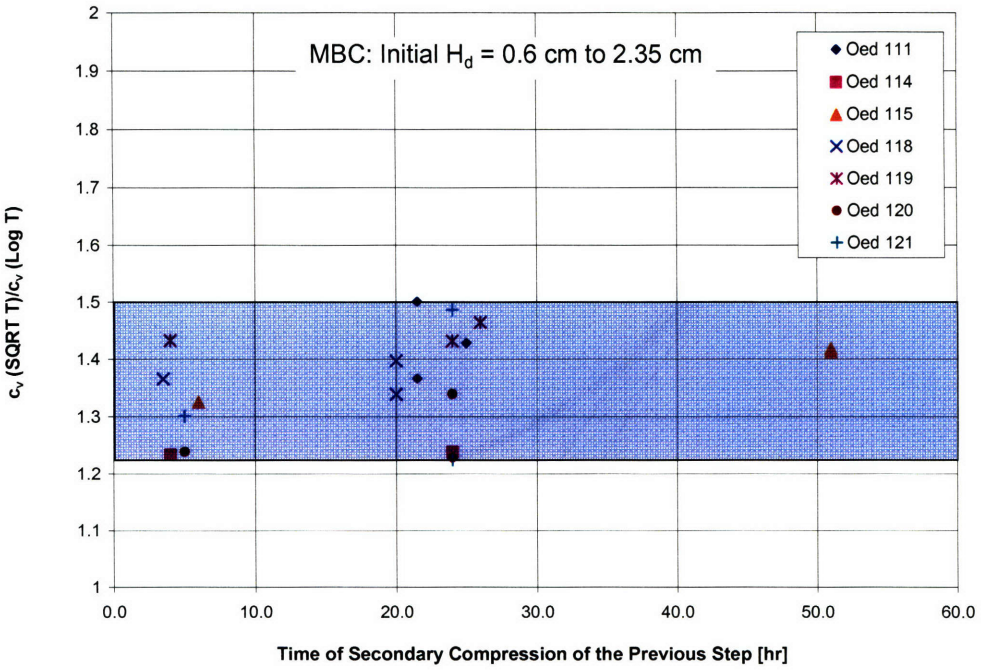

Figure 5.42 c_v analysis graph for MBC

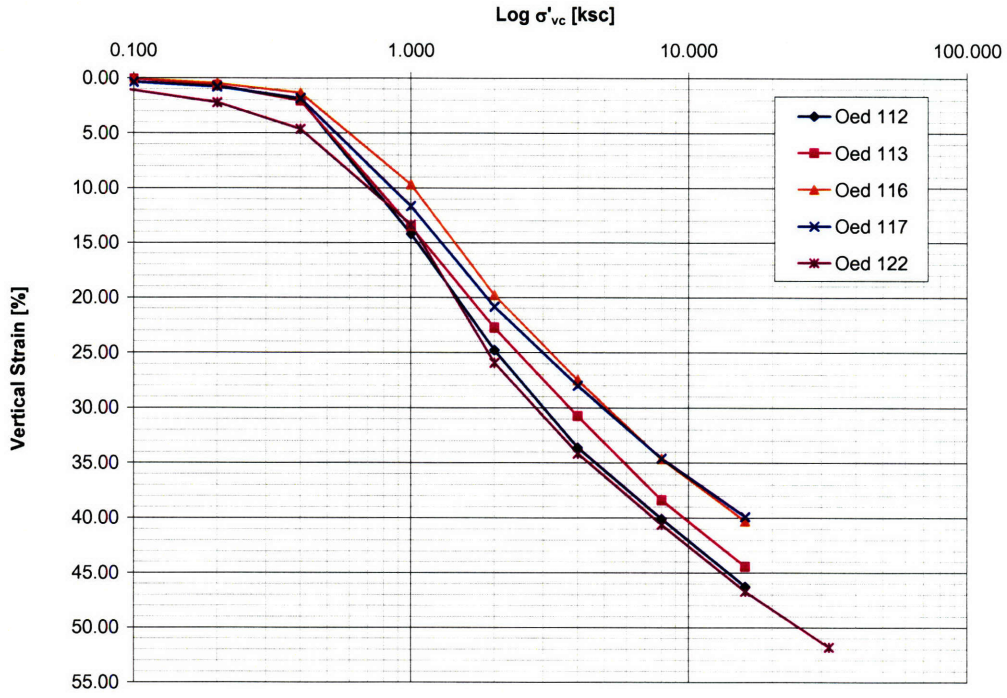

Figure 5.43 Summary of compression curves for the oedometer tests for SBM

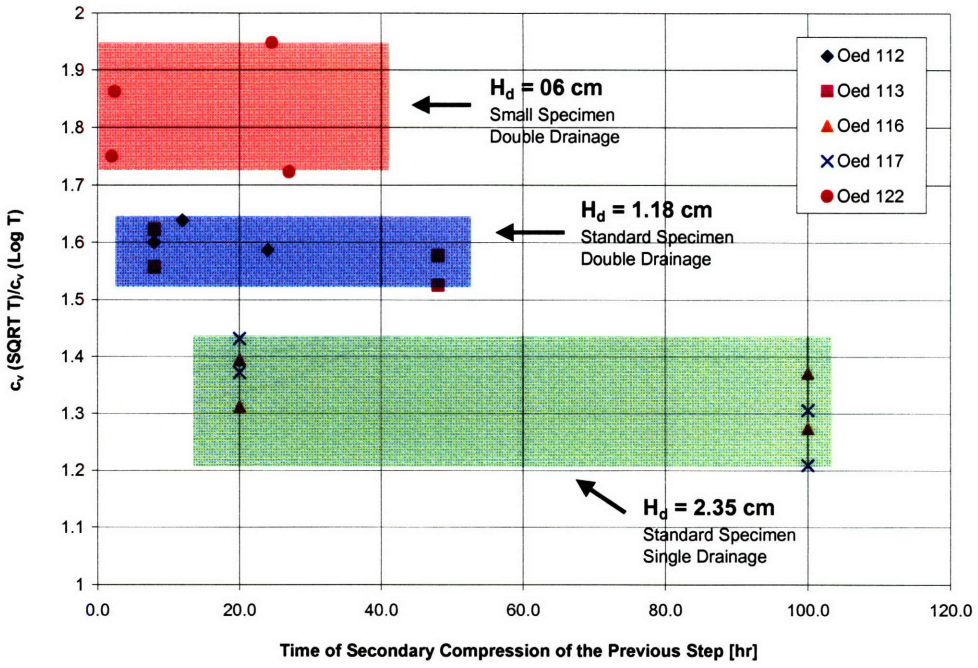

Figure 5.44 c_v analysis graph for SBM

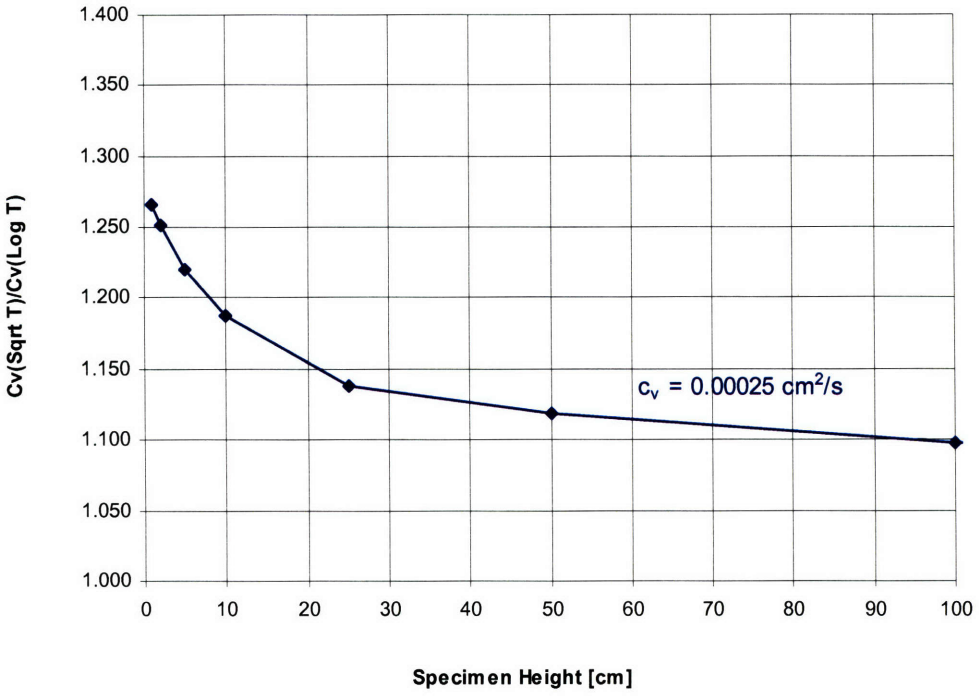

Figure 5.45(a) c_v ratio versus drainage height

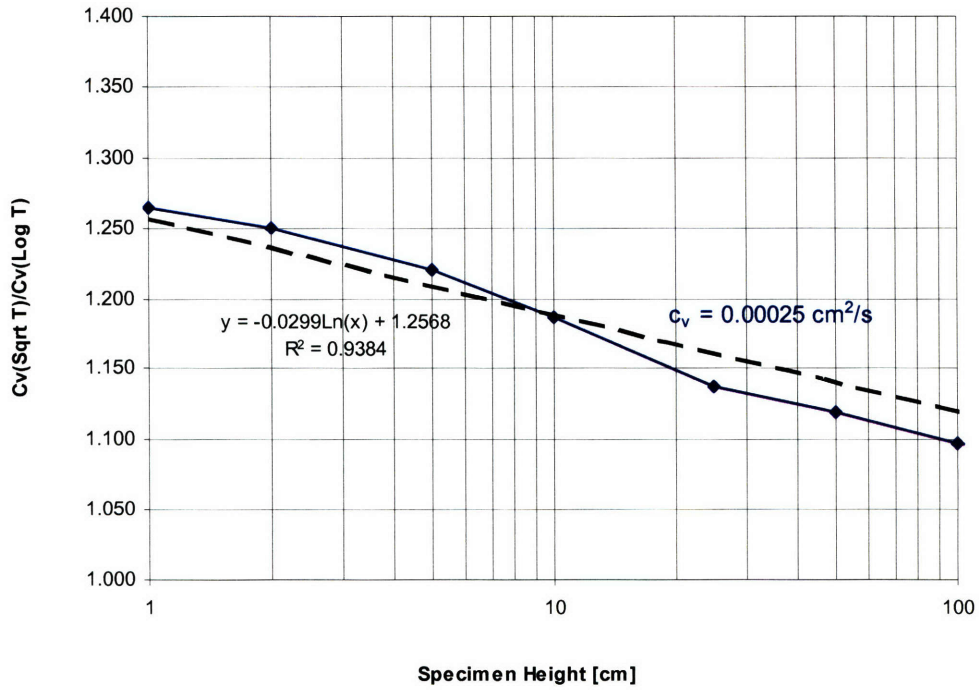

Figure 5.45(b) c_v ratio versus logarithm of drainage height

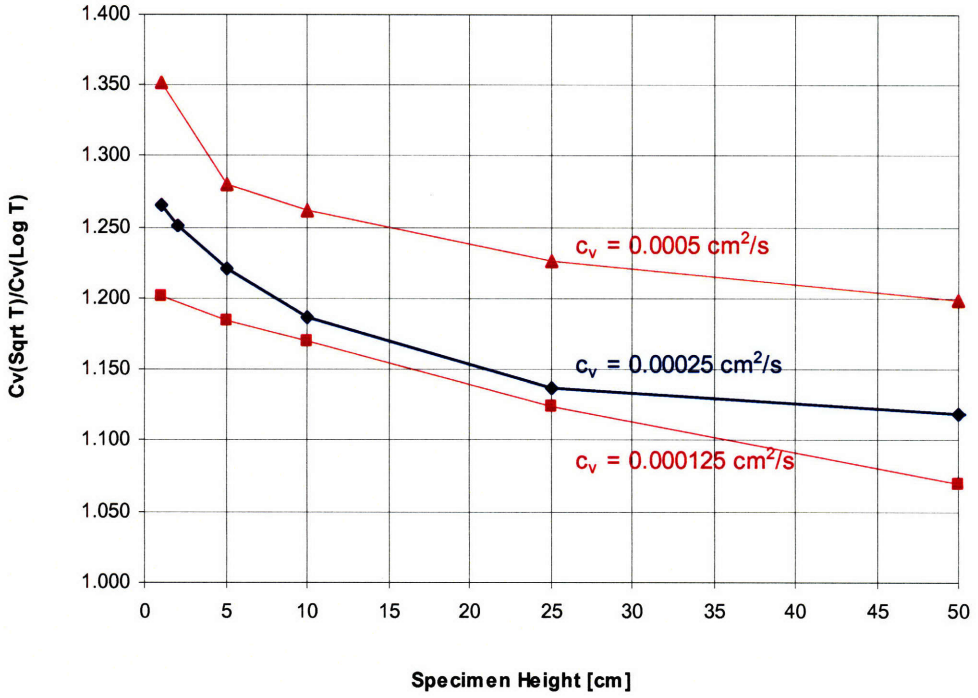

Figure 5.46 Effects of input c_v on the oedometer simulation

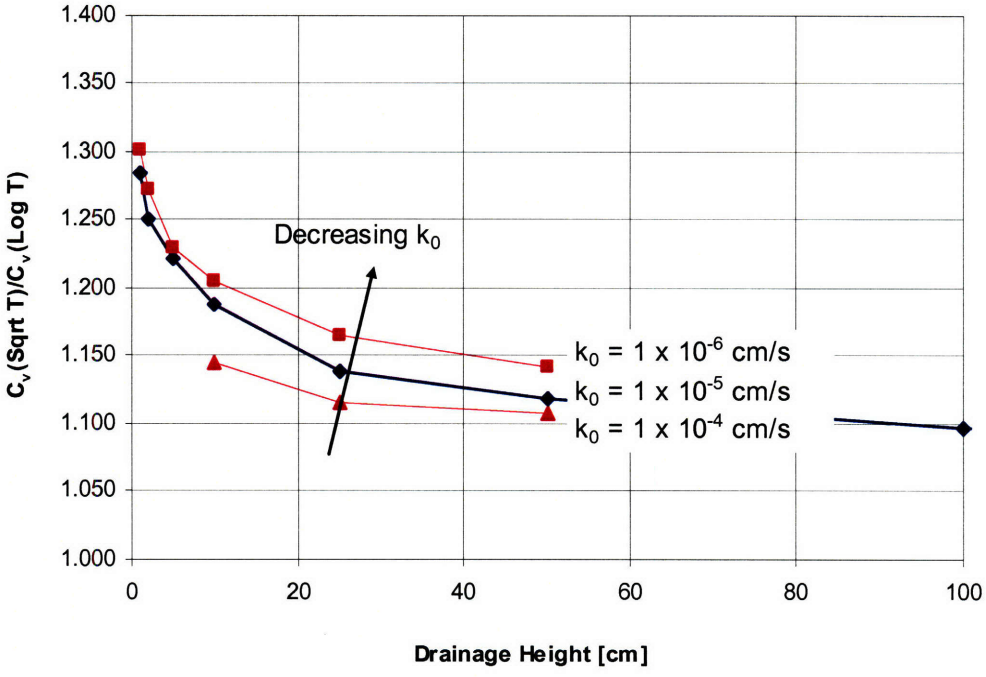

Figure 5.47 Effects of initial hydraulic conductivity on the oedometer simulation

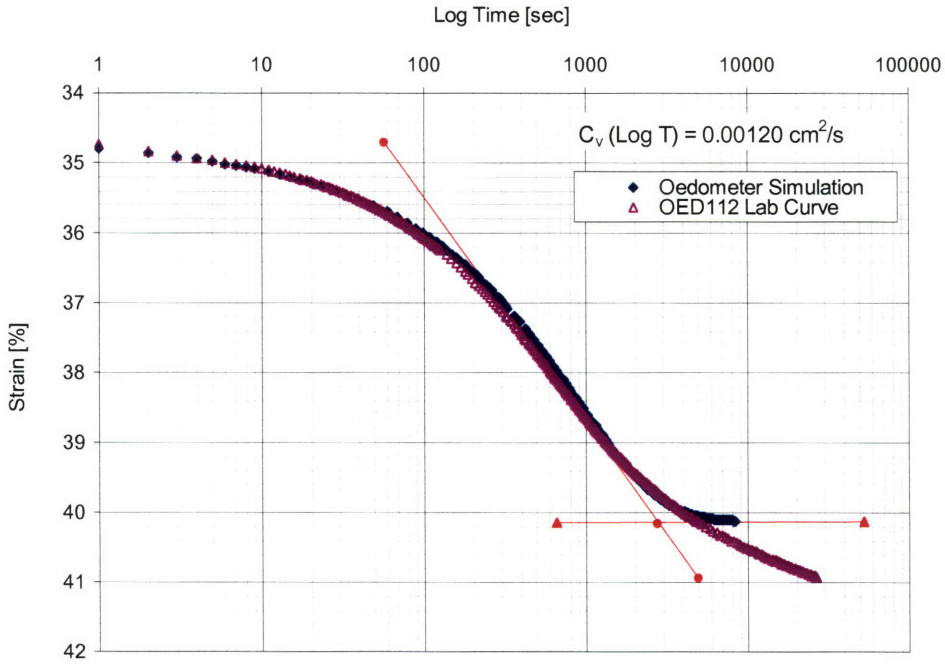

Figure 5.48 Comparison between laboratory consolidation curve (Oed112) and the predicted consolidation curve based on the oedometer simulation

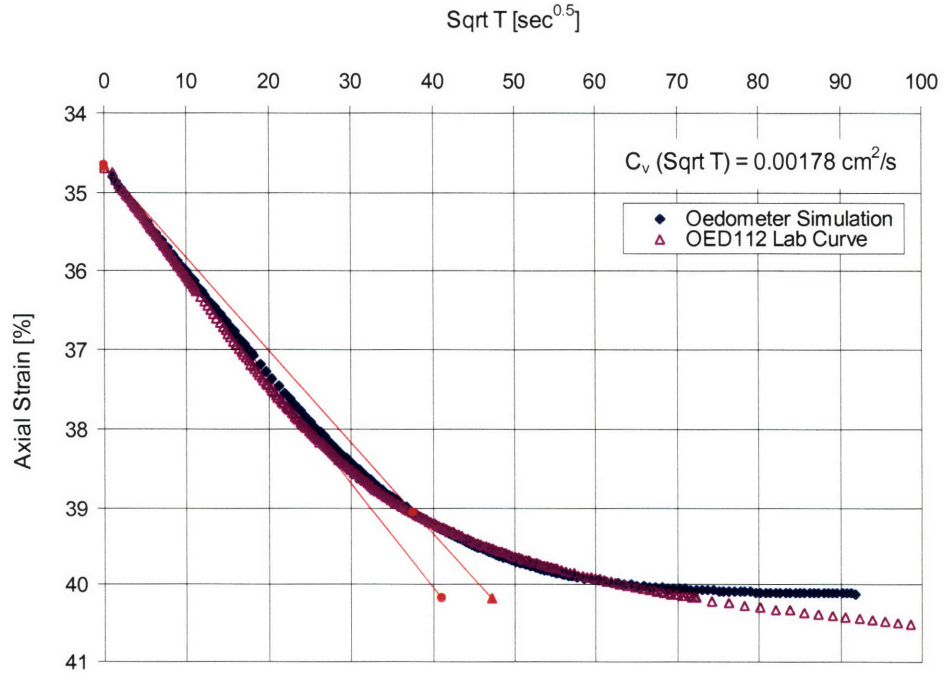

Figure 5.49 Comparison between laboratory consolidation curve (Oed112) and the predicted consolidation curve based on the oedometer simulation

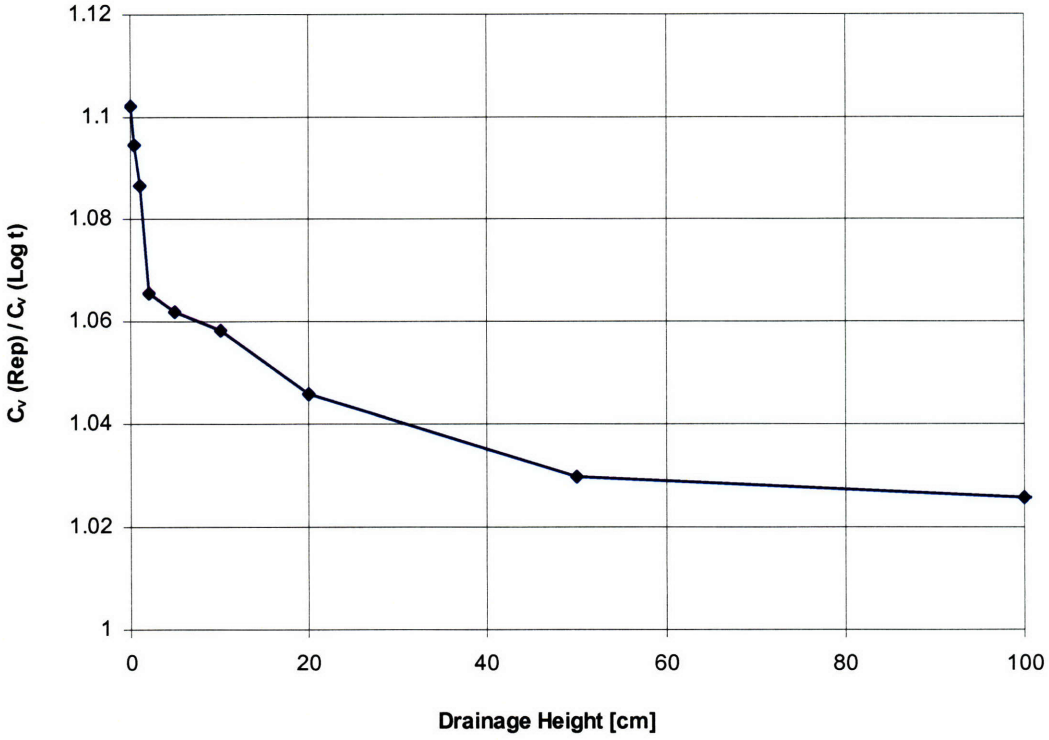

Figure 5.50 Graph between c_v(rep)/c_v(log t) and drainage height (H_d)

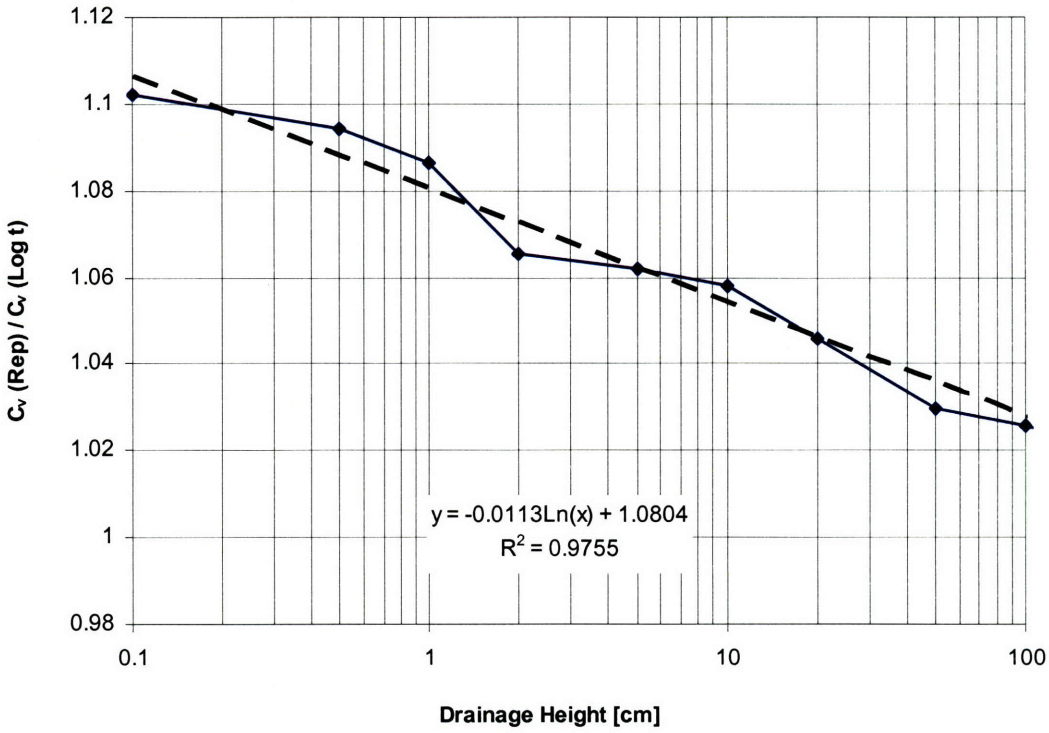

Figure 5.51 Graph between c_v(rep)/c_v(log t) and log(H_d)

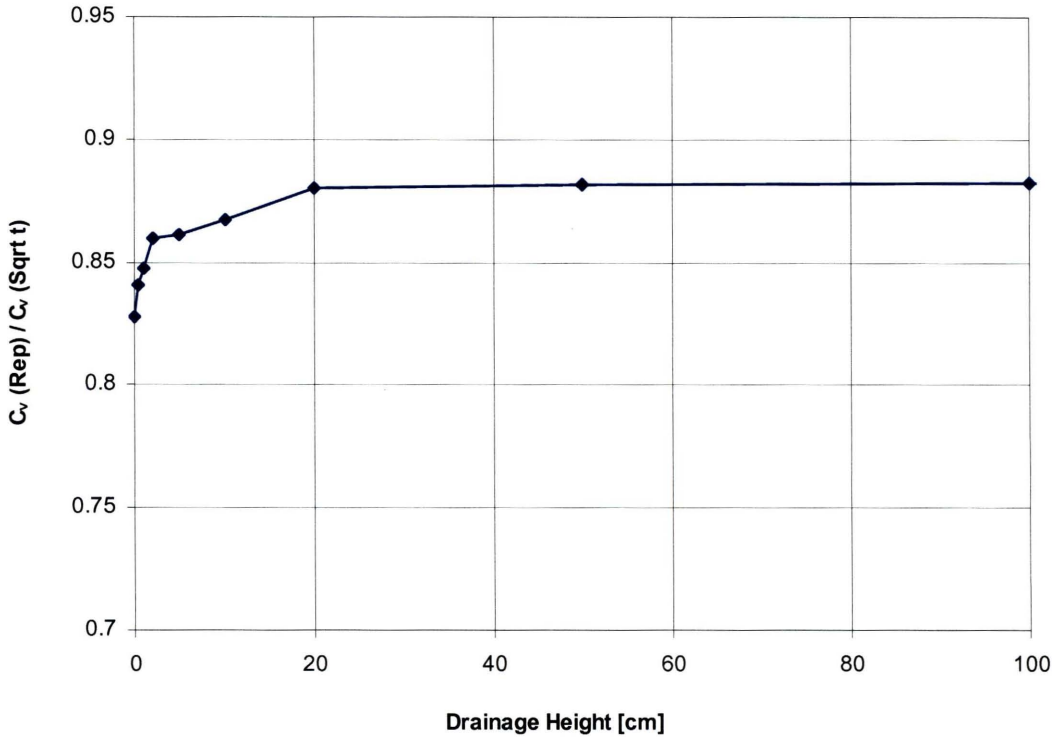

Figure 5.52 Graph between c_v(rep)/c_v(Sqrt t) and drainage height (H_d)

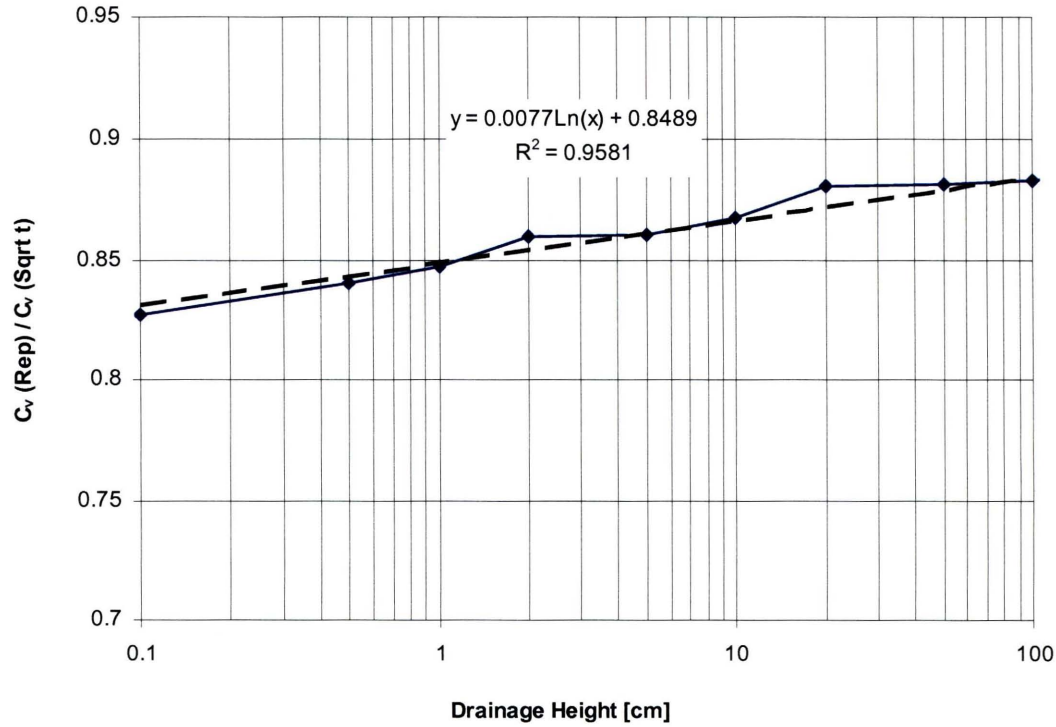

Figure 5.53 Graph between c_v(rep)/c_v(Sqrt t) and log(H_d)

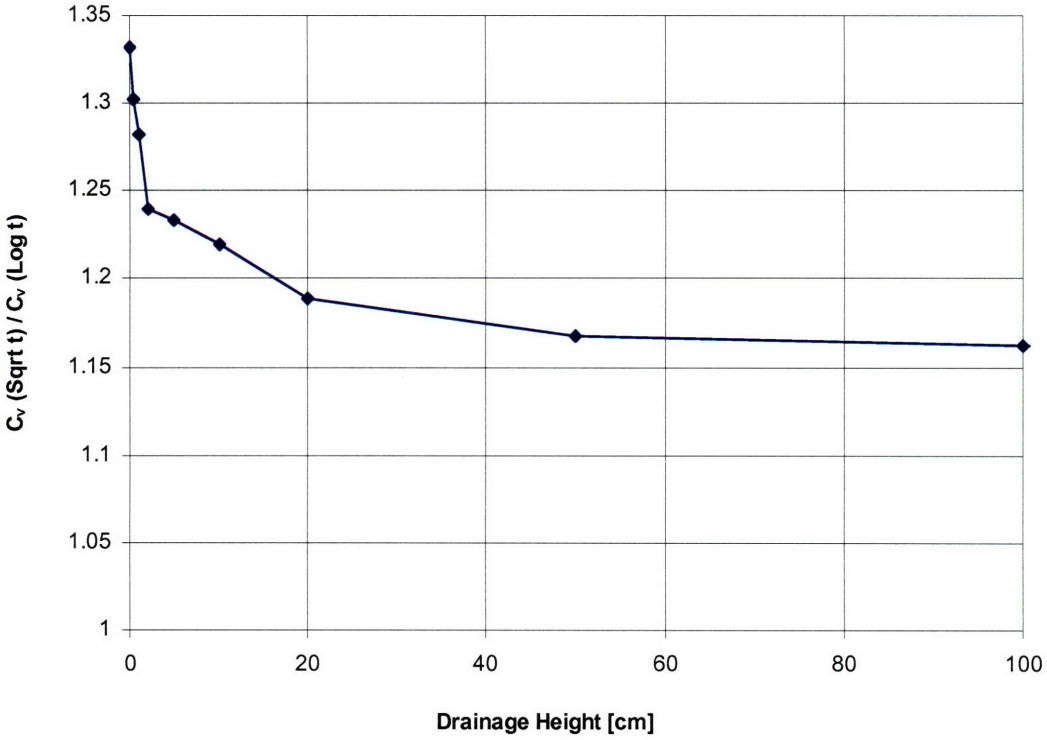

Figure 5.54 Graph between c_v(Sqrt t)/c_v(log t) and drainage height (H_d)

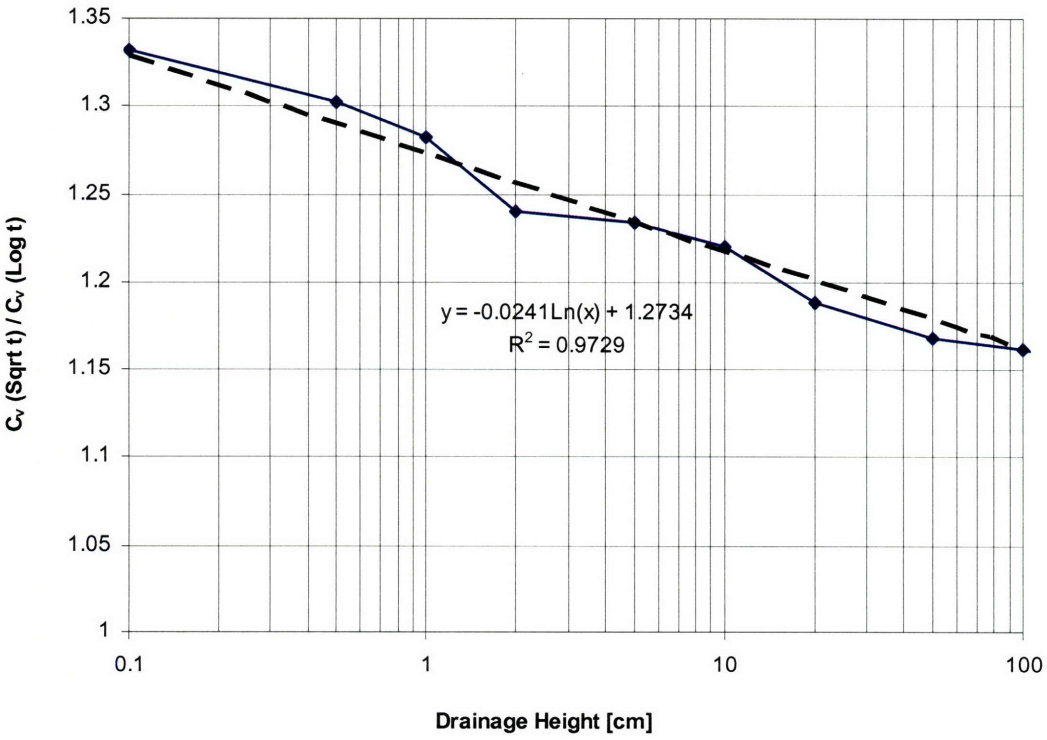

Figure 5.55 Graph between c_v(Sqrt t)/c_v(log t) and log (H_d)

Test Number	Imposed Hydraulic Gradient	Average Imposed Normalized Excess Pore Pressure, $\Delta u_e/\sigma'_v$ (AVG) [%]	Strain Rate [%/hr]
crs639	84	4.4	0.18
	113	2.4	
	226	3.2	
crs640	55	1.1	0.2
	110	1.1	
crs649	1068	36.0	0.2
crs652	1140	33	0.2

Table 5.1 Summary of GCRS tests for MBC

Test Number	Imposed Hydraulic Gradient	Average Imposed Normalized Excess Pore Pressure, $\Delta u_e/\sigma'_v$ (AVG) [%]	Strain Rate [%/hr]
crs654	362	50.8	0.09
crs656	537	42.4	0.1
crs662	354	66.4	0.088
crs663	371	61.5	0.1
crs674	224	38.4	0.375
crs680	157.5	34.4	0.5
	442.1	40.1	
crs683	180	37.7	0.5
	363	46.6	
crs686	282	42.3	3
crs687	202	46.1	1.45

Table 5.2 Summary of GCRS tests for SBM

Test No.	$\Delta\sigma'_v/\sigma'_v$ [%]	$\Delta u/\sigma'_v$ [%]	$\Delta\sigma'v/\Delta u$ [–]	Strain rate [%/hr]
crs654	-5.1	55.3	-0.093	0.09
	-5.0	50.1	-0.100	0.09
crs656	-3.5	35.6	-0.099	0.10
	-3.9	36.7	-0.107	0.10
crs662	-9	66.4	-0.136	0.088
crs663	-10.4	65.4	-0.159	0.10
	-7.5	57.7	-0.130	0.10
Reference	0	0	-	-
Average	-5.9	50.1	-0.118	0.095

Table 5.3 Summary of the GCRS tests with strain rate of 0.1%/hr with varying imposed hydraulic gradient for SBM

Test No.	$\Delta\sigma'_v/\sigma'_v$ [%]	$\Delta u/\sigma'_v$ [%]	$\Delta\sigma'v/\Delta u$ [–]	Strain rate [%/hr]
crs674	-3.81	35.11	-0.109	0.375
	-4.03	36.10	-0.112	0.375
crs680	-3.80	34.40	-0.110	0.500
	-3.60	38.75	-0.093	0.500
crs683	-4.00	36.70	-0.109	0.500
	-4.35	40.75	-0.107	0.500
crs686	0.00	42.30	0	3.000
crs687	0.00	46.10	0	1.450
Average from 0.1%/hr strain rate test	-3.3	37.9	-0.086	0.821

Table 5.4 Summary of the GCRS tests with varying strain rate for SBM

Test No.	Drainage Height (H_d) [cm]	Time to Secondary Compression (t_{sec}) [hr]
111	1.18	24
114	1.18	4, 24
115	1.18	6, 51
118	2.35	4, 20
119	2.35	5, 24
120	0.6	5, 24
121	0.6	5, 24 + Back Pressure to 4 ksc

Table 5.5 Summary of the MBC oedometer tests

SUMMARY OF CONSOLIDATION TEST RESULTS

Oedometer No. 111

Sample: Maine Blue Clays (MBC), Double Drainage

Increment Number	Consolidation Stress (kg/cm^2)	Rate of Secondary (%/log time)	Primary Time (min)	Primary Strain (%)	Compression Ratio (%/log stress)	C /CR (-)	Time for Secondary Compresison in Previous (hr)	Cv Sqrt Time (cm^2/min)	Cv Log Time (cm^2/min)
1	0.100	0.010	1.8	0.07	-	-	-	-	-
2	0.200	0.011	3.2	0.21	-	-	-	-	-
3	0.400	0.019	1.7	0.40	-	-	-	-	-
4	1.000	0.114	3.6	0.93	-	-	-	-	-
5	2.000	0.218	11.3	2.34	-	-	-	-	-
6	4.000	0.363	4.9	4.70	8.88	0.041	21.5	2.8689	1.9111
7	8.000	0.250	3.5	7.57	9.10	0.027	21.5	2.8758	2.1040
8	16.000	0.235	2.3	10.40	9.37	0.025	25.0	5.1047	3.5731

Oedometer No. 114

Sample: Maine Blue Clays (MBC), Double Drainage, Small Specimen

Increment Number	Consolidation Stress (kg/cm^2)	Rate of Secondary (%/log time)	Primary Time (min)	Primary Strain (%)	Compression Ratio (%/log stress)	Ca/CR (-)	Time for Secondary Compresison in the Previous Step [hr]	C_v Sqrt Time (cm^2/min)	C_v Log Time (cm^2/min)
0	0.1			0					
1	0.2	0.016	3.7	0.52	-	-	-	-	-
2	0.4	0.058	1.8	0.88	-	-	-	-	-
3	1.0	0.095	1.9	1.54	-	-	-	-	-
4	2.0	0.180	1.6	3.01	-	-	-	-	-
5	4.0	0.613	4.1	5.45	-	-	-	-	-
~~6~~	~~8.0~~	~~0.255~~	~~214.1~~	~~8.50~~			~~24.0~~	~~2.3608~~	~~0.0124~~
7	16.0	0.679	1.2	12.17	8.75	0.078	4.0	0.3375	0.2735
8	32.0	0.439	0.8	16.89	8.88	0.049	24.0	0.4660	0.3761

Oedometer No. 115

Sample: Maine Blue Clays (MBC), Double Drainage

Increment Number	Consolidation Stress (kg/cm^2)	Rate of Secondary (%/log time)	Primary Time (min)	Primary Strain (%)	Compression Ratio (%/log stress)	Ca/CR (-)	Time for Secondary Compresison in the Previous Step [hr]	C_v Sqrt Time (cm^2/min)	C_v Log Time (cm^2/min)
1	0.1	0.014	0.8	0.38	-	-	-	-	-
2	0.2	0.028	3.7	0.66	-	-	-	-	-
3	0.4	0.043	2.2	1.03	-	-	-	-	-
4	1.0	0.081	1.9	1.76	-	-	-	-	-
5	2.0	0.310	14.1	3.08	-	-	-	-	-
6	4.0	0.495	9.4	6.37	13.64	0.036	51.0	0.3071	0.2173
7	8.0	0.316	3.6	9.73	12.88	0.025	6.0	0.5754	0.4339
8	16.0	0.301	2.2	12.80	12.83	0.023	51.0	0.9500	0.6694

Table 5.6 Summary of oedometer test results for MBC (continue on the next page)

Oedometer No. 118

Sample: Maine Blue Clays (MBC), Single Drainage

1	0.1	0.017	4.2	0.03	-	-	-	-	-
2	0.2	0.005	2.7	0.26	-	-	-	-	-
3	0.4	0.046	16.9	0.63	-	-	-	-	-
4	1.0	0.083	14.8	1.41	-	-	-	-	-
5	2.0	0.251	34.3	2.48	-	-	-	-	-
6	4.0	0.471	25.3	5.62	10.43	0.045	20.0	0.3990	0.2978
7	8.0	0.289	16.6	8.67	9.66	0.030	3.5	0.6036	0.4419
8	16.0	0.281	9.6	11.35	8.90	0.032	20.0	0.9420	0.6740

Oedometer No. 119

Sample: Maine Blue Clays (MBC), Single Drainage

1	0.1	0.039	0.1	0.17	-	-	-	-	-
2	0.2	0.079	1.4	0.93	-	-	-	-	-
3	0.4	0.054	2.5	1.48	-	-	-	-	-
4	1.0	0.077	15.6	2.27	-	-	-	-	-
5	2.0	0.270	30.8	3.34	-	-	-	-	-
6	4.0	0.590	33.1	6.30	10.76	0.055	26.0	0.3588	0.2449
7	8.0	0.337	18.8	9.66	10.17	0.033	4.0	0.5366	0.3744
8	16.0	0.380	9.0	12.51	9.33	0.041	24.0	0.9429	0.6581

Oedometer No. 120

Sample: Maine Blue Clay, Double Drainage, Small Specimen

0	0.1			0					
1	0.2	0.018	0.8	0.54284	-	-	-	-	-
2	0.4	0.044	0.2	0.88	-	-	-	-	-
3	1.0	0.115	0.6	1.49	-	-	-	-	-
4	2.0	0.479	2.7	4.66	-	-	-	-	-
5	4.0	0.503	0.9	7.96	-	-	-	-	-
6	8.0	0.368	0.5	11.27	10.59	0.035	24.0	0.9105	0.6795
7	16.0	0.320	0.4	14.53	10.59	0.030	5.0	1.1617	0.9375
8	32.0	0.281	0.3	18.01	11.03	0.025	24.0	1.3953	1.1352

Table 5.6 Summary of oedometer test results for MBC (continue on the next page)

Oedometer No. 121

Sample: Maine Blue Clays (MBC), Double Drainage, 4ksc BP

Increment Number	Consolidation Stress (kg/cm^2)	Rate of Secondary (%/log time)	Primary Time (min)	Primary Strain (%)	Compression Ratio (%/log stress)	Ca/CR (-)	Time for Secondary Compresison in the Previous Step [hr]	C_v Sqrt Time (cm^2/min)	C_v Log Time (cm^2/min)
1	0.1	0.036	5.9	0.56	-	-	-	-	-
2	0.2	0.029	5.2	0.83	-	-	-	-	-
3	0.4	0.054	1.1	1.11	-	-	-	-	-
4	1.0	0.075	1.8	1.81	-	-	-	-	-
5	2.0	0.231	1.7	2.61	-	-	-	-	-
6	4.0	0.488	9.4	5.37	10.40	0.047	24.0	0.3515	0.2481
7	8.0	0.335	3.6	8.62	10.12	0.033	5.0	0.5680	0.4531
8	16.0	0.332	2.0	11.72	10.16	0.033	24.0	0.9547	0.7859

Table 5.6 Summary of oedometer test results for MBC

Test No.	Drainage Height (H_d) [cm]	Time to Secondary Compression (t_{sec}) [hr]
112	1.18	8, 12, 24
113	1.18	8, 48
116	2.35	20, 100
117	2.35	20, 100
122	0.6	2, 27

Table 5.7 Summary of the SBM oedometer tests

SUMMARY OF CONSOLIDATION TEST RESULTS

Oedometer No. 112

Sample: San Franscisco Bay Mud (SBM), Double Drainage

1	0.1	0.004	1.5	0.07	-	-	-	-	-
2	0.2	0.062	11.7	0.68	-	-	-	-	-
3	0.4	0.331	11.0	1.96	-	-	-	-	-
4	1.0	1.752	120.9	14.19	-	-	-	-	-
5	2.0	1.235	87.4	24.66	35.4	0.035	24.0	0.1004	0.0630
6	4.0	0.947	66.5	33.43	26.7	0.036	12.0	0.1122	0.0685
7	8.0	0.978	45.9	39.96	21.6	0.045	24.0	0.1128	0.0711
8	16.0	0.670	47.9	46.13	20.9	0.032	8.0	0.0998	0.0623

Oedometer No. 113

Sample: San Franscisco Bay Mud (SBM), Double Drainage

1	0.1	0.004	1.5	0.07		-	-	-	-
2	0.2	0.053	5.3	0.66		-	-	-	-
3	0.4	0.497	13.7	2.06		-	-	-	-
4	1.0	1.449	79.5	13.55		-	-	-	-
5	2.0	1.346	75.8	22.65	28.5	0.047	48.0	0.1057	0.0693
6	4.0	0.811	60.2	30.62	25.8	0.031	8.0	0.1263	0.0779
7	8.0	0.912	47.7	38.33	22.4	0.041	48.0	0.1205	0.0764
8	16.0	0.631	44.7	44.30	19.9	0.032	8.0	0.1024	0.0658

Oedometer No. 116

Sample: San Franscisco Bay Mud (SBM), Single Drainage Test

1	0.1	0.003	1.9	0.07	-	-	-	-	-
2	0.2	0.051	12.1	0.49	-	-	-	-	-
3	0.4	0.098	21.2	1.36	-	-	-	-	-
4	1.0	0.690	1969.9	9.69	-	-	-	-	-
5	2.0	1.117	159.5	19.38	28.2	0.040	20.0	0.0109	0.0083
6	4.0	1.061	122.2	27.41	25.0	0.042	100.0	0.0118	0.0093
7	8.0	0.746	101.7	34.41	19.9	0.037	20.0	0.0138	0.0099
8	16.0	0.746	74.4	40.14	18.3	0.041	100.0	0.0144	0.0105

Table 5.8 Summary of oedometer test results for SBM (continue on the next page)

Oedometer No. 117

Sample: San Franscisco Bay Mud (SBM), Single Drainage

Increment Number	Consolidation Stress (kg/cm^2)	Rate of Secondary (%/log time)	Primary Time (min)	Primary Strain (%)	Compression Ratio (%/log stress)	C□/CR (-)	Time for Secondary Compresison in the Previous Step [hr]	C_v Sqrt Time (cm^2/min)	C_v Log Time (cm^2/min)
1	0.1	0.035	0.1	0.34	-	-	-	-	-
2	0.2	0.048	0.1	0.76	-	-	-	-	-
3	0.4	0.125	1.8	1.80	-	-	-	-	-
4	1.0	1.022	697.3	11.64	-	-	-	-	-
5	2.0	0.950	167.5	20.60	25.92	0.037	20.0	0.0127	0.0088
6	4.0	0.904	125.2	27.94	23.24	0.039	100.0	0.0096	0.0079
7	8.0	0.636	105.8	34.48	19.65	0.032	20.0	0.0123	0.0090
8	16.0	0.676	89.6	39.80	17.65	0.038	100.0	0.0119	0.0091

Oedometer No. 122

Sample: SBM, Double Drainage, Small Specimen

Increment Number	Consolidation Stress (kg/cm2)	Rate of Secondary (%/log time)	Primary Time (min)	Primary Strain (%)	Compression Ratio (%/log stress)	C□/CR (-)	Time for Secondary Compresison in the Previous Step (hr)	Cv Sqrt Time (cm2/min)	Cv Log Time (cm2/min)
0	0.1		0	0					
1	0.1	0.112	4.0	2.22	-	-	-	-	-
2	0.2	0.571	7.7	4.66	-	-	-	-	-
3	0.4	1.310	21.1	13.35	-	-	-	-	-
4	1.0	1.133	8.6	25.93	-	-	-	-	-
5	2.0	0.834	8.1	33.95	23.54	0.035	2.0	0.055	0.032
6	4.0	0.798	7.2	40.52	21.27	0.038	27.0	0.049	0.028
7	8.0	0.620	6.7	46.63	18.53	0.033	2.4	0.044	0.025
8	16.0	0.612	5.7	51.68	16.55	0.037	24.6	0.047	0.024

Table 5.8 Summary of oedometer test results for SBM

Input Parameter for Oedometer Simulation for Parametric Studies	
Initial Void Ratio, e_0	1
Initial Total Stress, σ_{v0} ksc]	1
Initial Hydraulic Conductivity, k_0 cm/sec]	1.0×10^{-7}
Coefficient of Hydraulic Conductivity, C_k	0.1
Input Coefficient of Consolidation, input c_v [cm^2/sec]	0.00025
Initial coeffcient of compressibility, a_v	0.029
Stress Increment, $\Delta\sigma_v$ [ksc]	1

Table 5.9 Input parameters for oedometer simulation for parametric studies

Input Parameter for Oedometer Simulation for c_v(rep)	
Initial Void Ratio, e_0	1.6
Initial Total Stress, σ_{v0} ksc]	4
Initial Hydraulic Conductivity, k_0 cm/sec]	5.5×10^{-8}
Coefficient of Hydraulic Conductivity, C_k	0.188
Input Coefficient of Consolidation, input c_v [cm^2/sec]	0.0015
Coeffcient of consolidation, C_c	0.468
Stress Increment, $\Delta\sigma_v$ [ksc]	4
Initial Specimen Height [cm]	0.1 to 100

Table 5.10 Input parameters for the oedometer simulation for c_v(rep) analysis

Chapter 6: Summary, Conclusions and Recommendations

The consolidation behavior of soft clay is a very complicated subject. The subject is complicated because it involves significant numbers of parameters, many of which are coupled and difficult to study individually. While the basic concept of one-dimensional consolidation is well established by Terzaghi, the actual behavior observed in laboratories or from field studies are significantly differ from the theory. It is an aim of this research to study the effects from hydraulic gradient and strain rate on the consolidation behavior of soft clay. Another objective is to study the scaling effect on the consolidation behavior.

6.1 Summary and Conclusions

The following sections provide conclusion from this research including the strain rate effects on consolidation behavior of soft clay, hydraulic gradient effects, scaling effects, and large strain problem simulations.

6.1.1 Strain Rate Effects on Consolidation behavior of Soft Clay

Strain rate is probably the easiest parameter to study in a controlled environment. The Constant Rate of Strain (CRS) tests are especially suited for testing the strain rate effect. However, the strain rate used in a test should, at the minimum, produce reasonable and observable base excess pore pressure. The test set up is relatively simple and the test requires short amount of times except for a very slow strain rate test.

This research studied the strain rate effects on two natural soils: Maine Blue clay (MBC) and San Francisco Bay mud (SBM) covering strain rate of 0.1 %/hr to 8 %/hr for MBC and 0.1 %/hr to 3 %/hr for SBM. Chapter 3 presents the summary of basic soil properties and details of the experimental program. Based on the strain rate tests presented in the chapter 5, it is clear that both soils exhibit very different consolidation behavior. While the MBC does not exhibit strain rate dependent behavior when the strain rate excess approximately 1.5 %/hr, the SBM clearly shows that the location of the virgin compression line (VCL) is dependent on the strain rate for the test. Figure 6.1 shows the summary strain rate graph for both soils in a normalized space.

The strain rate test results are plotted on the normalized space to allow direct comparison between the results from MBC and SBM tests. The normalized base excess pore pressure produced during the strain rate sensitivity tests of MBC and SBM differ significantly. The strain rate of the tests is normalized by the strain rate which produces the normalized base excess pore pressure of 2% for each soil. The normalized base

excess pore pressure of 2% is selected because it is low but clearly observable. This should be a reasonable representation of the strain rate that produces the same VCL as the end-of-primary VCL. The difference between the two soils strain rate dependent behavior is very clearly shown in the Figure 6.1.

While MBC shows no rate dependency behavior, the shifts of the VCL for SBM is approximately 15% per log cycle of increases in normalized strain rate. It should be noted that, while the tests yield valuable insight into the strain rate effects of MBC and SBM, extrapolation of the lab test results for uses in field application must be done with careful considerations of other factors that can significantly affect the extrapolation.

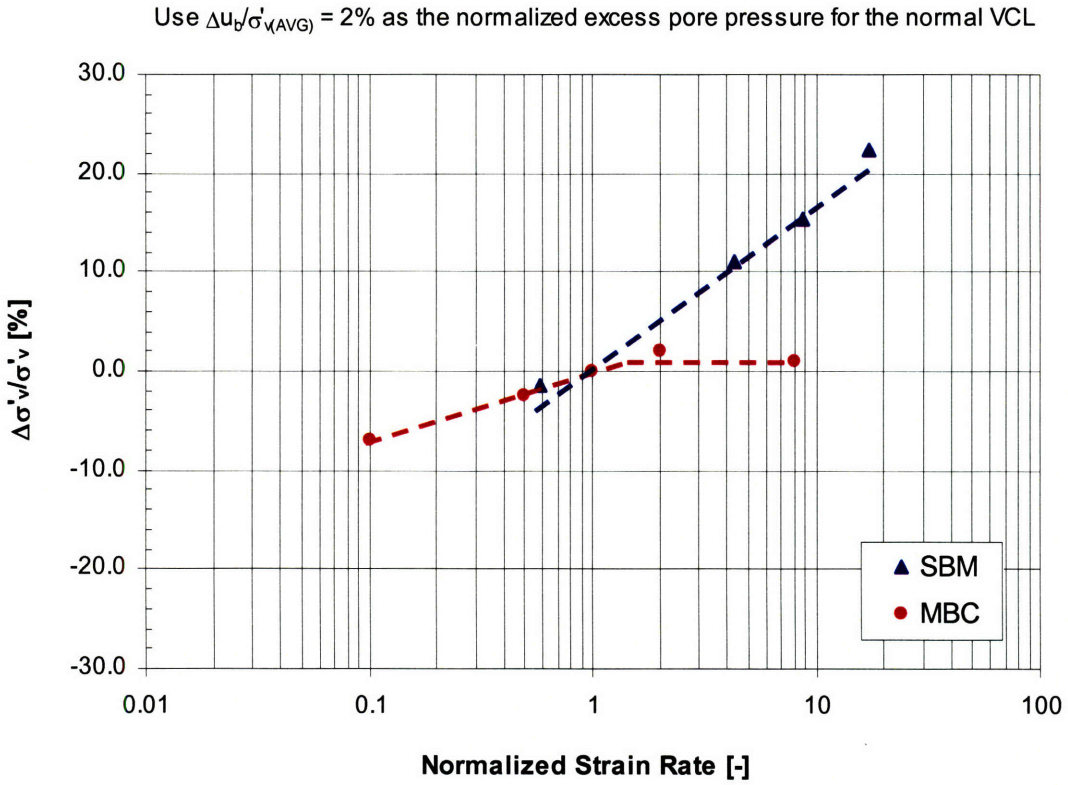

Figure 6.1 Summary of strain rate effects on MBC and SBM

Based on the test results, SBM is clearly a strain rate sensitive soil. For this type of soil, a special consideration has to be given to the settlement calculation for large soil layer. This is because the thicker the layer is, the more time it will consolidate before it reaches the end-of-primary. This will result in larger settlement than if the soil is not strain rate dependent. While not a direct part of this research, one would expect the preconsolidation pressure, σ'_p, to be strain rate dependent as well.

The main observation from the strain rate sensitivity test is that different soils have different strain rate dependent behavior. A more plastic soil such as SBM can exhibit

significant strain rate dependent behavior while a less plastic soil such as MBC may not exhibit the behavior at all at strain rate faster than 1.5 %/hr. It is important to thoroughly study the soil for strain rate effects before using laboratory test results for field applications.

Figure 6.2 shows comparison between predicted consolidation curves based on strain rate dependent and strain rate independent behaviors. The simulated oedometer consolidation curve in the figure 6.2 is based on the Taylor expansion of the Terzaghi's one dimensional consolidation theory (Taylor, 1948) for a specimen with drainage height of 1.9 cm. The calculation proceeds until the consolidation reaches 99% consolidation. The consolidation is then governed by a constant coefficient of secondary compression, C_α, to simulate the secondary compression occurring after the end-of-primary consolidation. The predicted consolidation curve based on the strain rate independent behavior is calculated using the same method but with drainage height of 100 cm. The predicted consolidation curve based on the strain rate dependent behavior is calculated by allowing the secondary compression to occur together with primary consolidation throughout the consolidation.

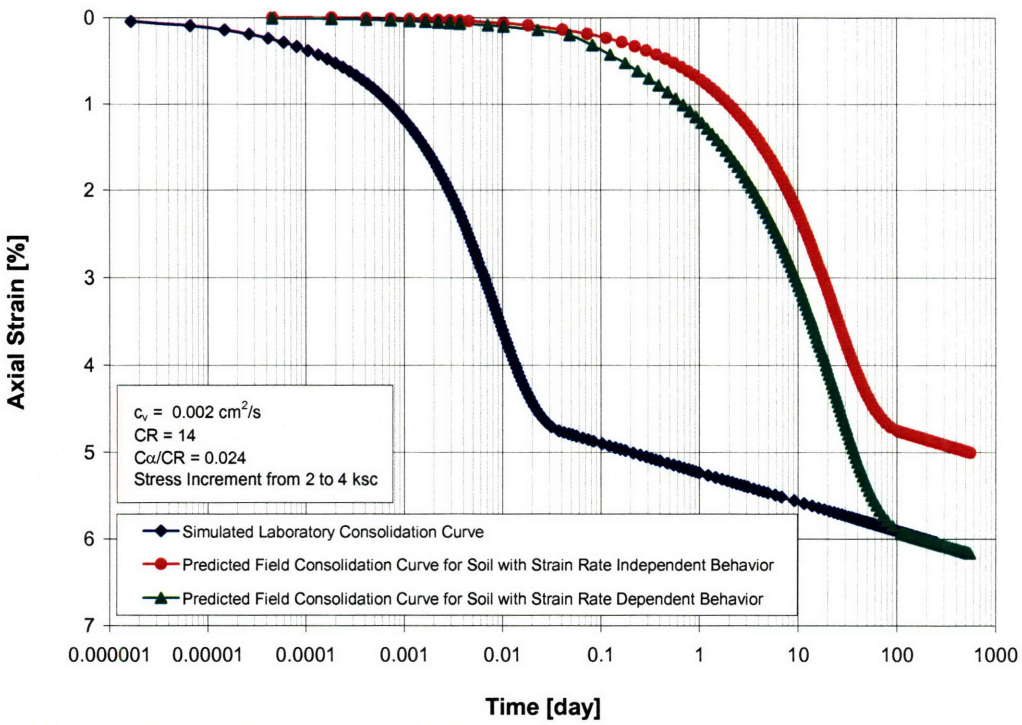

Figure 6.2 Comparison between the predicted vertical strain based on strain rate dependent and strain rate independent behavior soils

Figure 6.2 clearly shows that the predicted axial strain based on the strain rate dependent and independent behaviors are approximately 1% for the 100 cm soil layer. Consider that the axial strain at the end-of-primary consolidation is approximately 4.8%, this difference can cause the settlement predictions based on the strain rate dependent and independent behaviors to differ up to 21%. For a thicker soil layer, the differences can be very large and can result in major settlement miscalculation if the design does not take into account the strain rate dependent behavior properly.

6.1.2 Hydraulic Gradient Effects on Consolidation Behavior of Soft Clay

Hydraulic gradient is an important parameter because the gradient during a laboratory test can be vastly different from that occurring in the field. This difference is mainly the result of the difference in thickness of the soil specimen (used in the lab) and soil layer (in the field). For example, in a CRS test, the hydraulic gradient can reach 500 (at a very fast strain rate) while the hydraulic gradient in the field is usually very low (less then 20). The hydraulic gradient of an oedometer test can reach a much higher level (approximately 7000 for a double drainage test of 2 cm specimen with stress increment of 8 kg/cm^2) at the beginning of a load increment. The differences in the hydraulic gradient applied to the specimen in the laboratory test and that of in the field can cause errors in applying the results from the laboratory tests to field applications.

The effects of hydraulic gradient on the consolidation behavior of soft clay are very difficult to study because hydraulic gradient is coupled with the strain rate during the CRS and oedometer test. To separate the effect of hydraulic gradient from strain rate during the consolidation of soil, one need to control the hydraulic gradient separately while applying a constant rate of strain during a consolidation test. This research introduces this novel idea of testing for hydraulic gradient effects effectively in a relatively easy-to-perform laboratory test. This laboratory test is called the Gradient-controlled Constant Rate of Strain (GCRS) test. Chapter 3 presents the experimental technologies behind this test program. The tests cover strain rate of 0.1%/hr to 3%/hr and normalized base excess pore pressure ($\Delta u_e/\sigma'_{v(AVG)}$) of 2% to 66%.

The effects of hydraulic gradient can be observed from the shifts of the Virgin Compression Line (VCL) location. The higher the effects of the hydraulic gradient on the consolidation behavior of a soil, the larger the shift of the VCL will be. The shifts of the VCL can be quantified by normalized changes in the vertical effective stress ($\Delta\sigma'_v$) at an axial strain by the current vertical effective stress (σ'_v). Since the primary controlled parameter is the imposed gradient (or imposed base excess pore pressure), the normalized shifts of the VCL ($\Delta\sigma'_v/\sigma'_{v(AVG)}$) should be related to the level of imposed hydraulic gradient. It is also more useful to evaluate the results in term of normalized imposed base excess pore pressure ($\Delta u_e/\sigma'_{v(AVG)}$) rather than the absolute value of hydraulic gradient. Expressing the relationship between the shifts of the VCL and

$\Delta u_e/\sigma'_{v(AVG)}$ is not only more useful than that to a hydraulic gradient, but also allow for a more generalize representative of the effects.

The flow direction may also be a factor that might affect the consolidation behavior, in addition to, the imposed normalized excess pore pressure. This research focuses on the flow in the same loading direction (vertical).

The differences between the average vertical effective stress based on Wissa linear and nonlinear theory is less than 1% for the normalized base excess pore pressure, $\Delta u_b/\sigma'_v$, less than 25% (Gonzalez, 2000). The average excess pore pressure during the normal CRS loading phases in this research can be obtained based on Wissa linear CRS theory. The calculation of the average excess pore pressure during the Gradient-controlled CRS loading phase is more complicated. The GCRS loading involves flow of water through the base of specimen controlled by a pressure-volume control device where base pore pressure is constant. This causes the pore pressure distribution within the specimen to deviate from the distribution of the linear CRS theory. In addition, the pore pressure is imposed and we do not have a measurement of the CRS induced component of the excess pore pressure. The GCRS simulation is developed specifically for the interpretation of the GCRS tests. Chapter 4 discusses details of the GCRS simulation.

Figure 6.3 presents the graph between the normalized shifts of the VCL ($\Delta\sigma'_v/\sigma'_v$) versus the normalized base excess pore pressure ($\Delta u_e/\sigma'_v$). It is clear from the figure 6.3 that the VCLs shift to the left ($\Delta\sigma'_v/\sigma'_v$ is negative) when the soil is subjected to an imposed hydraulic gradient during the consolidation phase. The shifts of the VCLs to the left of a normal VCL indicate that the soil structure is weaker when subjected to a high hydraulic gradient during the consolidation process.

The shift of the VCLs can be explained by the increase in flow through specimen during the gradient-controlled consolidation phase. The increased flow lubricates the contact between soil particles and hence reduce the overall strength of the soil structure.

Based on the test results presented in the chapter 5, it is clear that both MBC and SBM show effects from hydraulic gradient during the consolidation. However, it is important to note that SBM exhibit somewhat larger effects than MBC. The hydraulic gradient effects on SBM are approximately 1.6 times higher than that of the MBC. The hydraulic gradient observed in a CRS or oedometer test is always higher than in the field. However, with better understanding of the hydraulic gradient effect, one can more accurately account for the effect and, thus, can potentially be used to improve the field design and analysis. Consider that the hydraulic gradient during an oedometer test is very high especially at the initial consolidation, the hydraulic gradient effects might change the shape of the oedometer consolidation curve.

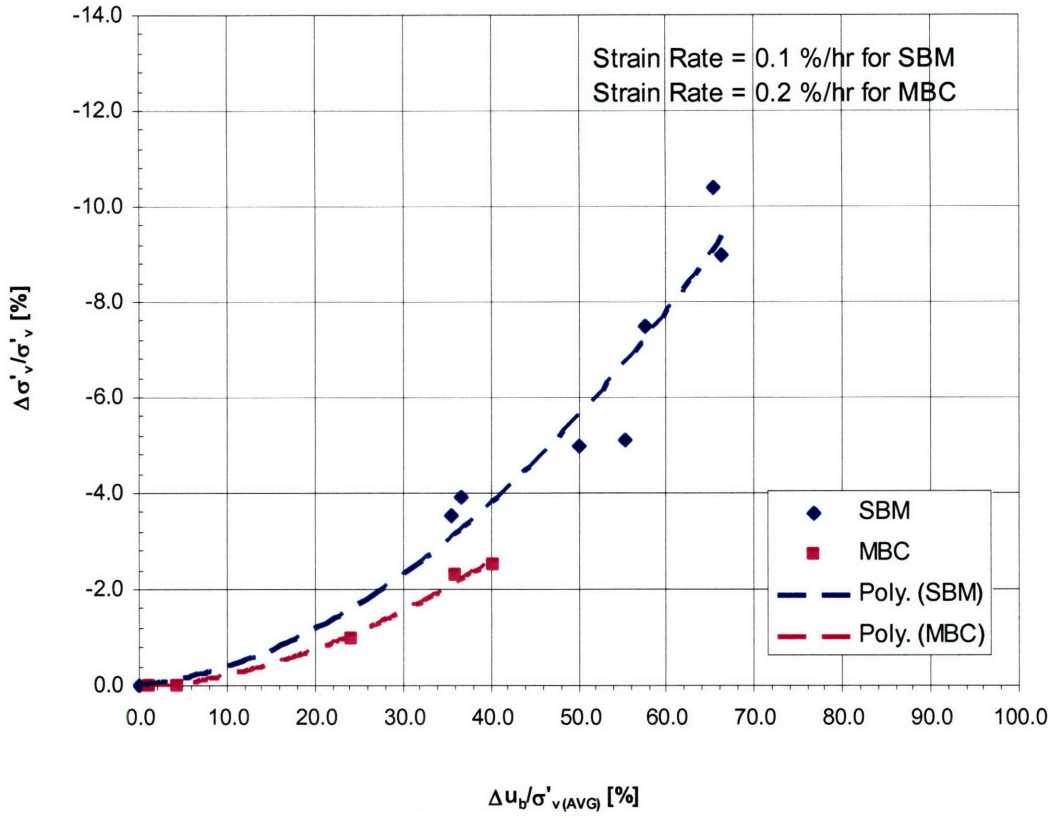

Figure 6.3 Normalized shifts of the VCL ($\Delta\sigma'_v/\sigma'_{v(AVG)}$) versus normalized base excess pore pressure ($\Delta u_e/\sigma'_{v(AVG)}$) for MBC and SBM

6.1.3 Scaling Effects

One of the most important parameters used in practice for the consolidation calculation of soil is the coefficient of consolidation, c_v. The coefficient of consolidation, c_v, is defined as

$$c_v = \frac{k_v}{m_v \cdot \gamma_w} \tag{6.1}$$

The c_v is the variable that governs the consolidation process as clearly shown in the Terzaghi's 1-D consolidation equation. c_v can be easily obtained from an oedometer test. However, there are significant debates as to what is an appropriate value of c_v for uses in a field application. There are many techniques that can be used to obtain the c_v from an oedometer test results. The two most well-known techniques are the square root of time ($\sqrt{t}$) method and logarithm of time (log t) method. Chapter 2 presents details of both methods. These methods generally yield different values of c_v. The c_v obtained

from $\sqrt{t}$ method is generally much higher (usually by 50% or higher) than that obtained from the log(t) method.

The differences make the selection of c_v for use in an engineering application problematic. It is also important to note that the drainage height normally found in an oedometer test is much smaller than that of an actual soil layer. Usually, an oedometer test specimen have a drainage height of 1 cm or larger (ASTM D2435 specifies the minimum initial specimen height of 1.2 cm which equals to 0.6 cm for a double drainage test). A soil layer, normally, has a drainage height in the order of meters.

The goal of the research is to determine whether the drainage height has an effect on the interpreted c_v for MBC and SBM. This is achieved by performing a series of oedometer tests with varying drainage heights and secondary compression range. Another goal is to develop a method to obtain a representative c_v for use in an engineering application. This goal can be achieved by combining the results from laboratory test with the results from a series of oedometer simulation.

Figure 6.4 and 6.5 presents the scaling effect graph for MBC and SBM, respectively. A scaling effect graph is, in essence, a plot between the c_v ratio [$c_v(\sqrt{t})/c_v(\log t)$] versus time to secondary compression (t_{sec}). The graph shows two things. The first thing that the graph shows is whether the drainage heights have effects on the c_v ratio. If the drainage height has effects on the c_v ratio, the c_v ratio obtained from different drainage height tests should be located in different regions in the graph. The graph also shows whether t_{sec} has an effect on the c_v ratio. If the t_{sec} has effects on the c_v ratio, there should be a clear trend of relationship between the two parameters.

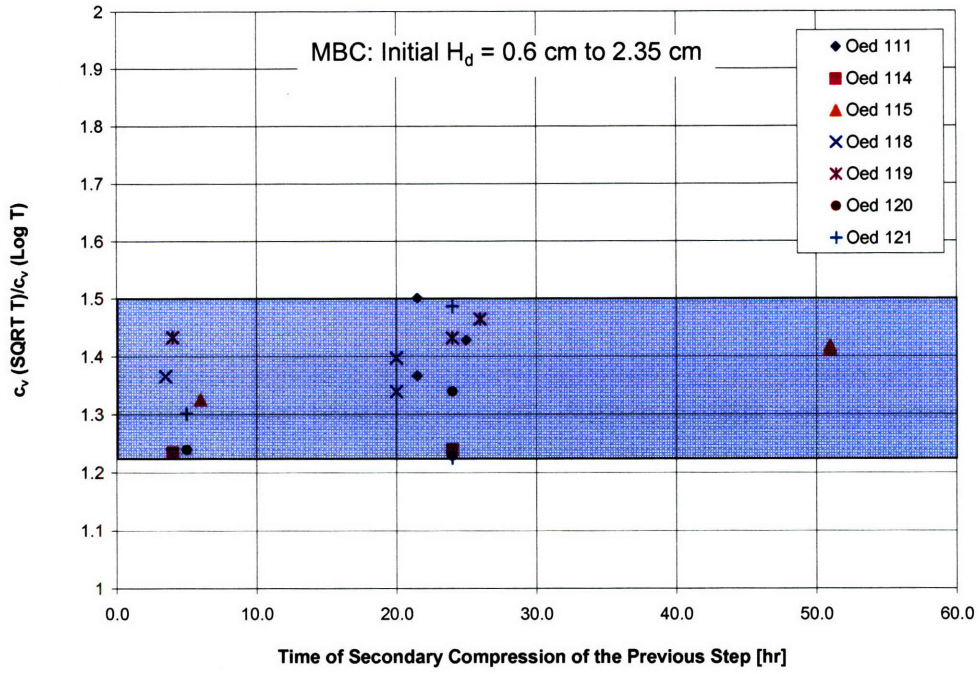

Figure 6.4 c_v ratio versus t_{sec} for MBC

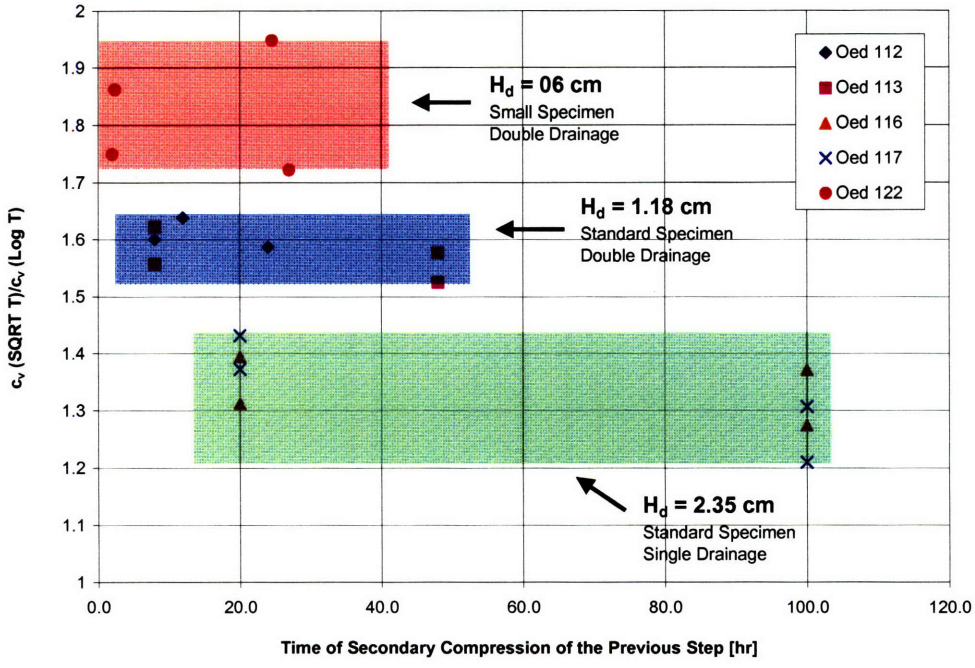

Figure 6.5 c_v ratio versus t_{sec} for SBM

Based on the test results, it is clear that the t_{sec} has no effect on the c_v ratio for both MBC and SBM. For example, with the t_{sec} of approximately 5 times difference (100 hr versus 20 hr for Oed116, SBM), there is no detectable differences between the c_v ratio from the load increment with t_{sec} of 20 hr and that of 100hr. This can be clearly observed from the figure 6.4 and 6.5.

However, when considering the drainage heights, the story changes significantly. The two soils exhibit very different behavior with regard to the scaling effects. While MBC does not exhibit any scaling effects, the SBM shows clear scaling effects. The c_v ratios of MBC are between 1.22 to 1.5 regardless of the drainage heights. The c_v ratio from the SBM tests, on the other hand, can be separated into three zones based on the drainage heights. At the largest drainage height (H_d = 2.35 cm), the SBM c_v ratios are the lowest (between 1.20 and 1.45 with an average c_v ratio of 1.32). When the drainage height decreases from 2.35 cm to 1.18 cm, the average c_v ratio increases from 1.32 to 1.59. At the smallest drainage height, the c_v ratio is the largest with the average of 1.84.

It is obvious that the smaller the drainage heights, the higher the c_v ratio. The results are consistent with the comparison between c_v ratio from a standard oedometer test with a large batch consolidation test (see chapter 2 for more details). The test results imply that for a larger soil layer, the c_v from $\sqrt{t}$ and log(t) methods should be very close.

The c_v based on $\sqrt{t}$ and log(t) are different mainly because the methods focus on different part of the consolidation curve. While the $\sqrt{t}$ method focuses on the initial part of the consolidation, the log(t) method utilizes the later portion of the consolidation curve for the interpretation of c_v value. Essentially, the c_v based on the $\sqrt{t}$ method is bias toward the initial consolidation behavior where the hydraulic gradient is much higher and the vertical deformation occur much faster than the later part. It should also be noted that the c_v is not a material properties. It is a combination of k and m_v which vary independently within a soil layer.

However, one question remains as to what is the representative c_v that one should use for an engineering application. Since the c_v from $\sqrt{t}$ and log(t) methods are different, a careful consideration must be taken in selecting a representative c_v. Instead of subjectively select one c_v based on one method over another or use an average values of c_v, the oedometer simulation can be used to obtain a representative c_v. Essentially, the input c_v of an oedometer simulation can be taken as a representative cv because it is the assumed correct c_v for the soil type (for this simulation). Since the simulation yields $c_v(\sqrt{t})$ and c_v(log t), both c_v can be compared to the representative c_v. A graph between the c_v(rep) and $c_v(\sqrt{t})$ or c_v(rep) and c_v(log t) and drainage height can be constructed based on the simulation results.

These graphs are valuable tools for obtaining the representative c_v when the $c_v(\sqrt{t})$ or c_v(log t) is known, i.e., from a laboratory test. Figure 6.6 and 6.7 present the graph between c_v(rep)/c_v(log t) and drainage height and the graph between c_v ratio [$c_v(\sqrt{t})$/c_v(log t)] and drainage height, respectively. Table 6.1 shows the input parameters used for the simulation.

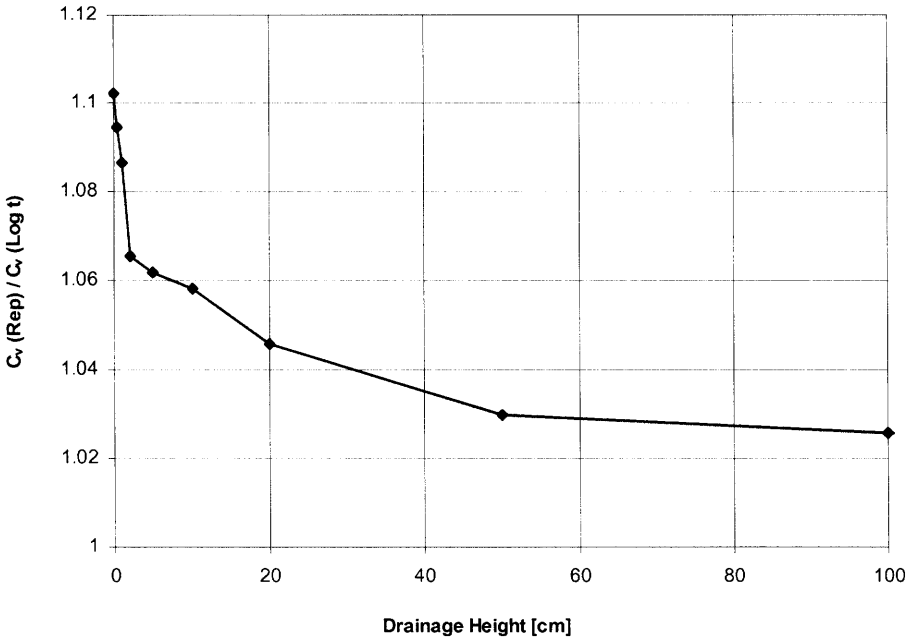

Figure 6.6 Graph between c_v(rep)/c_v(log t) and drainage height

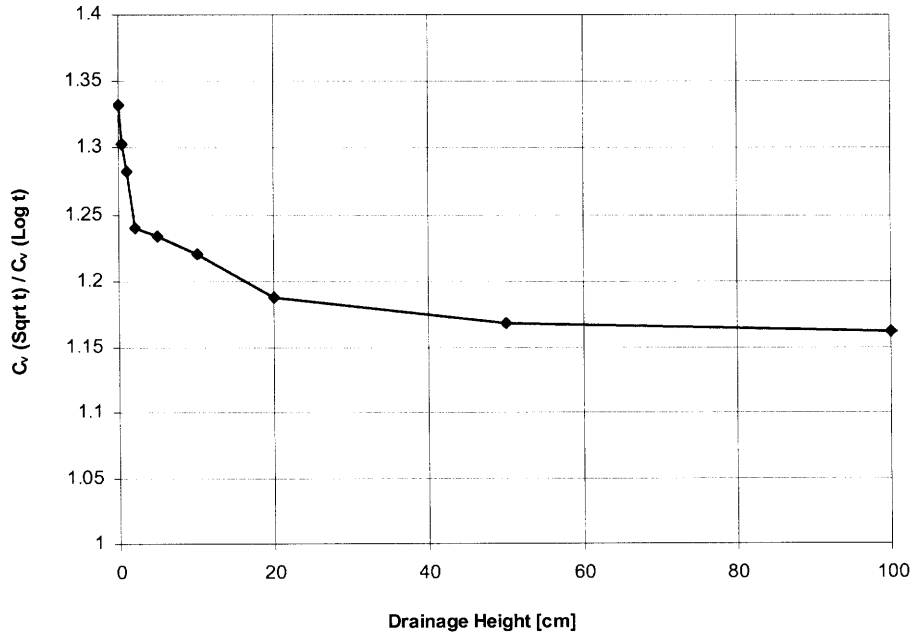

Figure 6.7 Graph between $c_v(\sqrt{t})$/c_v(log t) and drainage height

Input Parameter for Oedometer Simulation for c_v(rep)	
Initial Void Ratio, e_0	1.6
Initial Total Stress, σ_{v0} [ksc]	4
Initial Hydraulic Conductivity, k_0 cm/sec]	5.5×10^{-8}
Coefficient of Hydraulic Conductivity, C_k	0.188
Coefficient of Consolidation, c_v [cm^2/sec]	0.0015
Coeffcient of Compression, C_c	0.468
Stress Increment, $\Delta\sigma_v$ [ksc]	4
Initial Specimen Height [cm]	0.1 to 100

Table 6.1 Summary of the input parameters for the c_v(rep) simulations

It should be noted that the c_v(rep) graph is dependent on soil type (or input parameters). A series of oedometer simulation can be performed for each soil type. The simulation results can be collected into a database for uses in an engineering application.

6.2 Recommendations for Future Works

There are several future works that can greatly compliment this research and advance our understanding of consolidation behavior of soft clays. The following sections provide overview and concepts of possible future works.

6.2.1 Further Strain Rate Sensitivity Tests on Other Soil Types

One of the most important future works is the further studies of strain rate sensitivity of other soil types. Results from the study can be compiled into a database identifying which soils follow hypothesis A, which soils follow hypothesis B, and if some soils have behavior that somewhere between the two hypotheses. Due to complicated nature of soil structure, it is likely that different soil will exhibit different degree of strain rate dependent behavior. This database can be used to separate soils into categories based

on level of strain rate dependency. It can help in identifying the factors that directly or indirectly control or explain the strain rate dependent behavior.

On the engineering practice perspective, with extensive understanding of strain rate effects, a more accurate design and analysis can be achieved and thus can reduce the cost of the overall project.

6.2.2 Simulated Large Soil Layer Consolidation Test

Another novel concept to study the consolidation behavior of soft clay is to perform a series of laboratory test to simulate a large soil layer. Field consolidation testing can take a very long time and the boundary conditions are difficult to ascertain or control. Laboratory tests are usually limited to small specimens. However, laboratory test have a major advantage of well controlled boundary conditions. A large batch consolidation test in laboratory is both time consuming and generally expensive.

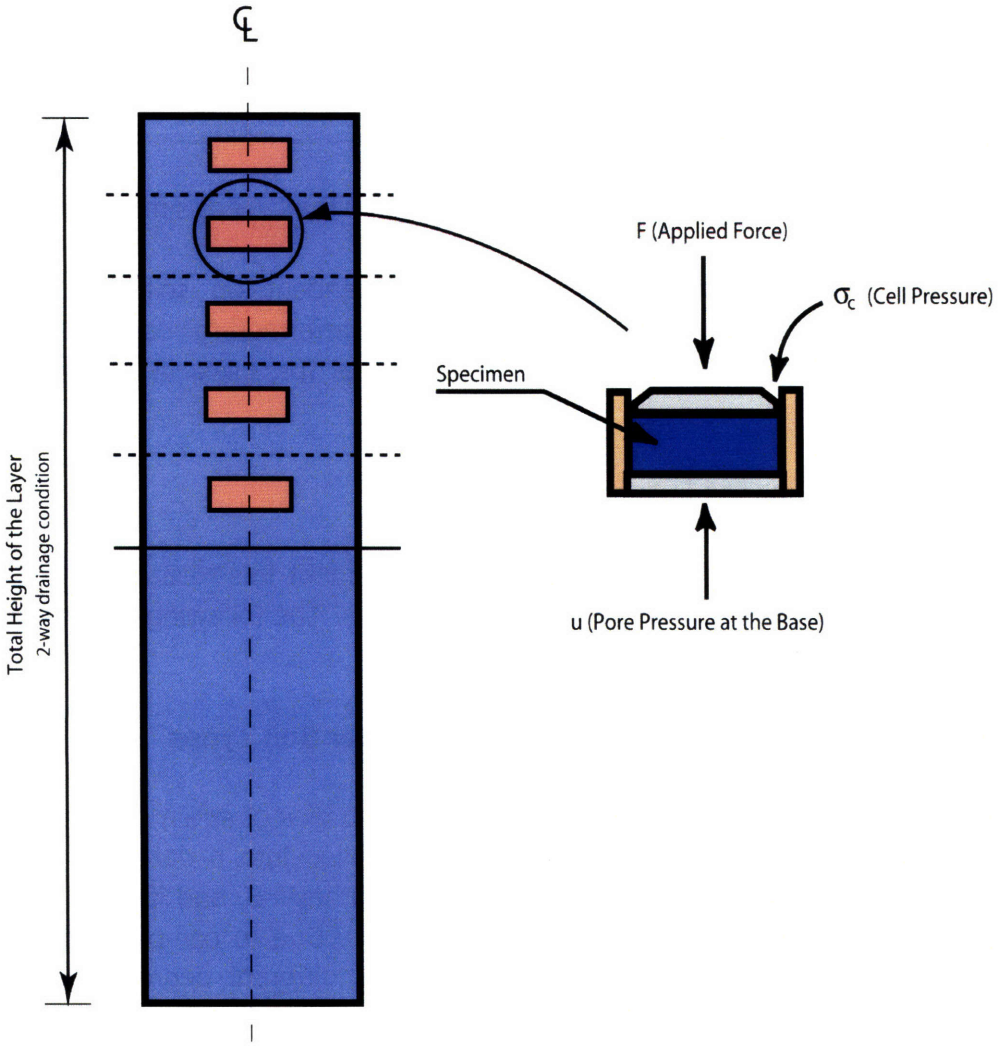

Figure 6.8 Sketch of consolidation test for the representative specimen of each sublayer

A new experimental program can be developed to test the consolidation behavior by simulating a large soil layer. A large soil layer can be separated into several small sublayers as shown in the Figure 6.8. The boundary conditions of each specimen representing the sublayer can be predicted based on Terzaghi's one-dimensional consolidation theory. With the known boundary conditions, a series of consolidation test, can be performed to simulate the specimens at the center of each layer. This experimental program requires a new type of device that can control vertical total stress or deformation, top boundary pore pressure, and base boundary pore pressure during the consolidation process.

6.2.2.1 Equipments

This three axis computer controlled device (*Controlled Elemental Consolidation Apparatus* (CECA) will allow one dimensional compression tests to be performed under conditions of uniform stress (including pore pressure) and imposed gradients. As a starting point, Terzaghi's solutions can be used to define the variation of average effective stress and hydraulic gradient applied to the specimen over time. The device can be a modification of the Trautwein CRS Consolidometer, two pressure-volume controllers, one 50 kN load frame, and a computer data acquisition/control system.

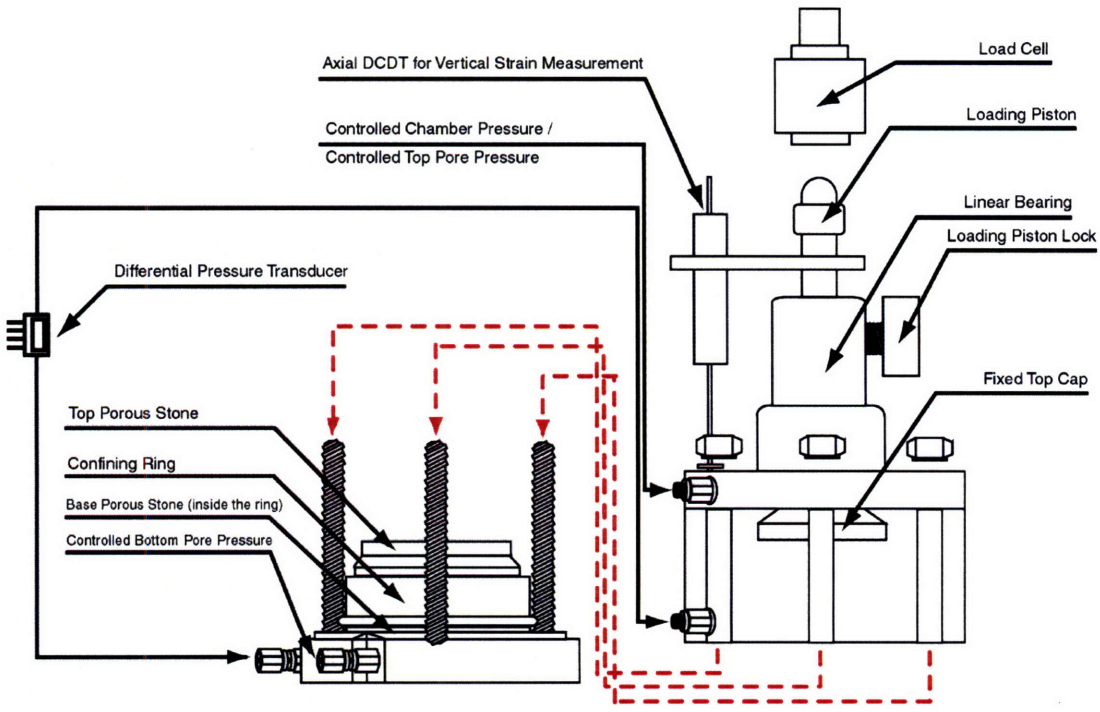

Figure 6.9 Schematic drawing of a possible CACE device

The CECA can be designed through selection of the appropriate transducers and gear drives to meet the following requirements. The computer will control the axial drive system to a vertical stress tolerance of 0.05 kPa and a strain rate of ± 0.5%. One pressure-volume controller will maintain the top pore pressure to the tolerance of ± 0.05 kPa. The second pressure-volume controller will be used to control the gradient using the output from a differential pressure transducer. The gradient should be controlled to ±0.1 tolerances. Due to the relatively long duration of the experiments, the apparatus should be enclosed in an environmental chamber with temperature control to ± 0.5°C. The basic experimental components and methodology are described in DaRe et al. (2001). Figure 6.9 provides a schematic of a possible design of the CECA device.

6.2.2.2 Data Interpretation

The measured strain versus time relationships from a range of layer heights and for a given stress increment must be compared to evaluate applicability of Hypothesis A or B. These relationships are directly measured with the oedometer and large batch consolidometer. However, each soil element consolidation test provides the relationship for one location in the soil layer and it will be necessary to integrate the measurements of several tests to obtain the settlement curve for the entire layer. One possible integration scheme is illustrated in figure 6.10 that uses a curve fit guided by conventional pore pressure isochrones. Other integration schemes are possible and it will be necessary to investigate several to understand the sensitivity of the findings to interpretation method.

Obviously, the choice of analysis method becomes less important as the number of test locations increase. However, testing time is a major consideration and the proposal is based on simulating five elements. The set of time curves representing layers between 2 and 150 cm thickness will be used to evaluate the rate of consolidation and the rate of secondary compression as a function of layer thickness. This will allow direct comparison with Hypothesis A and B predictions. Preliminary calculations predict more than 4% strain difference between the two Hypotheses for the increment between 200 and 400 kPa for RBBC.

With this experimental program, we can study the large soil layer consolidation in a controlled environment with relatively inexpensive cost. The main obstacle for such project is the time require for the test itself. Due to the fact that the laboratory test tries to simulate an elemental consolidation of the center of each layer, the time require to finish consolidated the element can be extremely long especially the element of the center layer (where the water drain out the slowest).

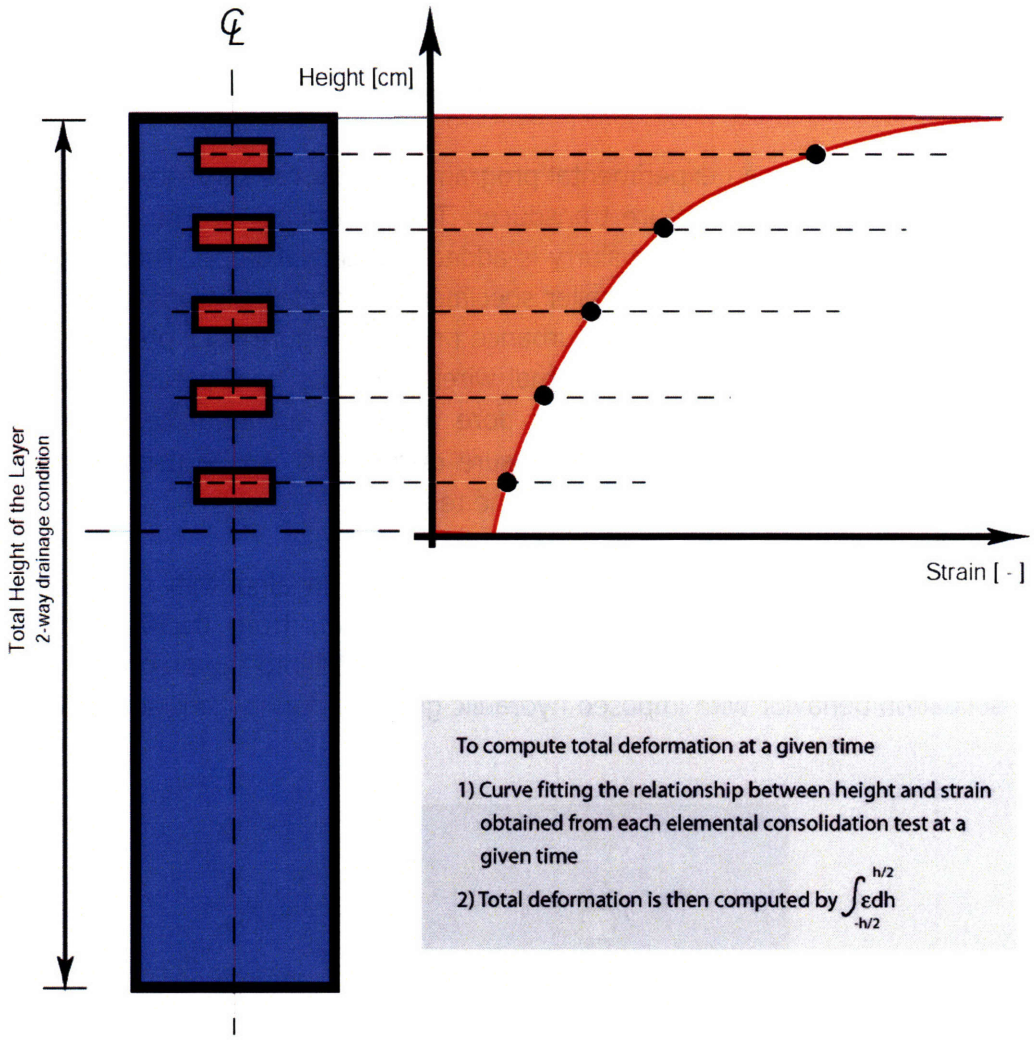

Figure 6.10 Sketch of a possible data interpretation of consolidation from CACE tests

A conceptual framework can be formulated to describe the observed aspects of consolidation and compression behavior as a function of hydraulic gradient and strain rate. This conceptual framework will guide the development of a plan to recommend a testing methodology for the profession to measure consolidation properties of a deposit and apply the results to the field scale. This proposed technique will take into consideration the accuracy, cost, and time required for the tests.

6.2.3 Incorporation of Real-time Hydraulic Gradient Control to GCRS Tests

Further study of hydraulic gradient effects is also very important. The study of hydraulic gradient effects can be further improved by incorporate a real-time hydraulic gradient control into the experimental program. It is also greatly beneficial to develop a reliable method to measure internal excess pore pressure during the tests. The measurement of

internal excess pore pressure is difficult without causing disturbance to the soil structure or allowing some extra excess pore pressure to dissipate out of the specimen.

It is possible to construct an experimental program to test a resedimented soil with very small wireless excess pore pressure transducer. The transducer can be installed inside the consolidation chamber prior the slurry is added and consolidated. The resedimented specimen is, then, can be cut into smaller specimens with internal transducers in place. With this method, we eliminate the disturbance problem. Figure 6.11 presents a sketch of a soil specimen with pre-installed internal wireless excess pore pressure transducer. With internal measurement of the excess pore pressure, an accurate pore pressure distribution can be obtained. The pore pressure distribution can be used to obtain an accurate average vertical effective stress for the test.

The GCRS simulation can also be improved to include an algorithm to simulate the correction factor graph covering typical strain rate (i.e., from 0.1%/hr to 3%/hr) automatically. The transient calculation can also be included into the program to capture the consolidation behavior with imposed hydraulic gradient during transient state.

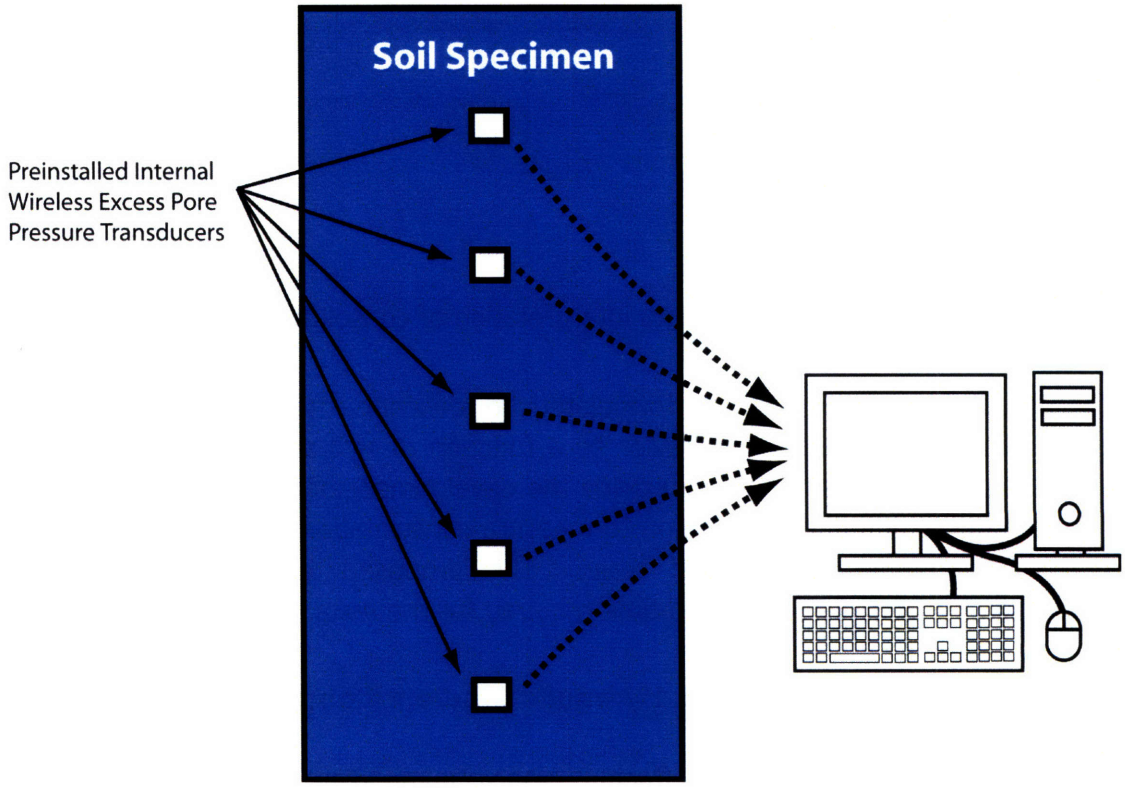

Figure 6.11 Sketch of a soil specimen with pre-installed internal wireless excess pore pressure transducer

6.2.4 Additional Scaling Effect Study on Oedometer Tests

The study of scaling effect can also be expanded to cover more soil types and more drainage heights. The aspect ratio of the specimen should be kept the same to avoid the problems with different level of side friction applied to the specimen during tests. Another problem that needs to be considered is that a specimen height cannot be too small. The ASTM D2435 specifies the minimum initial specimen height of 1.2 cm (or at the minimum 10 times the maximum particle diameter). This specimen height translates to the minimum drainage height of 0.6 cm. Therefore, any oedometer tests with a drainage height less than 0.6 cm should be avoided.

Additional scaling effect tests should focus on the drainage height starting from 0.6 cm and double the drainage height for each subsequent test up to drainage height of 10 cm. The drainage height of 10 cm is selected as the higher end of the limit for practical purpose. Consolidation of a specimen with drainage height larger than 10 cm will take significant time, not to mention that a natural soil specimen that size is very difficult to obtain and often very expensive. For example, a SBM specimen with drainage height of 10 cm can take 45 days or more to complete a single load increment (20 days for primary consolidation and at least 25 days for the secondary compression). A complete oedometer test, in this case, can take up to 9 – 12 months.

The results from double drainage test of a 2.4 cm height specimen (H_d = 1.2 cm) can also be compared to the results from the single drainage test of a 1.2 cm height specimen. The tests can be used to study the effects of side friction.

To avoid the difficulty with obtaining large natural soil specimens, the tests can be performed with a resedimented soil instead. But the difference between the natural and resedimented soil behavior must also be taken into consideration. Generally, undisturbed natural soil samples are preferred because the observed behavior in laboratory should reflect that in the field more closely than that of resedimented soil. Figure 6.12 presents a sketch of specimens covering 5 different drainage heights (from 0.6 cm to 10 cm).

It should be noted that while the relationship between simulated c_v ratio and drainage height is similar to that of the measured c_v ratio, the values of simulated c_v ratio and measured c_v ratio are significantly different. It is important to investigate this difference.

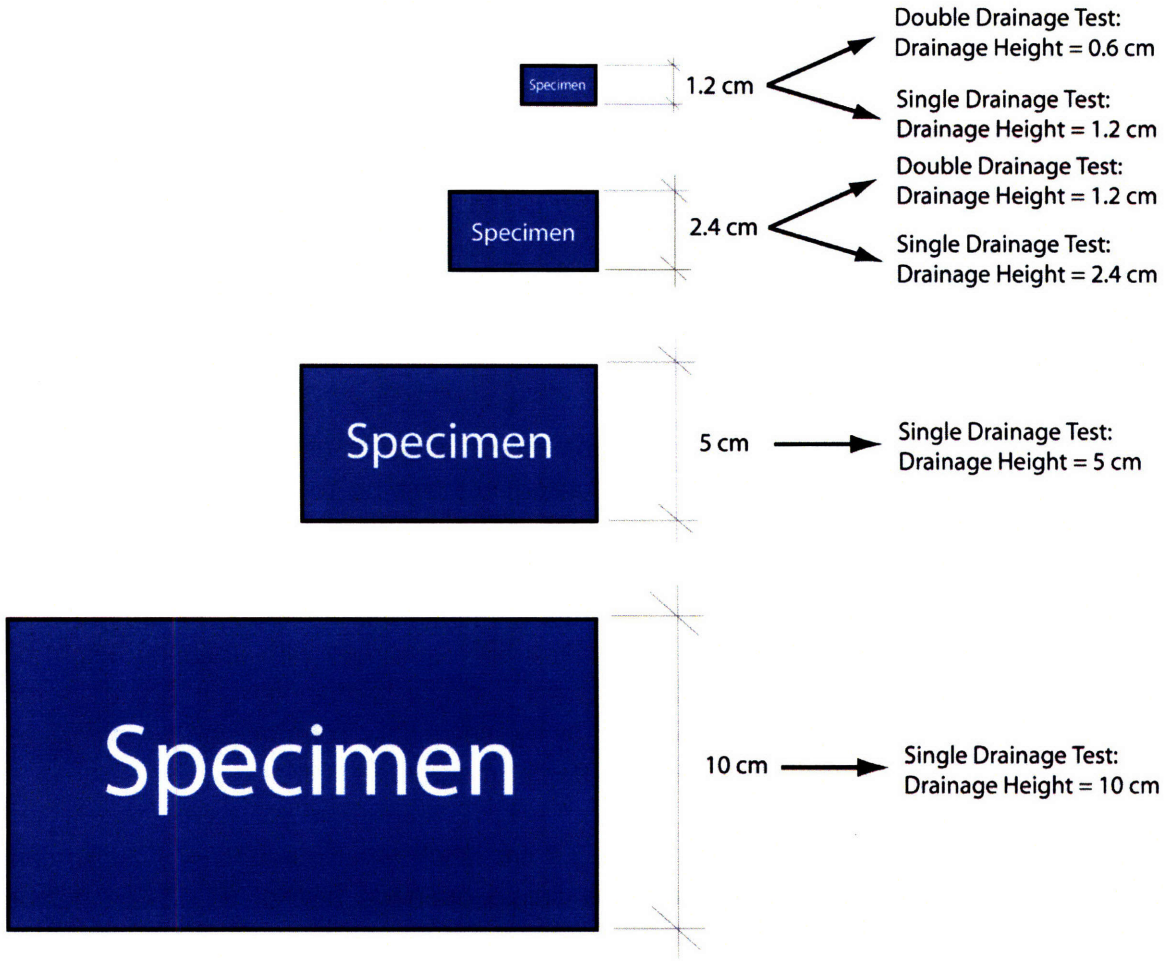

Figure 6.12 Sketch of oedometer specimens covering 5 different drainage heights from 0.6 to 10 cm

6.2.5 Further study of scaling effects

The results from strain rate sensitivity and hydraulic gradient effect tests can be incorporated into a numerical simulation model. The predictions from the model can be used to compare with the test results to study the scaling issues further.

Chapter 7: References

1. ASTM D 2435 – 04, "Test Methods for One-Dimensional Consolidation Properties of Soils Using Incremental Loading", *Annual Book of ASTM Standard*, ASTM International.

2. ASTM D 4186 – 89, "Test Methods for One-Dimensional Consolidation Properties of Soils Using Controlled-Strain Loading", *Annual Book of ASTM Standard*, ASTM International.

3. Chartier, M. (2005), Data from Constant Rate of Strain test for strain rate sensitivity study of Maine Blue clay (CRS594).

4. Da Re, G., Santagata, M.C., and Germaine, J.T. (2001), "LVDT Based System for the Measurement of the Prefailure Behavior of Geomaterials", *Geotechnical Testing Journal*, ASTM, Vol. 24, No. 3, pp. 288-298.

5. Fox, P. J. (1996), "Analysis of Hydraulic Gradient Effects for Laboratory Hydraulic Conductivity Testing", *Geotechnical Testing Journal*, Volume 19, Issue 2, pp. 181-190

6. Germaine, J. T. (2002), Personal communication regarding the consolidation behavior of large RBBC batch consolidation and coefficient of consolidation relative to laboratory oedometer test.

7. Germaine, J. T. (2003), Personal communication regarding the appropriate strain rate for the Gradient-controlled Constant Rate of Strain (GCRS) test for Maine Blue clay and San Francisco Bay mud.

8. Germaine, J. T. (2007), Constant Rate of Strain Test Results for Strain Rate Sensitivity study of Maine Blue Clay (CRS860, CRS861, and CRS862).

9. Gonzalez, J. H. (2000), "Experimental and Theoretical Investigation of Constant Rate of Strain Consolidation", Massachusetts Institute of Technology S.M. Thesis.

10. Holtz, R. D. and Kovacs, W. D. (1981), "An introduction to Geotechnical Engineering", *Prentice-Hall Civil Engineering and Engineering Mechanics Series*, Prentice-Hall, Inc.

11. Imai, G. and Tang, Y.X. (1992), "A Constitutive Equation of One-Dimensional Consolidation Derived from Inter-connected tests", *Soils and Foundations*, 32(2), pp. 83-96.

12. Imai, G. (1995), "Analytical Examinations of the Foundations to Formulate Consolidation Phenomena with Inherent Time-dependent", *Int. Symp. On Compression and Consolidation of Clayey Soils – IS-Hiroshima's 95*, Hiroshima, 2, pp. 891-935.

13. Jamiolkowski, M., Ladd, C.C., Germaine, J.T., and Lancellotta, R. (1985), "New Developments in Field and Laboratory testing of Soils", *Proc., 11th. International Conference on Soil Mechanics and Foundation Engineering, San Francisco*, 1, 57-153.

14. Ladd C.C., Foott, R., Ishihara, K., Schlosser, F., and Poulos, H.G. (1977). "Stress-deformation and strength characteristics." *General Report, Proc. 9th Int. Conf. Soil Mech. Found. Engrg.*, 2, 421-494

15. Ladd, C.C., Whittle, A.J., and Legaspi, D.E. (1994), "Stress-Deformation Behavior of an Embankment on Boston Blue Clay", *Proceedings of Settlement' 94, Geotechnical Engineering Division/ASCE*, pp. 1730-1759

16. Lambe T. W. and Whitman R. V. (1979), "Soil Mechanics, SI Version", John Wiley & Sons, New York, pp. 32-37, 406-412.

17. Leroueil, S., Kabbaj, M., Tavenas, F., and Bouchard, R. (1985), "Stress-strain-strain rate Relation for The Compressibility of Sensitive Natural Clays", G*eotechnique*, Vol. 35, No.2, pp. 159-180.

18. Leroueil, S. and Marques, M.E.S. (1996), "Importance of Strain rate and Temperature Effects in Geotechnical Engineering", *Geotechnical Special Publication No. 61*, ASCE, New York, pp. 1-60.

19. Leroueil S. (1996), "Compressibility of Clays: Fundamental and Practical Aspects", *Journal of Geotechnical Engineering, American Society of Civil Engineers, Geotechnical Engineering Division*, Vol. 122, No.7, pp.534-543.

20. Mesri, G., and Godlewski, P.M. (1977), "Time- and Stress-Compressibility Interrelationship", *Journal of Geotechnical Engineering*, ASCE, Vol. 103, No. 5, pp. 417-430.

21. Mesri, G., and Choi, Y.K. (1985), "The Uniqueness of The End-of-primary (EOP) void ratio-effective stress relationship", *Proc. 11th ICSMFE*, San Francisco, 2, pp. 587-590.

22. Mesri, G., and Castro, A. (1987), "C_α/C_c Concept and K_0 during Secondary Compression", *Journal of Geotechnical Engineering*, Vol. 113, No. 3, pp. 230-247.

23. Mesri, G., Shahien, M., and Feng, T.W. (1995), "Compressibiliity Parameters during Primary Consolidation", *Int. Symp. On Compression and Consolidation of Clayey Soils – IS-Hiroshima's 95*, Hiroshima, 2, pp. 1021-1037.

24. Mesri, G., Stark, T.D., Ajlouni, M.A., and Chen, C.S. (1997), "Secondary Compression of Peat with or without Surcharging", *Journal of Geotechnical and Geoenvironmental Engineering*, Vol. 123, No. 5, pp. 411-421.

25. Mitchell, J. K. (1993), "Fundamental of Soil Behaviors", John Wiley & Sons, New York.

26. Nguyen, H.Q. (2007), "Reanalysis of the Settlement of a Levee on Soft Bay Mud", Massachusetts Institute of Technology.

27. Olson, R.E. (1985), "State of the Art: Consolidation Testing", *Consolidation of Soils: Testing and Evaluation, ASTM Special Technical Publication 892*, pp. 7-70.

28. Olson, R.E. (1998), "Settlement of Embankments on Soft Clays", *Journal of Geotechnical and Geoenvironmental Engineering*, Vol. 124, No. 4, pp. 278-288.

29. Sheahan, T.C. and Watters, P.J. (1997), "Experimental Verification of CRS Consolidation Theory", *Journal of geotechnical and Geoenvironmental Engineering*, Vol. 123, No. 5, pp. 430-437.

30. Terzaghi, K. (1923), "Die Berechnug der Durchlassigkeitsziffer des Tones aus dem Verlauf der hydronamischen Spannungserscheinungen." *Akademie der Wissenschaften in Wien. Sitzungsberichte. Mathematischnaturwissenschaftliche Klasse.* Part IIa, 132(3-4), 125-138. (Reprinted in *From Theory to Practice in Soil Mechanics*, Wiley, New York, 1960.)

31. Wissa, A.E.Z, Christian, J.T., Davis, E.H., and Heiberg, S. (1971), "Consolidation at Constant Rate of Strain", *Journal of Soil Mech. Found. Div.*, ASCE, 97(SM10), pp. 1393-1413.

Appendix A

Summary Table of Soil Specimen Properties

- Initial Void Ratio
- Natural Water Content
- Compression Ratio
- $C\alpha\varepsilon/CR$
- Coefficient of Consolidation

CRS test results

- Compression Curve (ε_a vs log σ'_v)
- Strain Rate Graph ($\dot{\varepsilon}$ vs ε)
- Normalized Base Excess Pore Pressure Graph ($\Delta u_b/\sigma'_v$ vs ε)

Oedometer Test Results

- Compression Curve
- Consolidation Curve in Square Root of Time Space for Each Load Increment (ε vs $\sqrt{t}$)
- Consolidation Curve in Logarithm of Time Space for Each Load Increment (ε vs log t)

A.1 Summary Table CRS and Oedometer Test

Test No.	Soil Type	Initial Void Ratio, e0	Natural Water Content [%]	Strain Rate [%/hr]	Note
crs639	MBC	0.907	31.01	0.18	GCRS Test
crs640	MBC	0.865	32.44	0.2	GCRS Test
crs649	MBC	0.967	33.39	0.2	GCRS Test
crs652	MBC	0.910	34.12	0.2	GCRS Test
crs594	MBC	-	-	1, 8	Strain Rate Test
crs860	MBC	0.911	32.44	0.5, 1.0	Strain Rate Test
crs861	MBC	0.960	34.23	1, 2	Strain Rate Test
crs862	MBC	-	-	1, 0.1	Strain Rate Test
crs654	SBM	2.548	77.78	0.09	GCRS Test
crs656	SBM	2.081	78.31	0.1	GCRS Test
crs662	SBM	2.301	73.10	0.088	GCRS Test
crs672	SBM	2.371	80.51	0.1, 0.75, 1.5	Strain Rate Test
crs674	SBM	2.294	76.47	0.375	GCRS Test
crs680	SBM	2.854	97.17	0.5	GCRS Test
crs683	SBM	2.776	98.43	0.5	GCRS Test
crs686	SBM	2.533	81.55	3	GCRS Test
crs687	SBM	2.752	95.78	1.45	GCRS Test
crs691	SBM	2.786	98.18	0.75, 1.5, 3.0	Strain Rate Test
Test No.	**Soil Type**	**Initial Void Ratio, e0**	**Natural Water Content [%]**	**Compression Ratio, CR**	**Cae/CR**
oed111	MBC	0.879	30.72	9.12	0.0311
oed114	MBC	0.904	31.50	8.82	0.0635
oed115	MBC	0.888	31.46	13.12	0.0281
oed118	MBC	0.906	30.51	9.66	0.0355
oed119	MBC	0.903	29.53	10.09	0.0429
oed120	MBC	0.904	31.42	10.74	0.0301
oed121	MBC	0.892	30.17	10.23	0.0376
oed112	SBM	2.579	78.82	26.12	0.0370
oed113	SBM	2.371	80.94	24.15	0.0378
oed116	SBM	2.581	74.59	22.85	0.0401
oed117	SBM	2.137	76.18	21.62	0.0366
oed122	SBM	2.435	81.42	19.97	0.0359

Table A.1 Summary of CRS and Oedometer Test

A.2 CRS Test Results

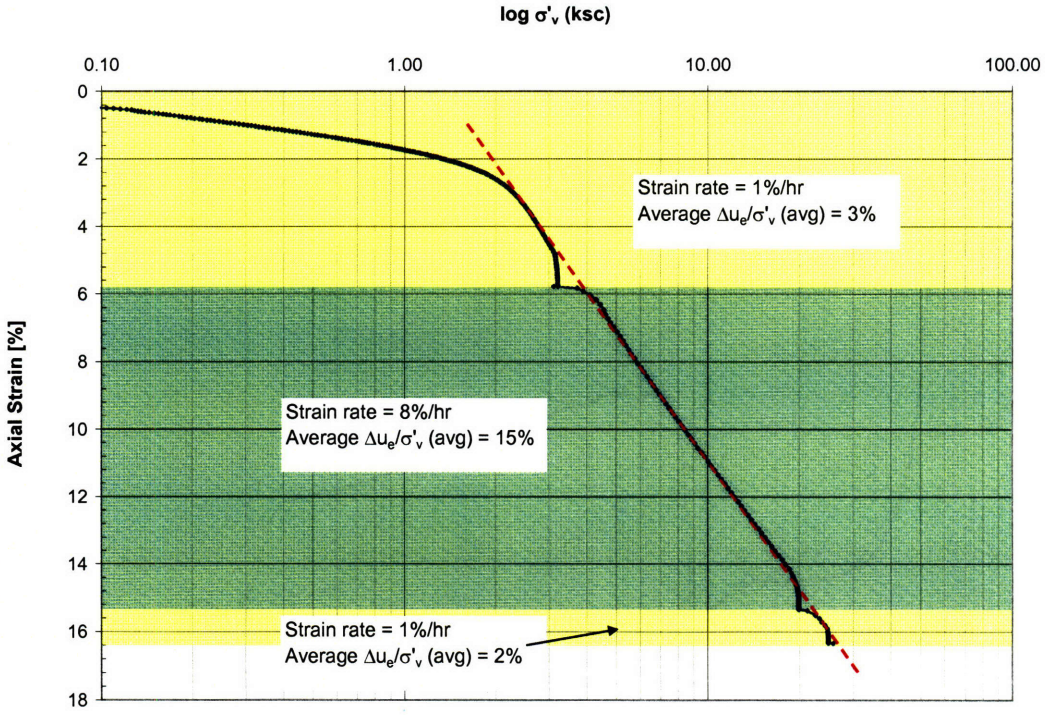

Figure A.1 Compression curve of CRS594

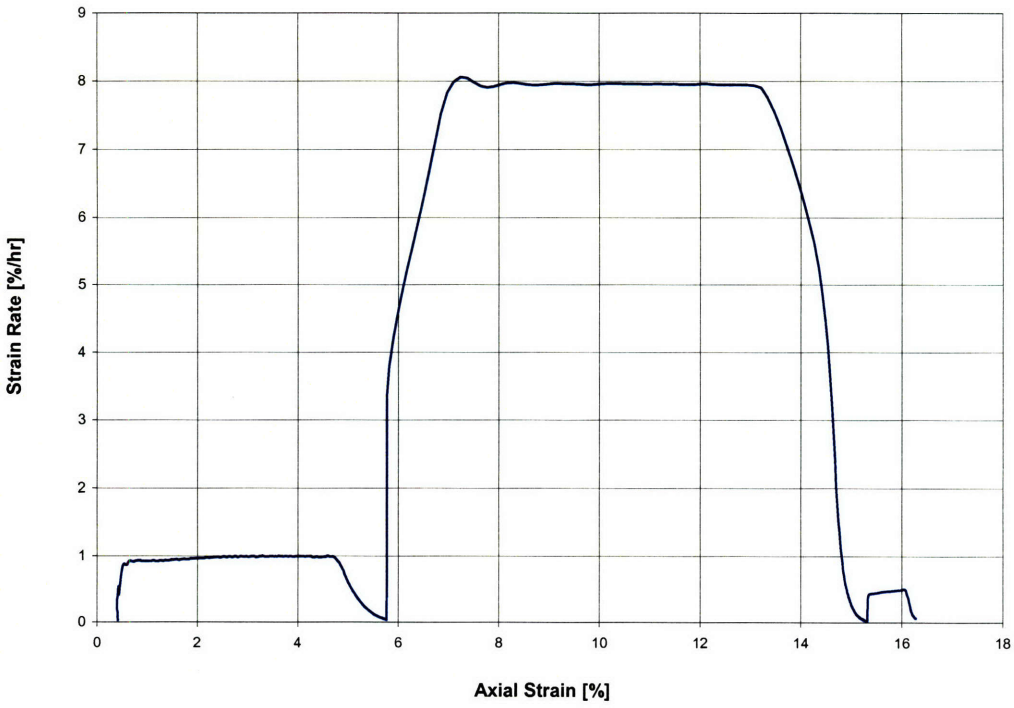

Figure A.2 Strain rate graph of CRS594

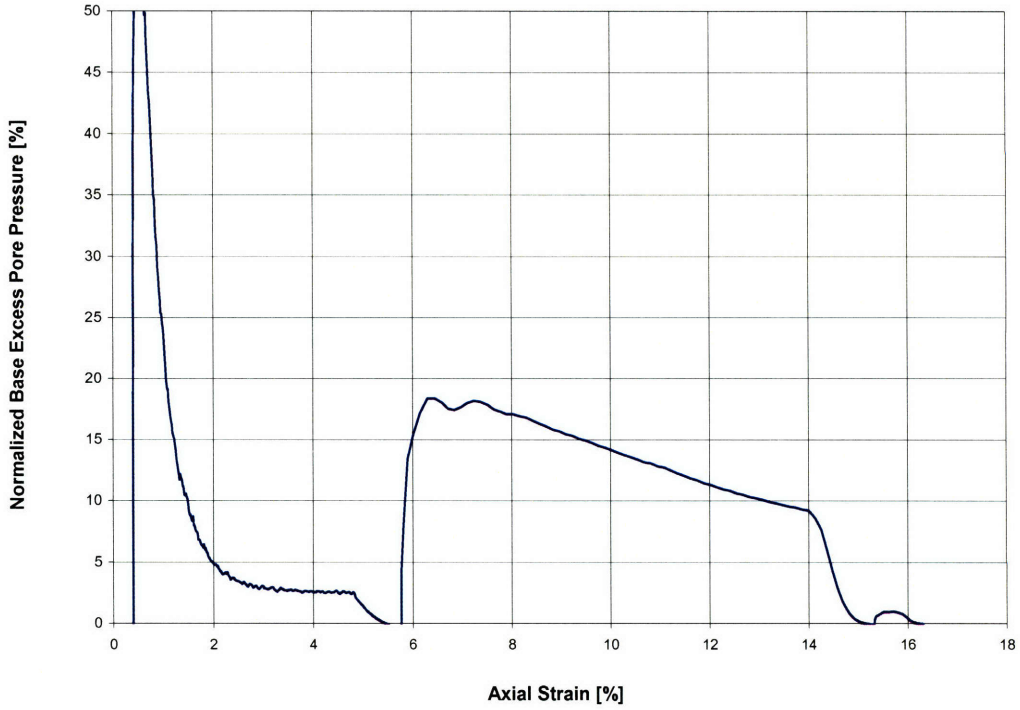

Figure A.3 Normalized base excess pore pressure graph of CRS594

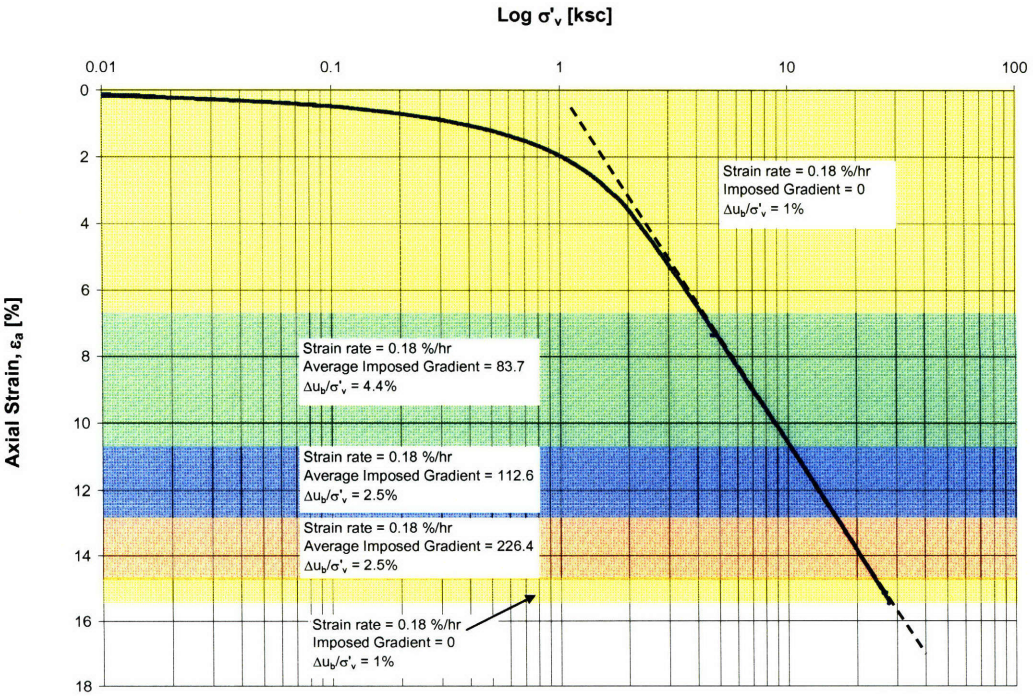

Figure A.4 Compression curve of CRS639

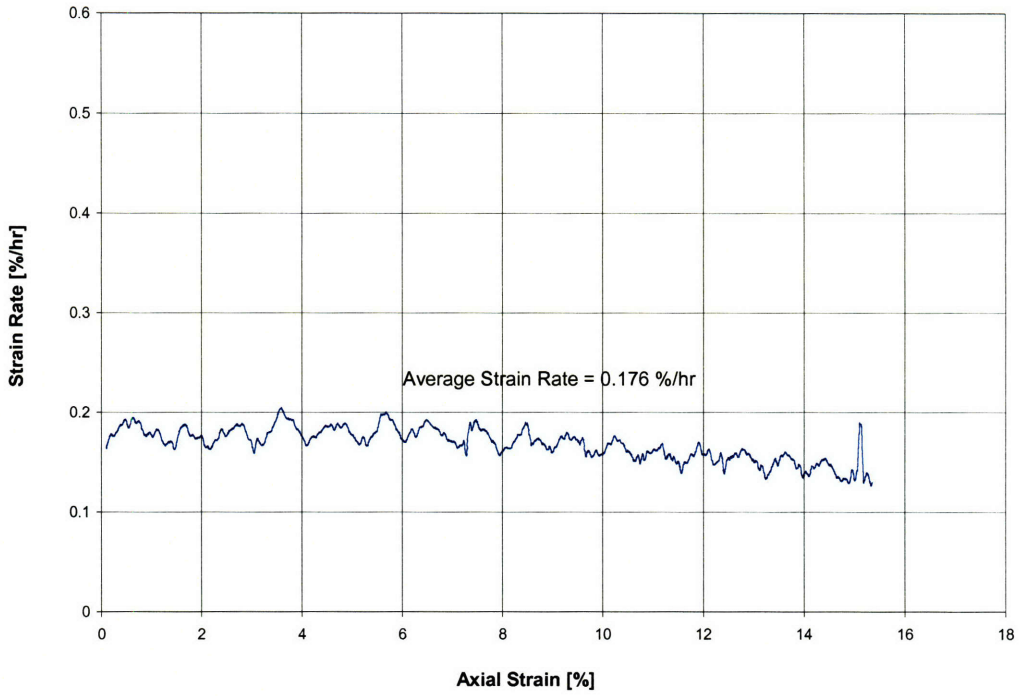

Figure A.5 Strain rate graph of CRS639

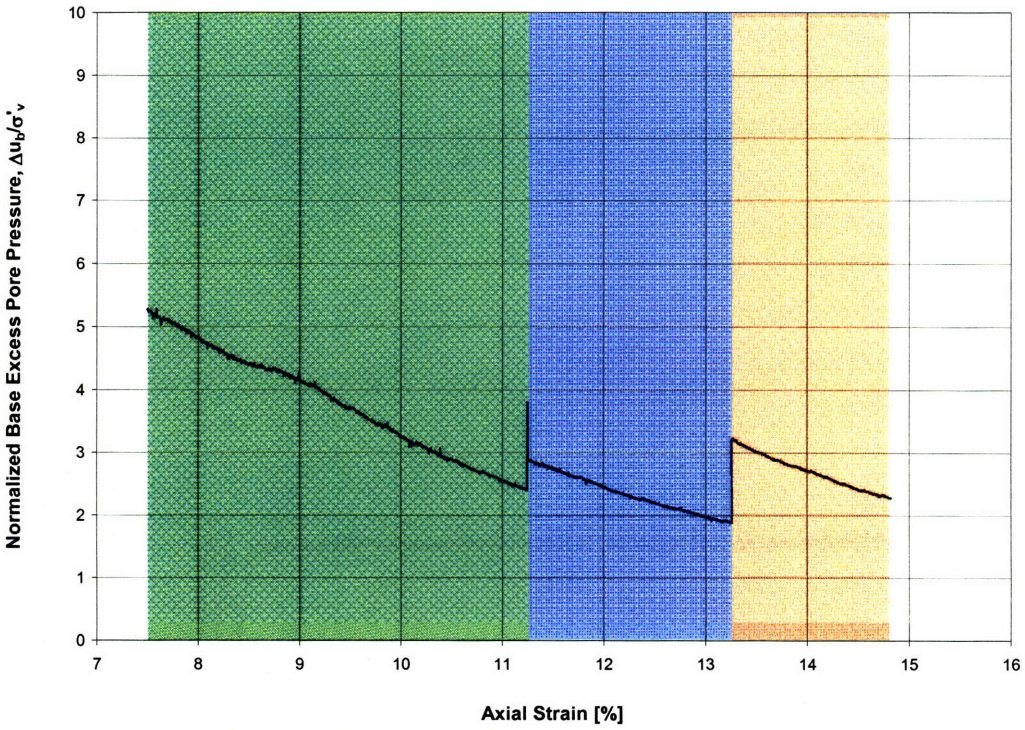

Figure A.6 Normalized base excess pore pressure graph of CRS639

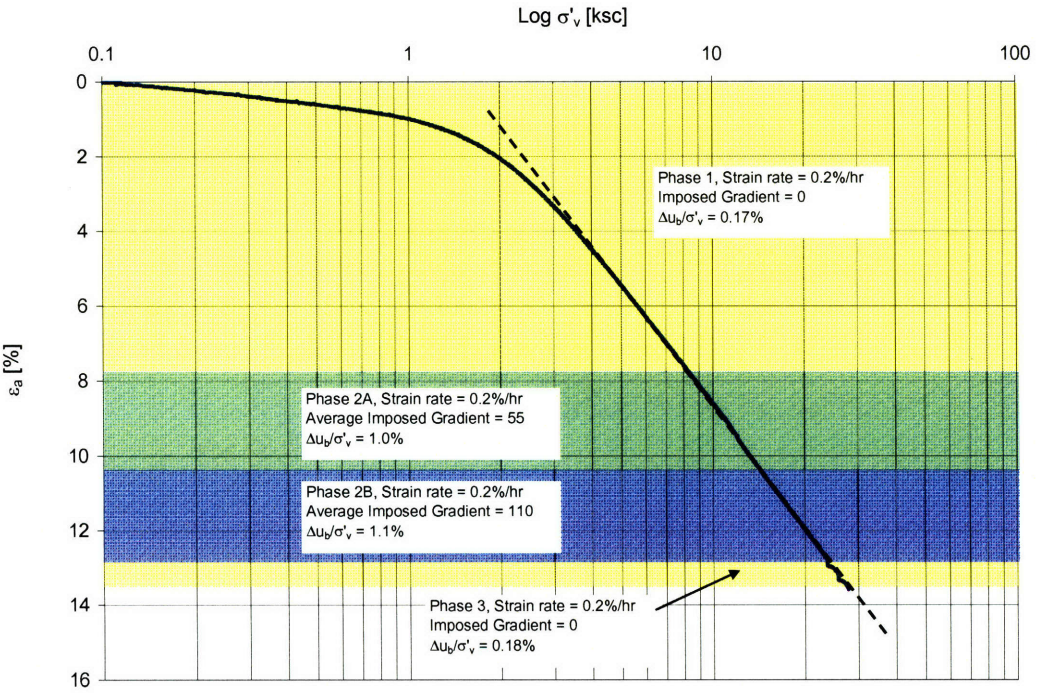

Figure A.7 Compression curve of CRS640

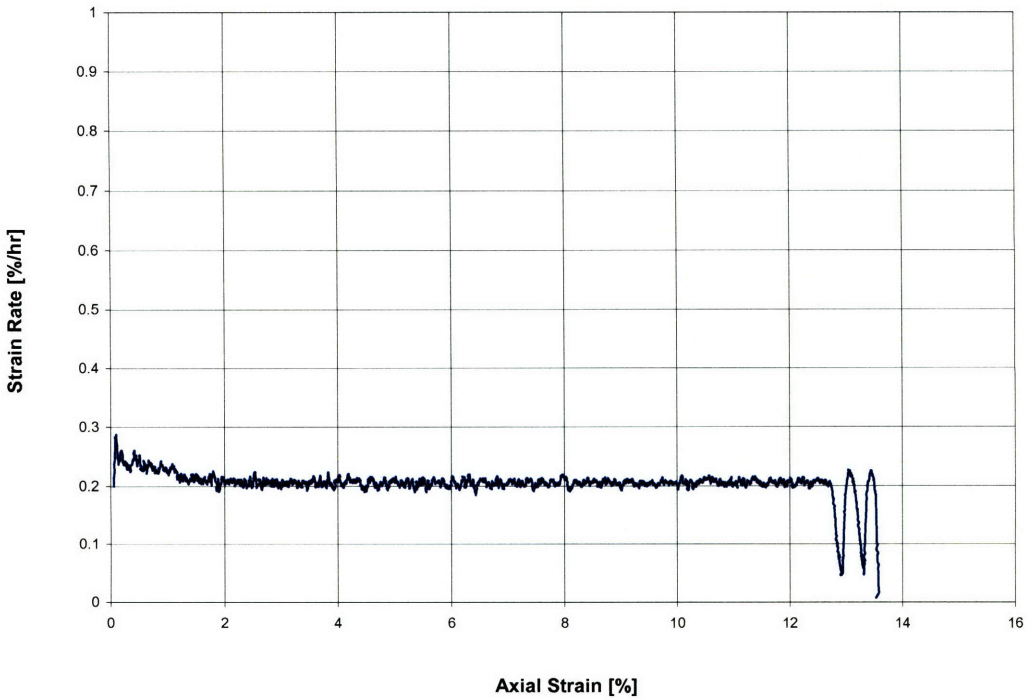

Figure A.8 Strain rate graph of CRS640

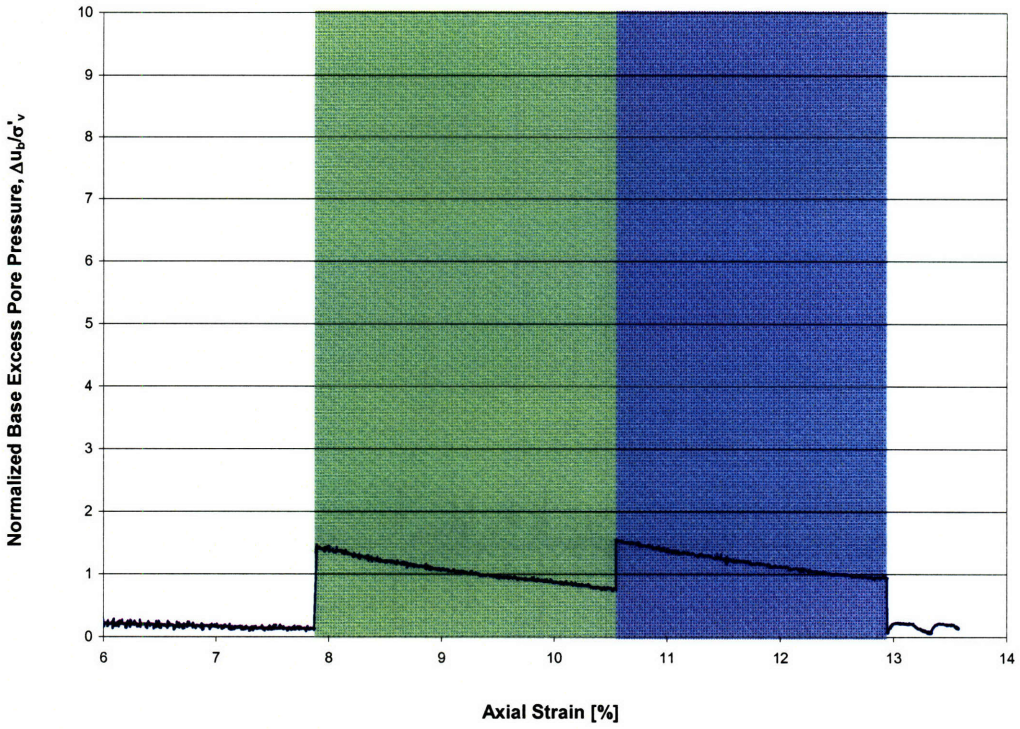

Figure A.9 Normalized base excess pore pressure graph of CRS640

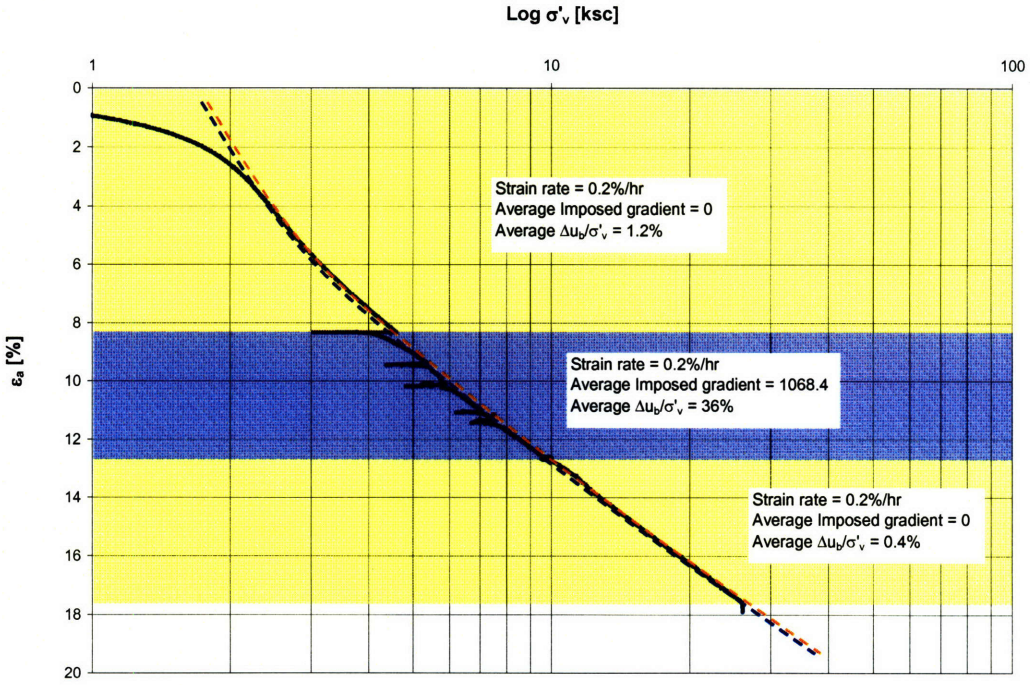

Figure A.10 Compression curve of CRS649

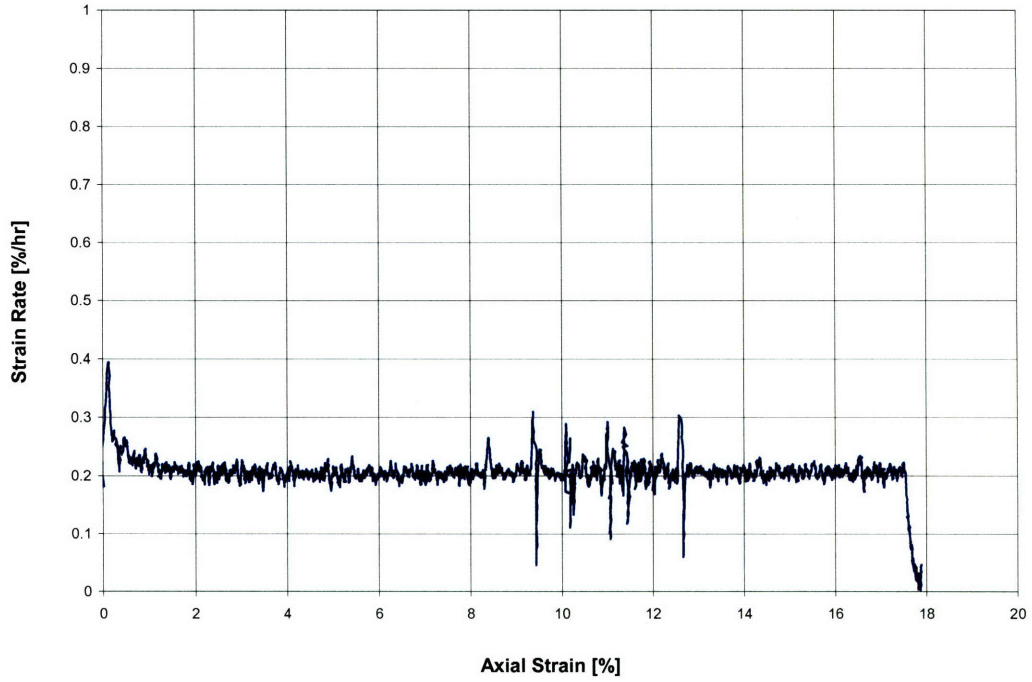

Figure A.11 Strain rate graph of CRS649

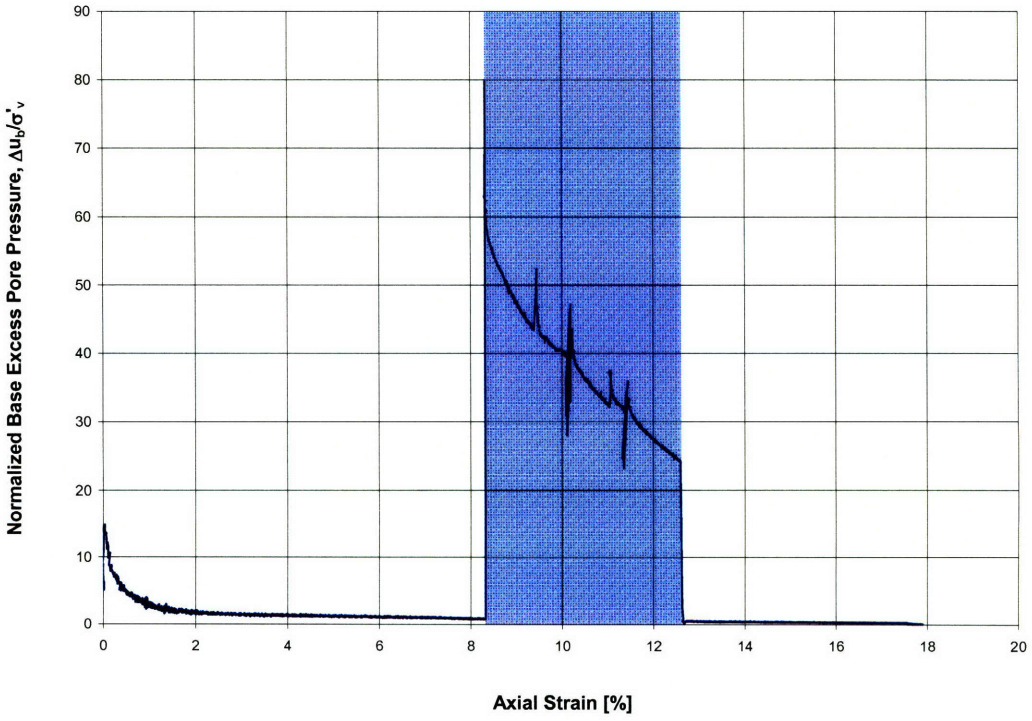

Figure A.12 Normalized base excess pore pressure graph of CRS649

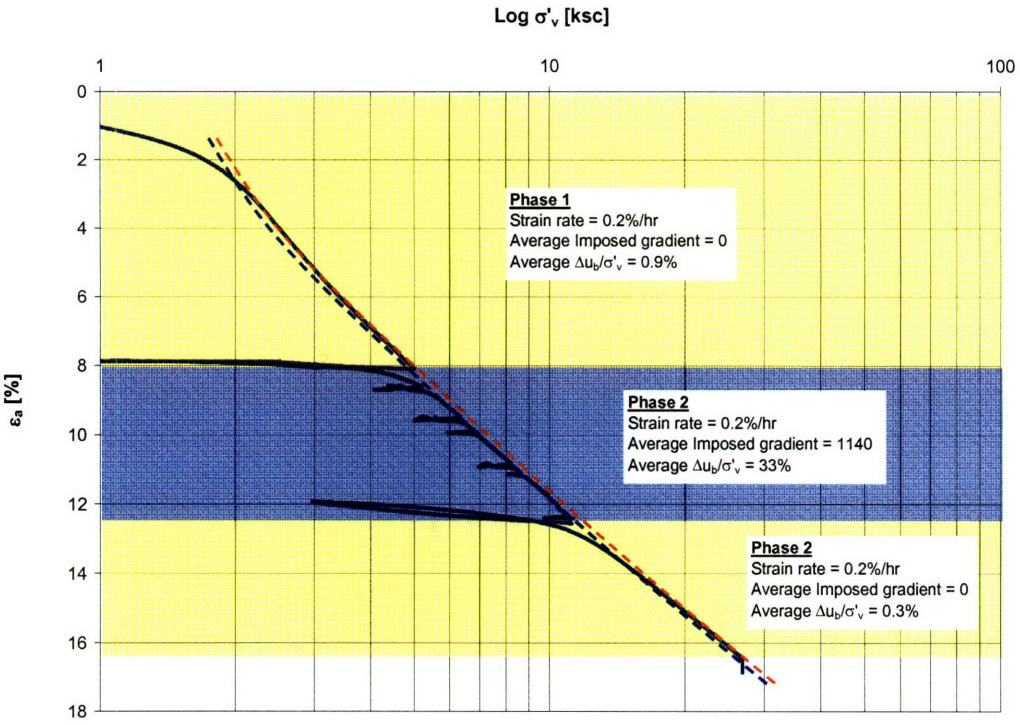

Figure A.13 Compression curve of CRS652

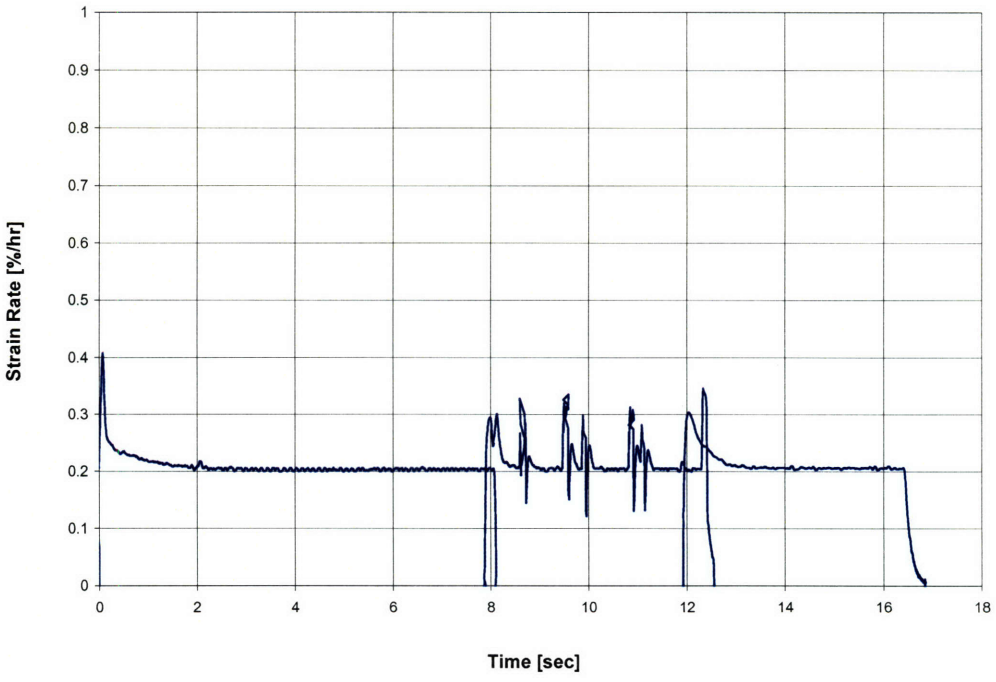

Figure A.14 Strain rate graph of CRS652

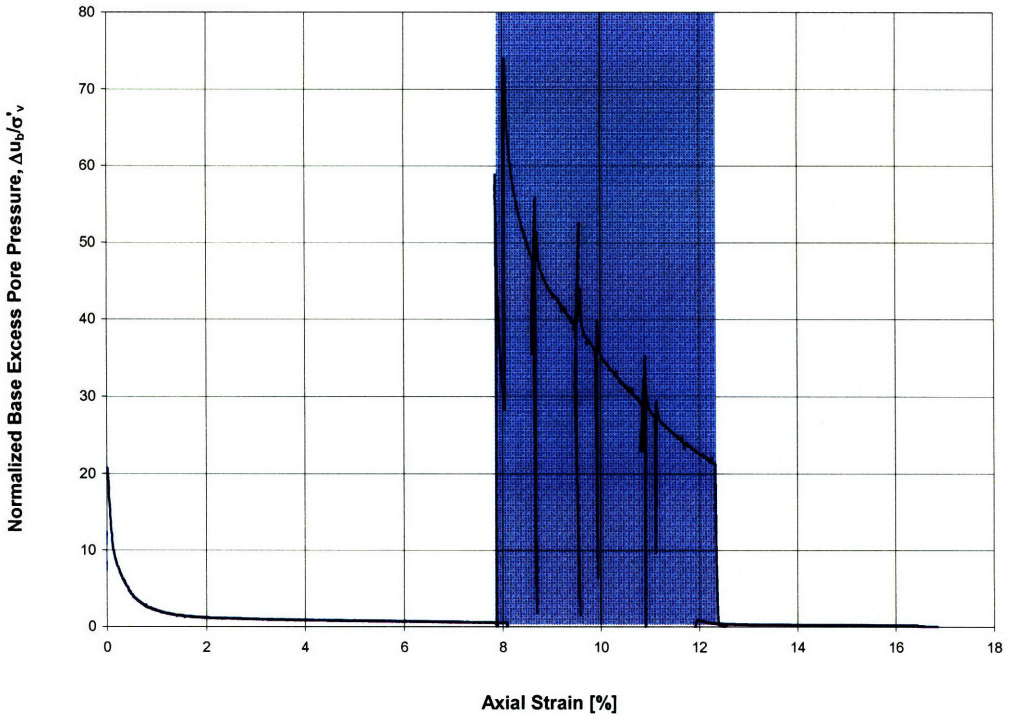

Figure A.15 Normalized base excess pore pressure graph of CRS652

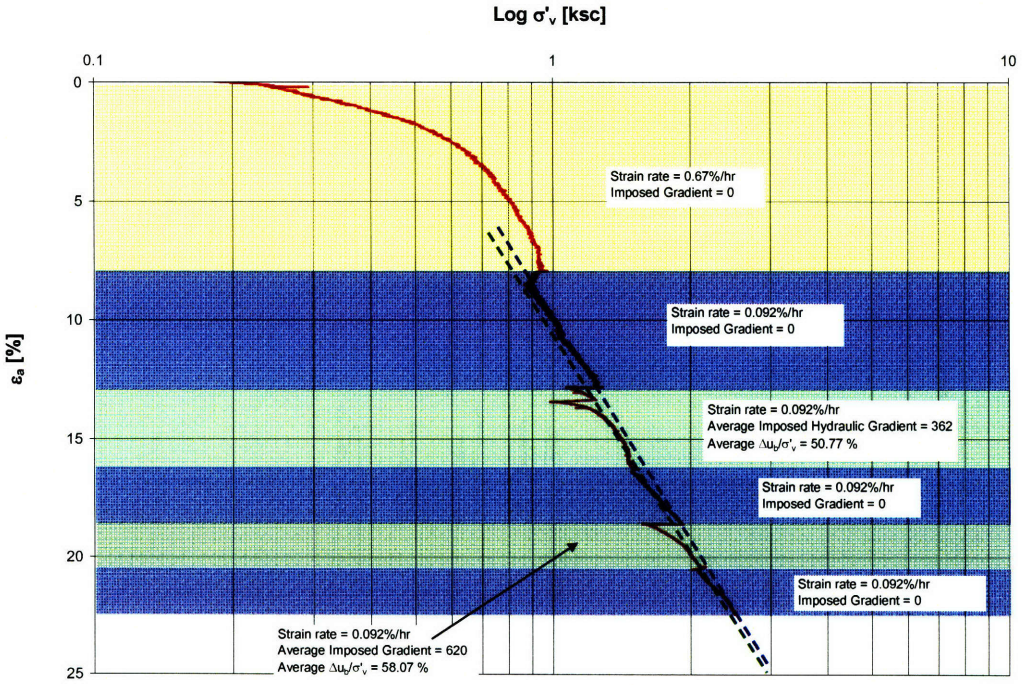

Figure A.16 Compression curve of CRS654

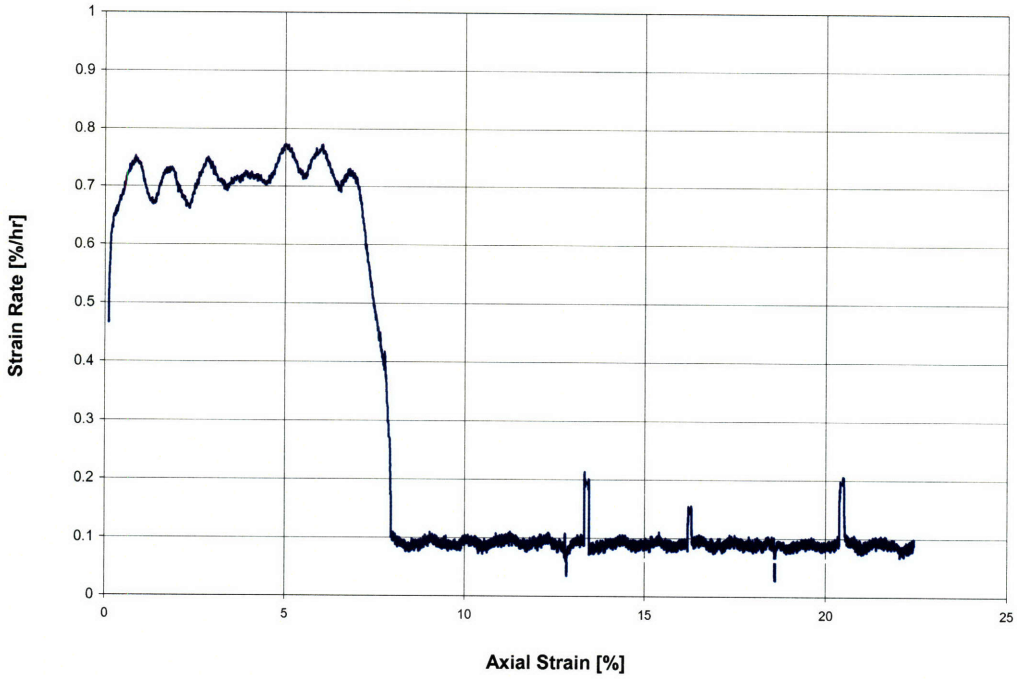

Figure A.17 Strain rate graph of CRS654

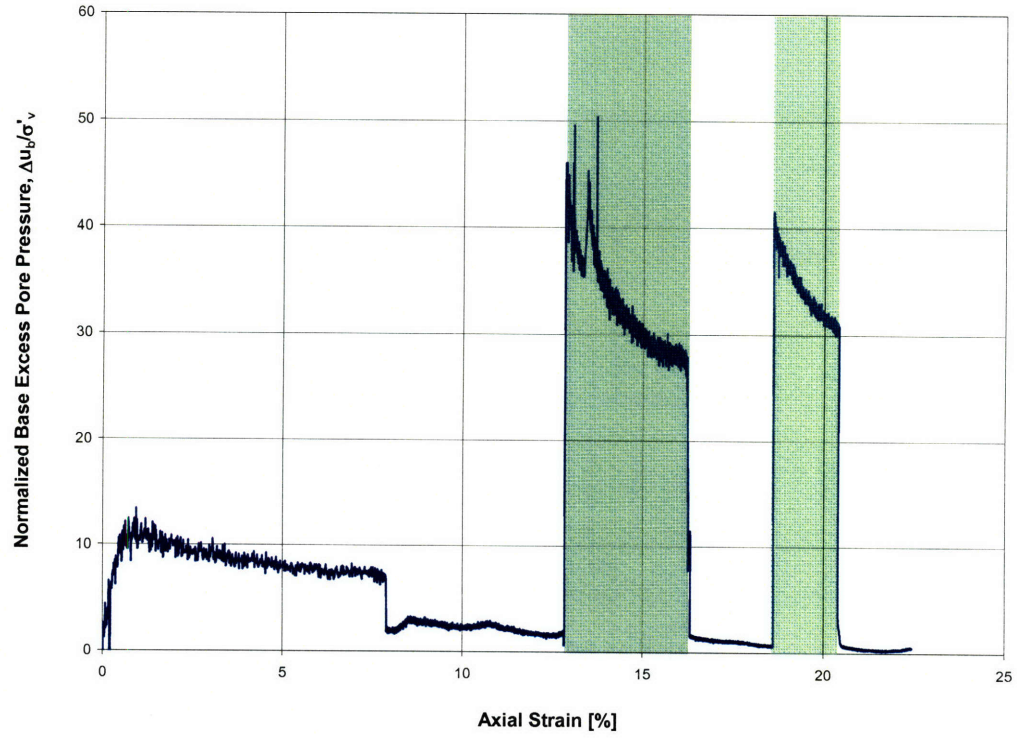

Figure A.18 Normalized base excess pore pressure graph of CRS654

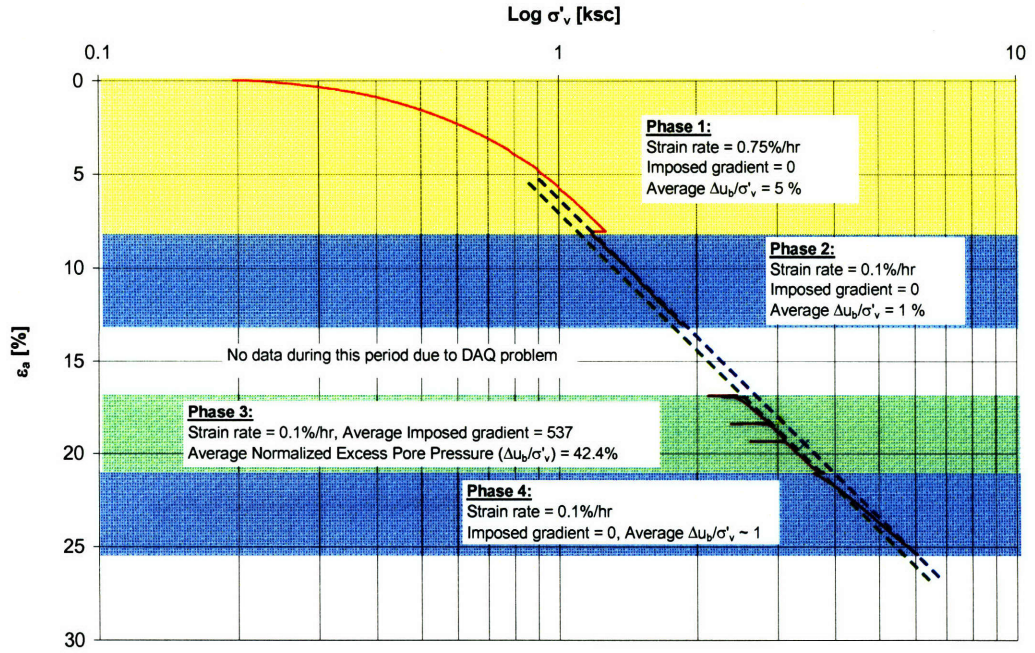

Figure A.19 Compression curve of CRS656

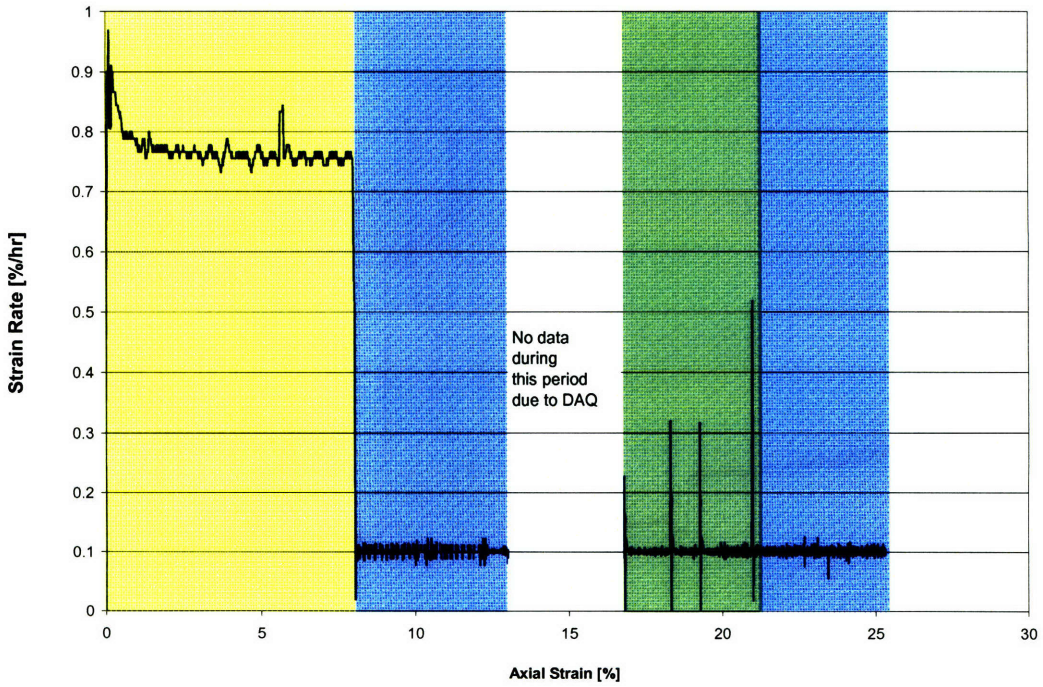

Figure A.20 Strain rate graph of CRS656

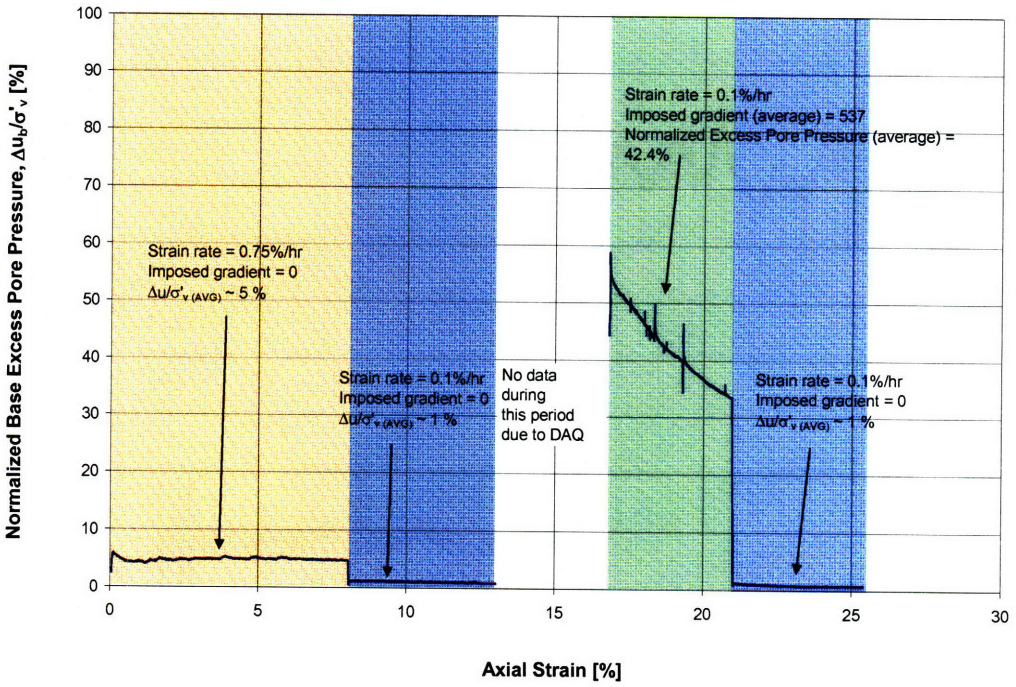

Figure A.21 Normalized base excess pore pressure graph of CRS656

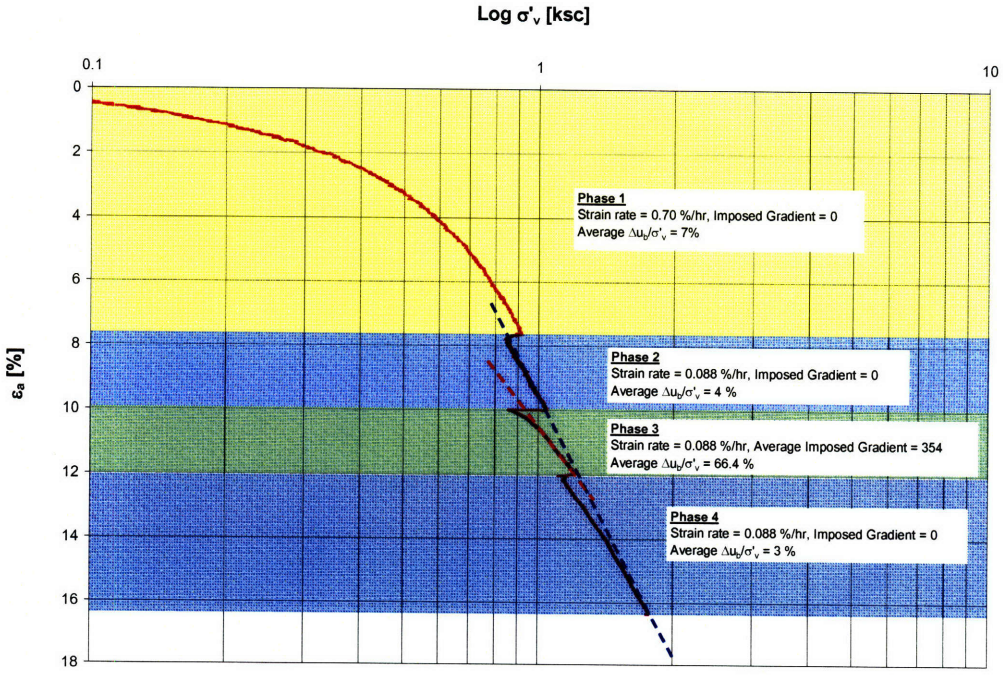

Figure A.22 Compression curve of CRS662

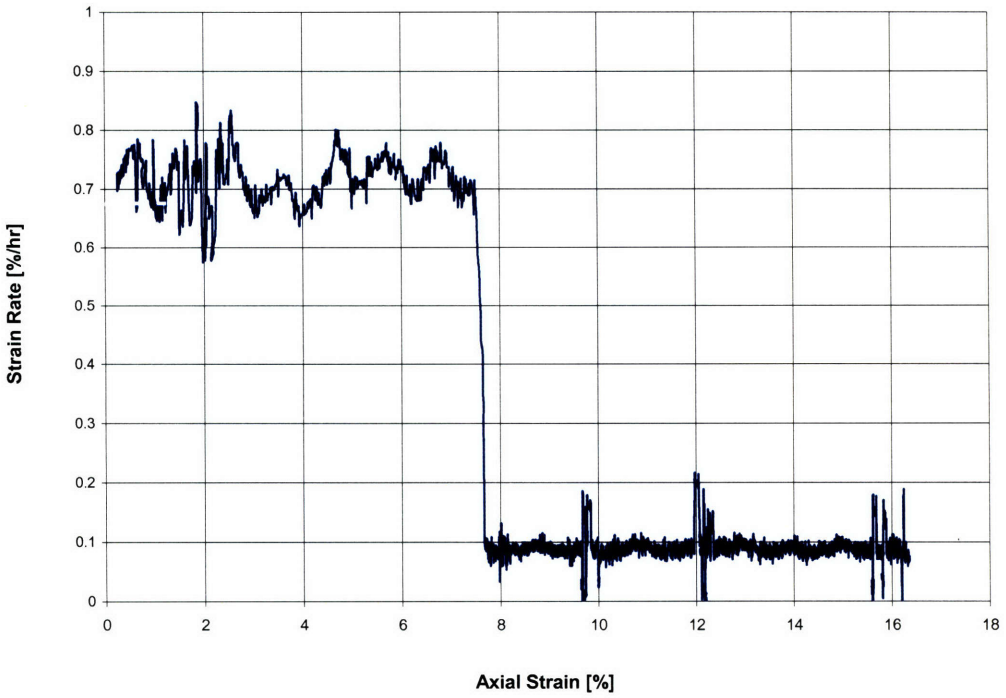

Figure A.23 Strain rate graph of CRS662

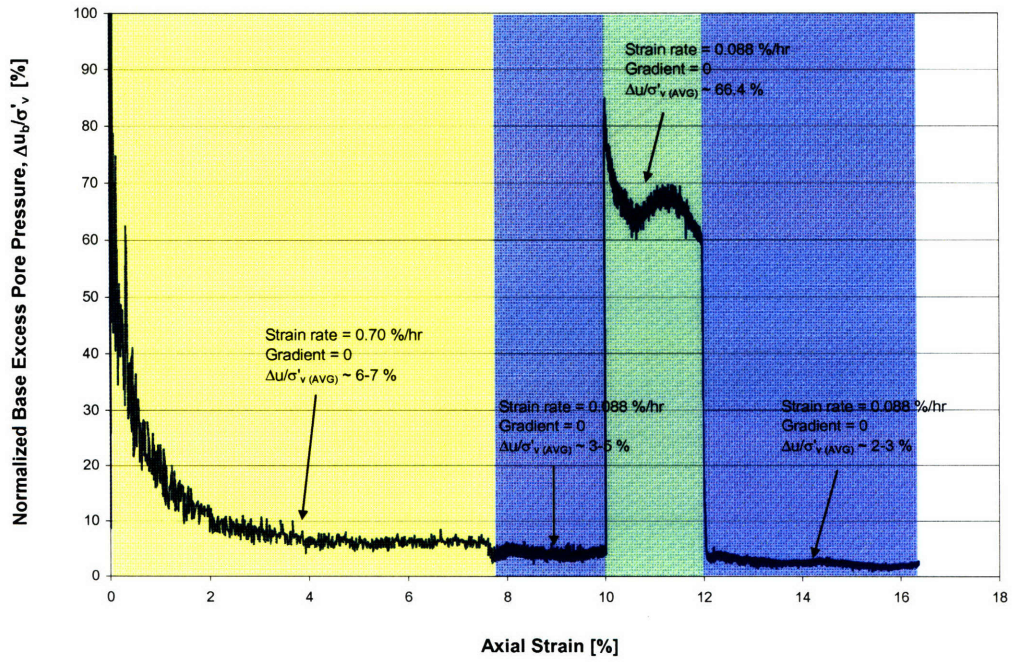

Figure A.24 Normalized base excess pore pressure graph of CRS662

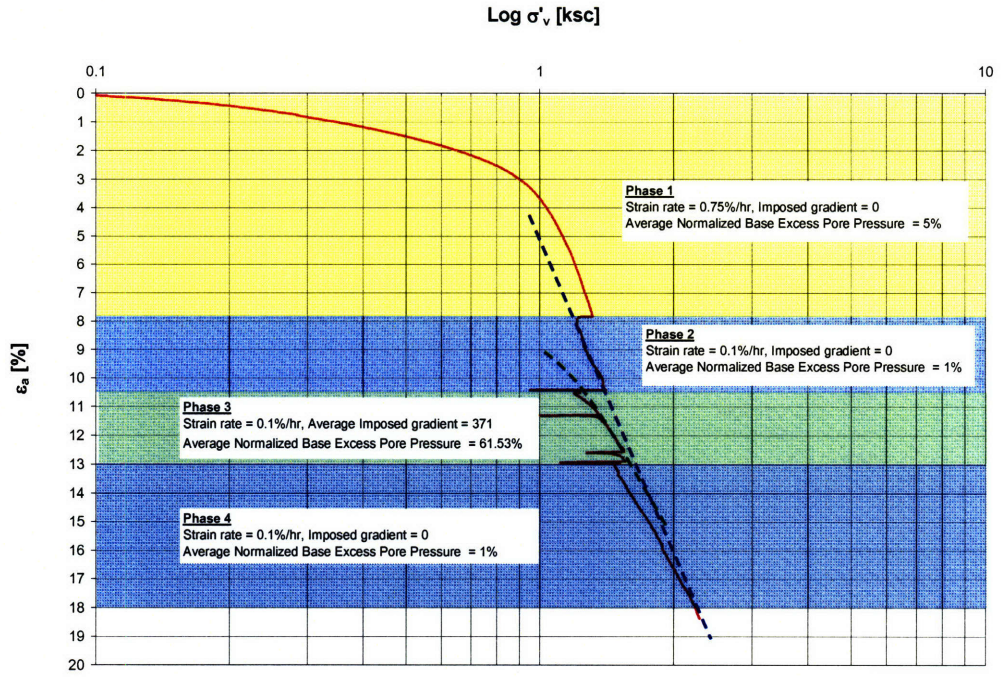

Figure A.25 Compression curve of CRS663

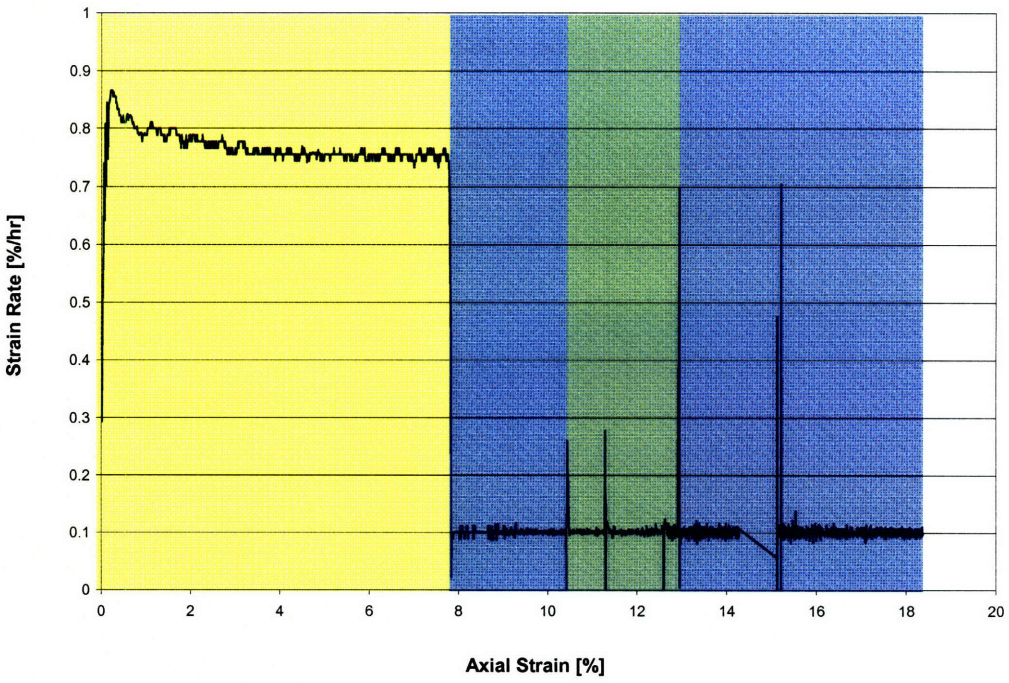

Figure A.26 Strain rate graph of CRS663

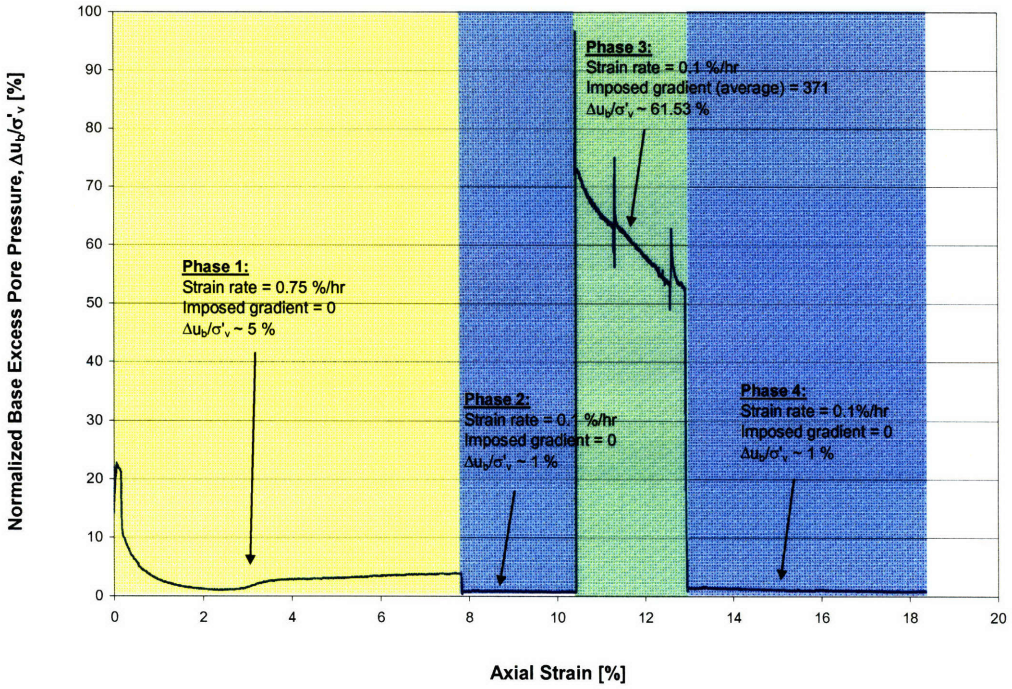

Figure A.27 Normalized base excess pore pressure graph of CRS663

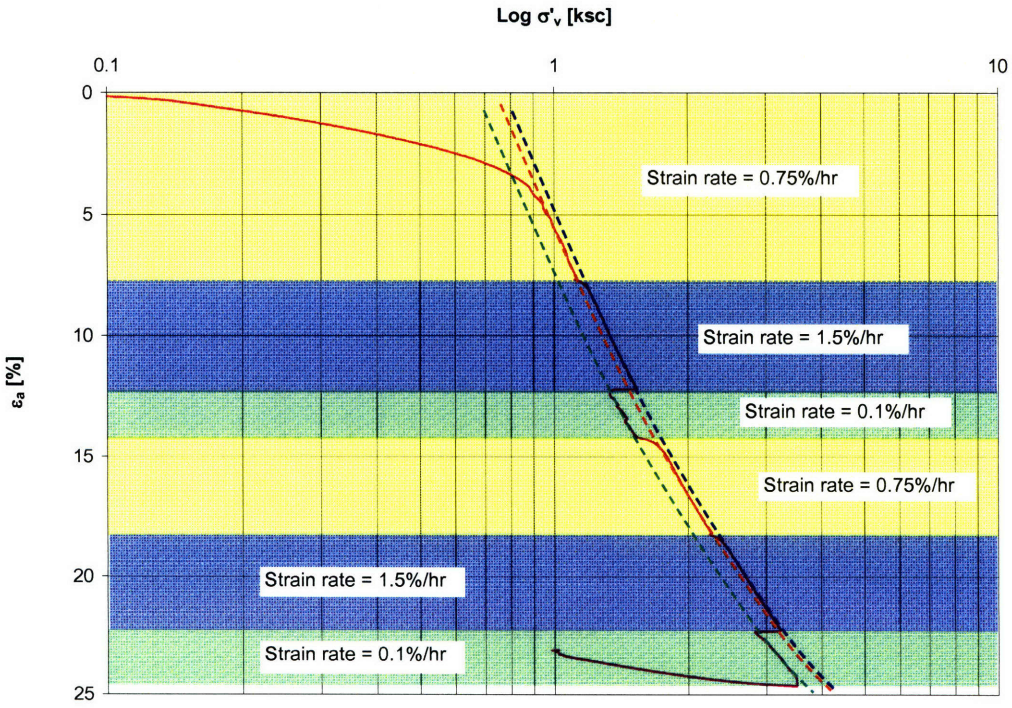

Figure A.28 Compression curve of CRS672

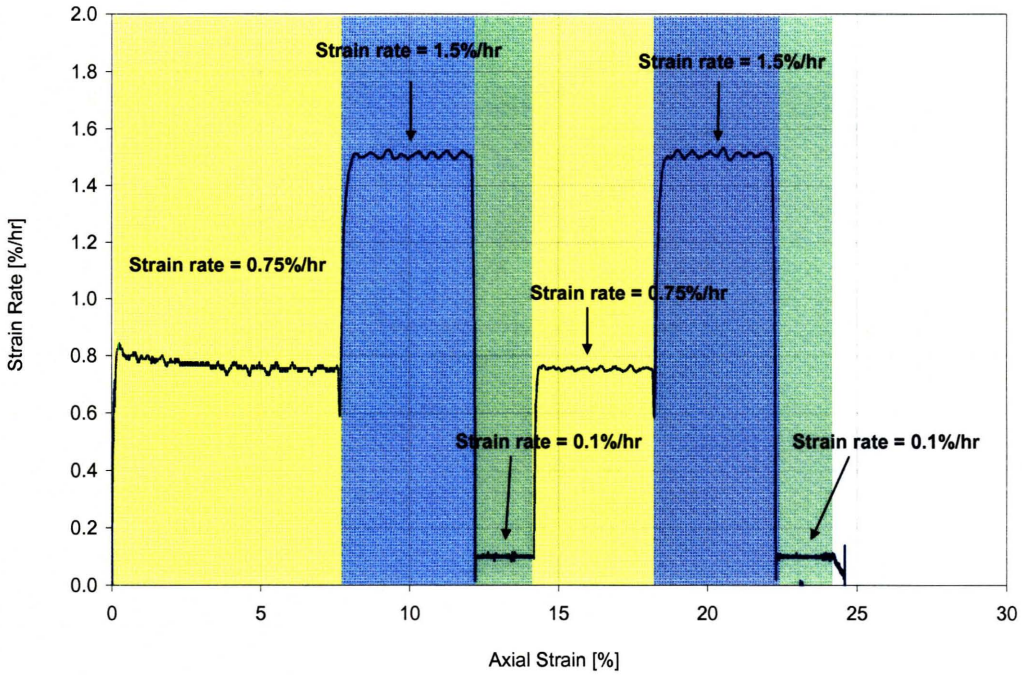

Figure A.29 Strain rate graph of CRS672

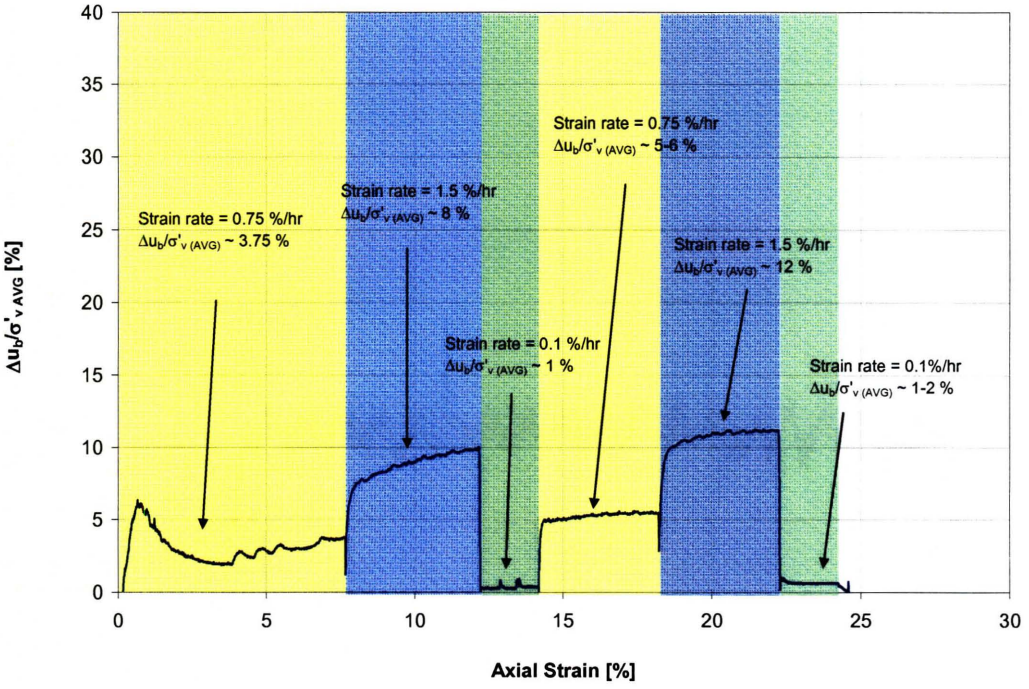

Figure A.30 Normalized base excess pore pressure graph of CRS672

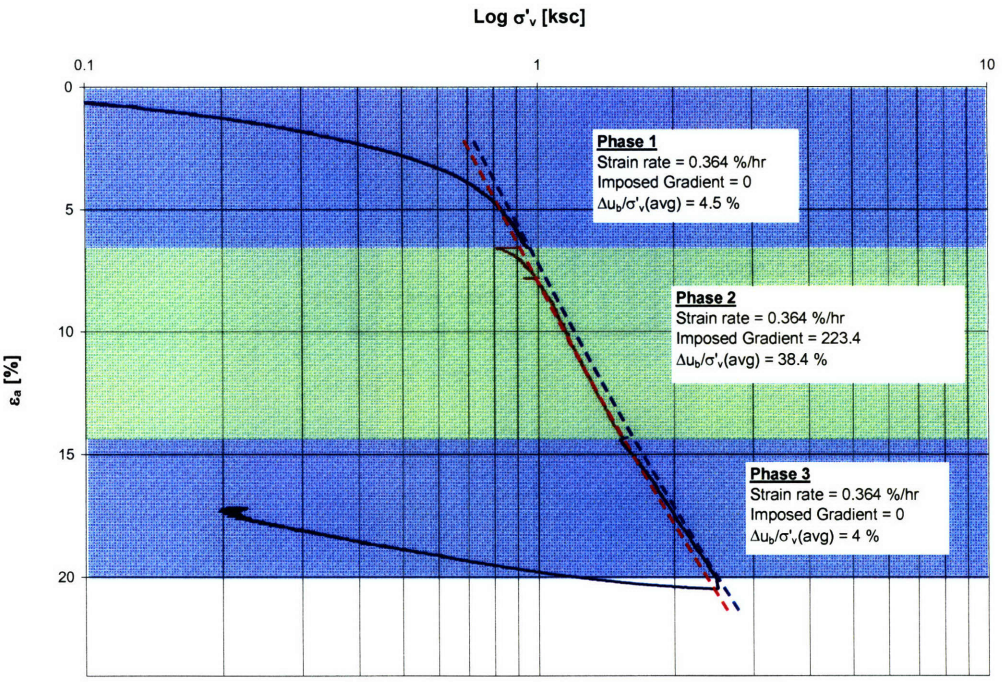

Figure A.31 Compression curve of CRS674

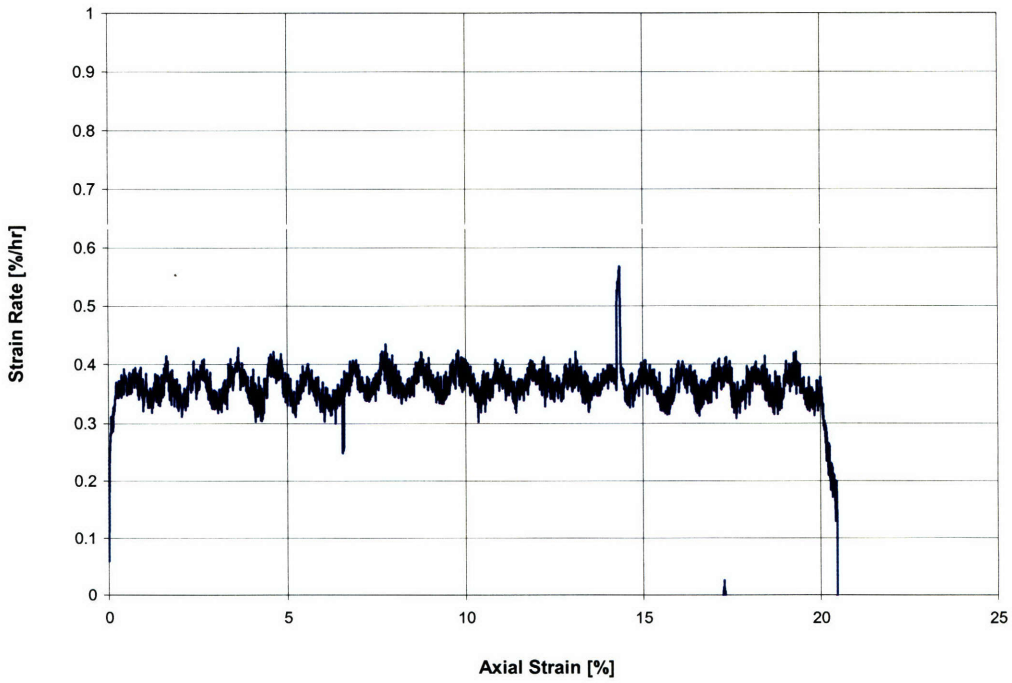

Figure A.32 Strain rate graph of CRS674

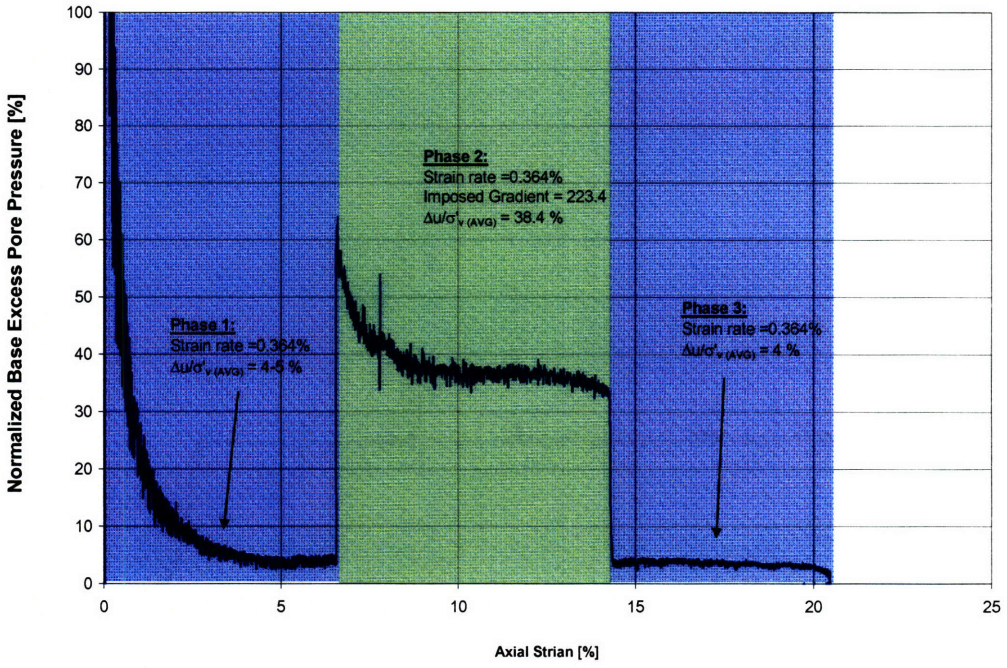

Figure A.33 Normalized base excess pore pressure graph of CRS674

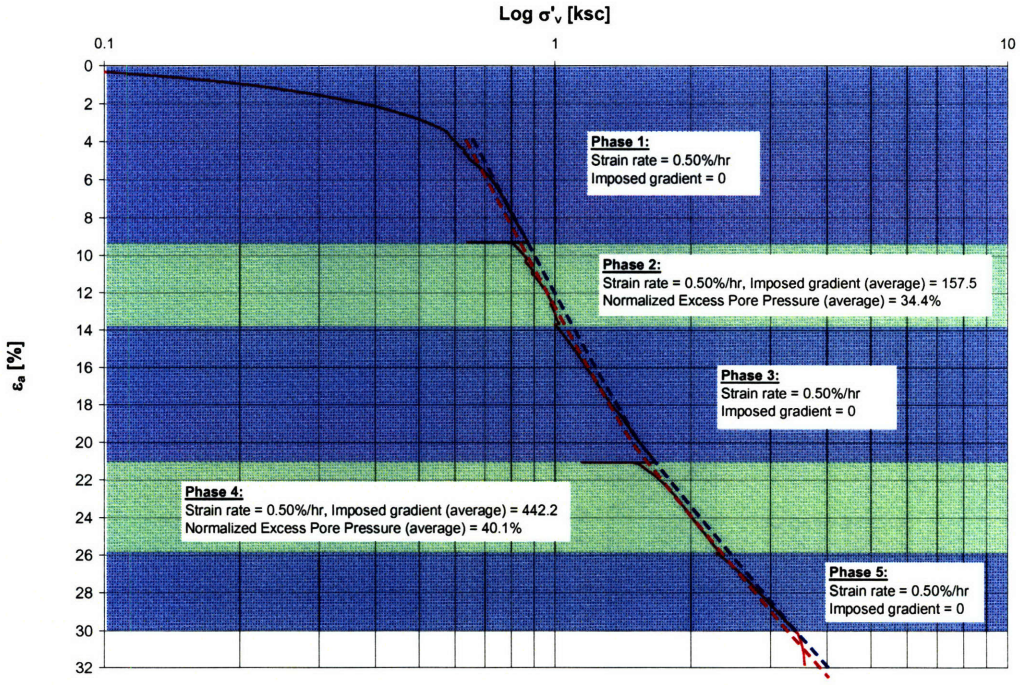

Figure A.34 Compression curve of CRS680

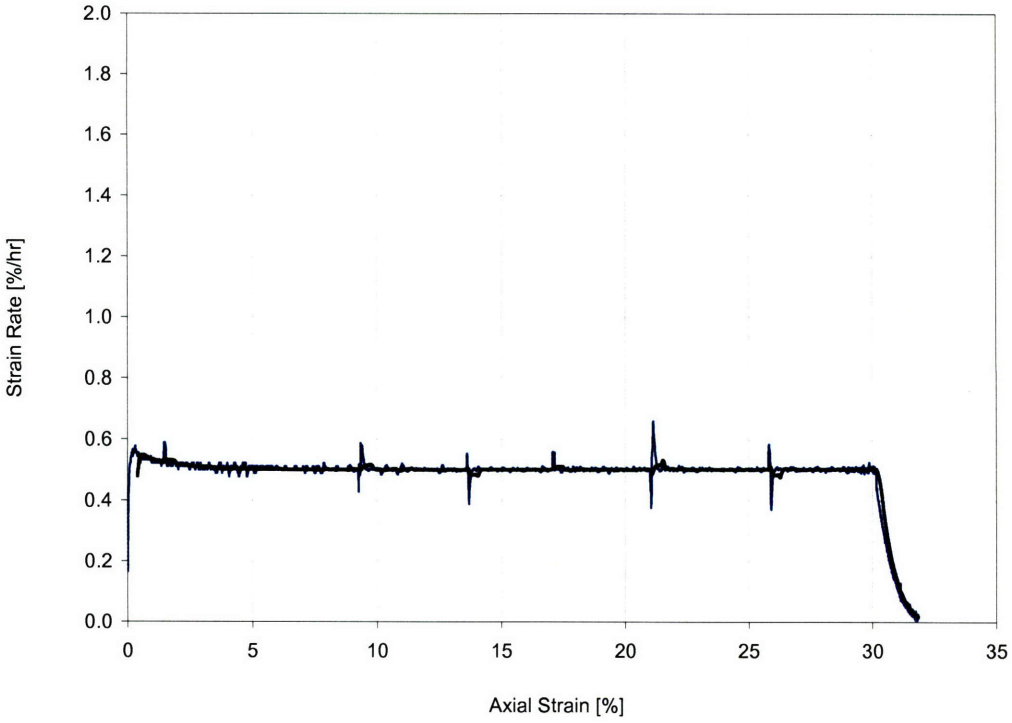

Figure A.35 Strain rate graph of CRS680

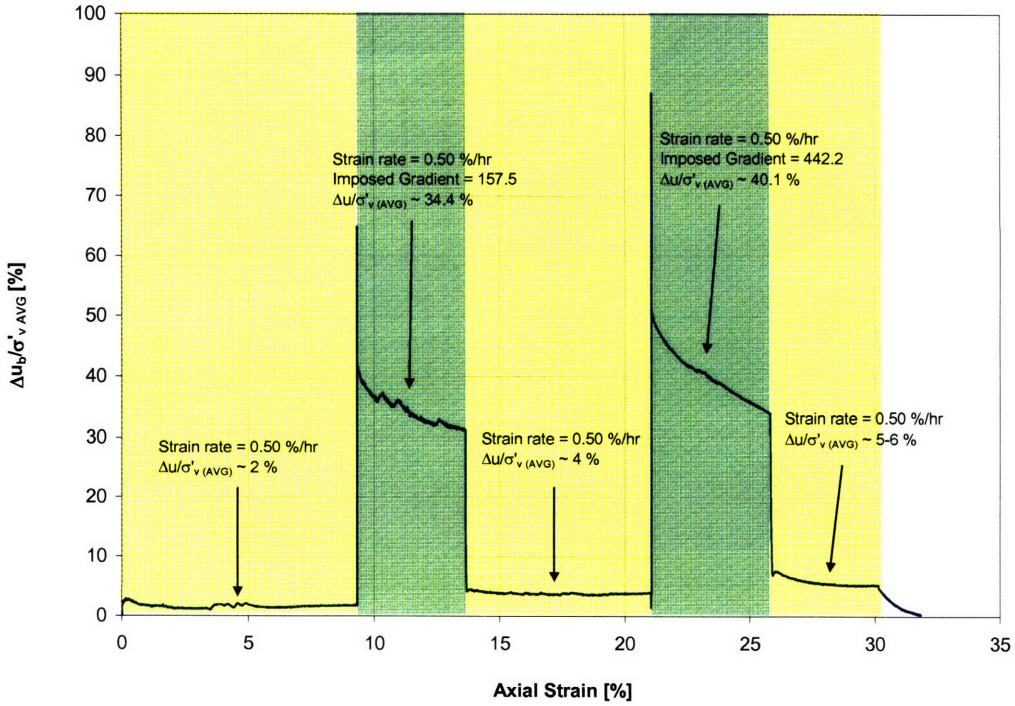

Figure A.36 Normalized base excess pore pressure graph of CRS680

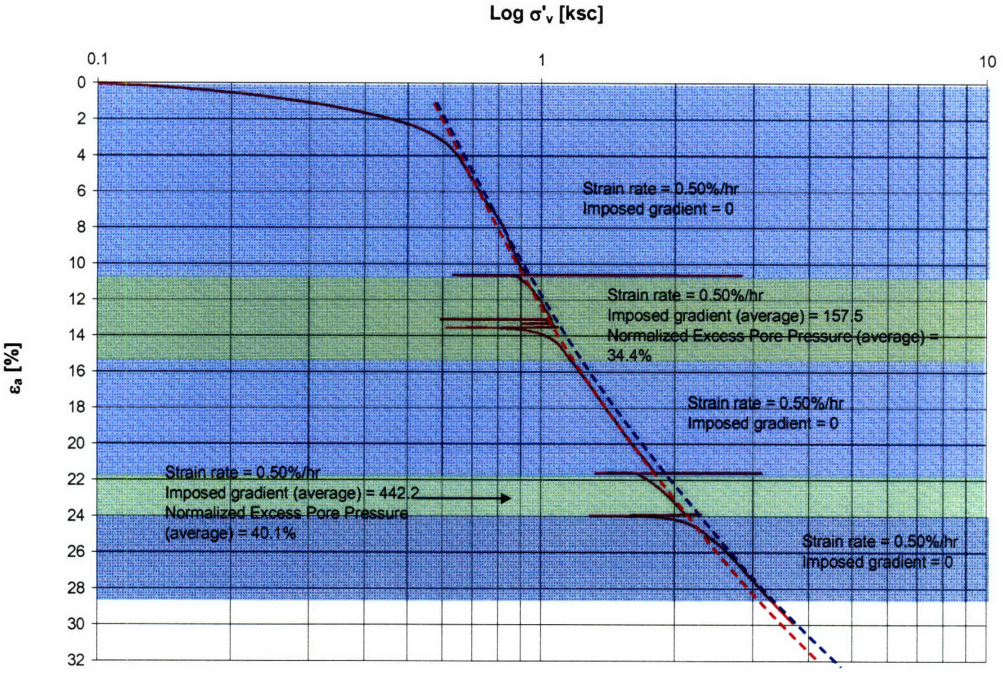

Figure A.37 Compression curve of CRS683

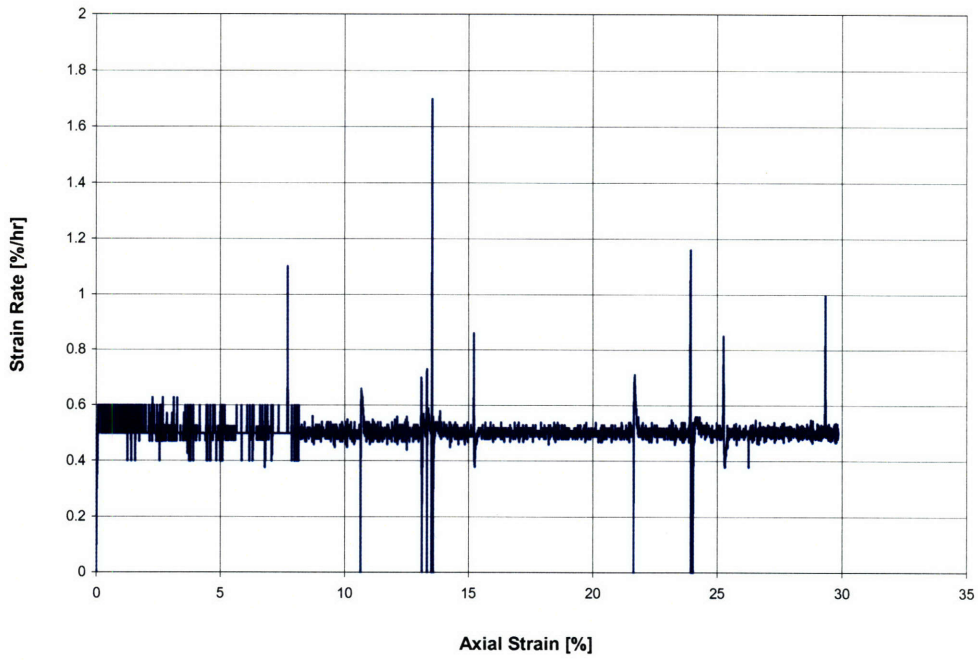

Figure A.38 Strain rate graph of CRS683

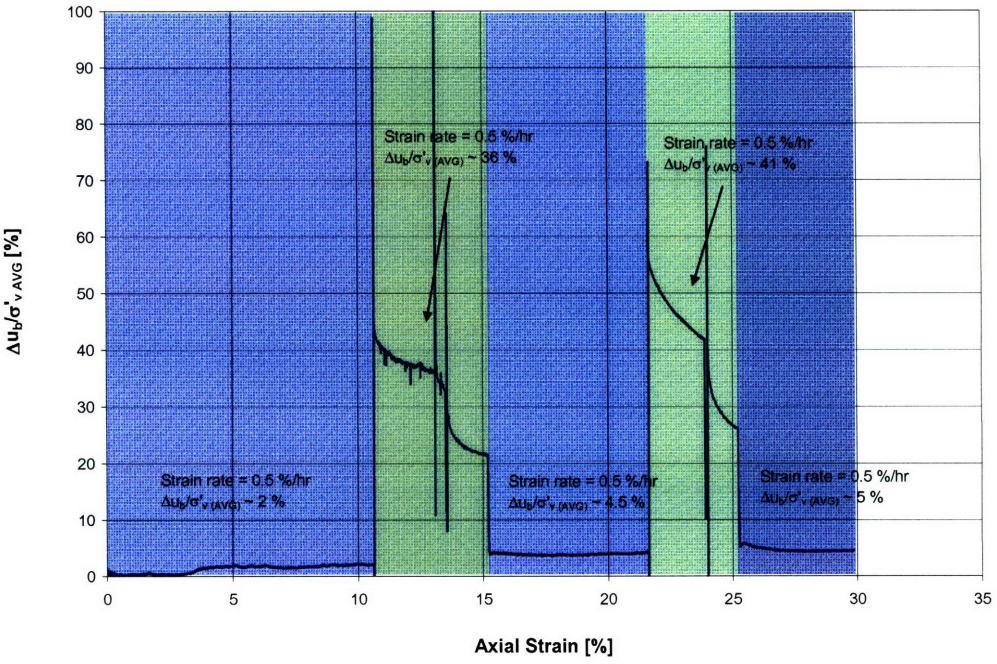

Figure A.39 Normalized base excess pore pressure graph of CRS683

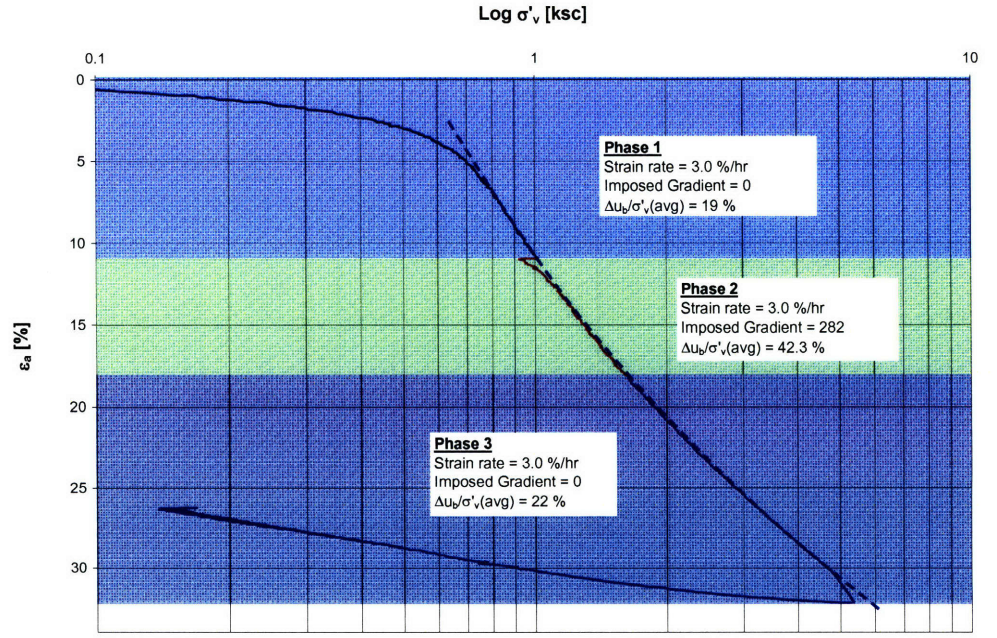

Figure A.40 Compression curve of CRS686

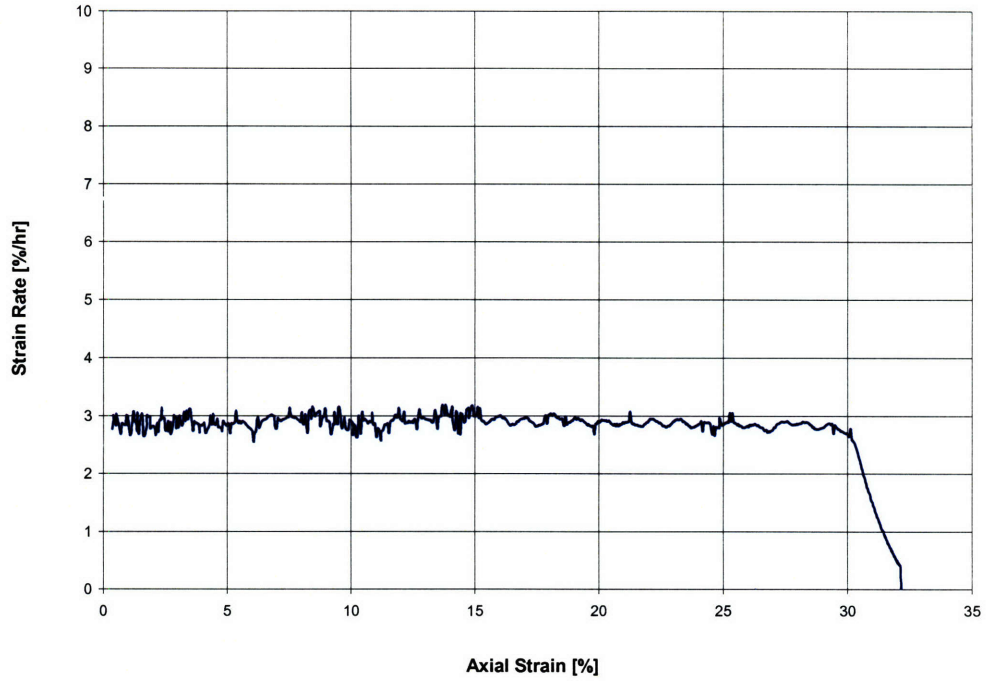

Figure A.41 Strain rate graph of CRS686

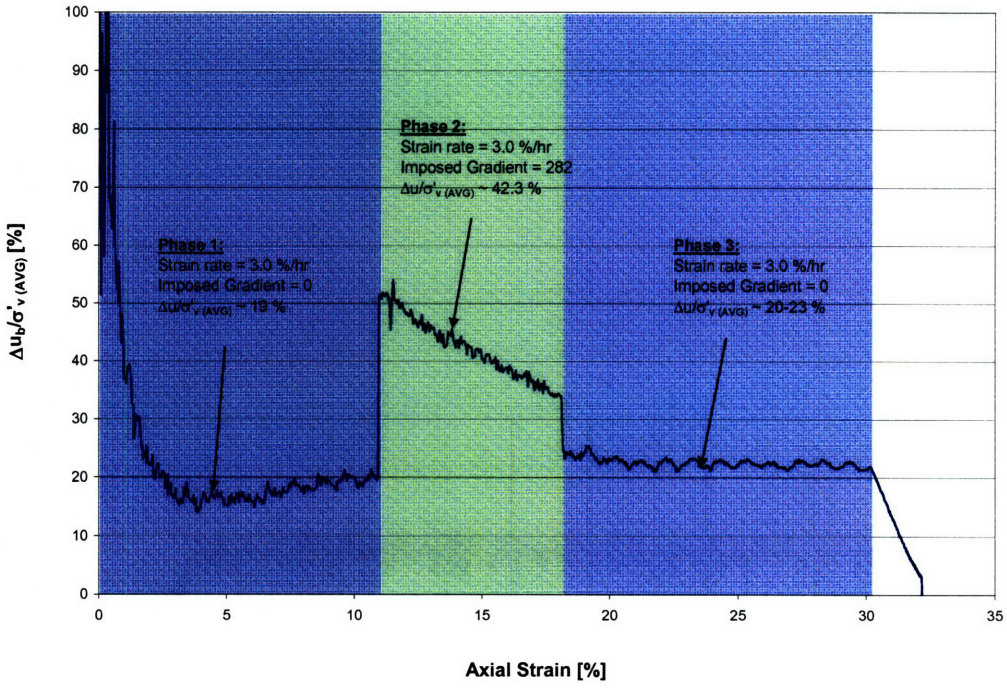

Figure A.42 Normalized base excess pore pressure graph of CRS686

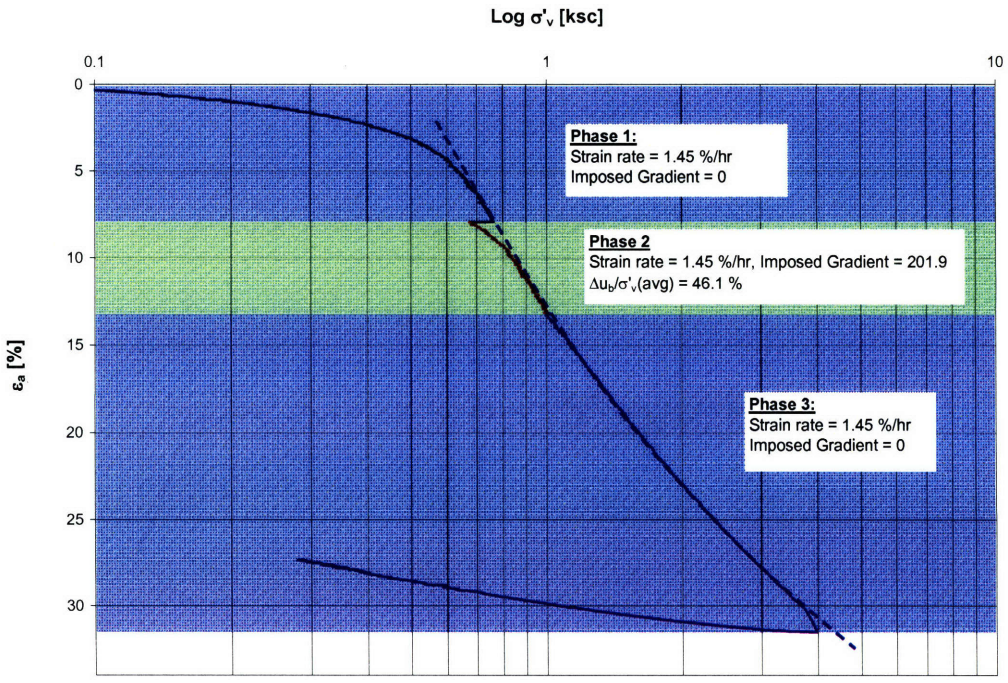

Figure A.43 Compression curve of CRS687

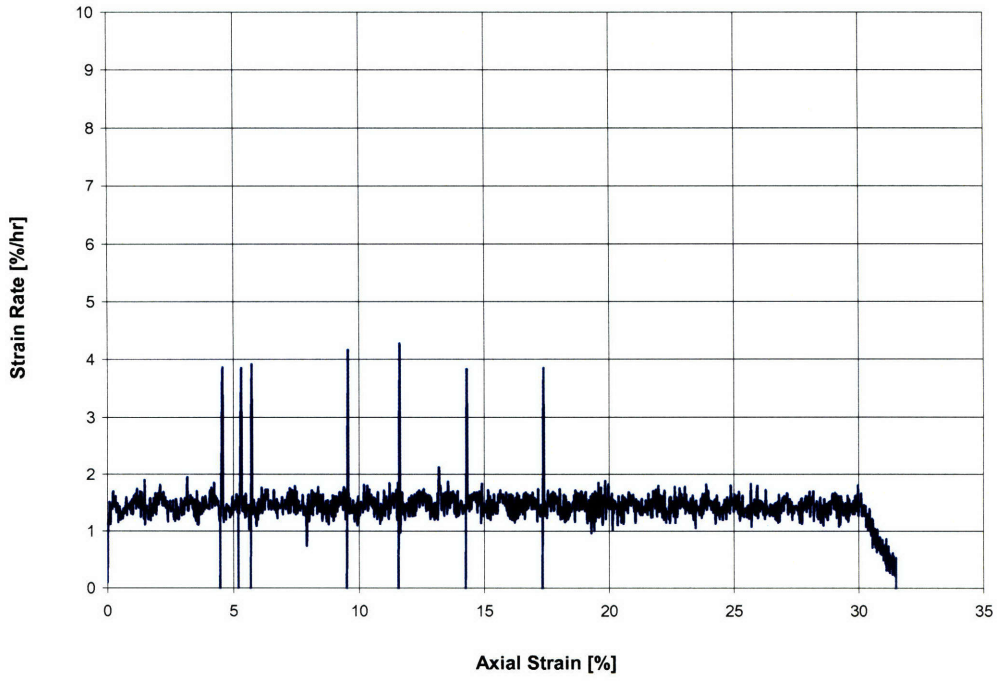

Figure A.44 Strain rate graph of CRS687

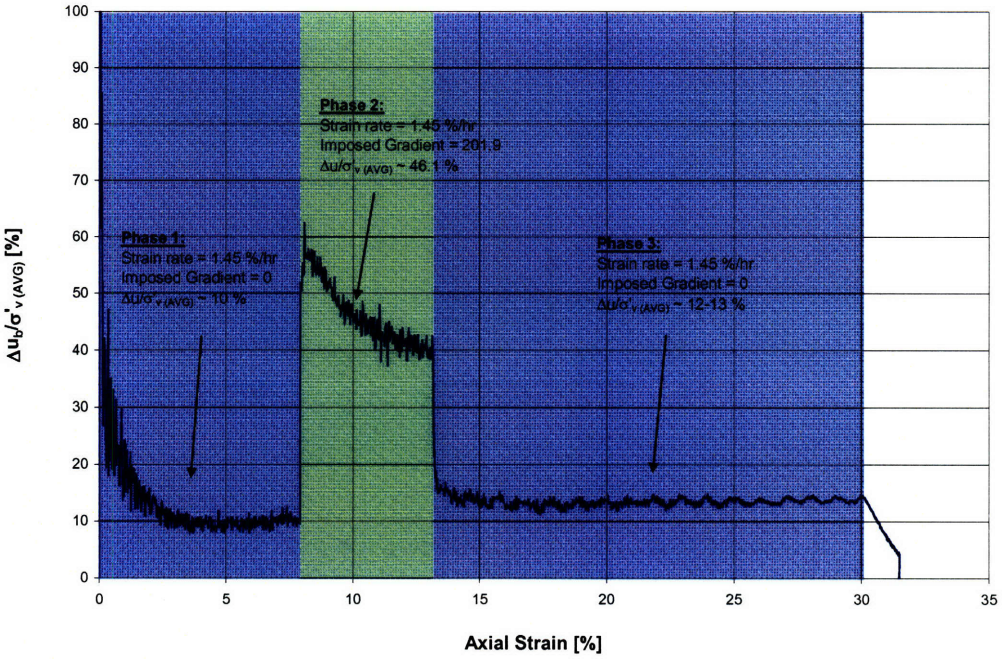

Figure A.45 Normalized base excess pore pressure graph of CRS687

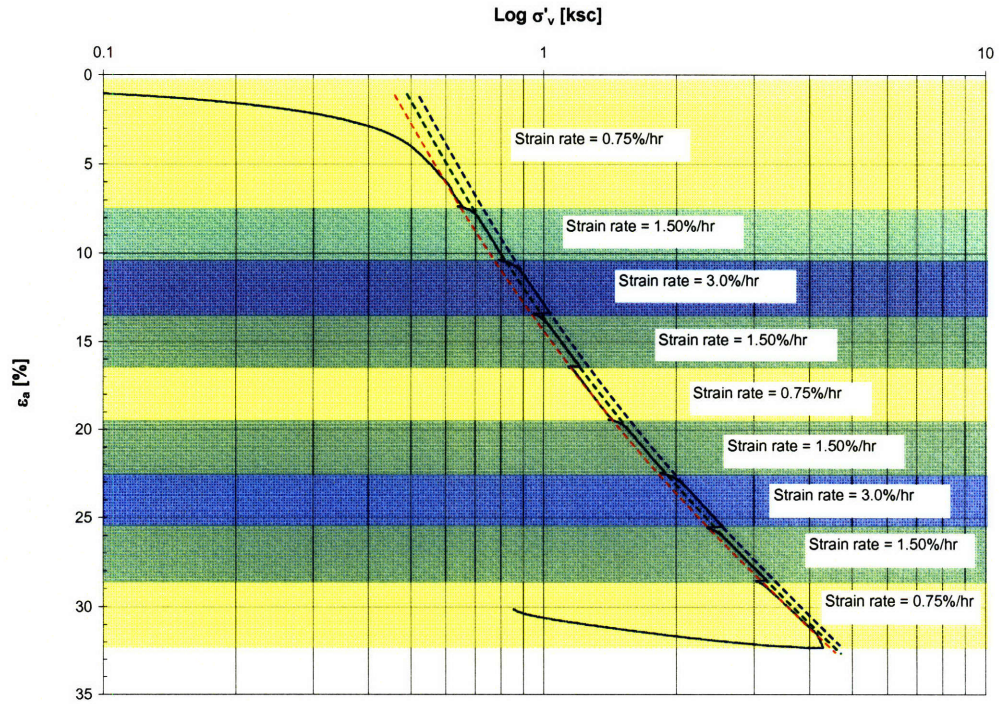

Figure A.46 Compression curve of CRS691

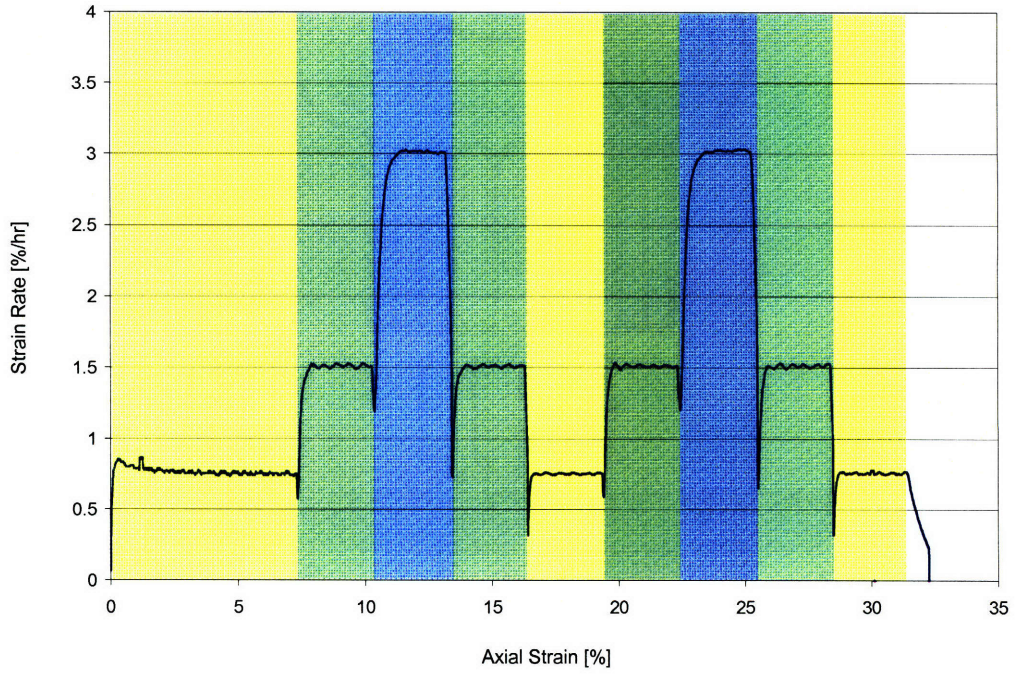

Figure A.47 Strain rate graph of CRS691

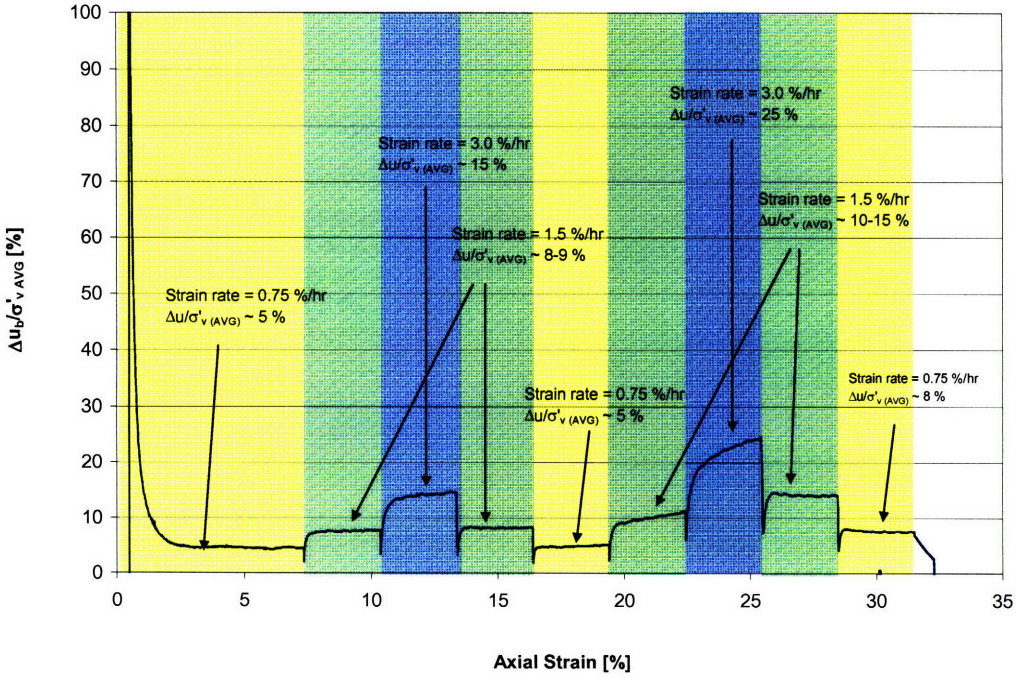

Figure A.48 Normalized base excess pore pressure graph of CRS691

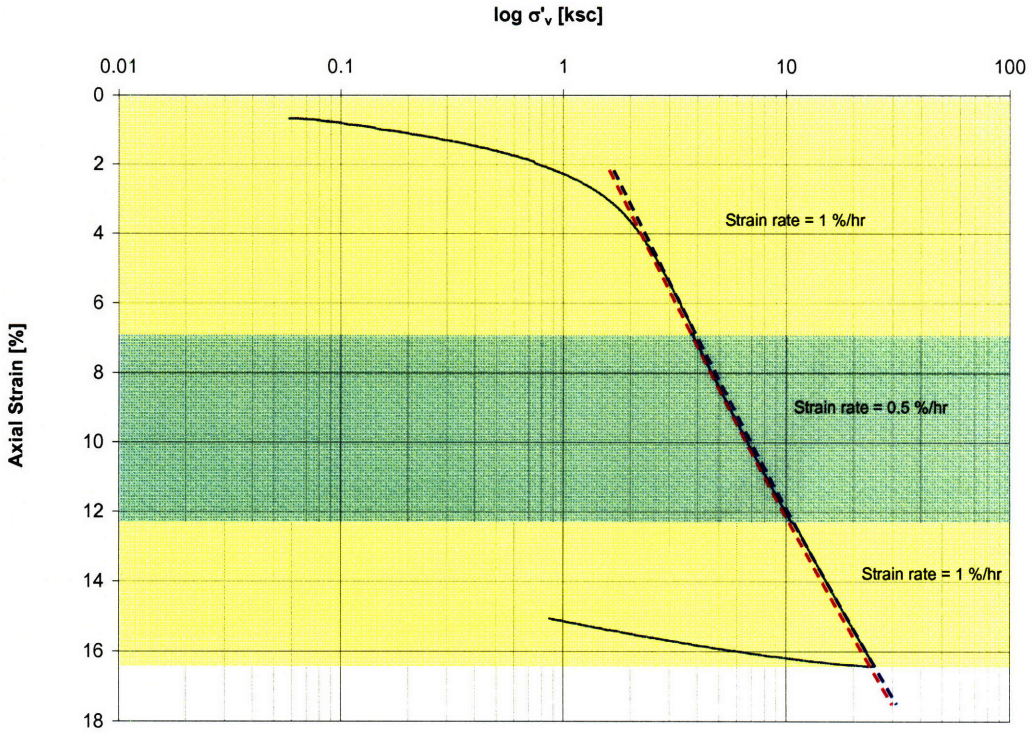

Figure A.49 Compression curve of CRS860

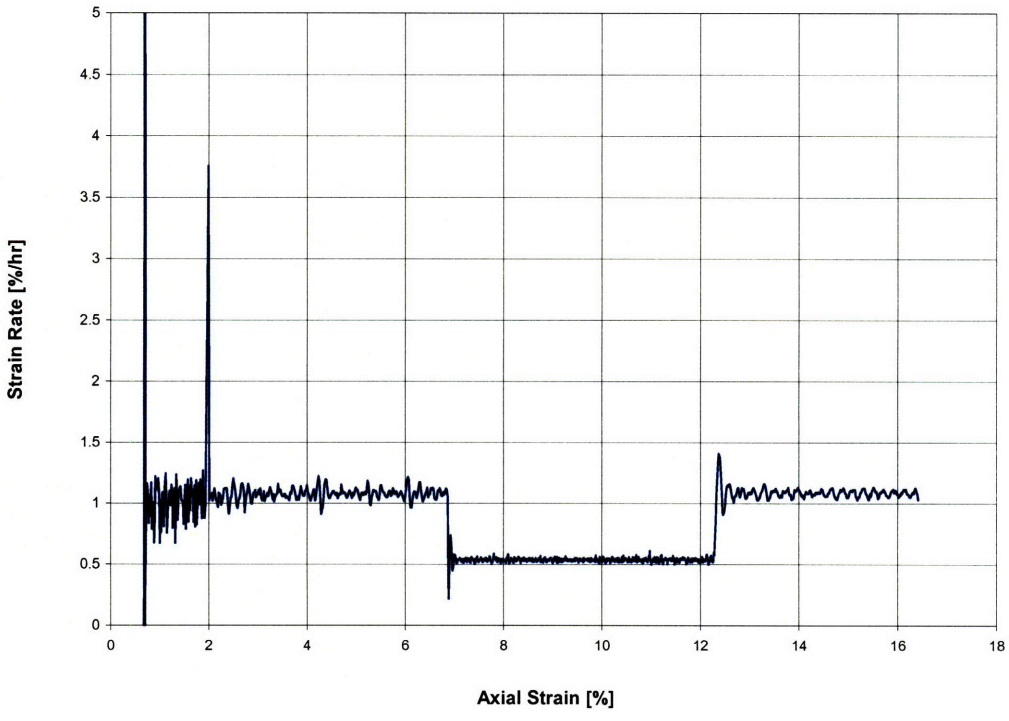

Figure A.50 Strain rate graph of CRS860

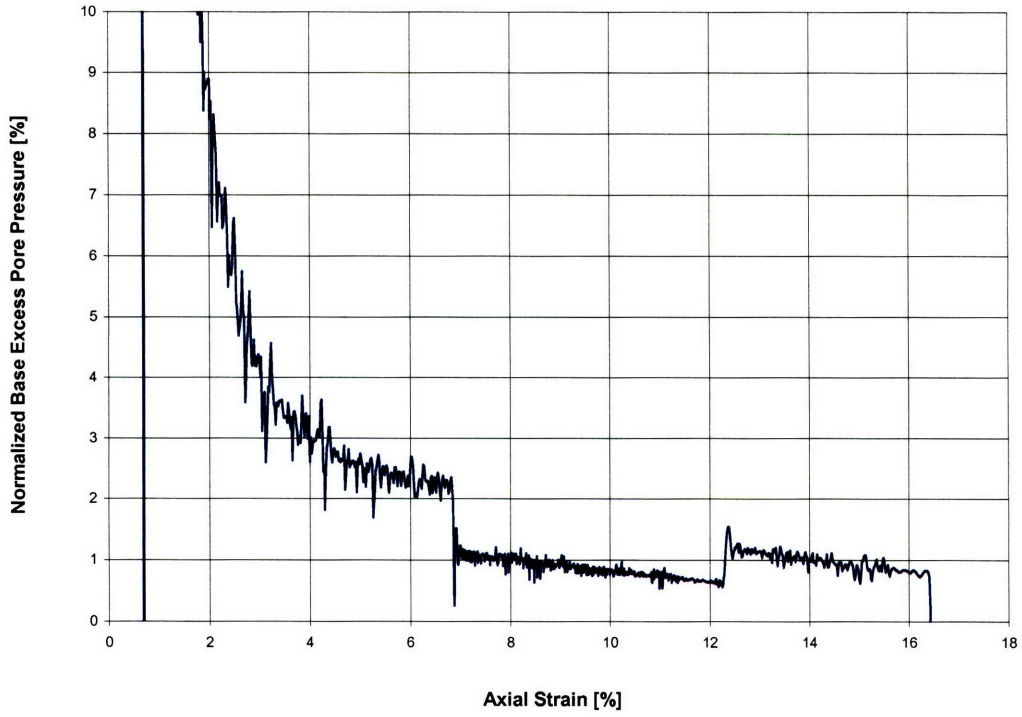

Figure A.51 Normalized base excess pore pressure graph of CRS860

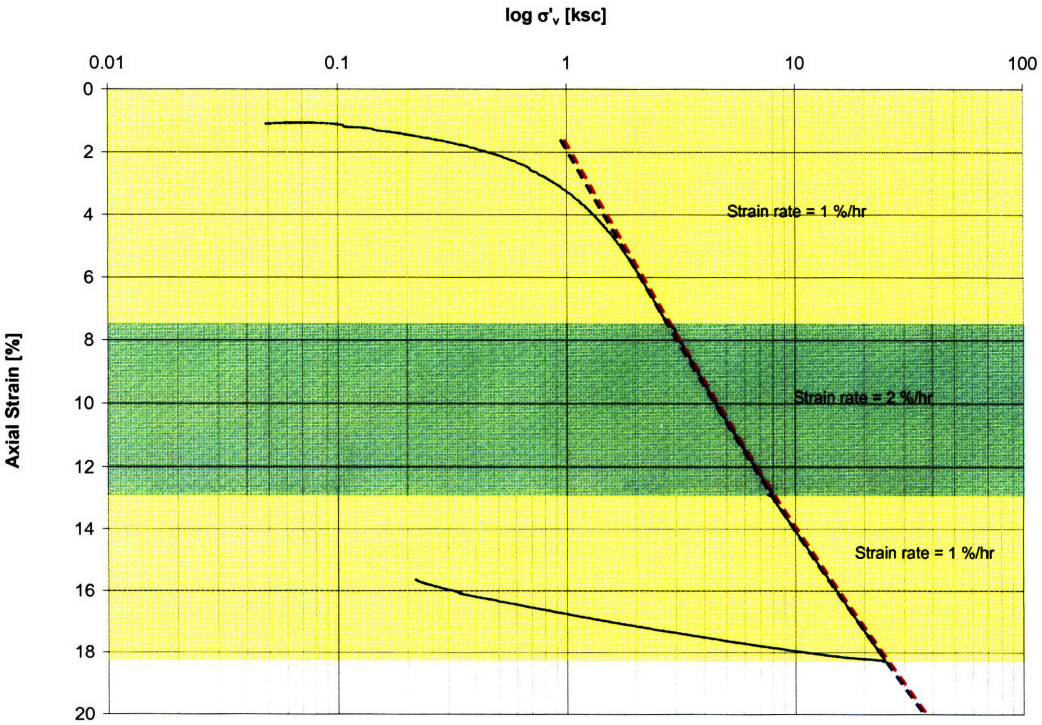

Figure A.52 Compression curve of CRS861

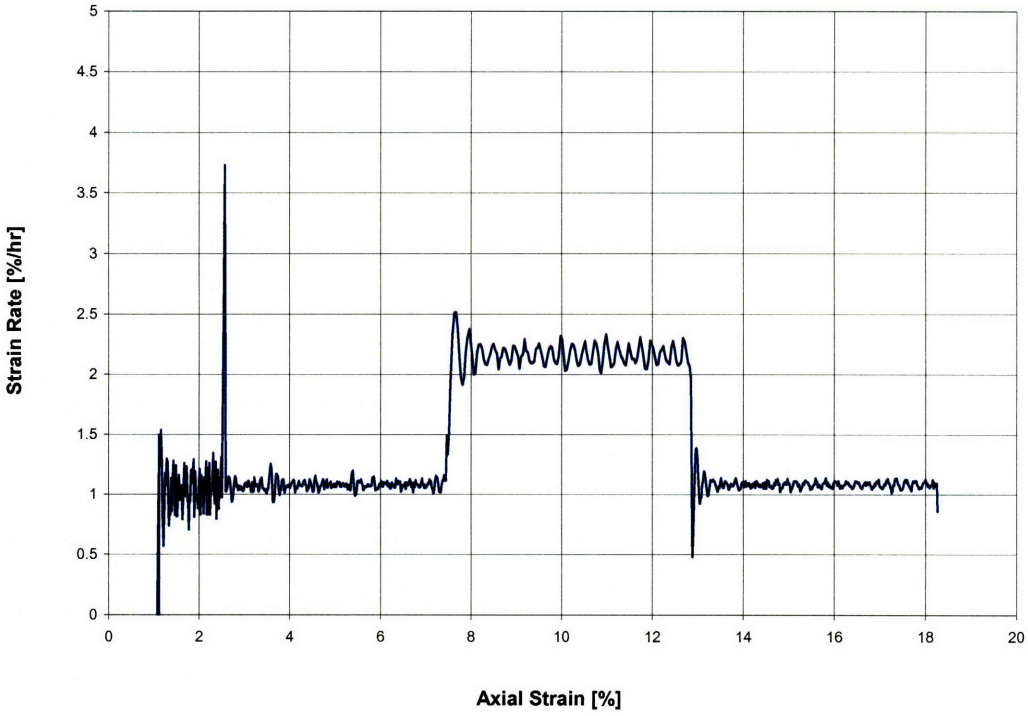

Figure A.53 Strain rate graph of CRS861

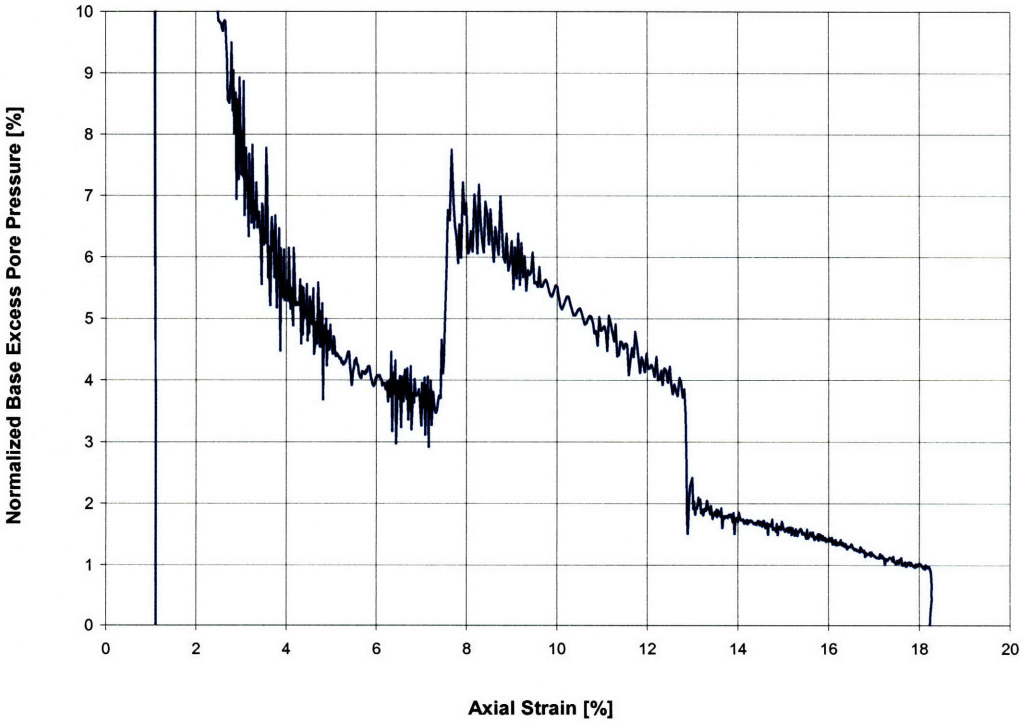

Figure A.54 Normalized base excess pore pressure graph of CRS861

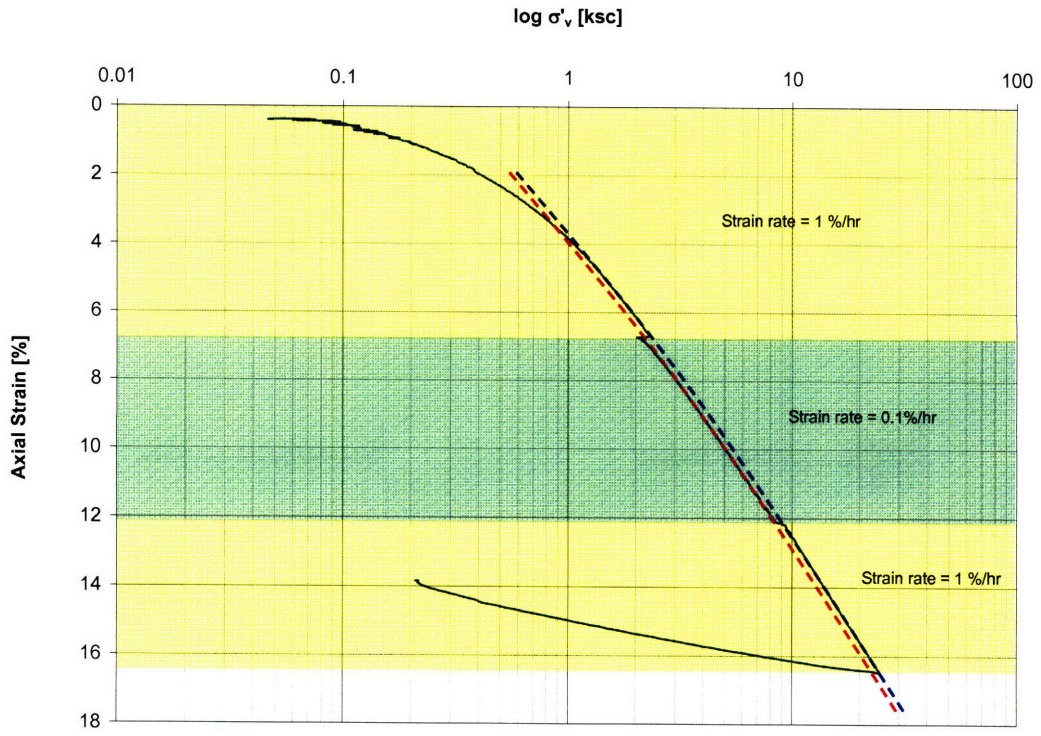

Figure A.55 Compression curve of CRS862

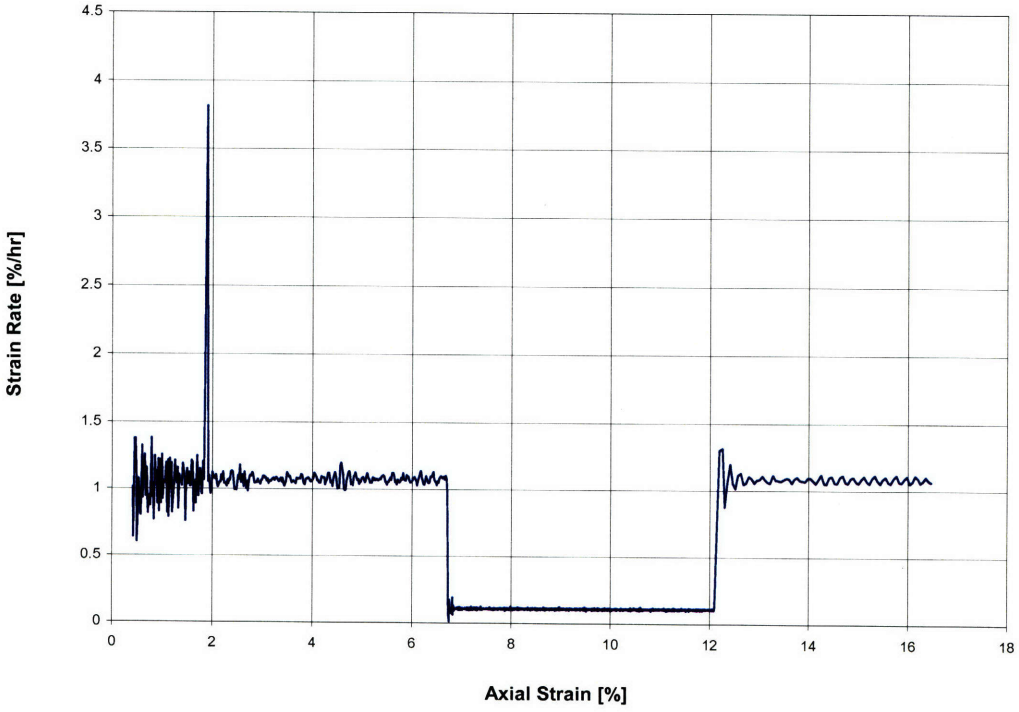

Figure A.56 Strain rate graph of CRS862

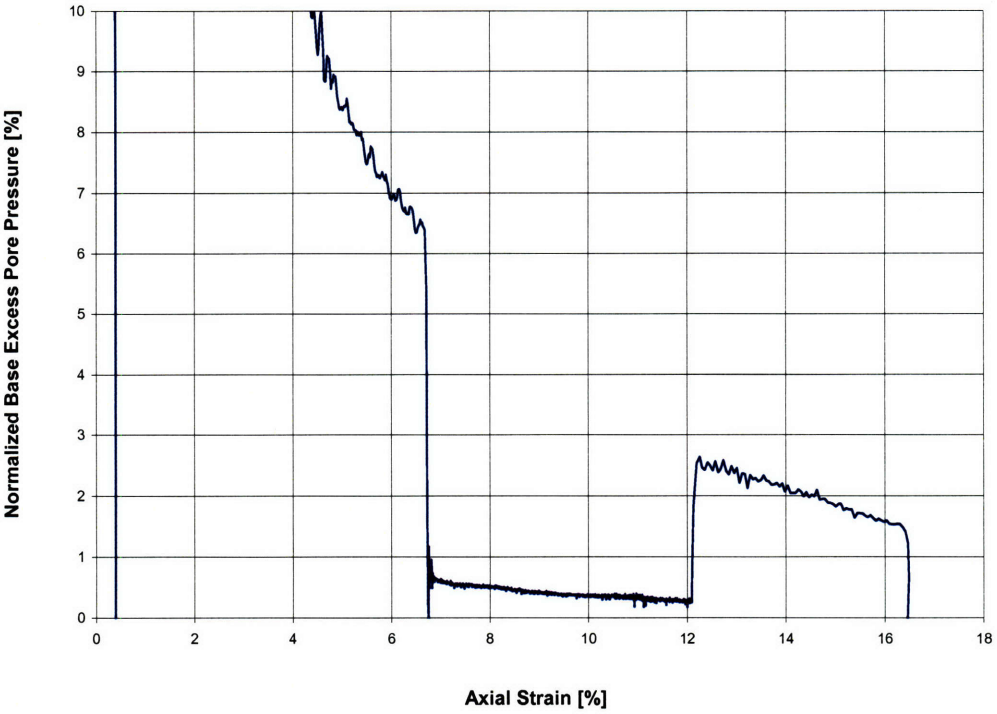

Figure A.57 Normalized base excess pore pressure graph of CRS862

A.3 Oedometer Test Results

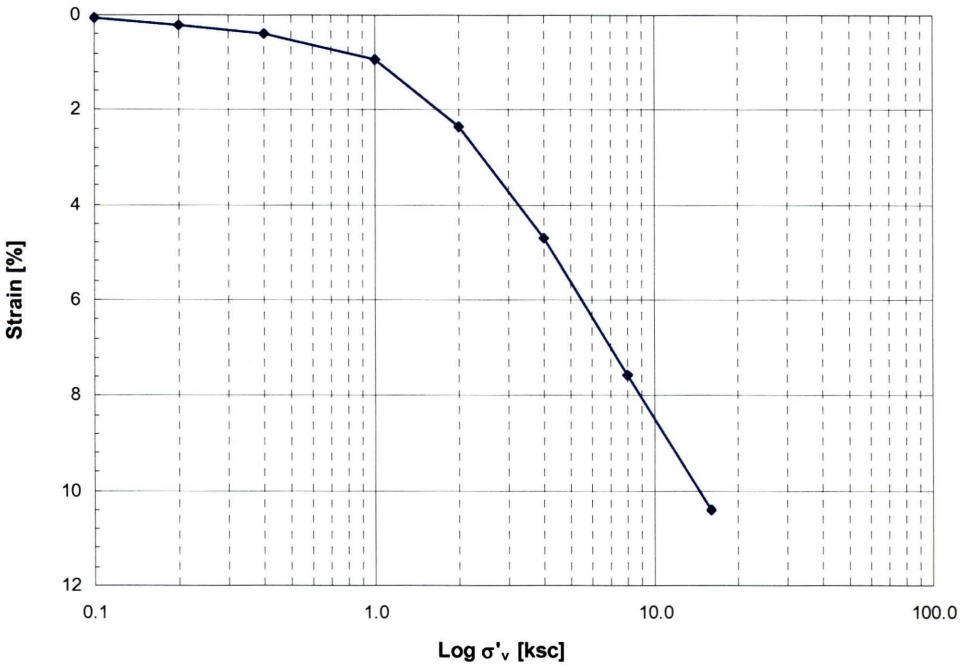

Figure A.58 Compression curve for Oed111

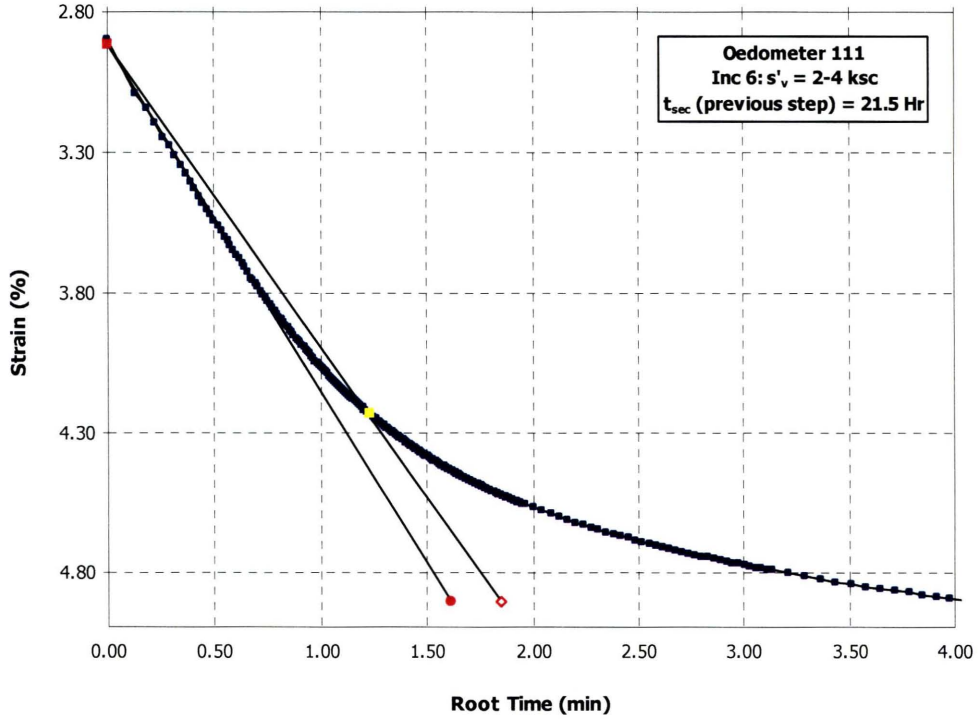

Figure A.59 Consolidation curve in $\sqrt{t}$ space for Oed111 Load Increment 6

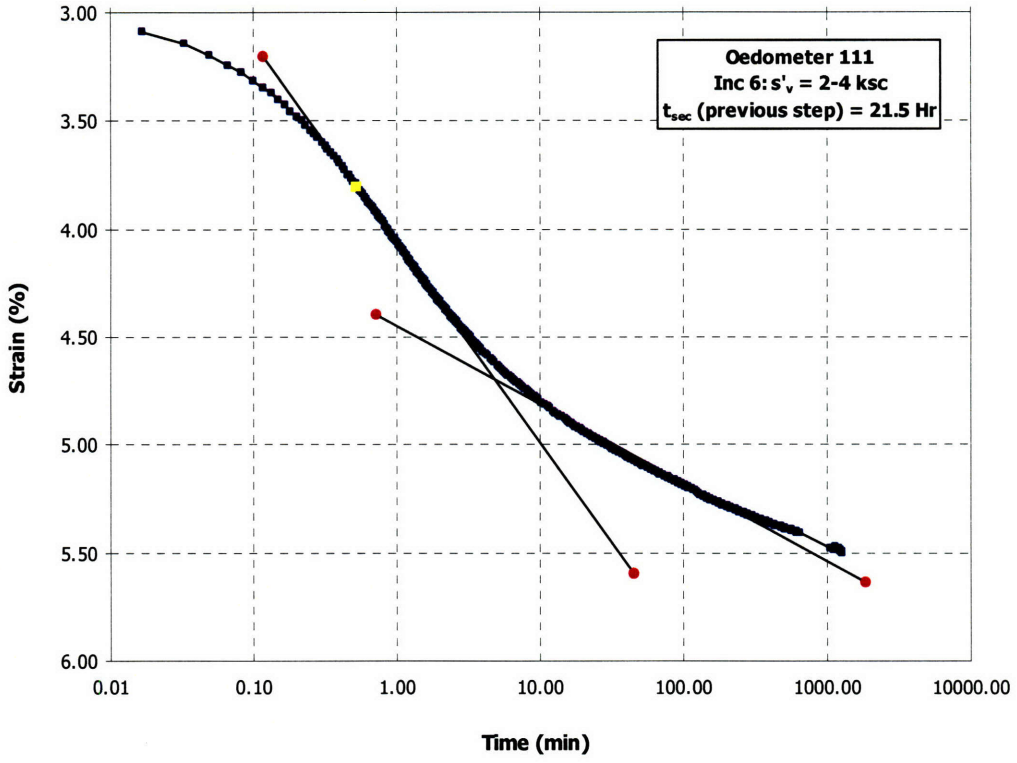

Figure A.60 Consolidation curve in Log time space for Oed111 Load Increment 6

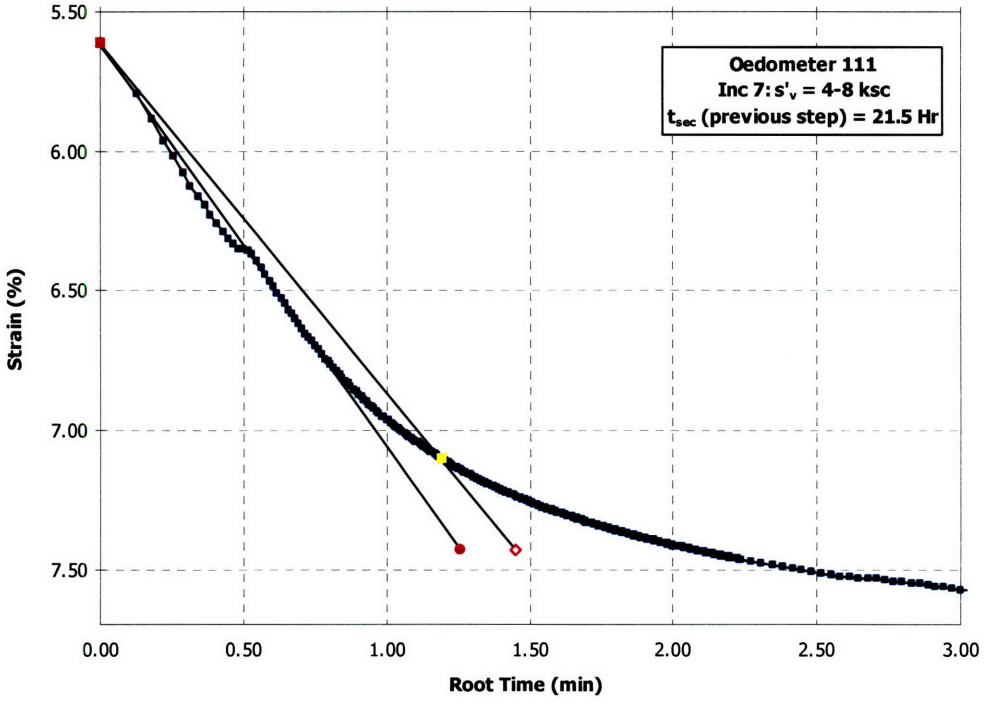

Figure A.61 Consolidation curve in $\sqrt{t}$ space for Oed111 Load Increment 7

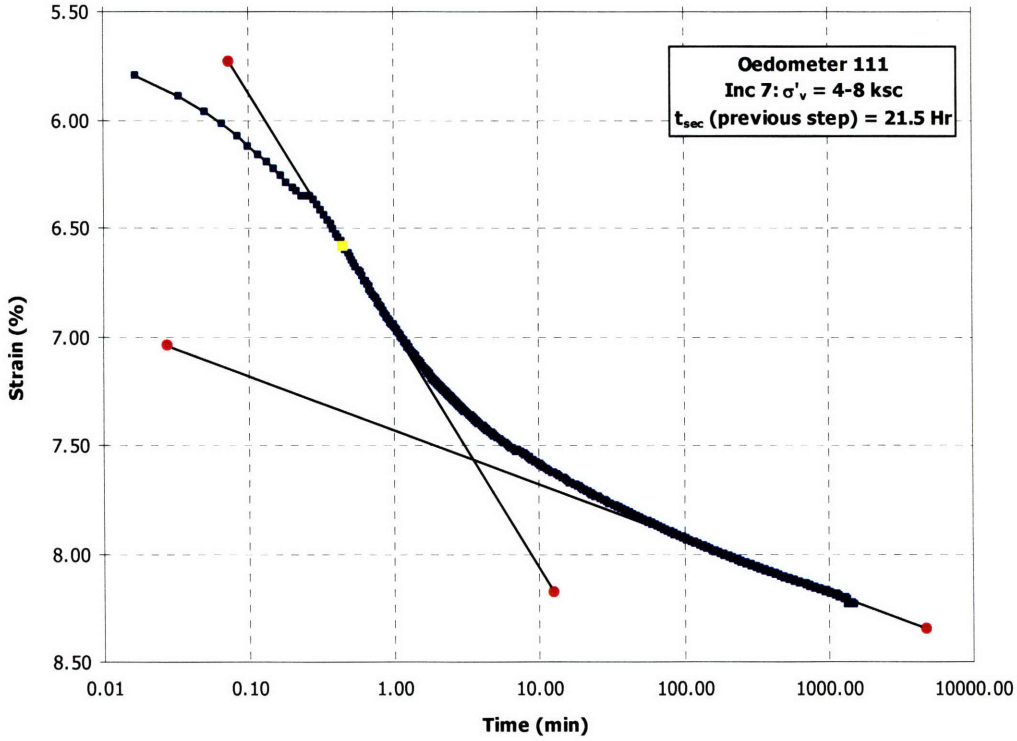

Figure A.62 Consolidation curve in Log time space for Oed111 Load Increment 7

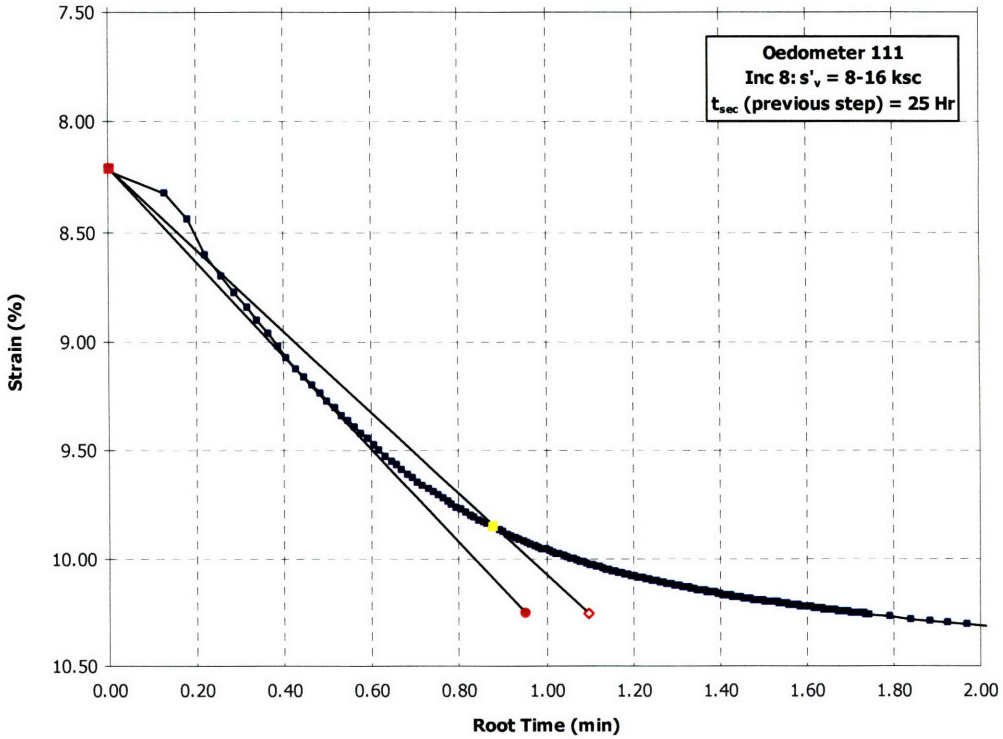

Figure A.63 Consolidation curve in $\sqrt{t}$ space for Oed111 Load Increment 8

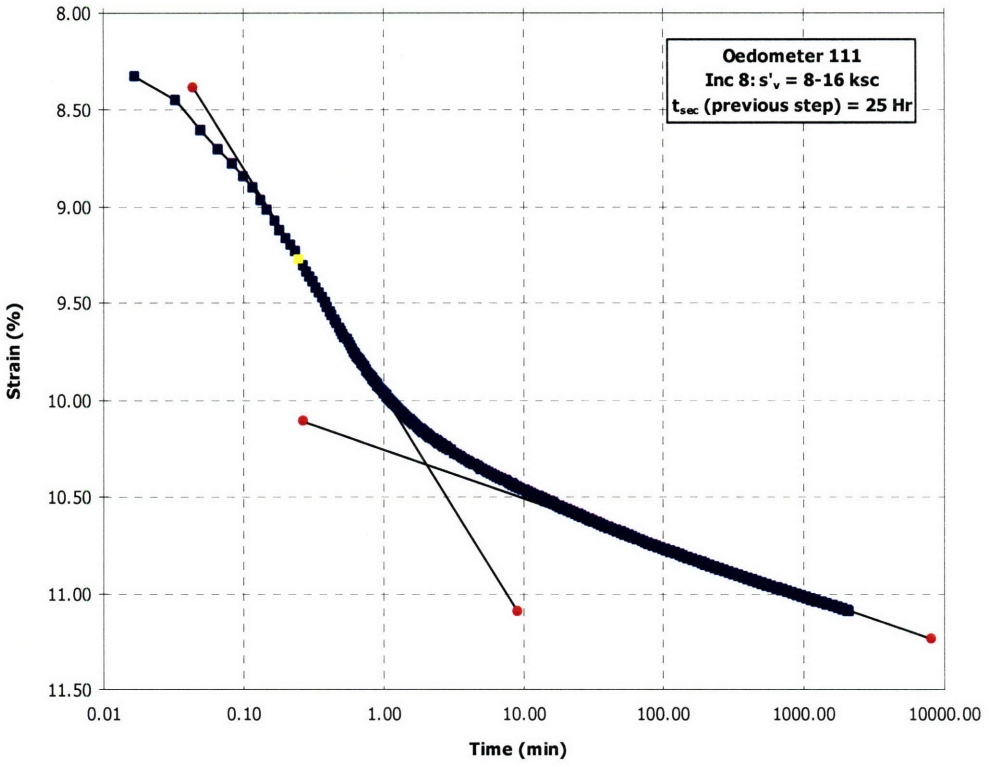

Figure A.64 Consolidation curve in Log time space for Oed111 Load Increment 8

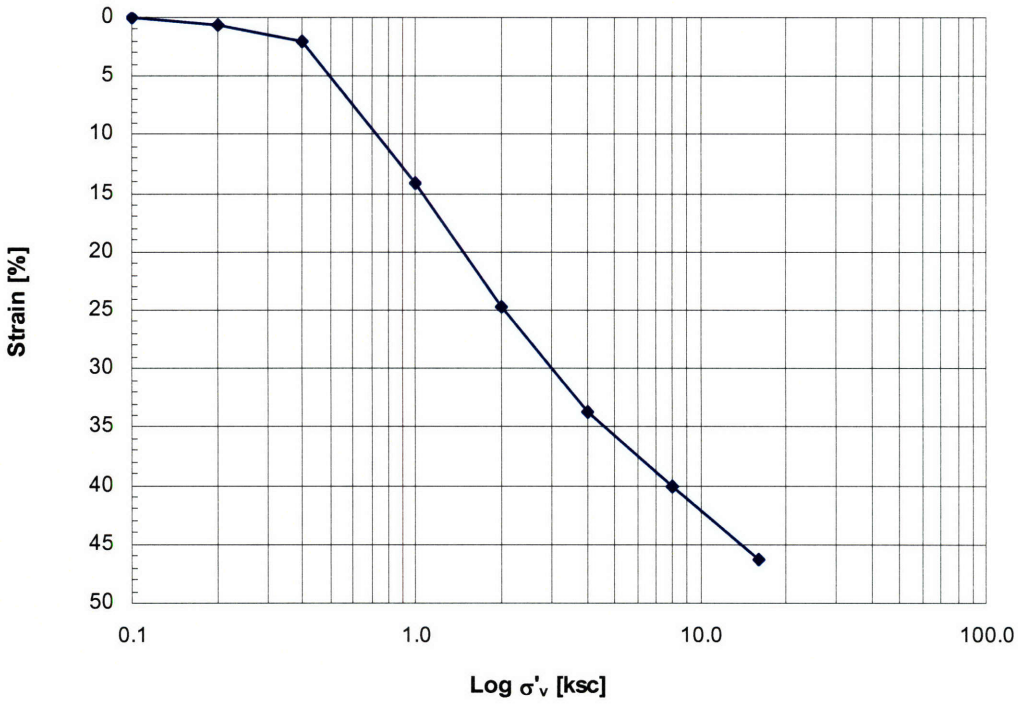

Figure A.65 Compression curve for Oed112

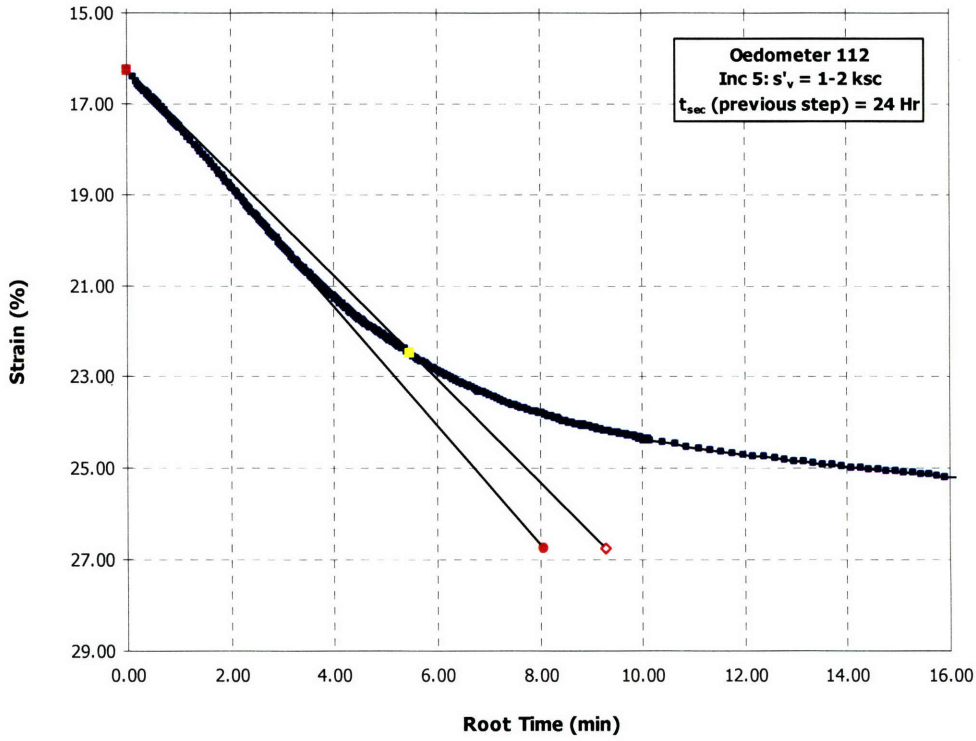

Figure A.66 Consolidation curve in $\sqrt{t}$ space for Oed112 Load Increment 5

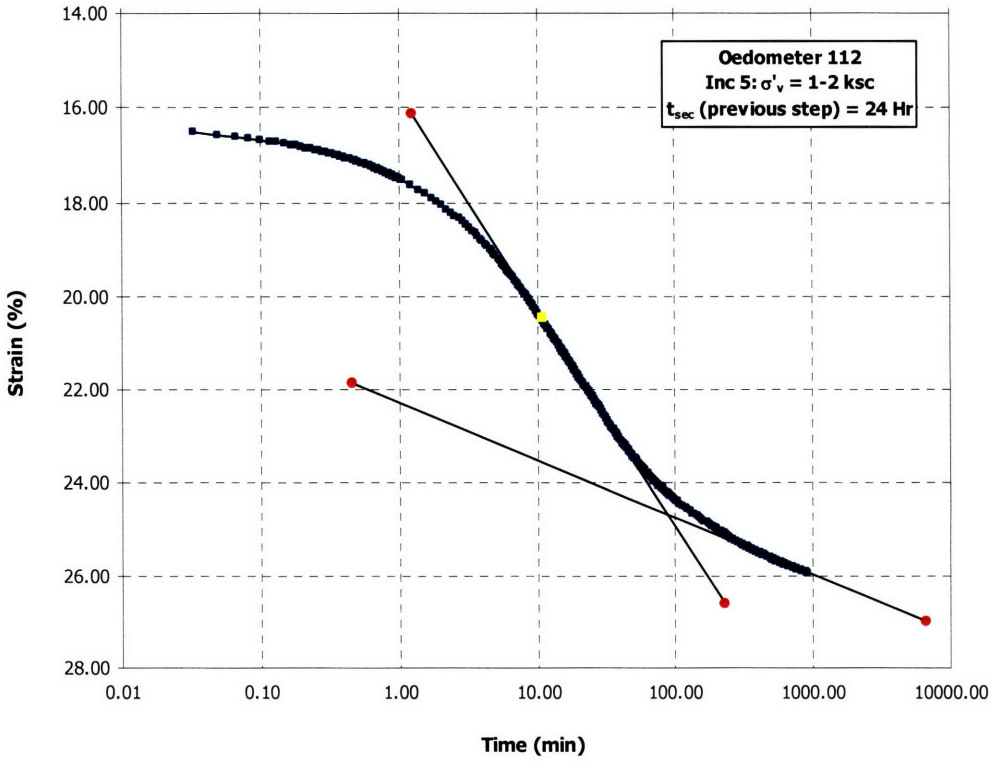

Figure A.67 Consolidation curve in Log time space for Oed112 Load Increment 5

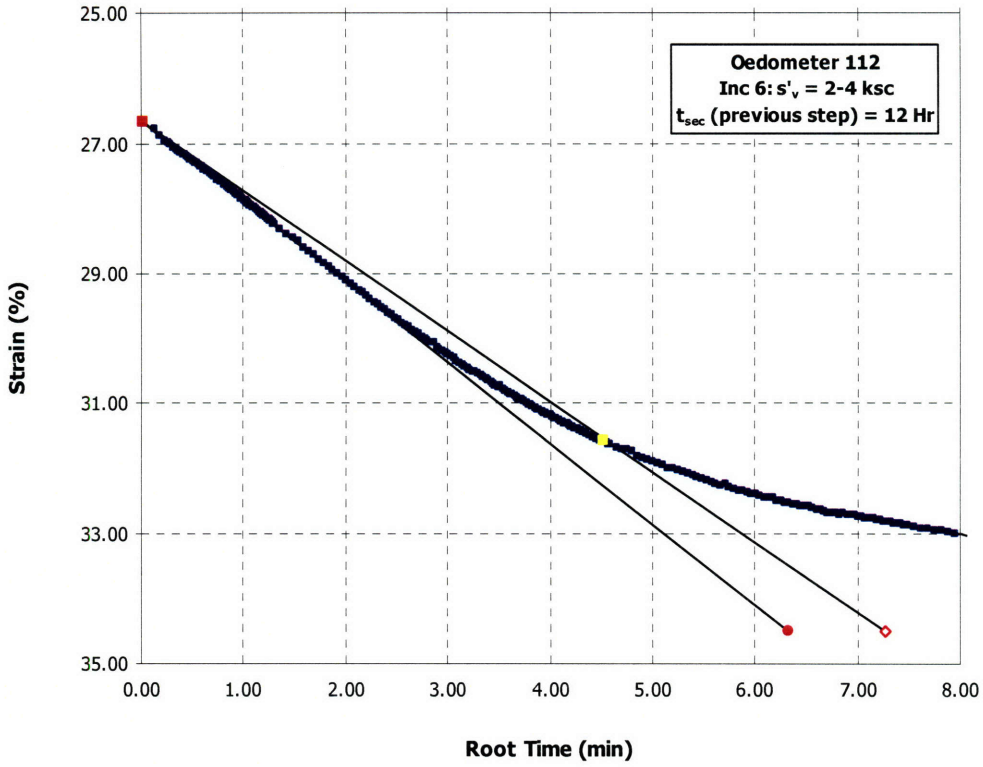

Figure A.68 Consolidation curve in $\sqrt{t}$ space for Oed112 Load Increment 6

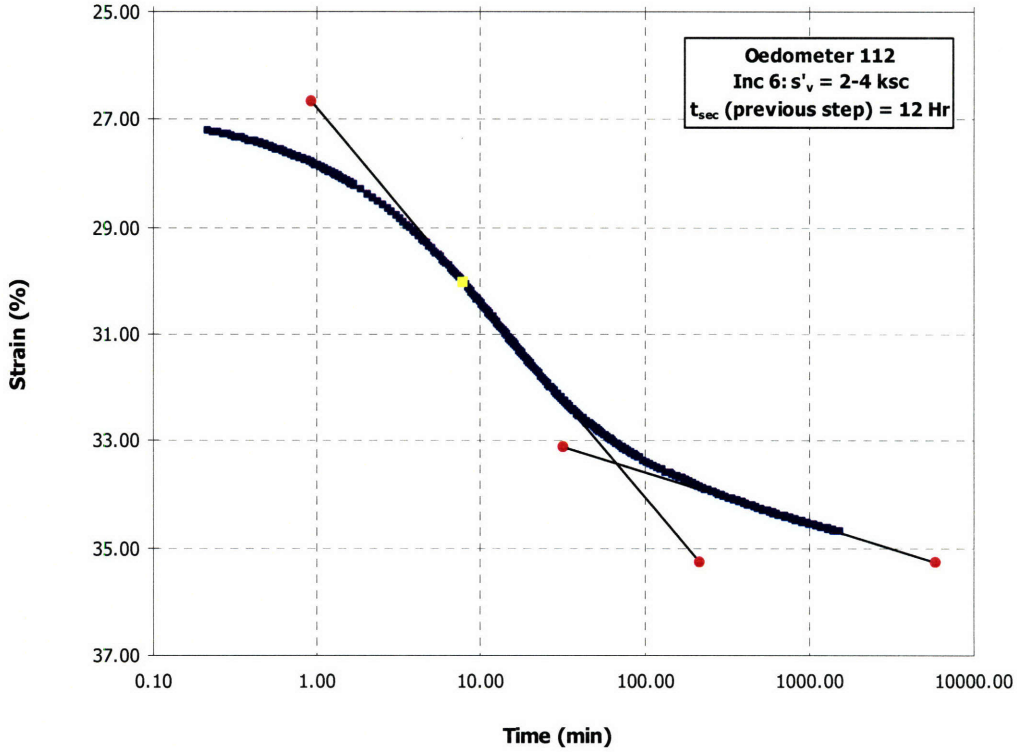

Figure A.69 Consolidation curve in Log time space for Oed112 Load Increment 6

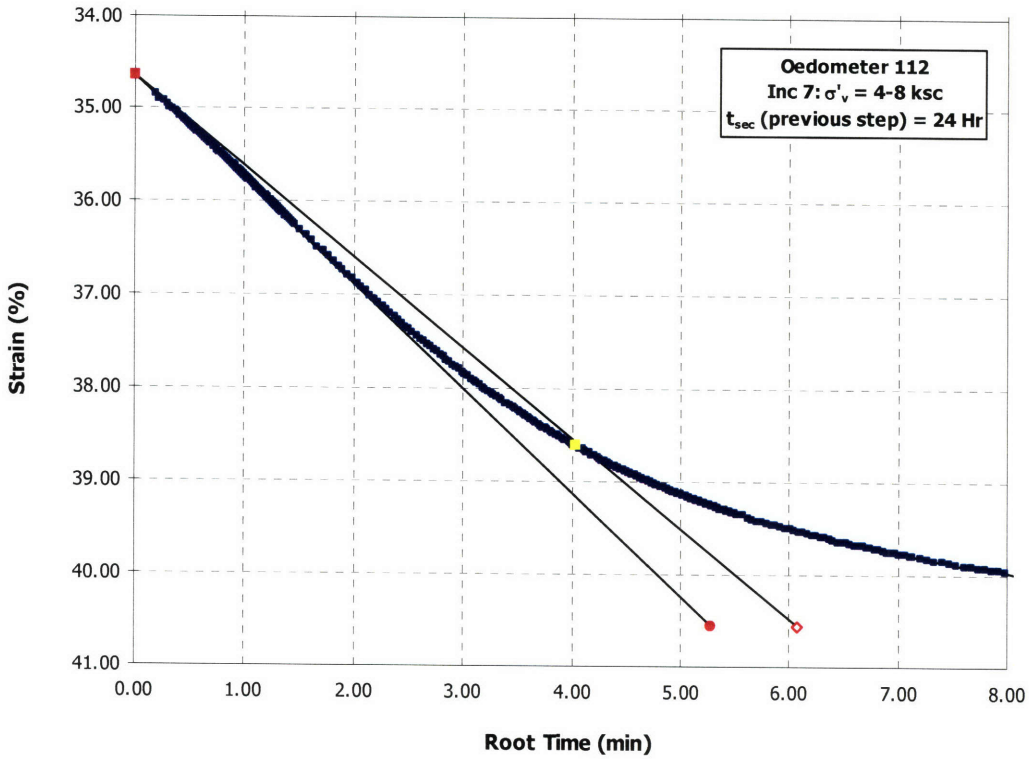

Figure A.70 Consolidation curve in $\sqrt{t}$ space for Oed112 Load Increment 7

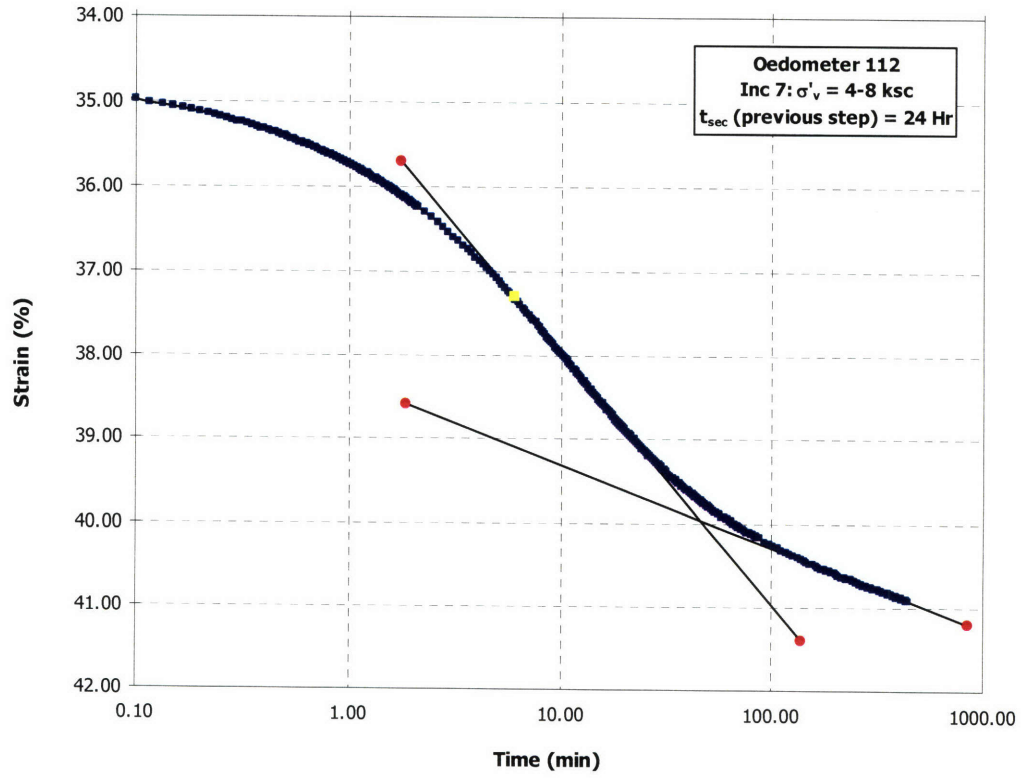

Figure A.71 Consolidation curve in Log time space for Oed112 Load Increment 7

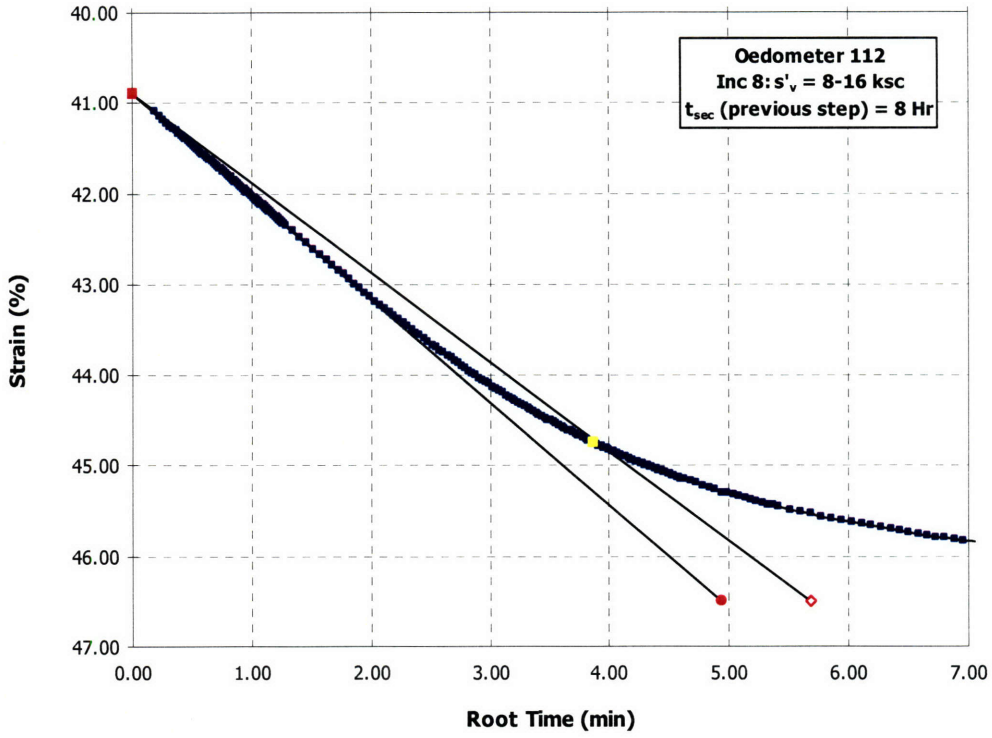

Figure A.72 Consolidation curve in $\sqrt{t}$ space for Oed112 Load Increment 8

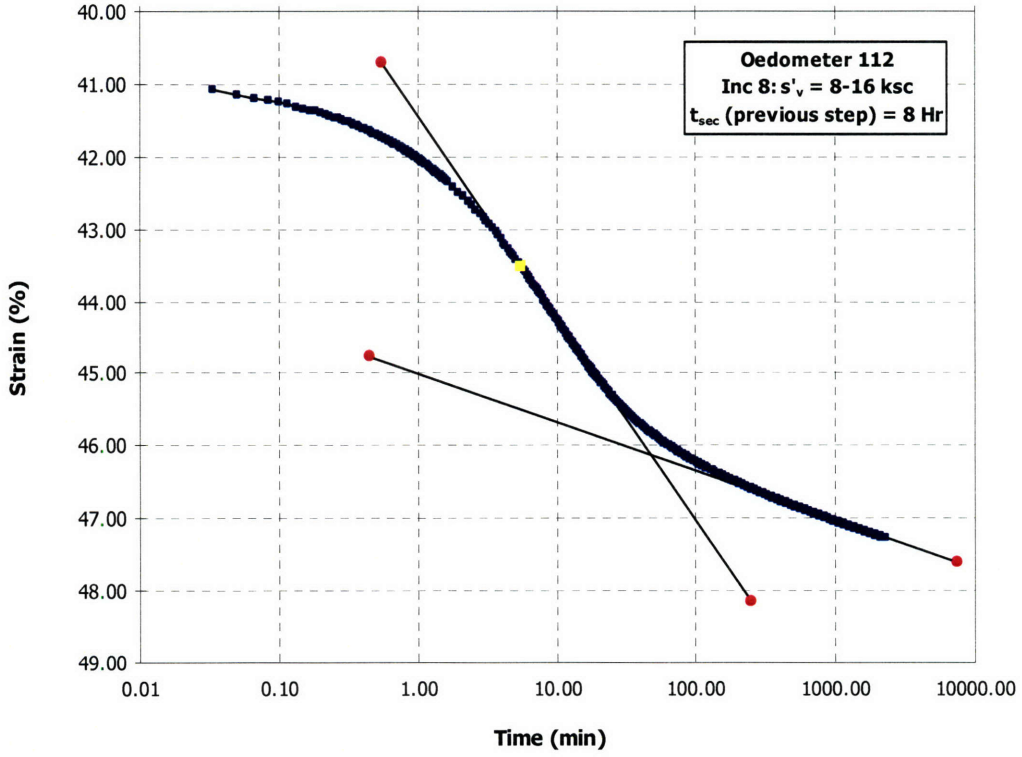

Figure A.73 Consolidation curve in Log time space for Oed112 Load Increment 8

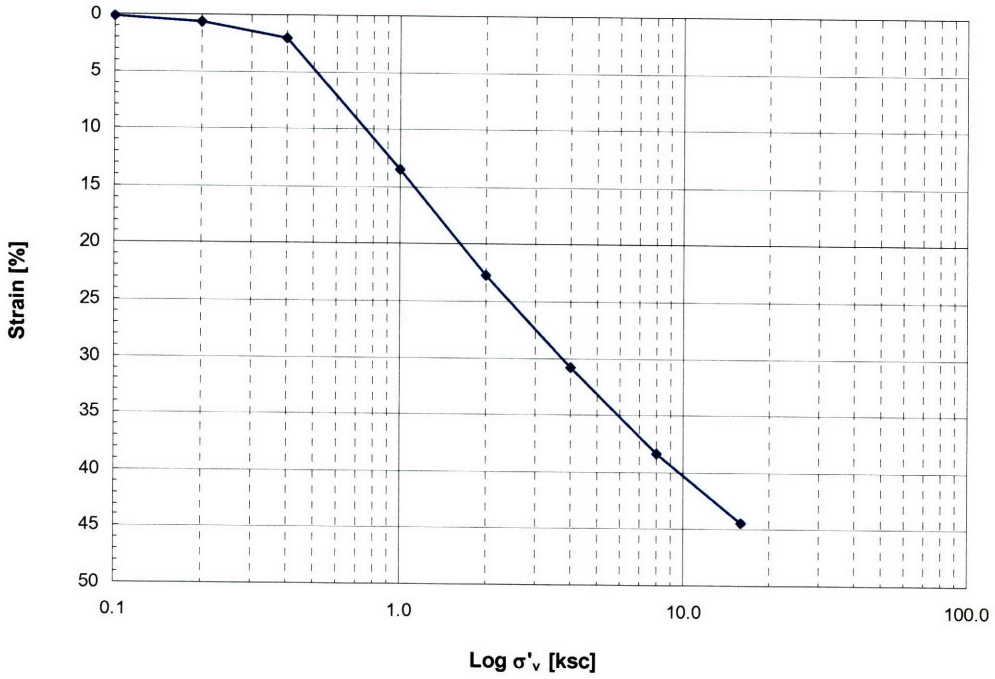

Figure A.74 Compression curve for Oed113

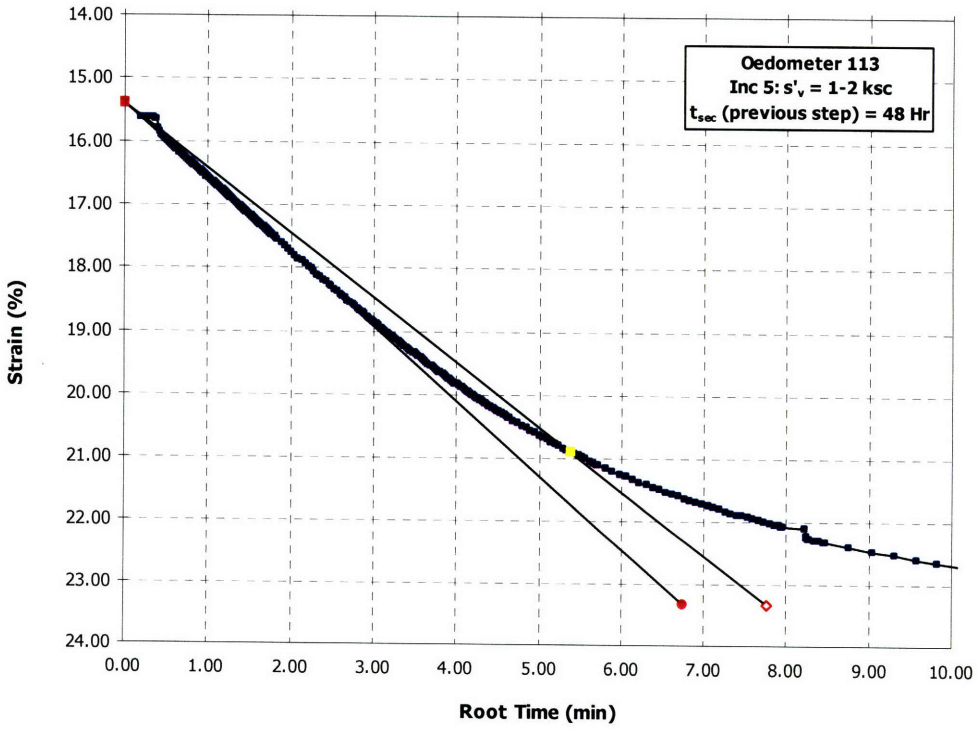

Figure A.75 Consolidation curve in $\sqrt{t}$ space for Oed113 Load Increment 5

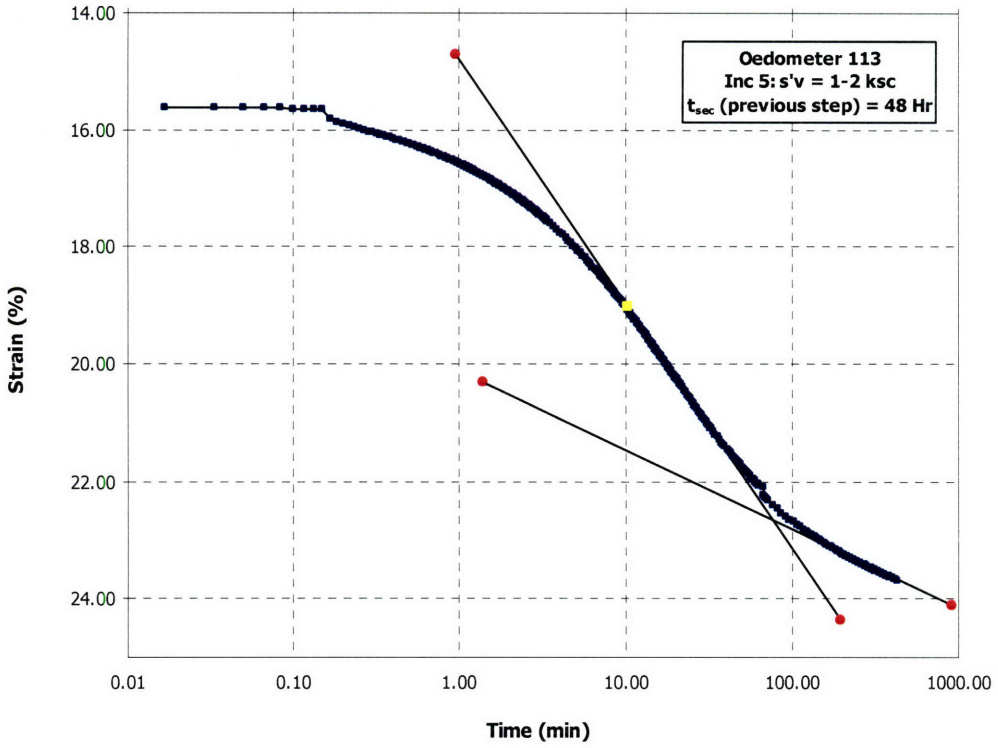

Figure A.76 Consolidation curve in Log time space for Oed113 Load Increment 5

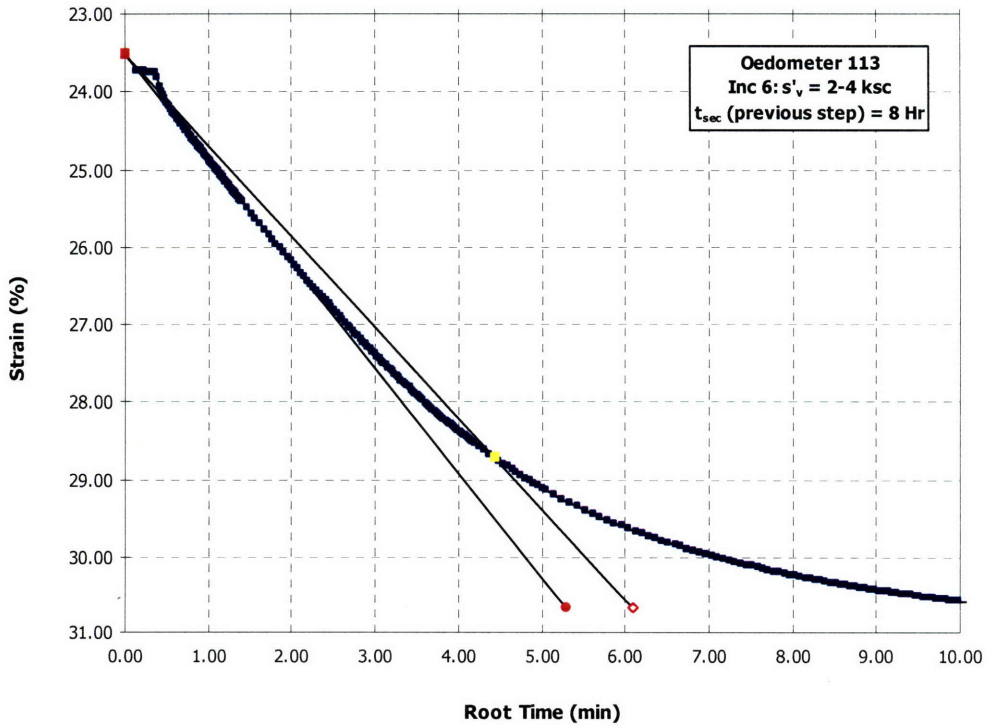

Figure A.77 Consolidation curve in $\sqrt{t}$ space for Oed113 Load Increment 6

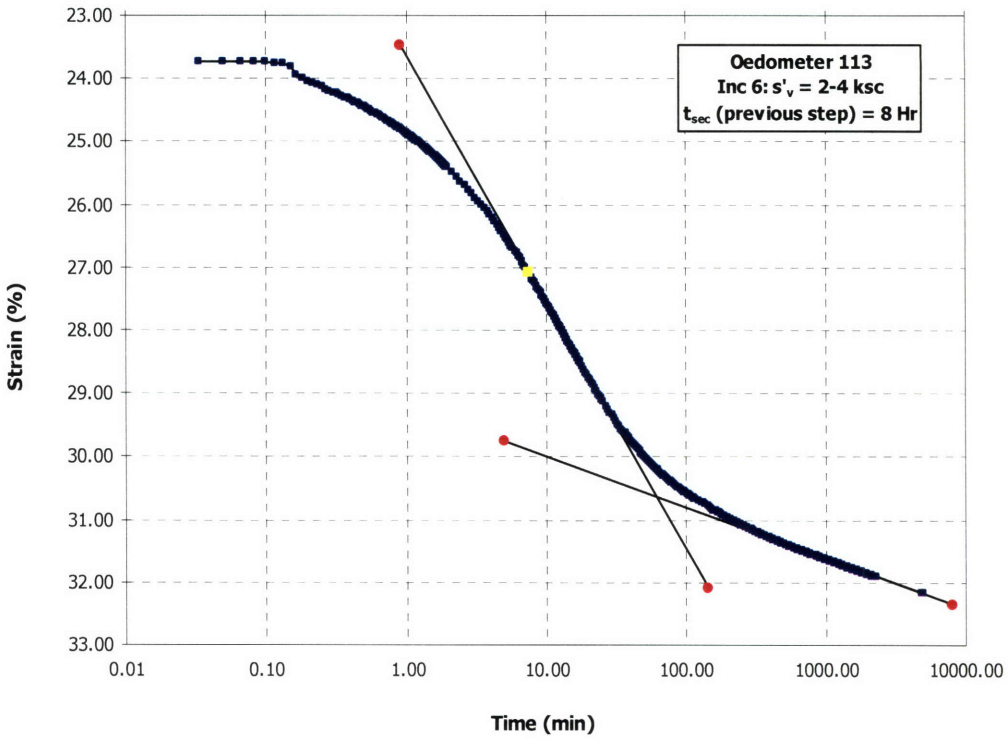

Figure A.78 Consolidation curve in Log time space for Oed113 Load Increment 6

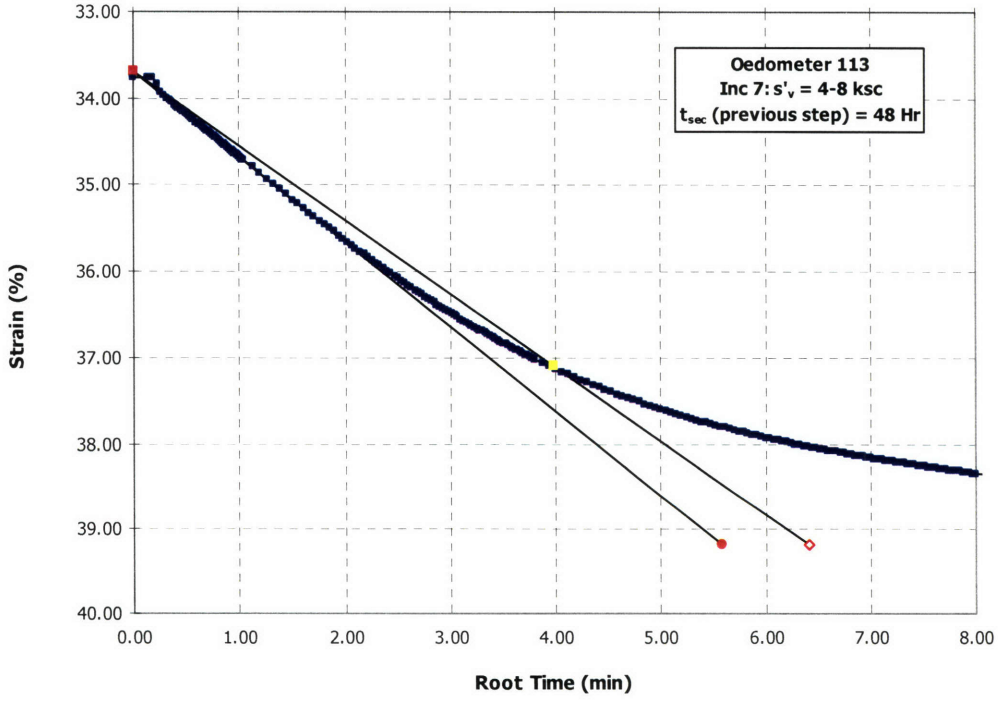

Figure A.79 Consolidation curve in $\sqrt{t}$ space for Oed113 Load Increment 7

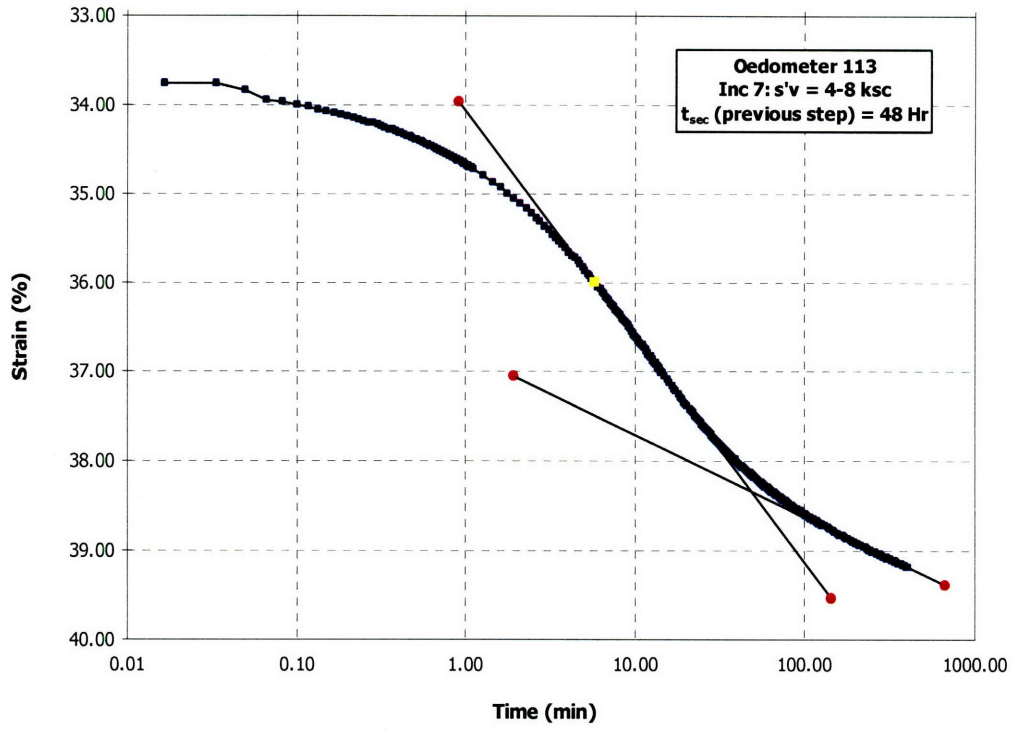

Figure A.80 Consolidation curve in Log time space for Oed113 Load Increment 7

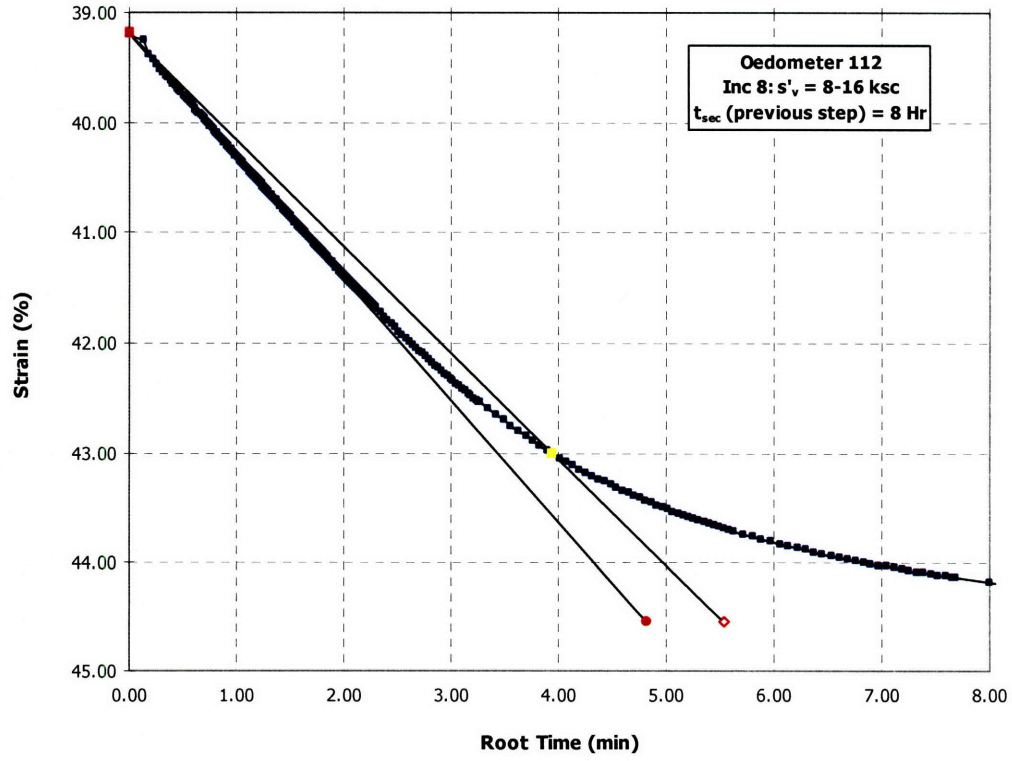

Figure A.81 Consolidation curve in $\sqrt{t}$ space for Oed113 Load Increment 8

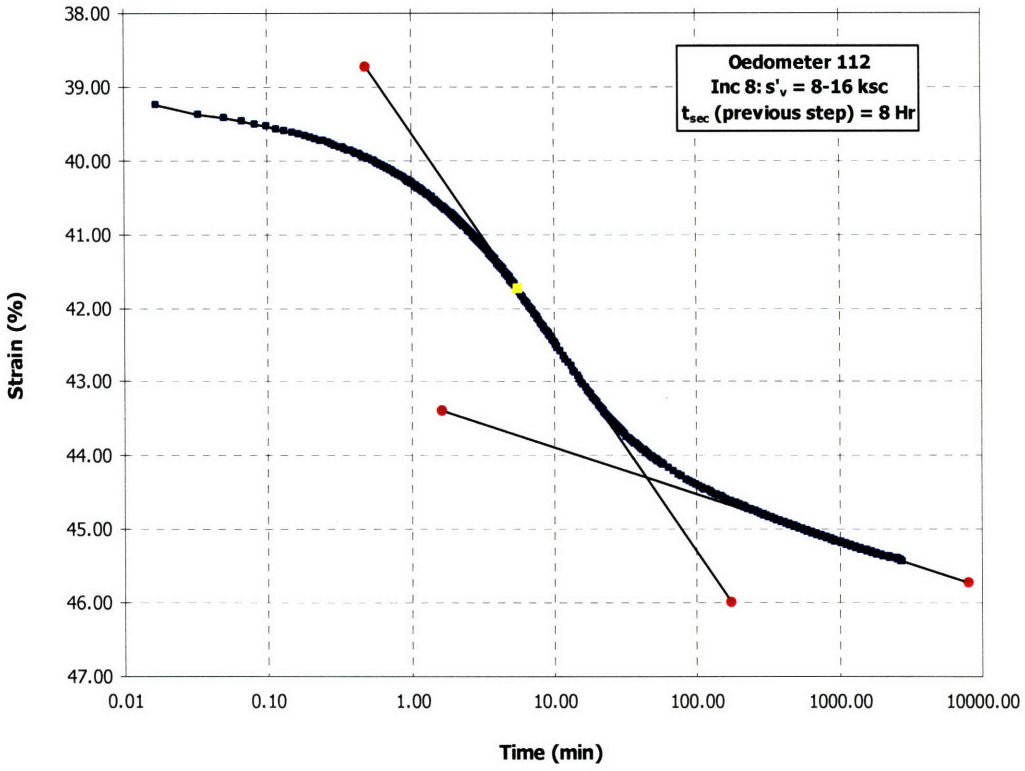

Figure A.82 Consolidation curve in Log time space for Oed113 Load Increment 8

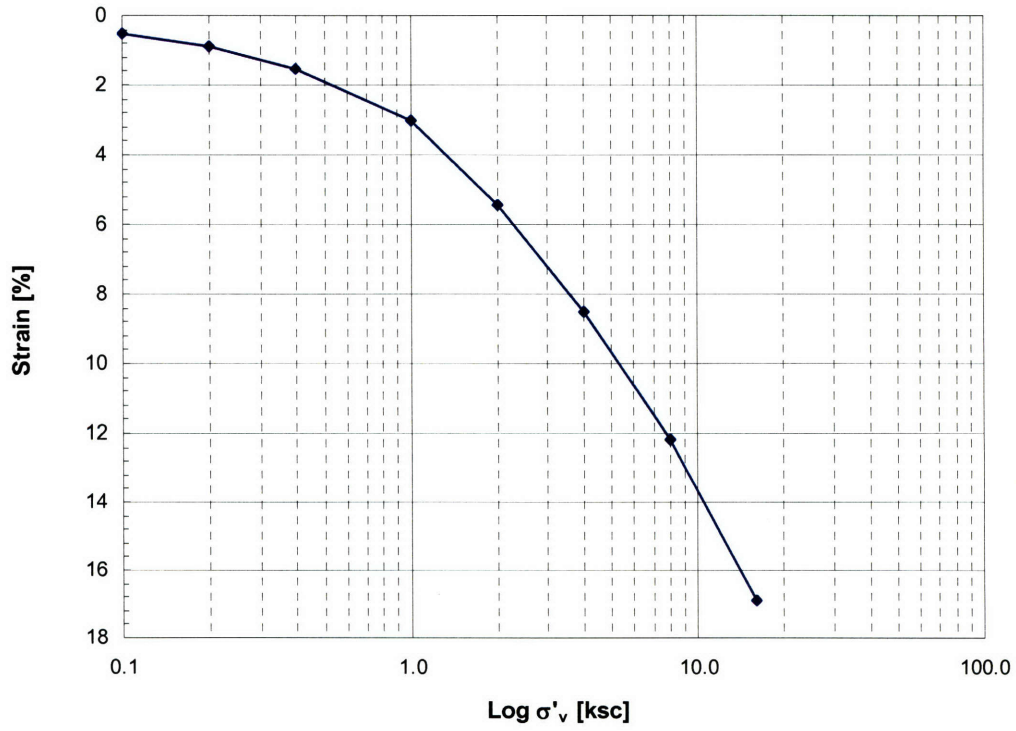

Figure A.83 Compression curve for Oed114

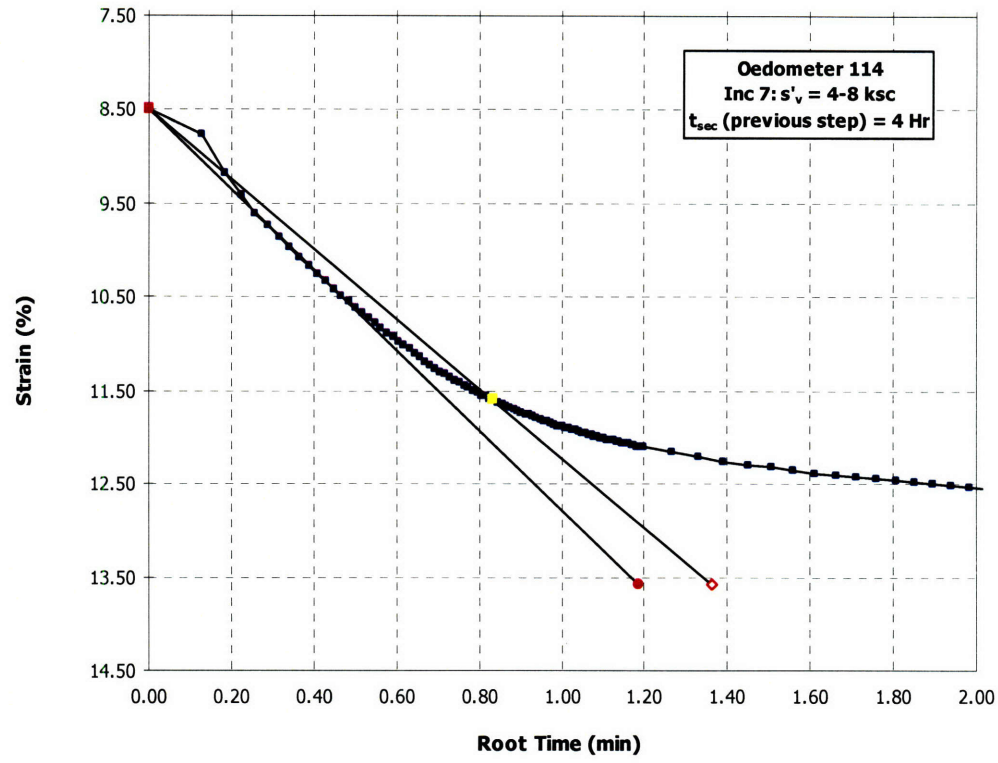

Figure A.84 Consolidation curve in $\sqrt{t}$ space for Oed114 Load Increment 7

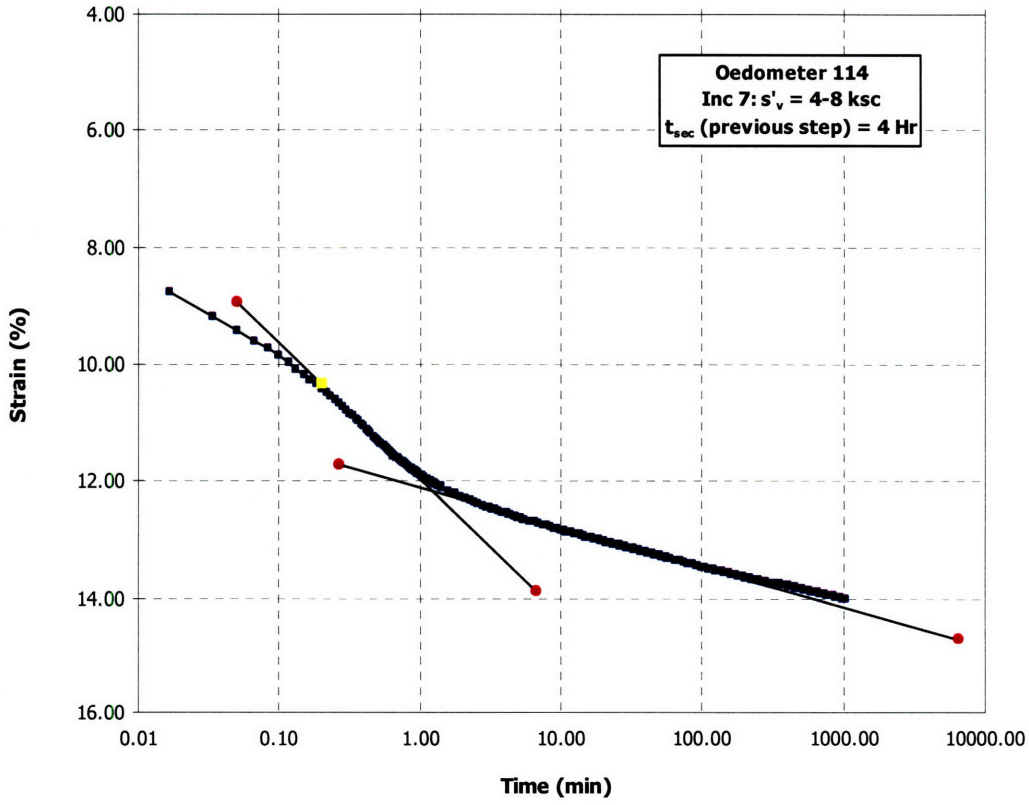

Figure A.85 Consolidation curve in Log time space for Oed114 Load Increment 7

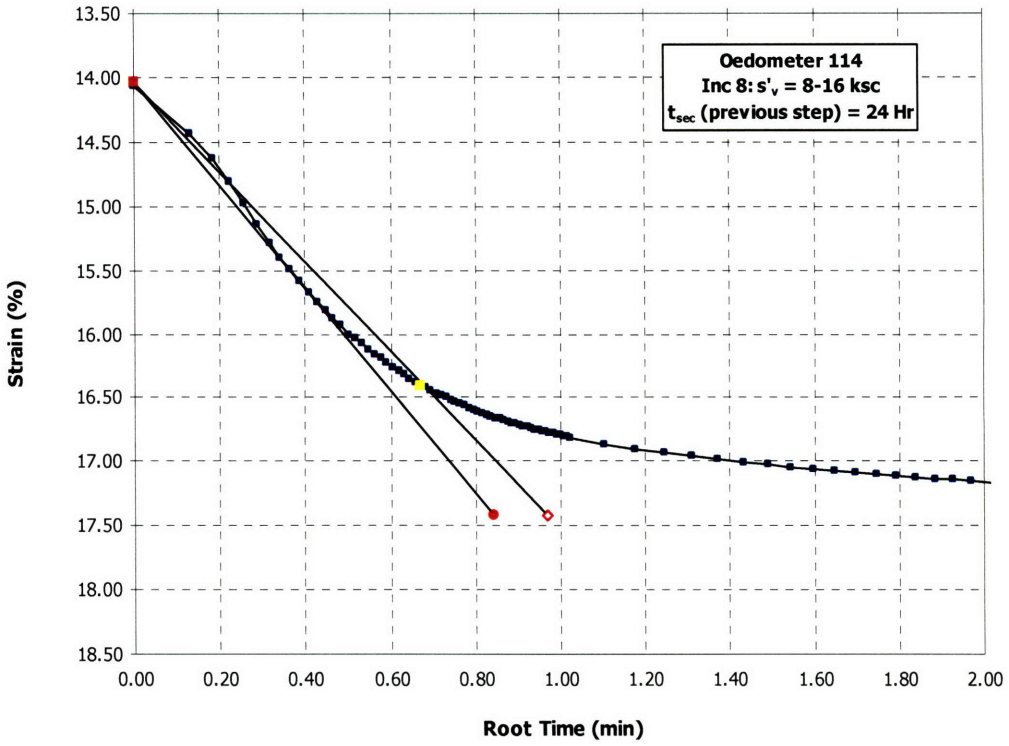

Figure A.86 Consolidation curve in $\sqrt{t}$ space for Oed114 Load Increment 8

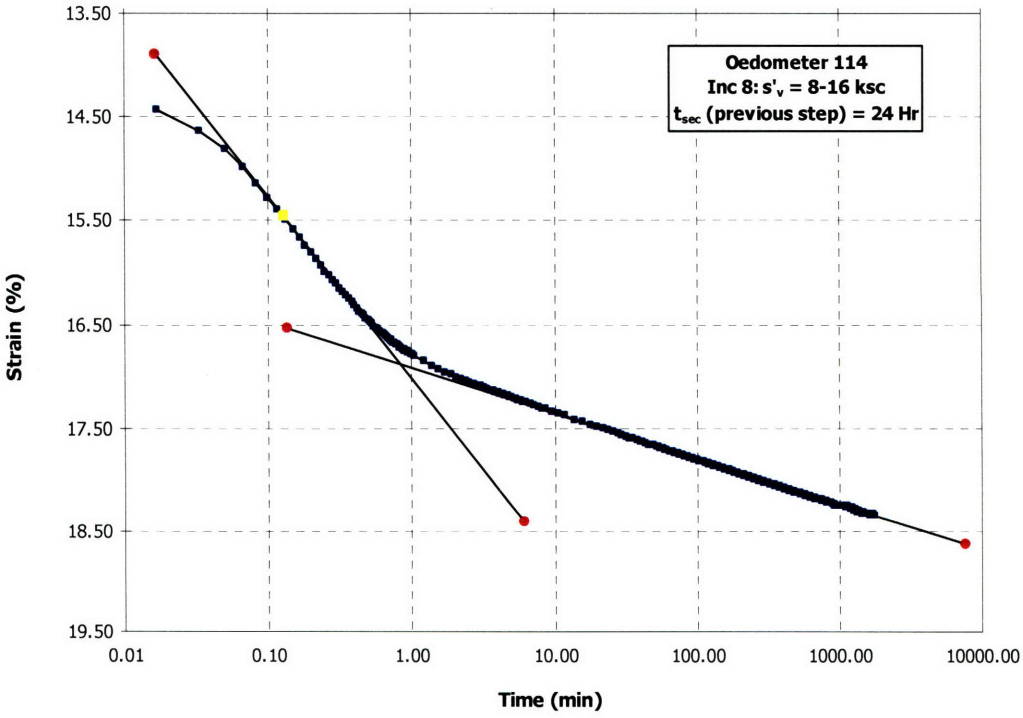

Figure A.87 Consolidation curve in Log time space for Oed114 Load Increment 8

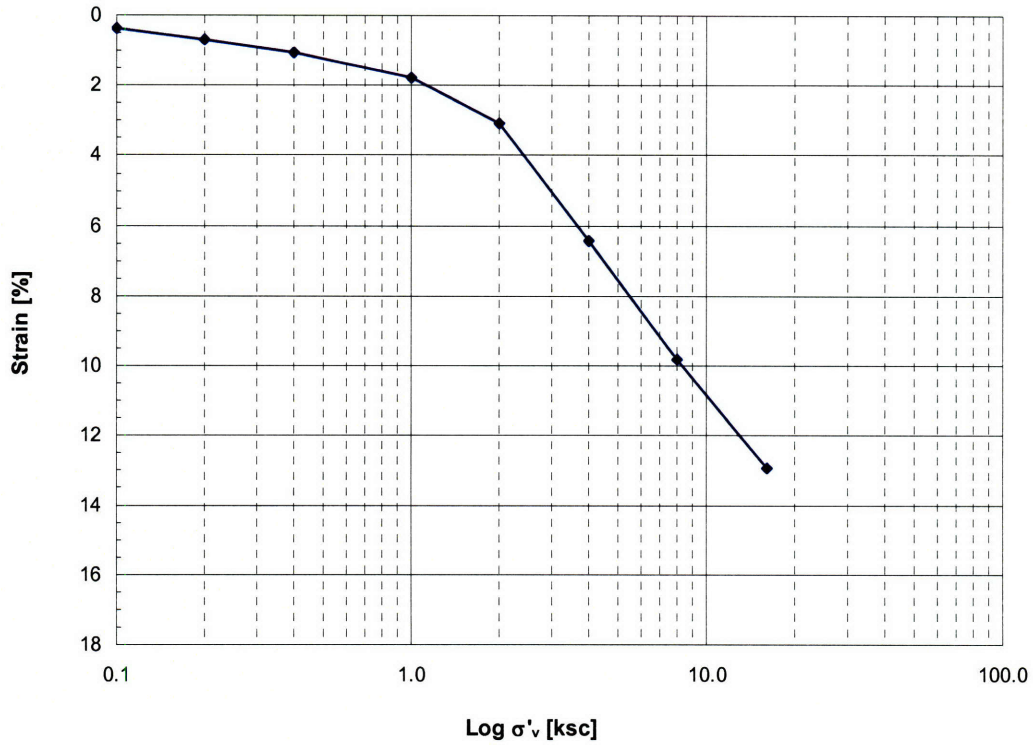

Figure A.88 Compression curve for Oed115

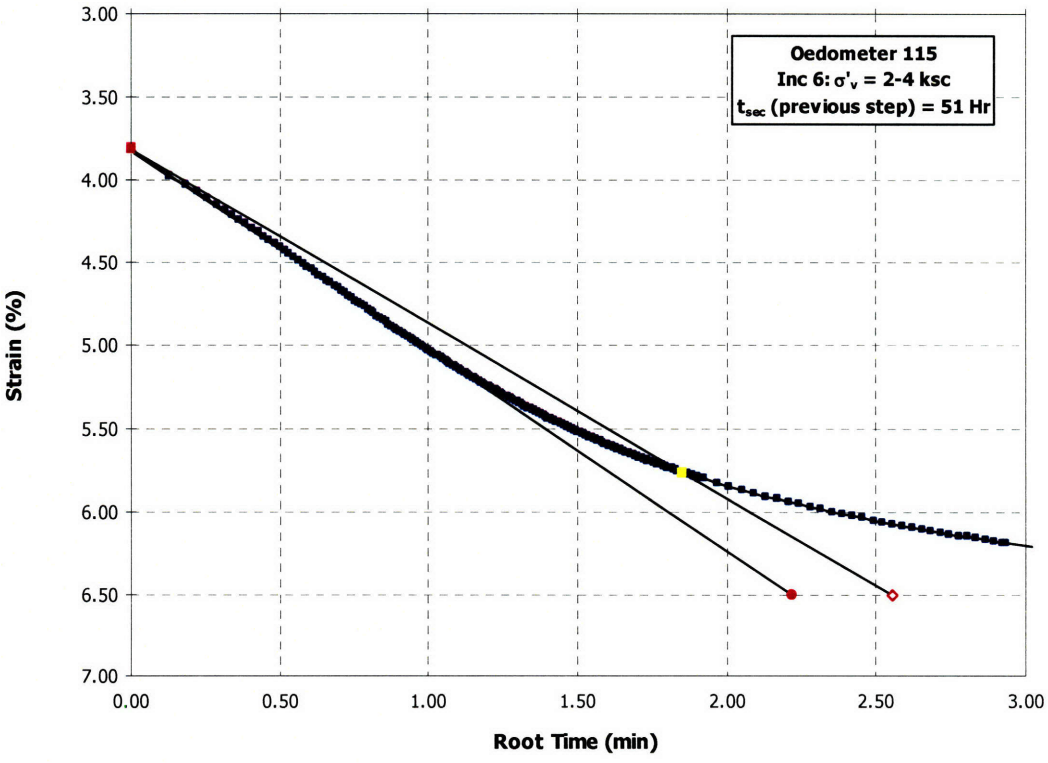

Figure A.89 Consolidation curve in $\sqrt{t}$ space for Oed115 Load Increment 6

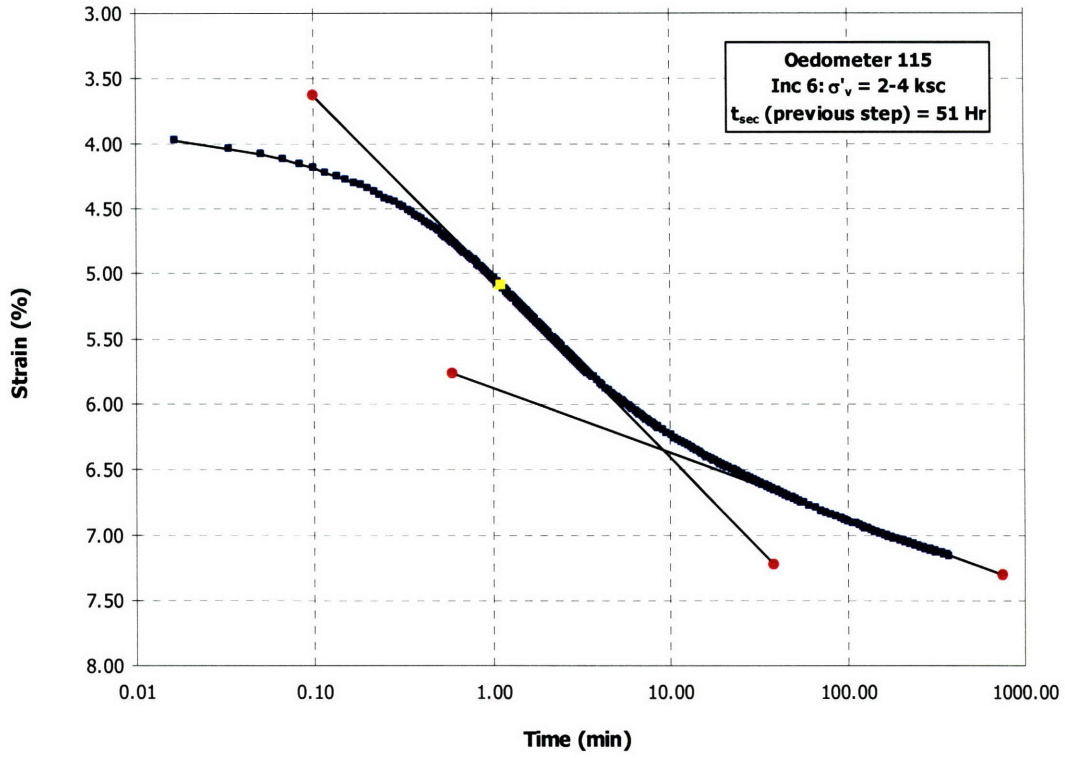

Figure A.90 Consolidation curve in Log time space for Oed115 Load Increment 6

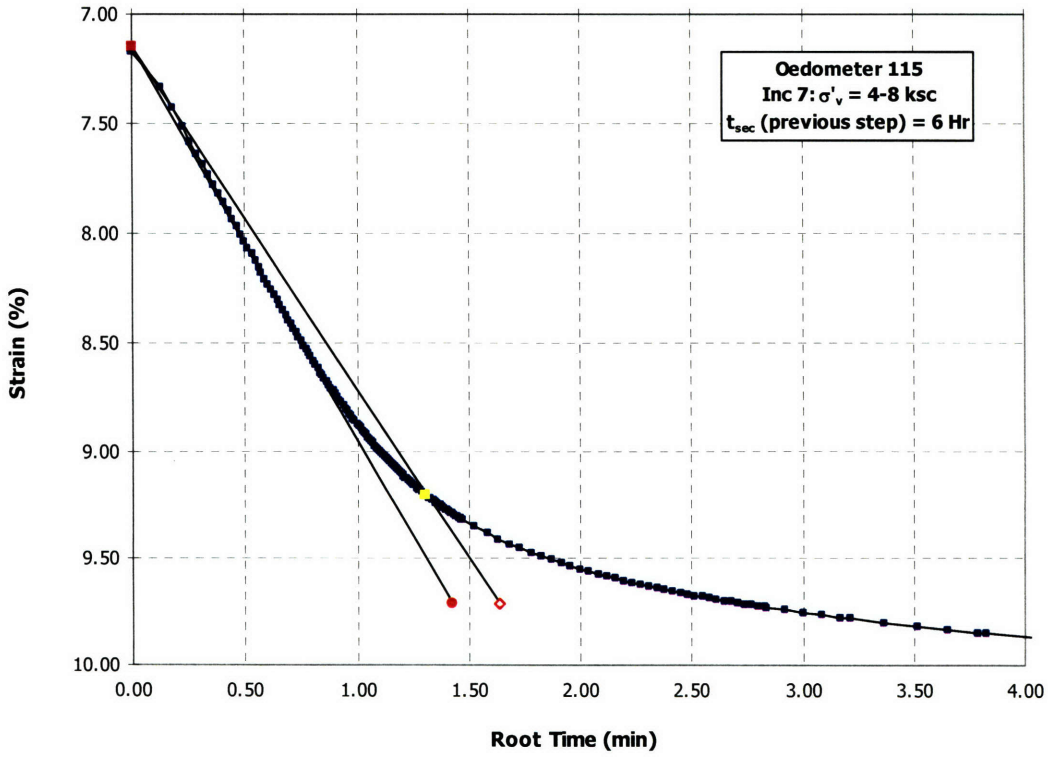

Figure A.91 Consolidation curve in $\sqrt{t}$ space for Oed115 Load Increment 7

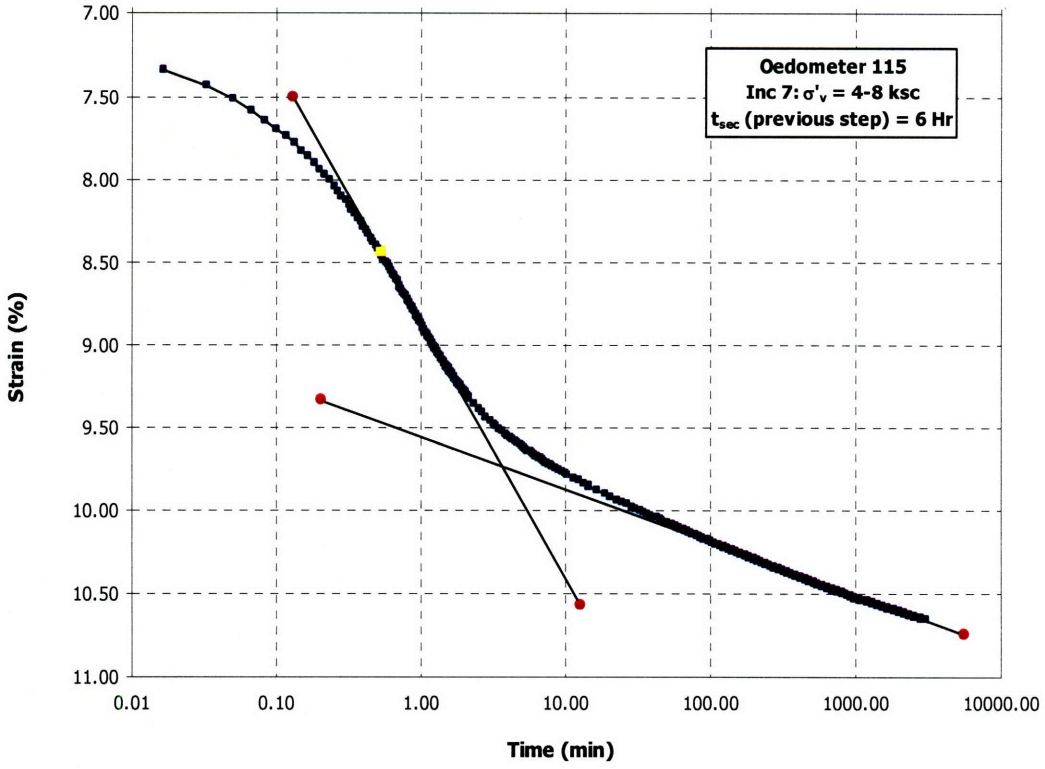

Figure A.92 Consolidation curve in Log time space for Oed115 Load Increment 7

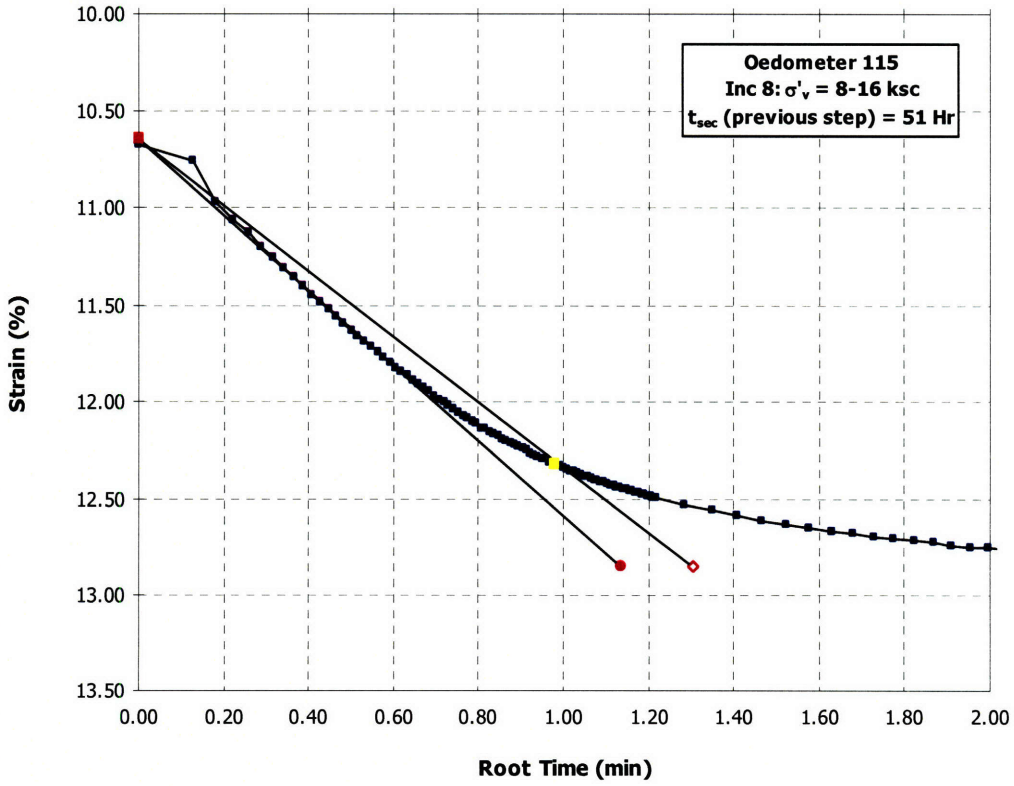

Figure A.93 Consolidation curve in $\sqrt{t}$ space for Oed115 Load Increment 8

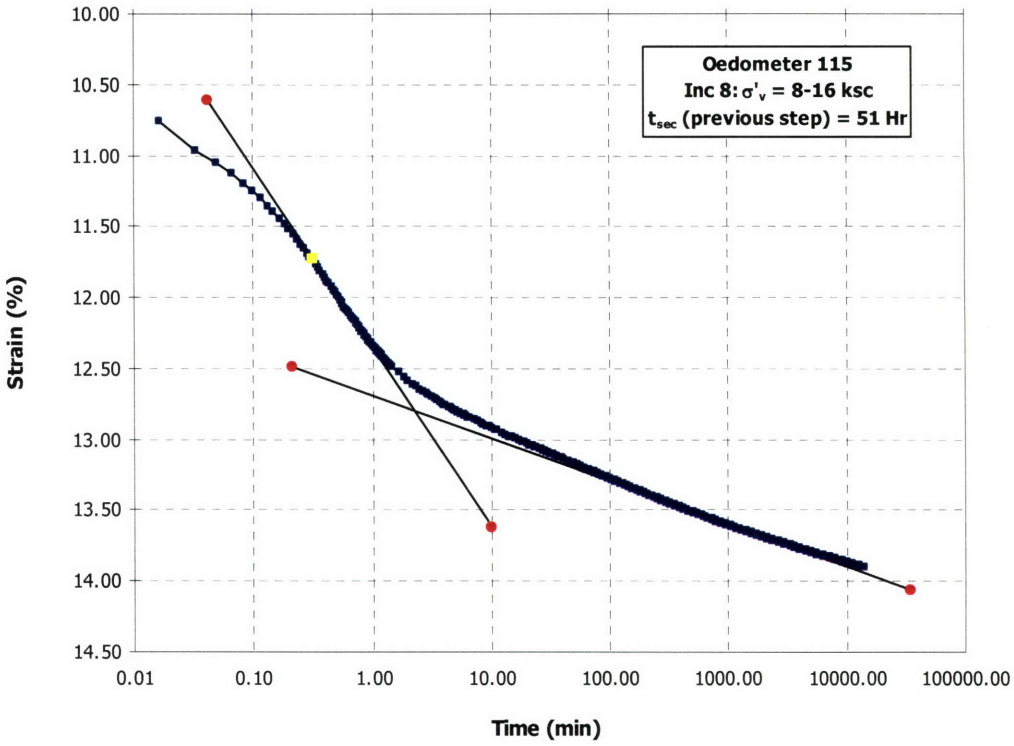

Figure A.94 Consolidation curve in Log time space for Oed115 Load Increment 8

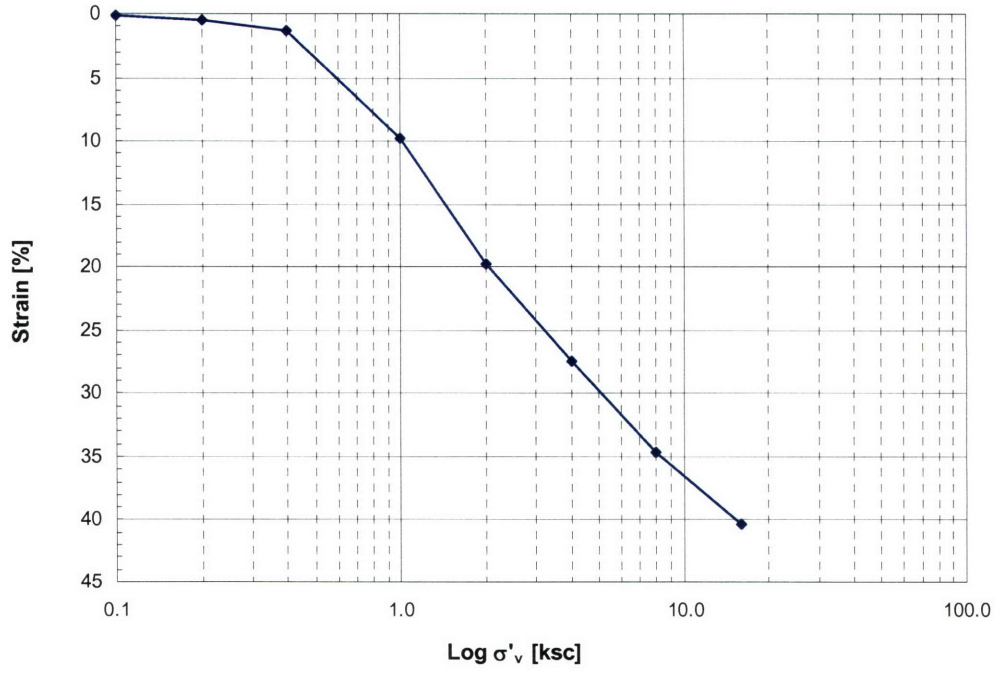

Figure A.95 Compression curve for Oed116

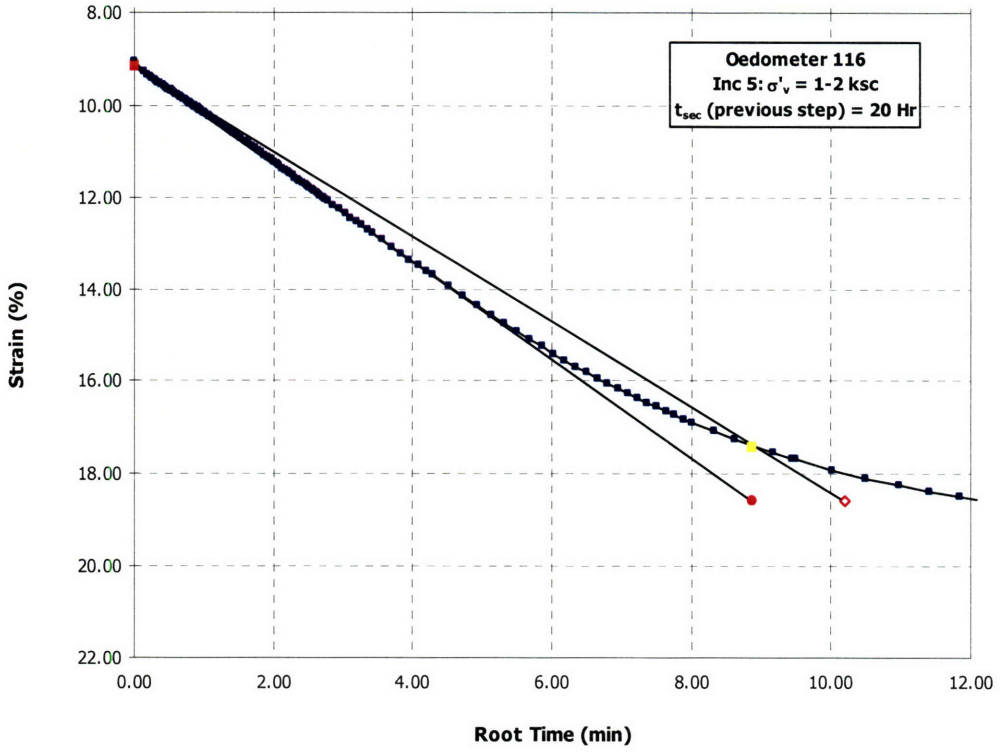

Figure A.96 Consolidation curve in $\sqrt{t}$ space for Oed116 Load Increment 5

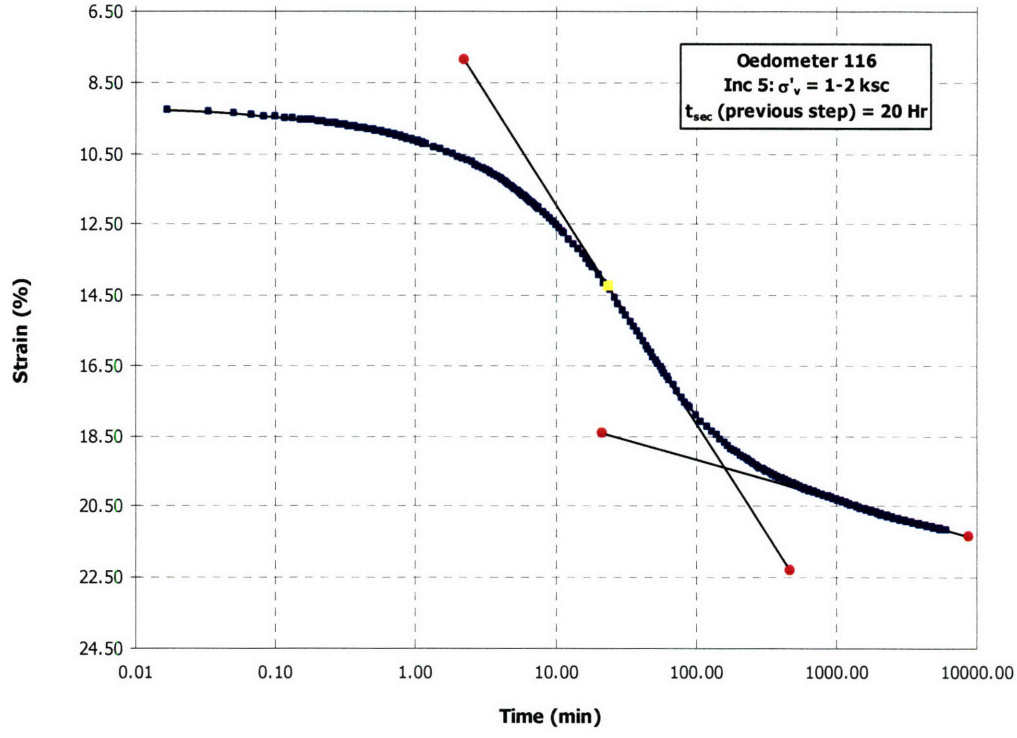

Figure A.97 Consolidation curve in Log time space for Oed116 Load Increment 5

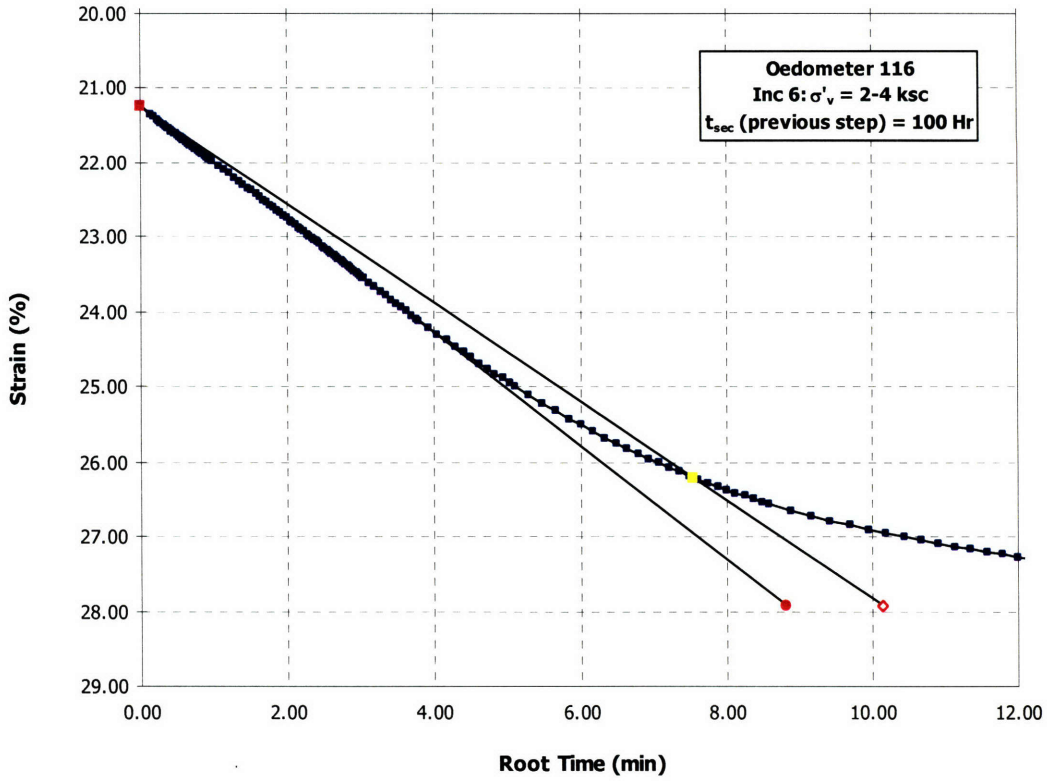

Figure A.98 Consolidation curve in $\sqrt{t}$ space for Oed116 Load Increment 6

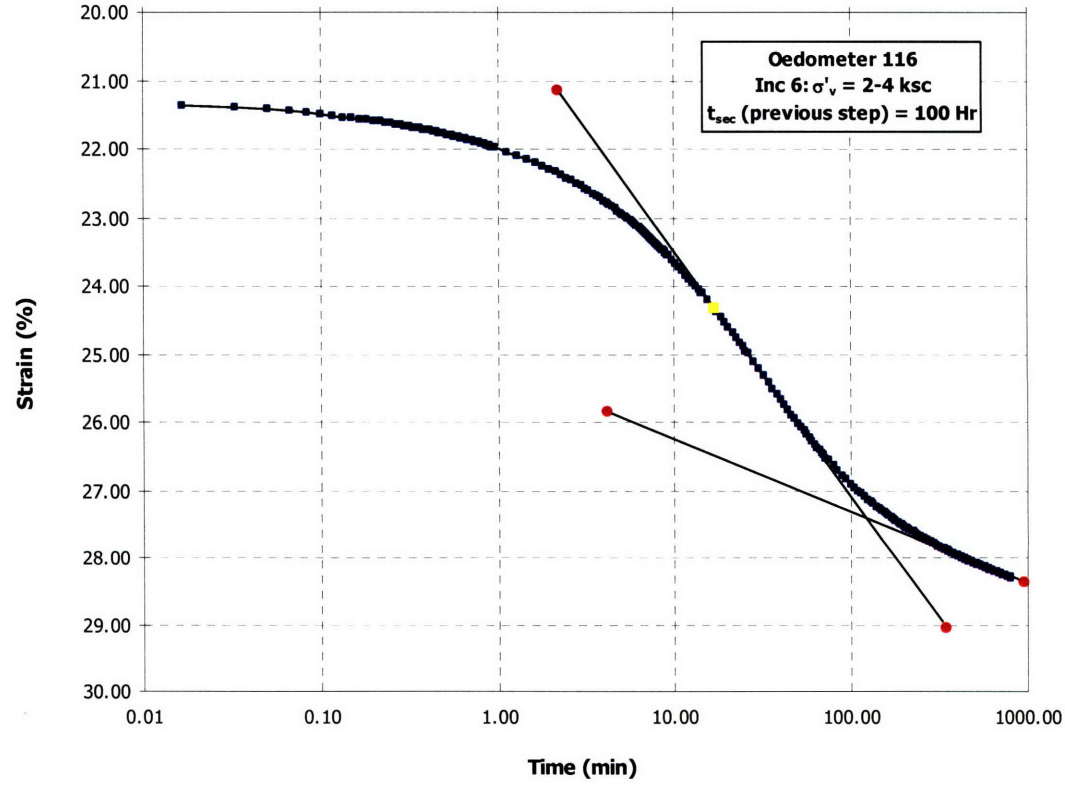

Figure A.99 Consolidation curve in Log time space for Oed116 Load Increment 6

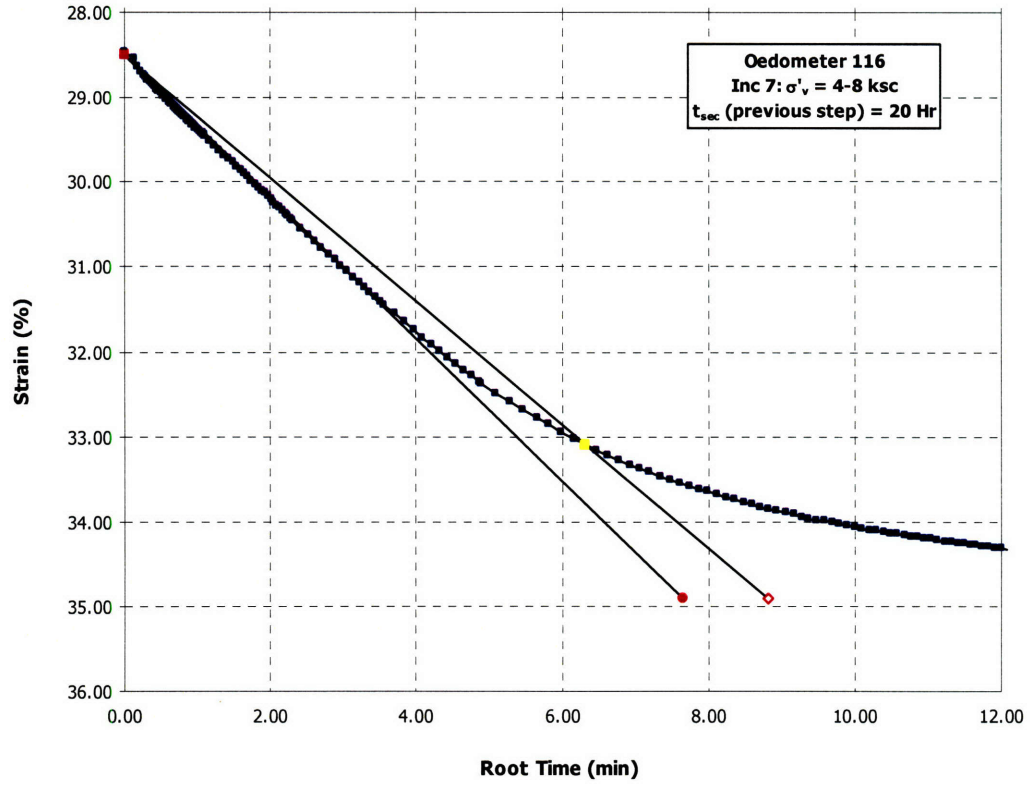

Figure A.100 Consolidation curve in $\sqrt{t}$ space for Oed116 Load Increment 7

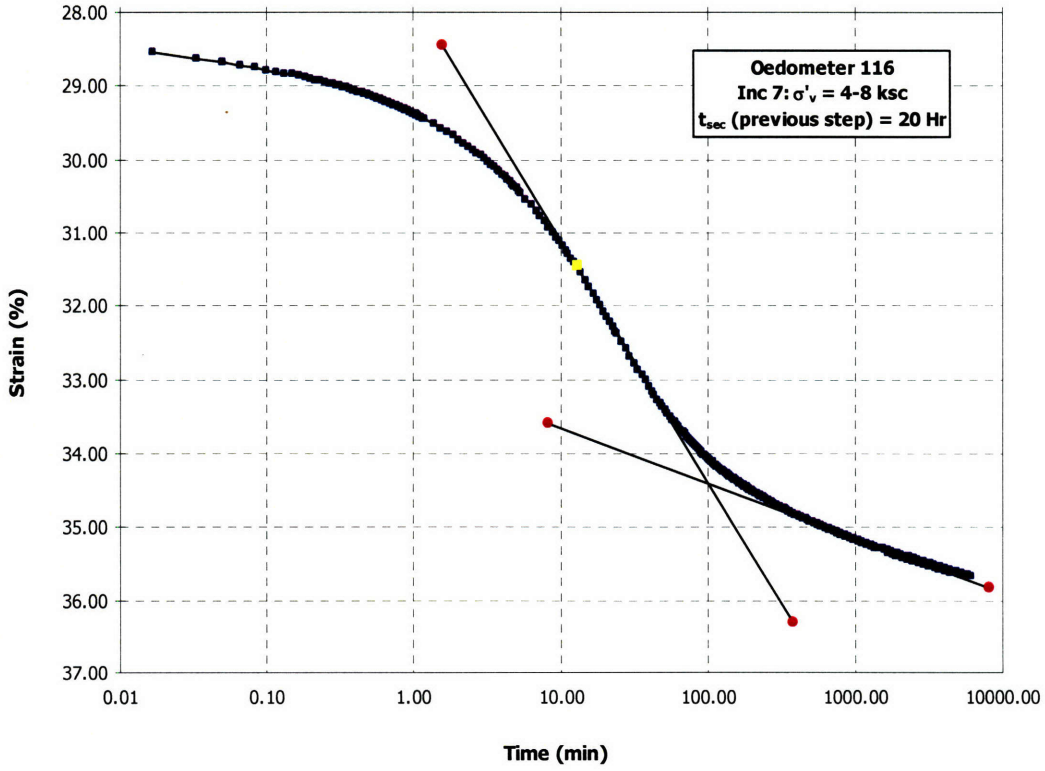

Figure A.101 Consolidation curve in Log time space for Oed116 Load Increment 7

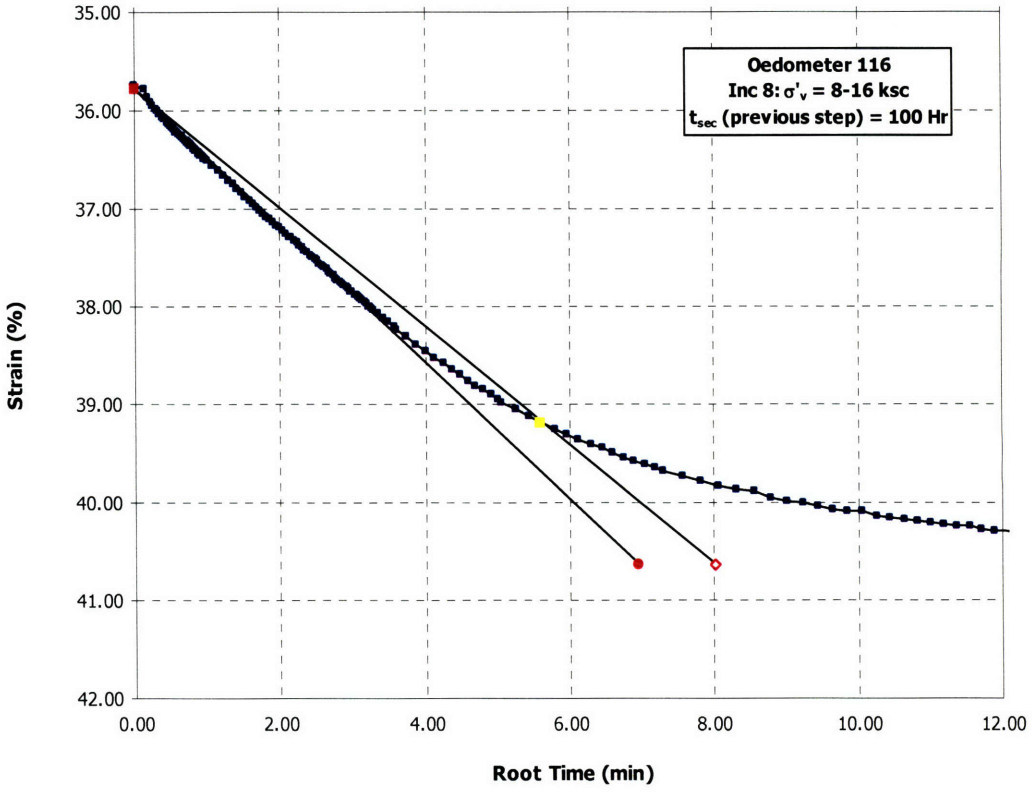

Figure A.102 Consolidation curve in $\sqrt{t}$ space for Oed116 Load Increment 8

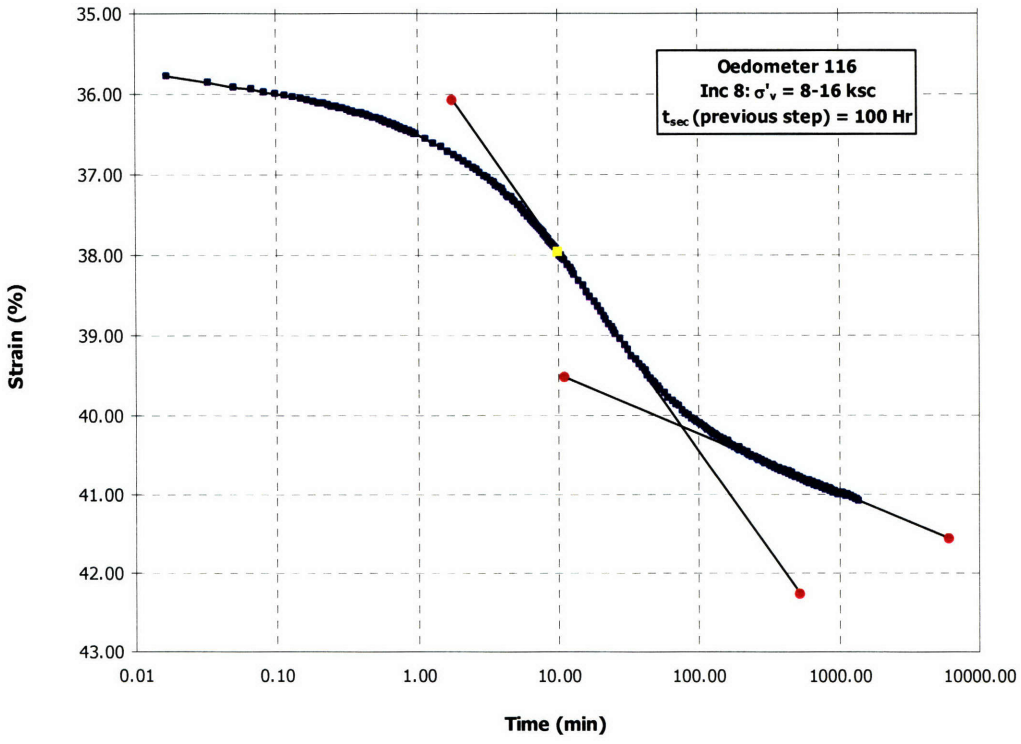

Figure A.103 Consolidation curve in Log time space for Oed116 Load Increment 8

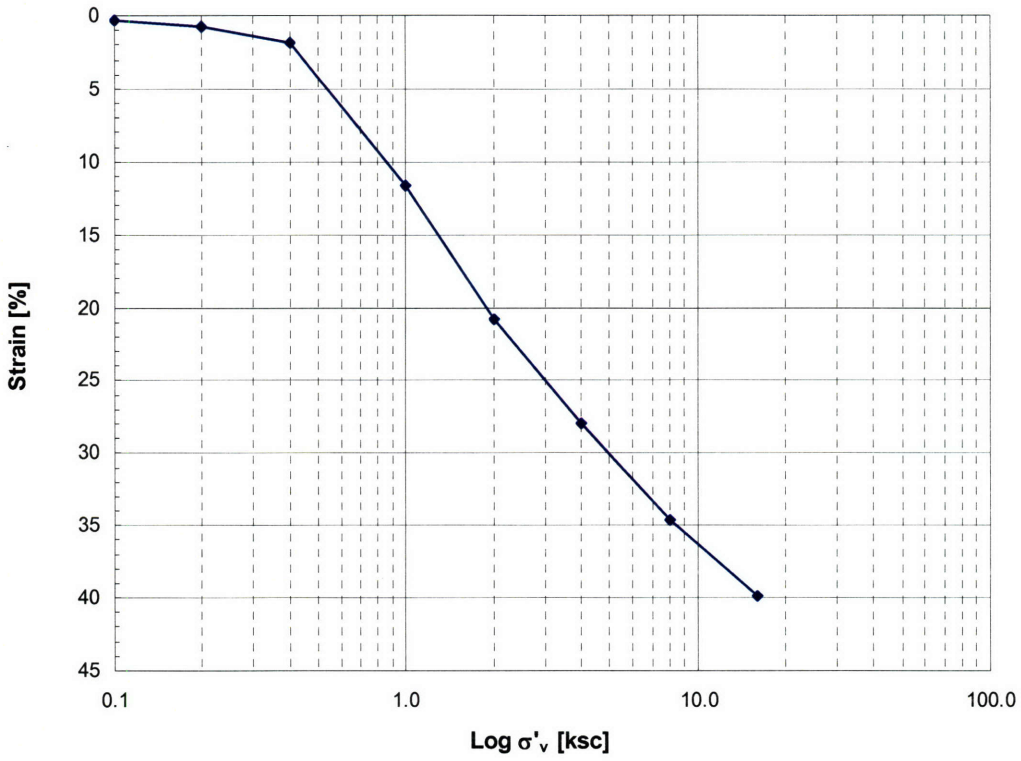

Figure A.104 Compression curve for Oed117

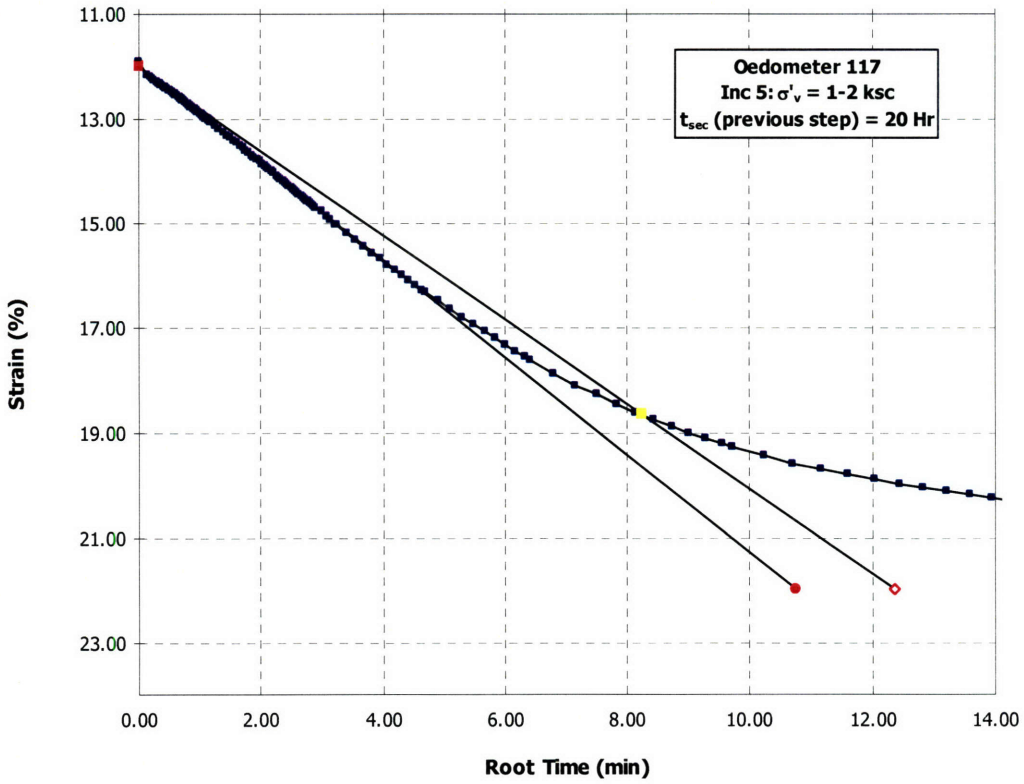

Figure A.105 Consolidation curve in $\sqrt{t}$ space for Oed117 Load Increment 5

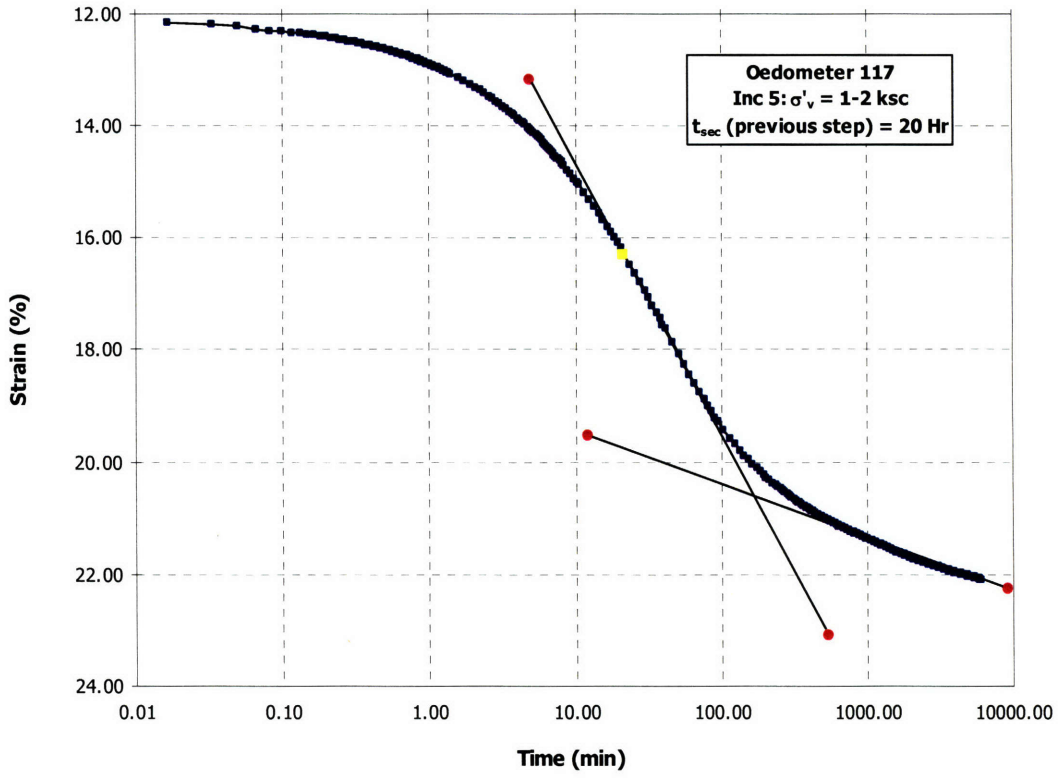

Figure A.106 Consolidation curve in Log time space for Oed117 Load Increment 5

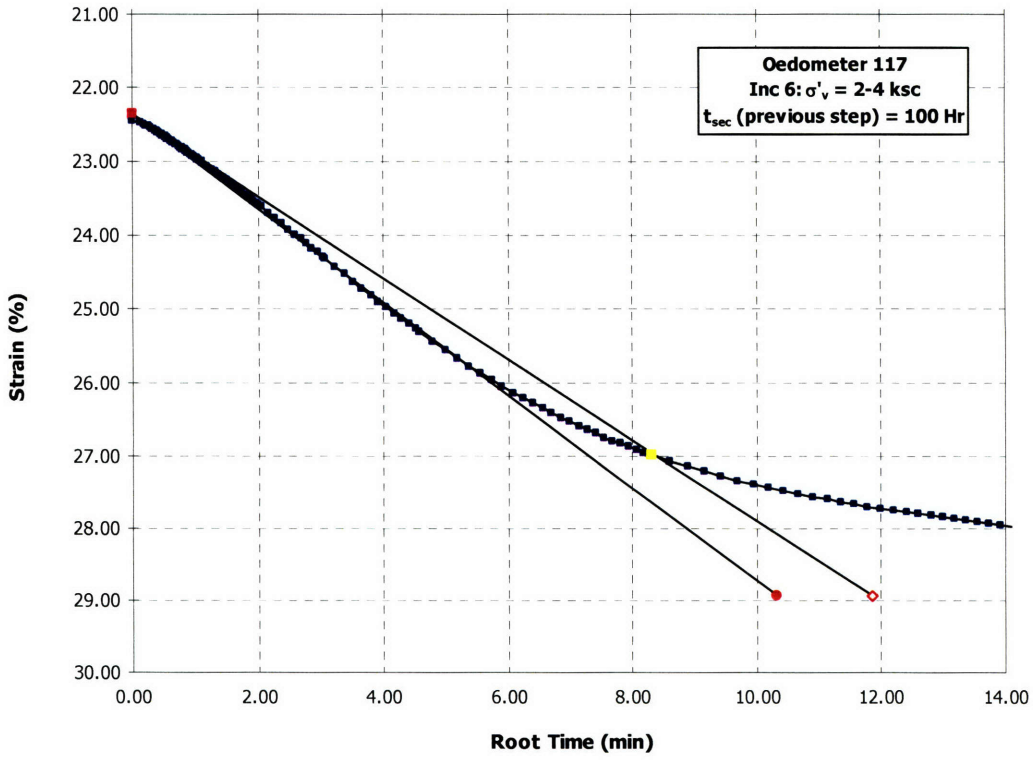

Figure A.107 Consolidation curve in $\sqrt{t}$ space for Oed117 Load Increment 6

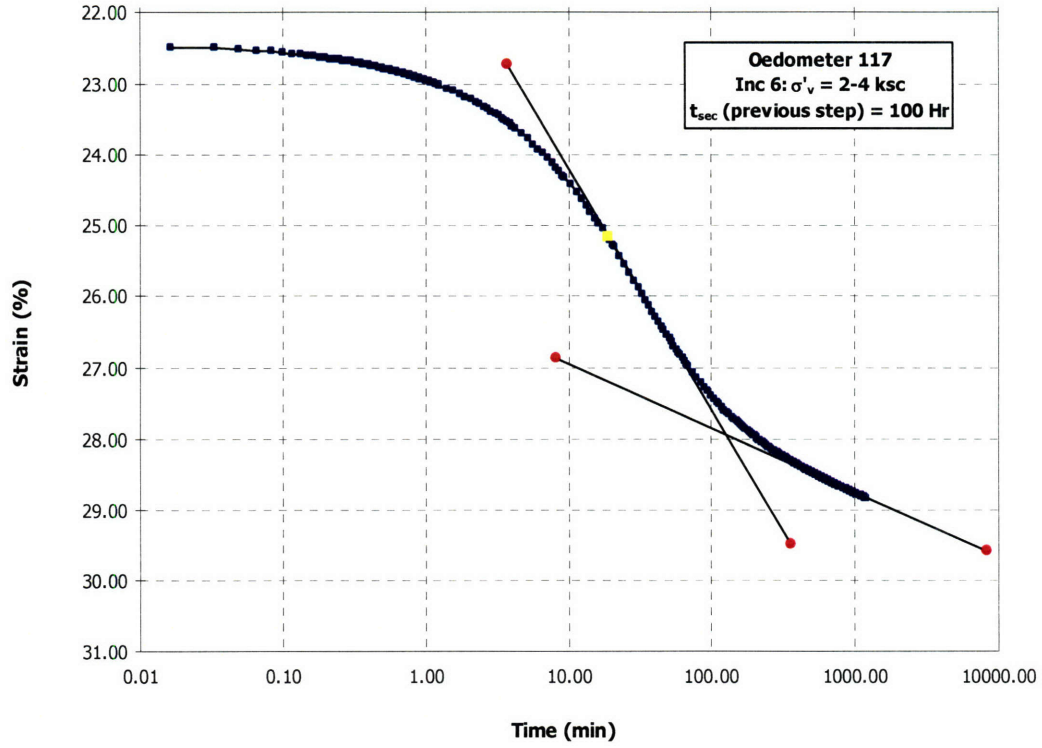

Figure A.108 Consolidation curve in Log time space for Oed117 Load Increment 6

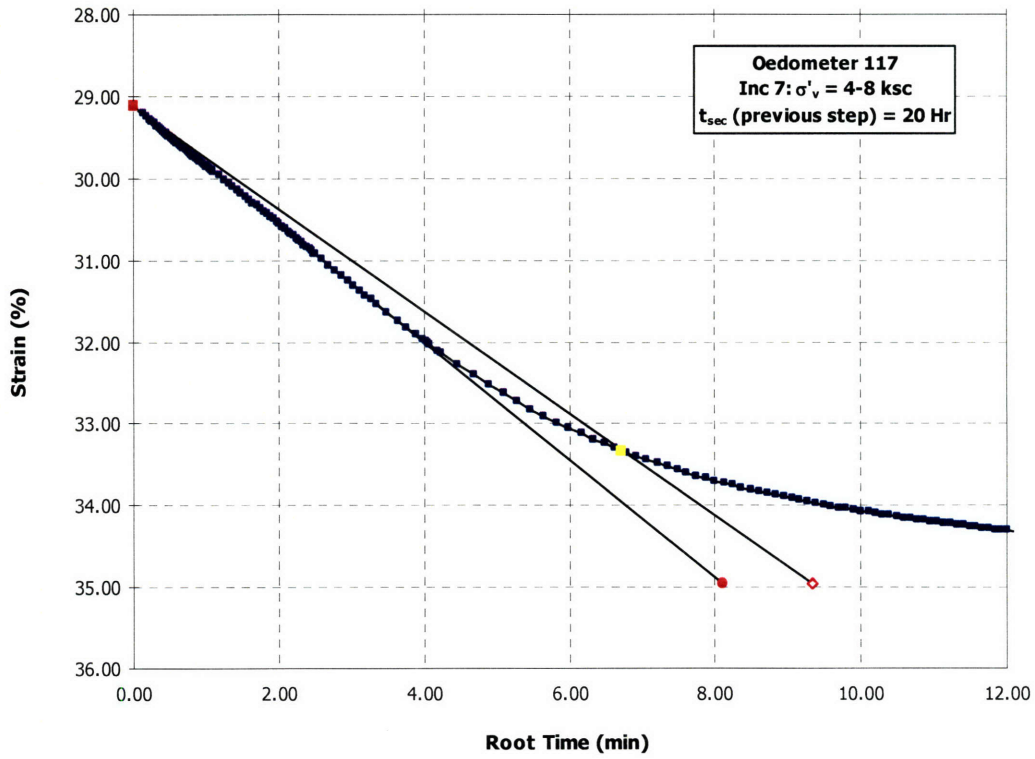

Figure A.109 Consolidation curve in $\sqrt{t}$ space for Oed117 Load Increment 7

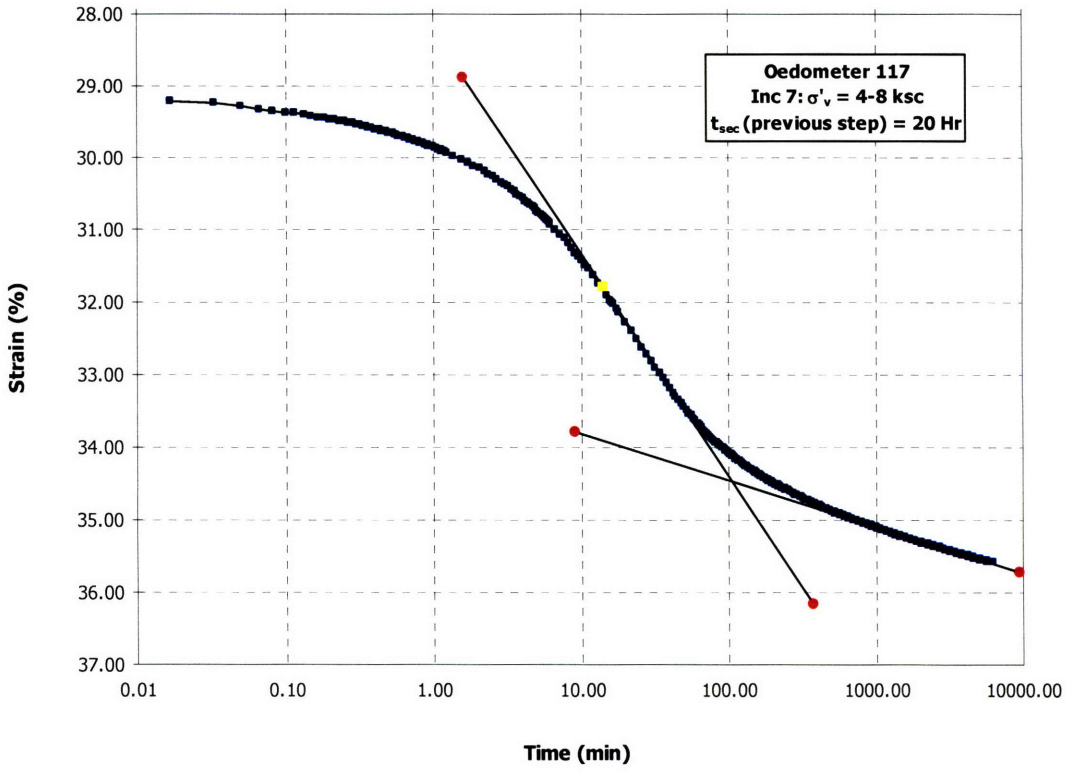

Figure A.110 Consolidation curve in Log time space for Oed117 Load Increment 7

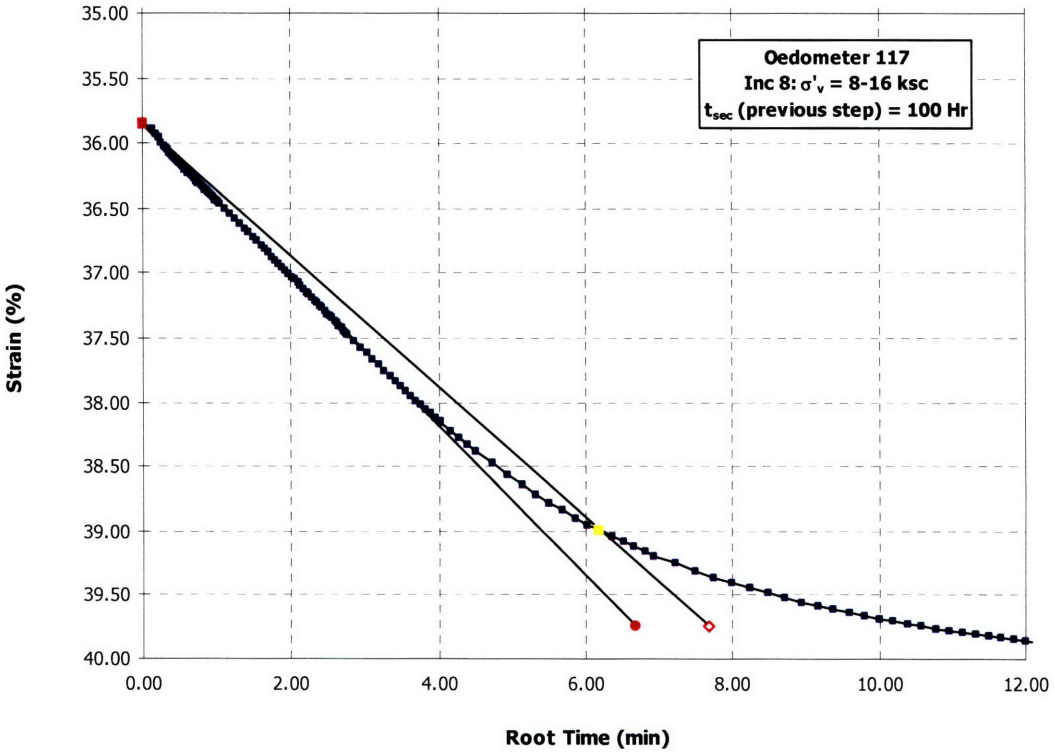

Figure A.111 Consolidation curve in $\sqrt{t}$ space for Oed117 Load Increment 8

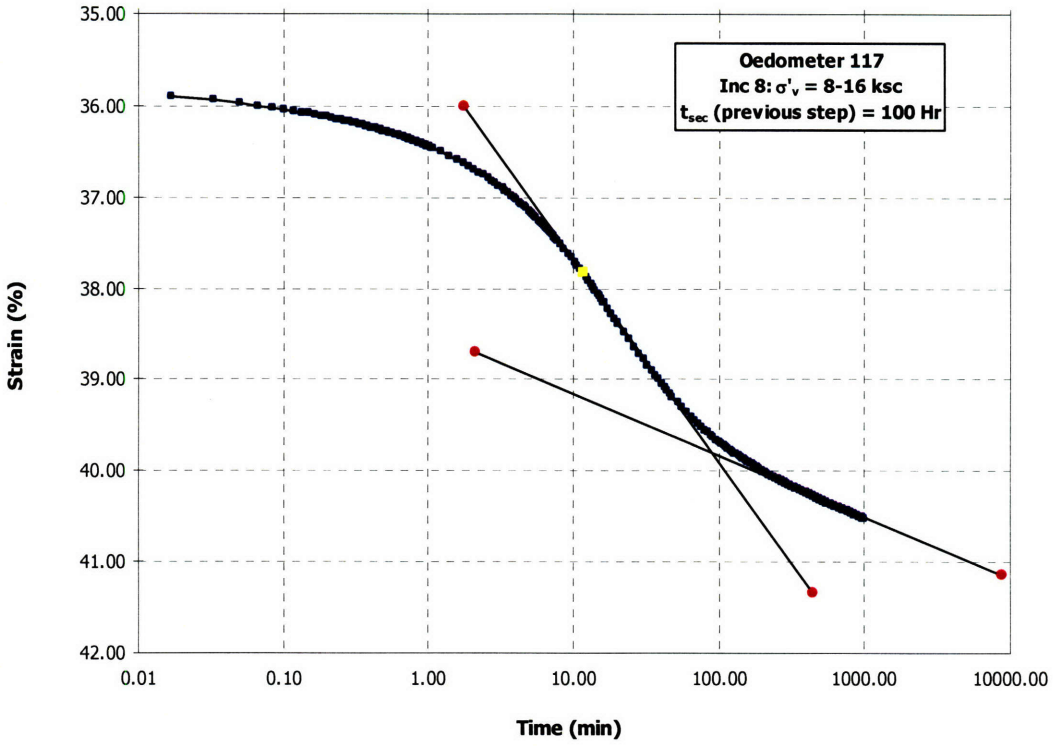

Figure A.112 Consolidation curve in Log time space for Oed117 Load Increment 8

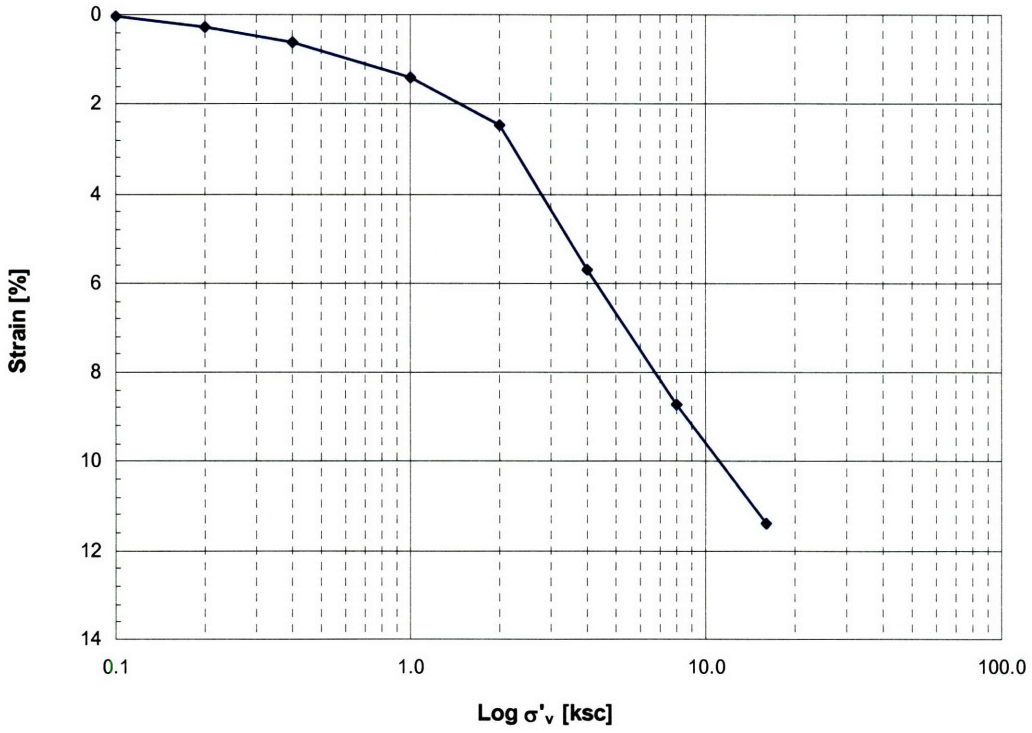

Figure A.113 Compression Curve for Oed118

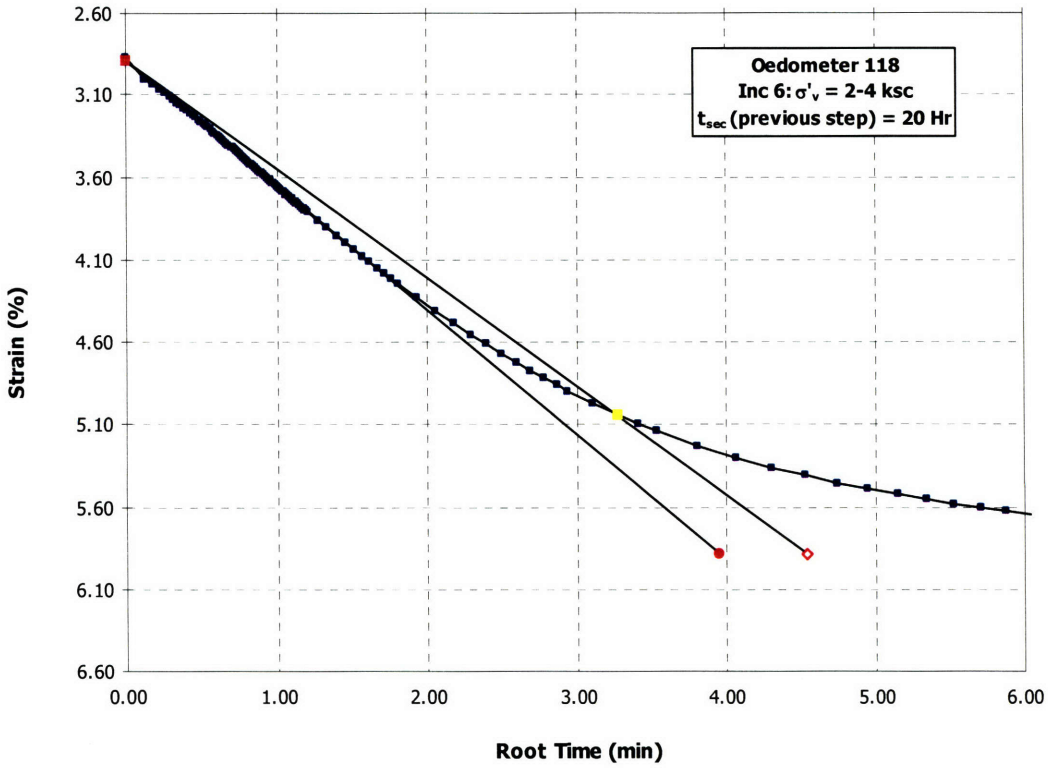

Figure A.114 Consolidation curve in $\sqrt{t}$ space for Oed118 Load Increment 6

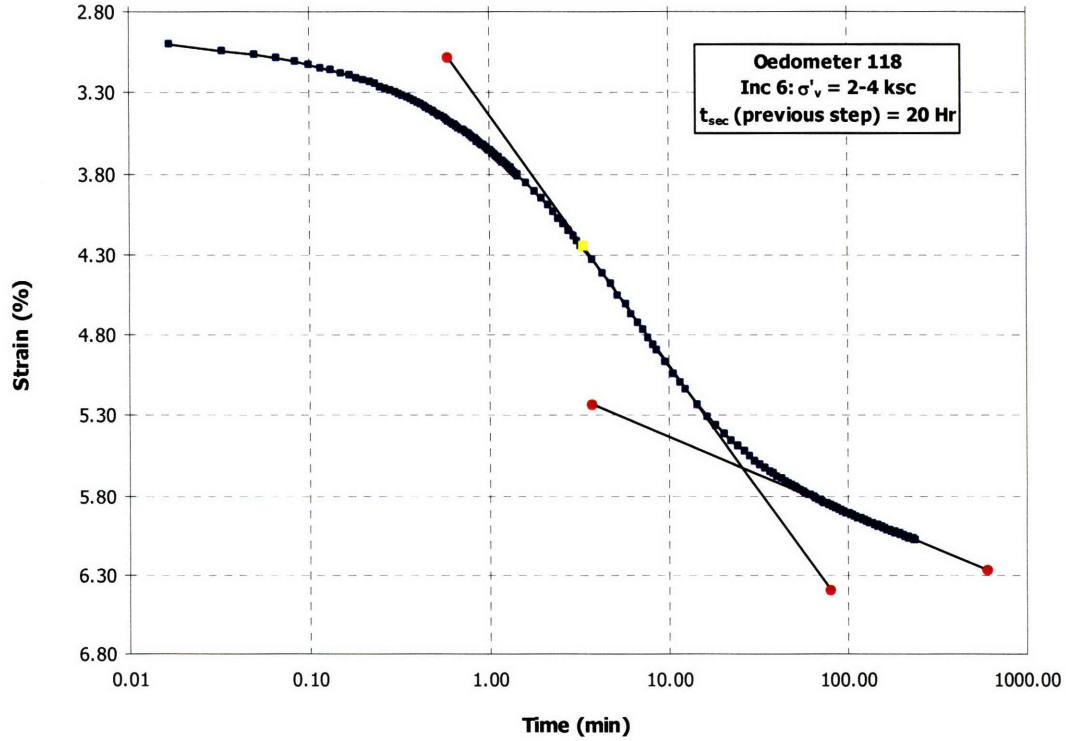

Figure A.115 Consolidation curve in Log time space for Oed118 Load Increment 6

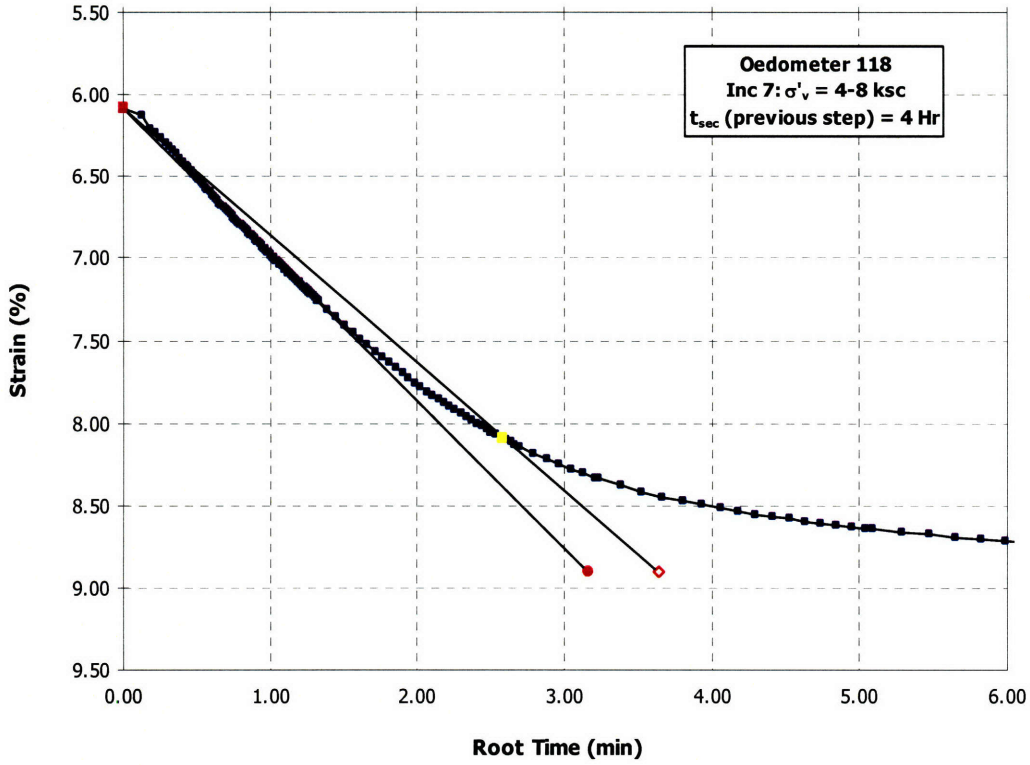

Figure A.116 Consolidation curve in $\sqrt{t}$ space for Oed118 Load Increment 7

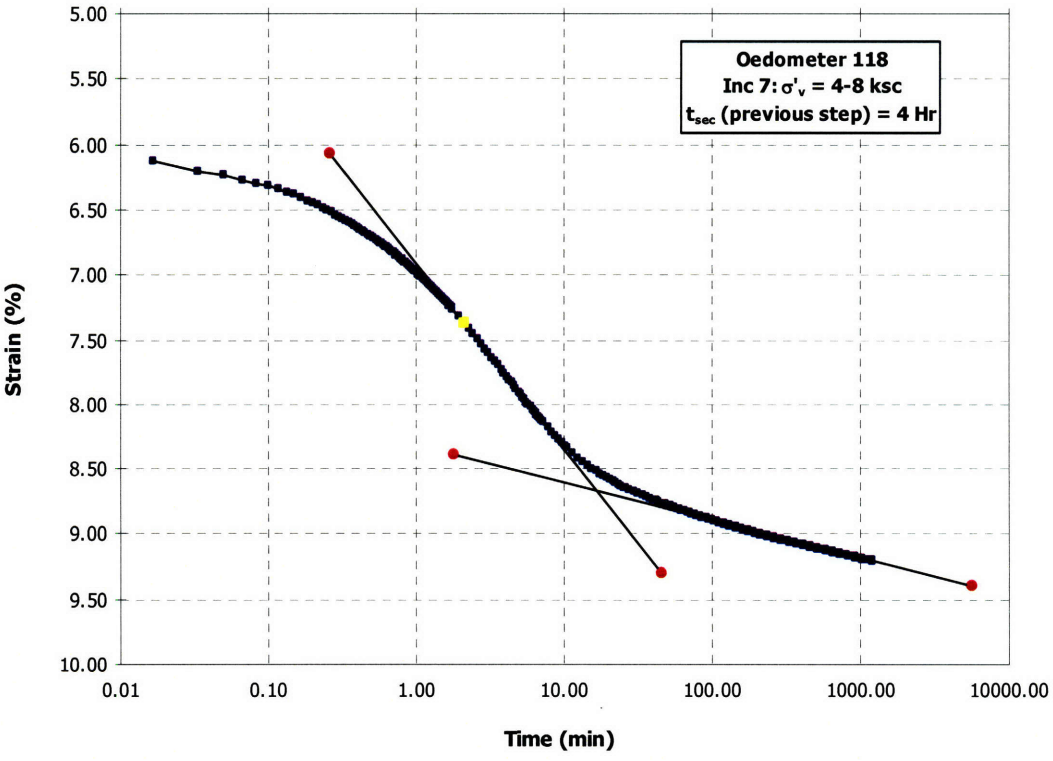

Figure A.117 Consolidation curve in Log time space for Oed118 Load Increment 7

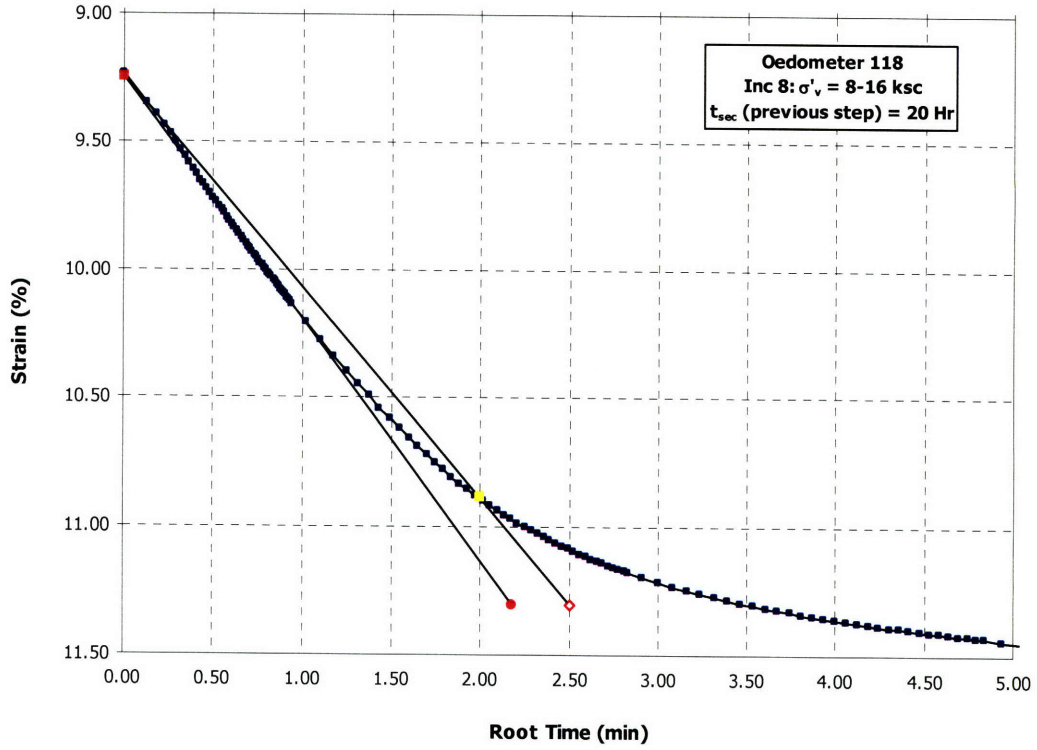

Figure A.118 Consolidation curve in $\sqrt{t}$ space for Oed118 Load Increment 8

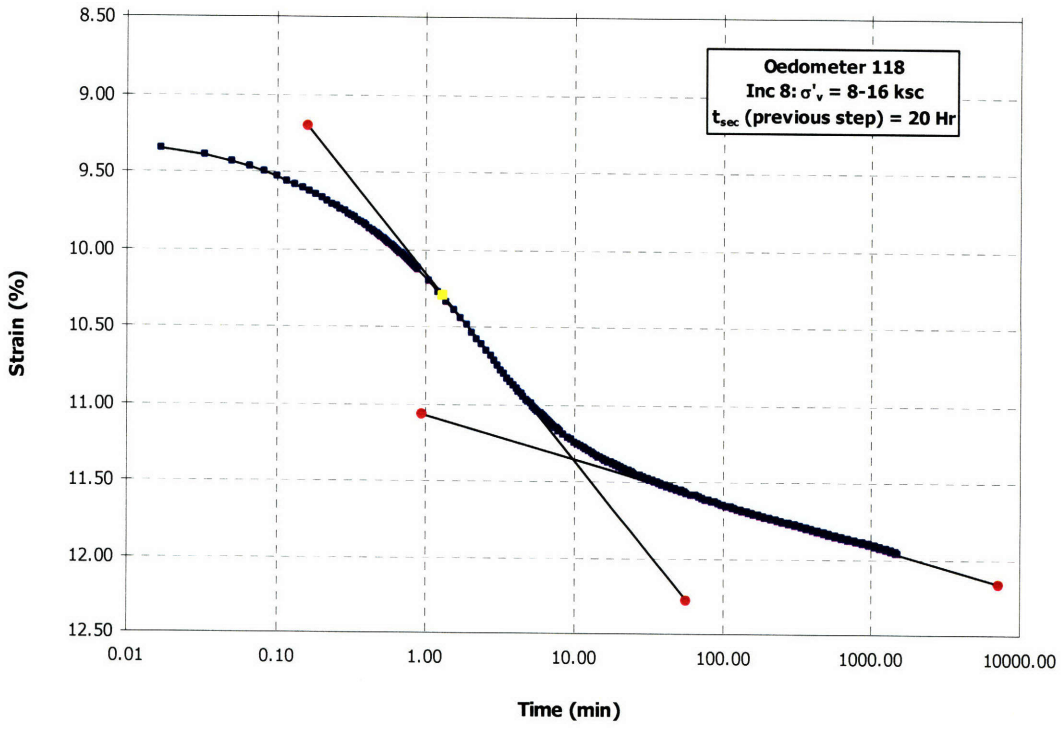

Figure A.119 Consolidation curve in Log time space for Oed118 Load Increment 8

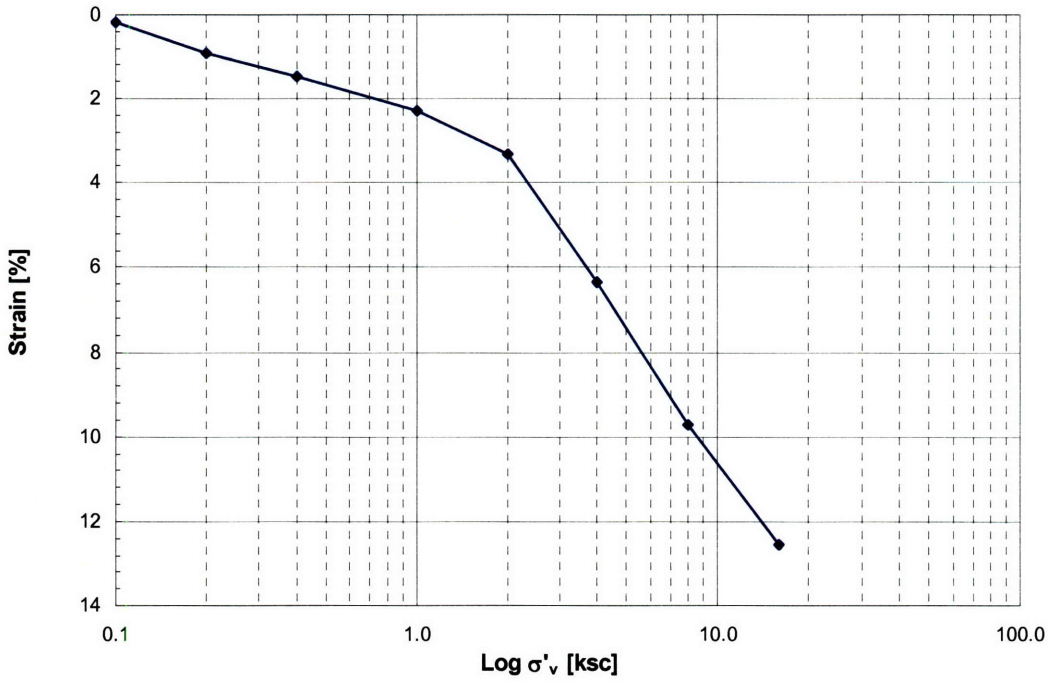

Figure A.120 Compression Curve for Oed119

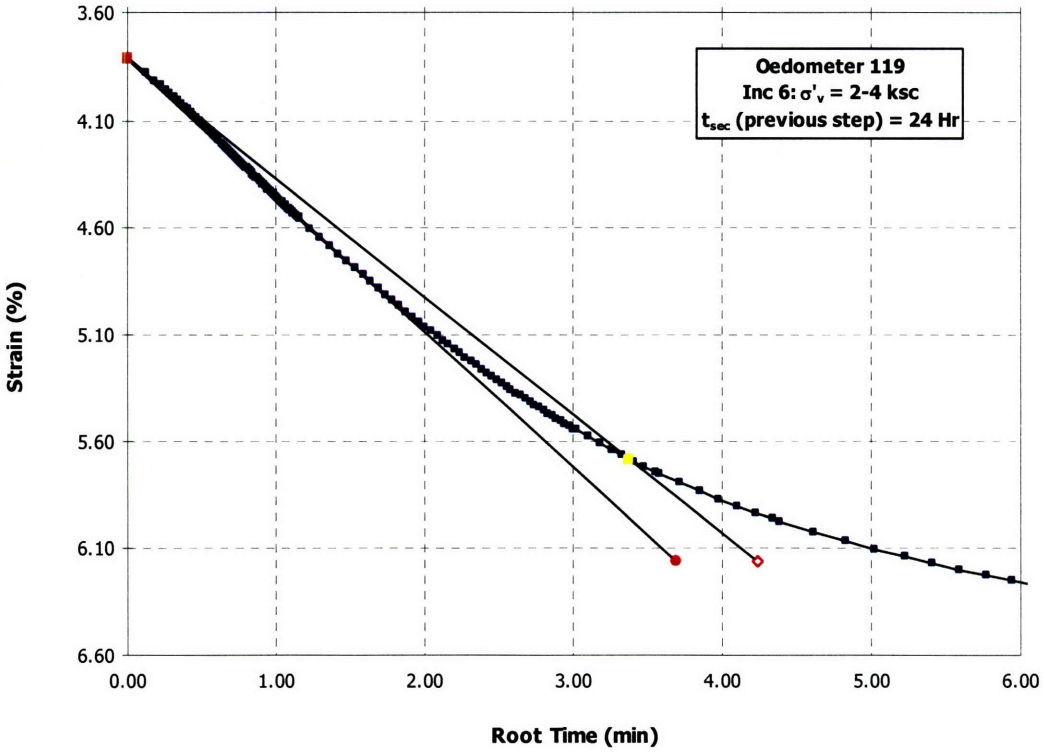

Figure A.121 Consolidation curve in $\sqrt{t}$ space for Oed119 Load Increment 6

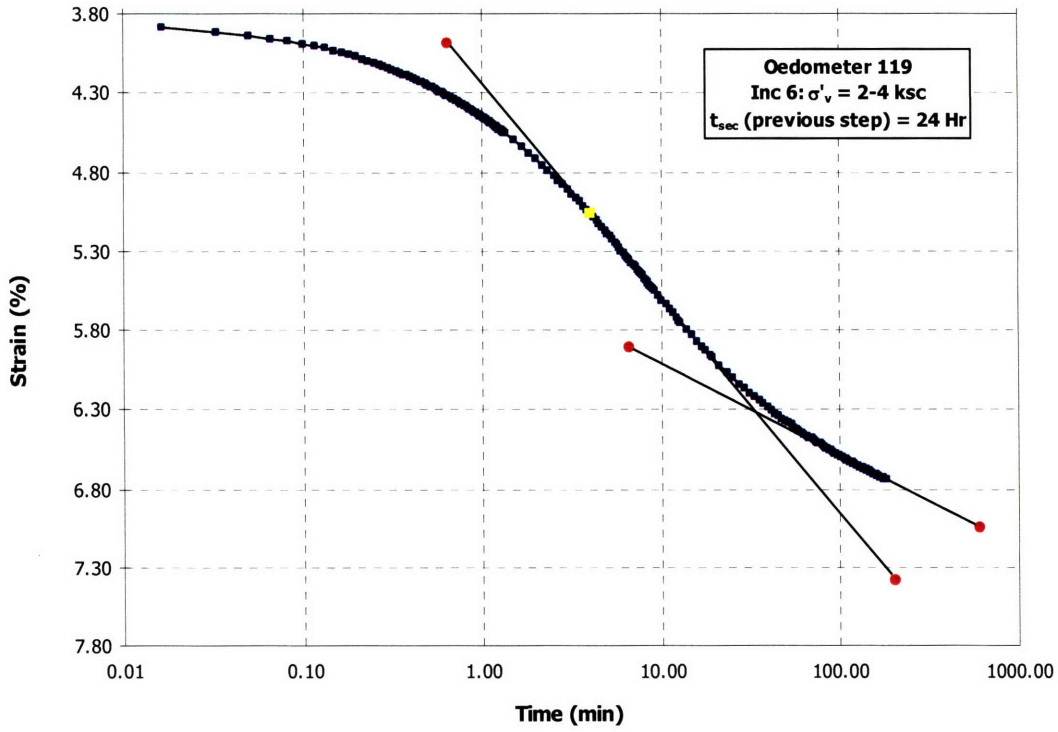

Figure A.122 Consolidation curve in Log time space for Oed119 Load Increment 6

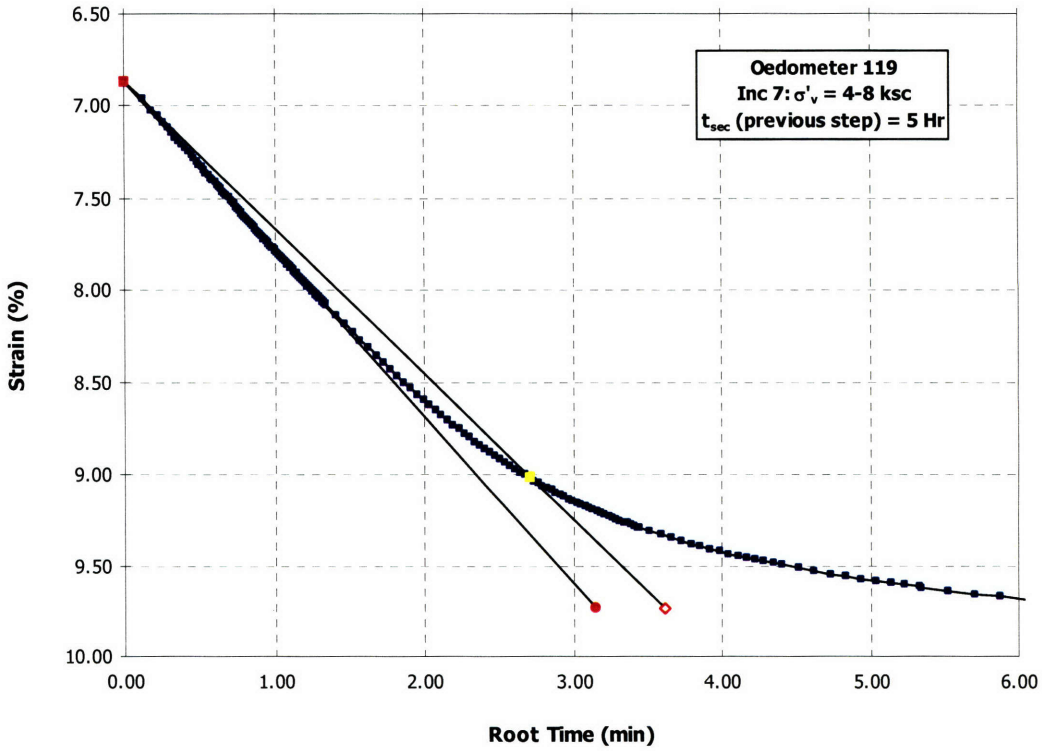

Figure A.123 Consolidation curve in $\sqrt{t}$ space for Oed119 Load Increment 7

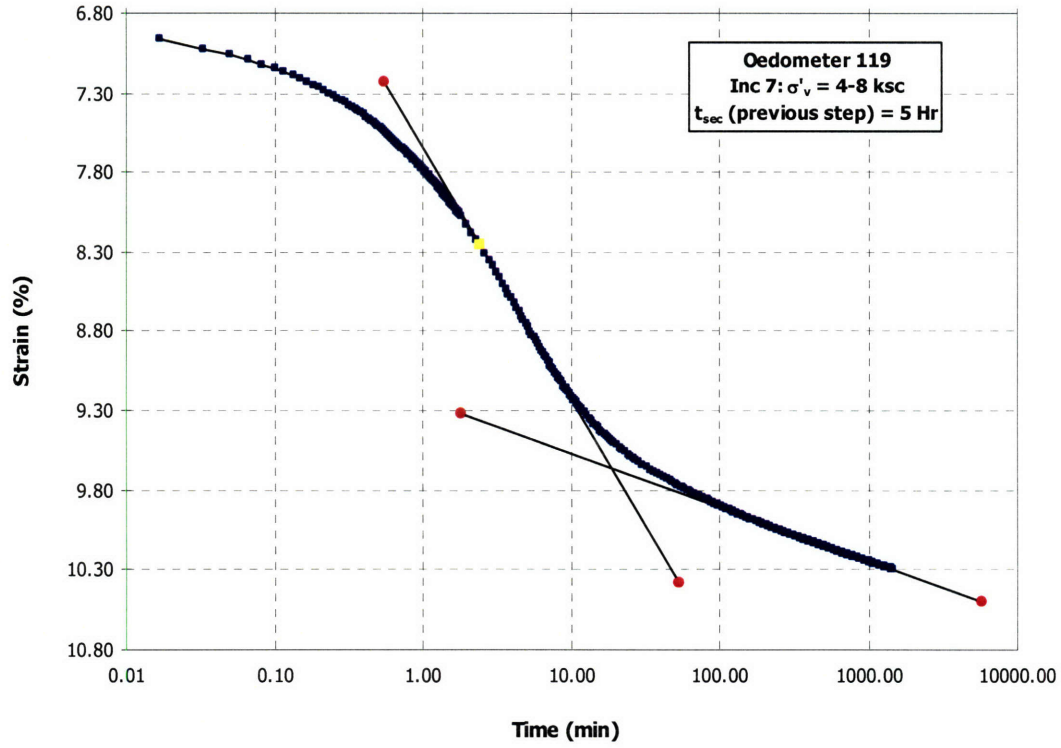

Figure A.124 Consolidation curve in Log time space for Oed119 Load Increment 7

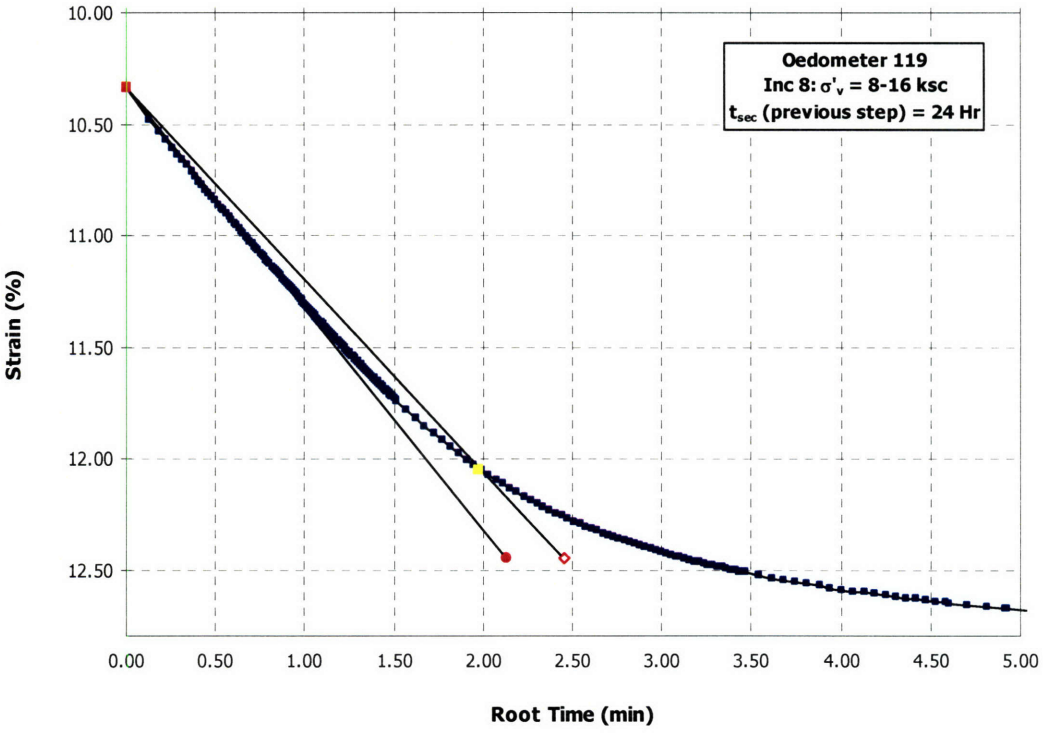

Figure A.125 Consolidation curve in $\sqrt{t}$ space for Oed119 Load Increment 8

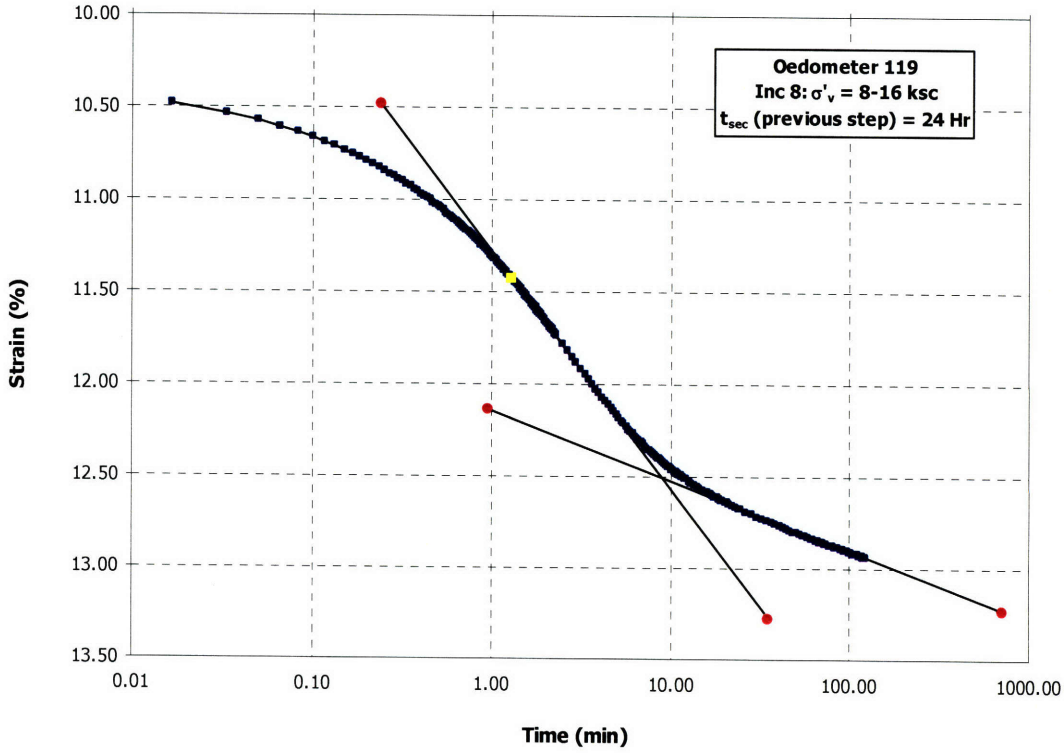

Figure A.126 Consolidation curve in Log time space for Oed119 Load Increment 8

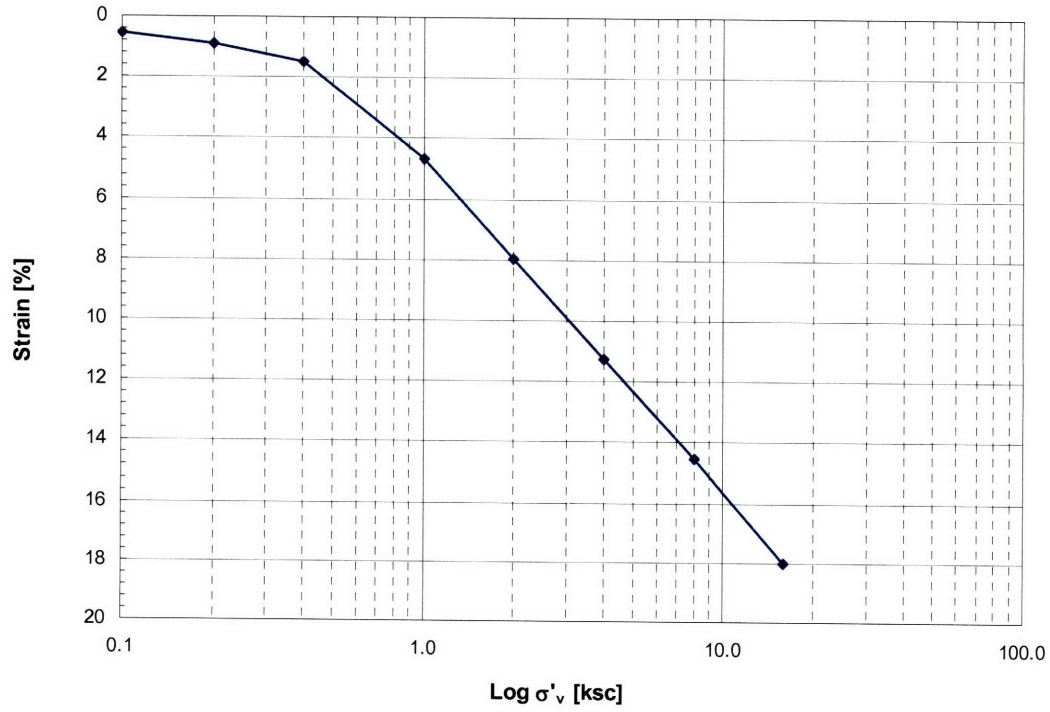

Figure A.127 Compression Curve for Oed120

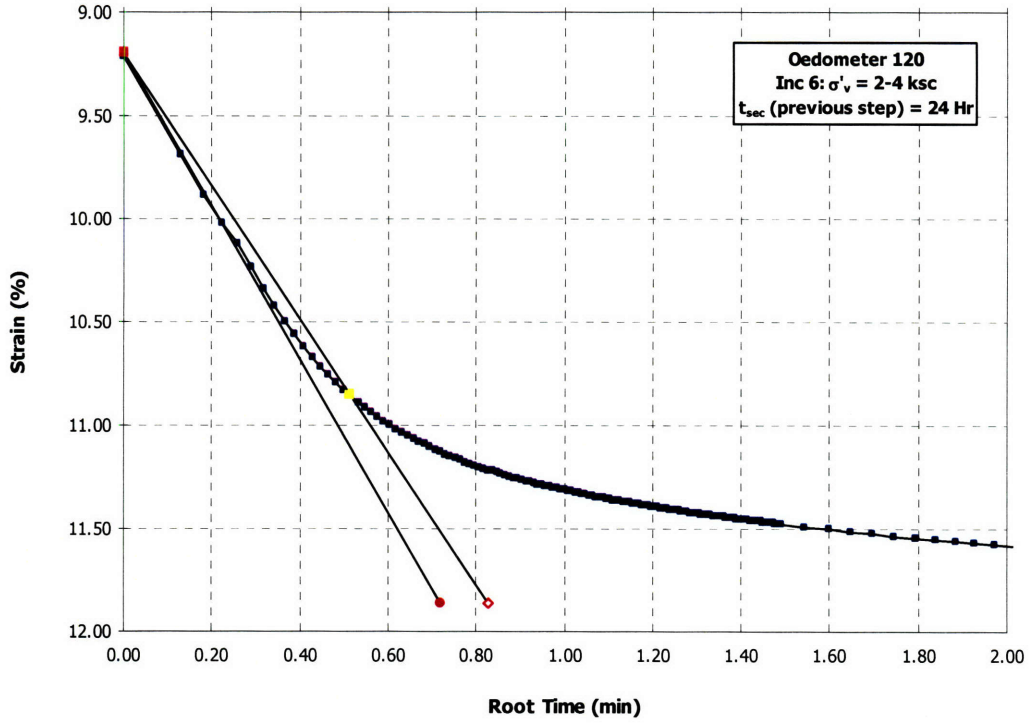

Figure A.128 Consolidation curve in $\sqrt{t}$ space for Oed120 Load Increment 6

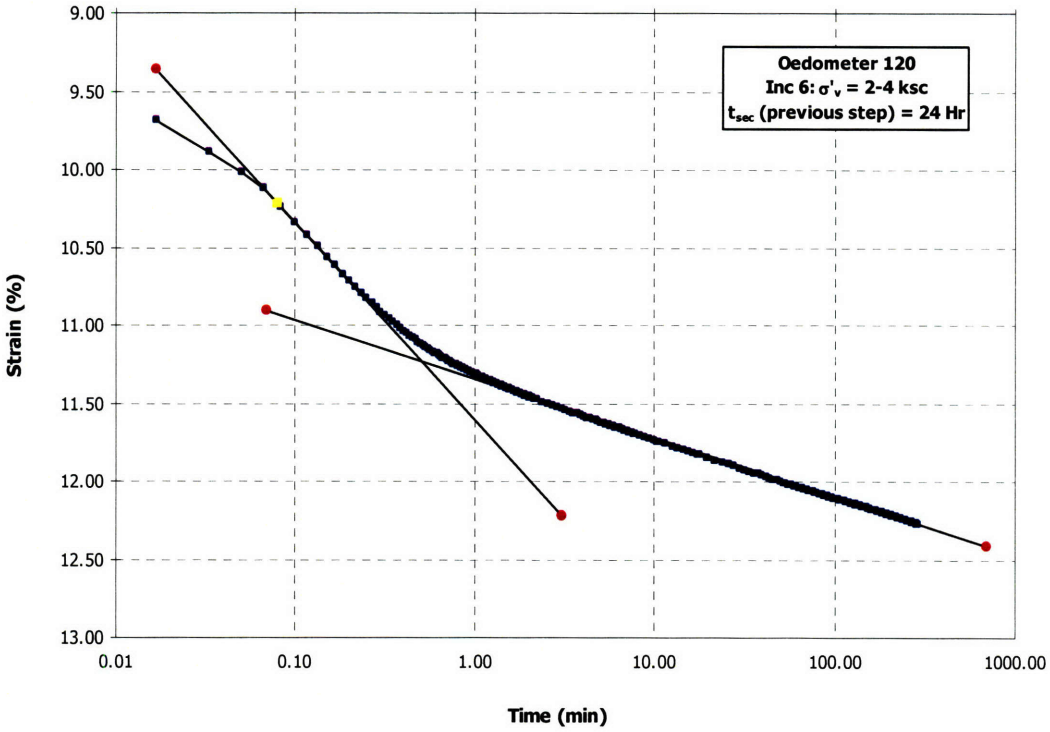

Figure A.129 Consolidation curve in Log time space for Oed120 Load Increment 6

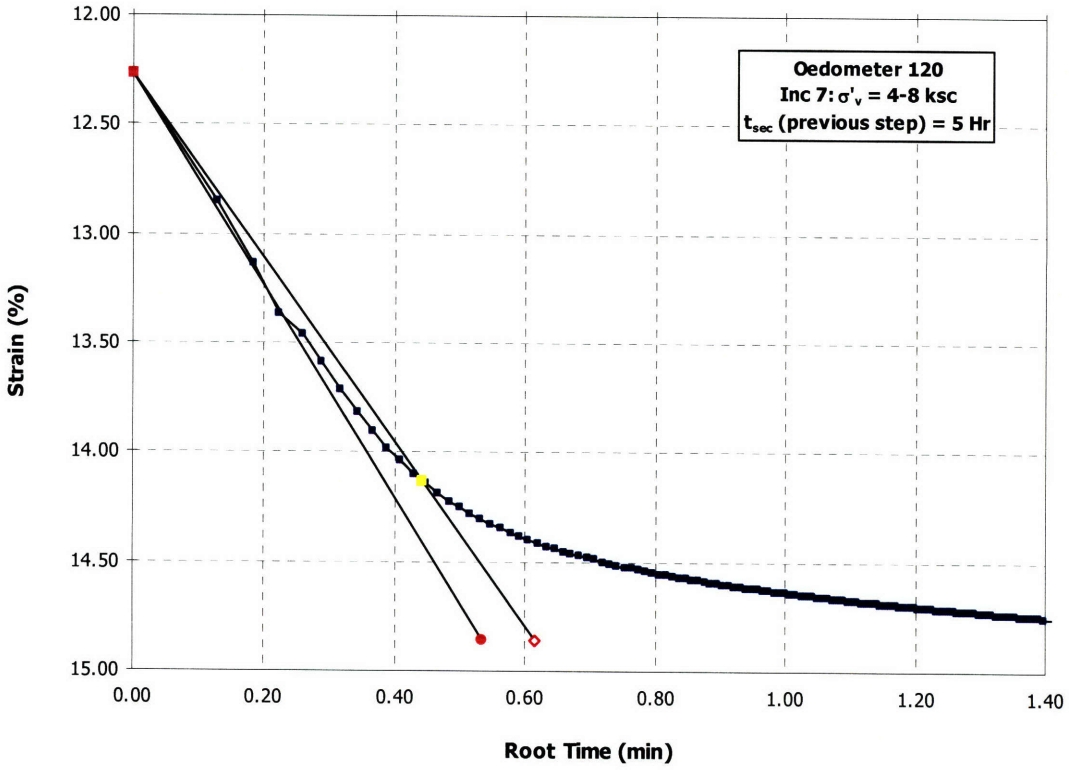

Figure A.130 Consolidation curve in $\sqrt{t}$ space for Oed120 Load Increment 7

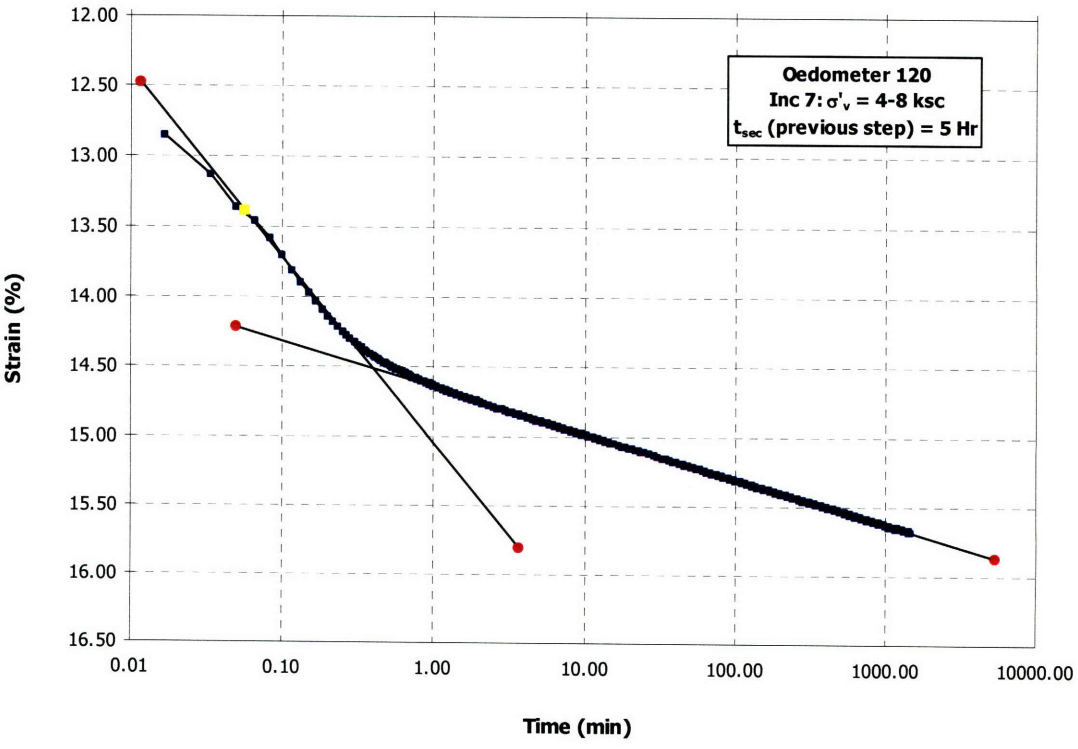

Figure A.131 Consolidation curve in Log time space for Oed120 Load Increment 7

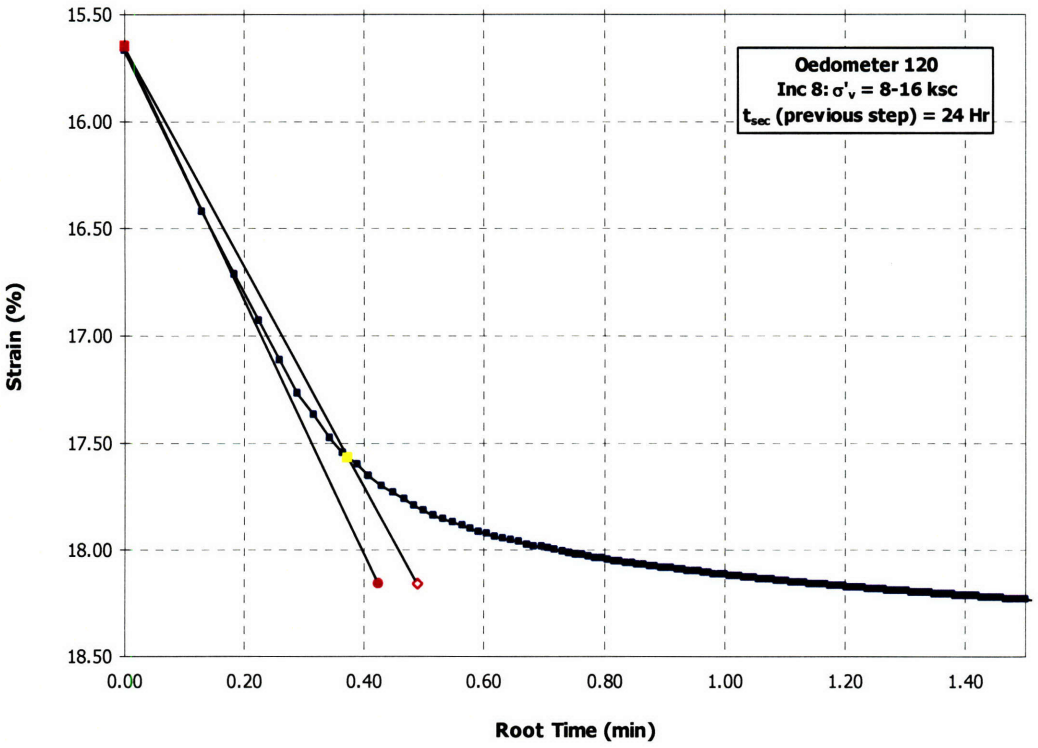

Figure A.132 Consolidation curve in $\sqrt{t}$ space for Oed120 Load Increment 8

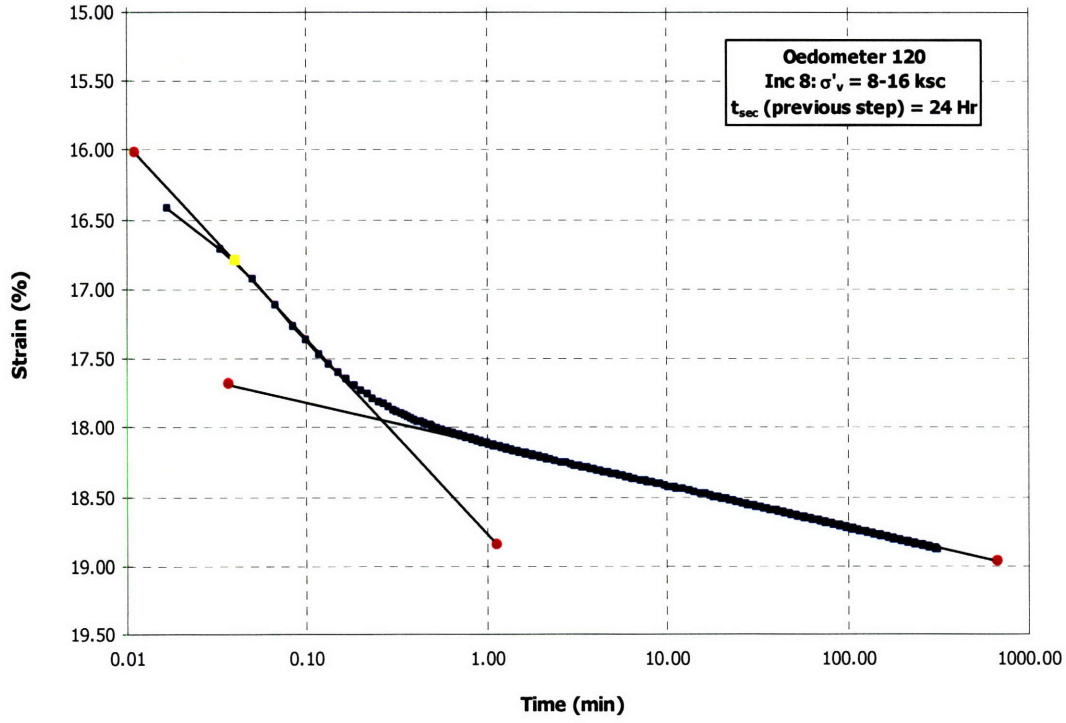

Figure A.133 Consolidation curve in Log time space for Oed120 Load Increment 8

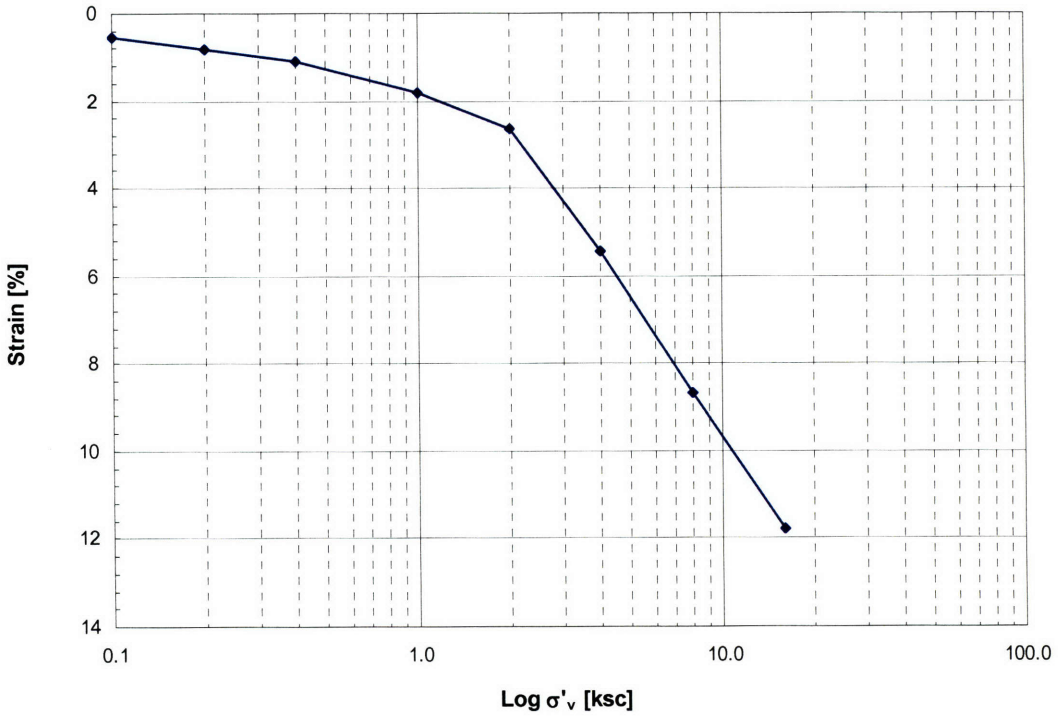

Figure A.134 Compression Curve for Oed121

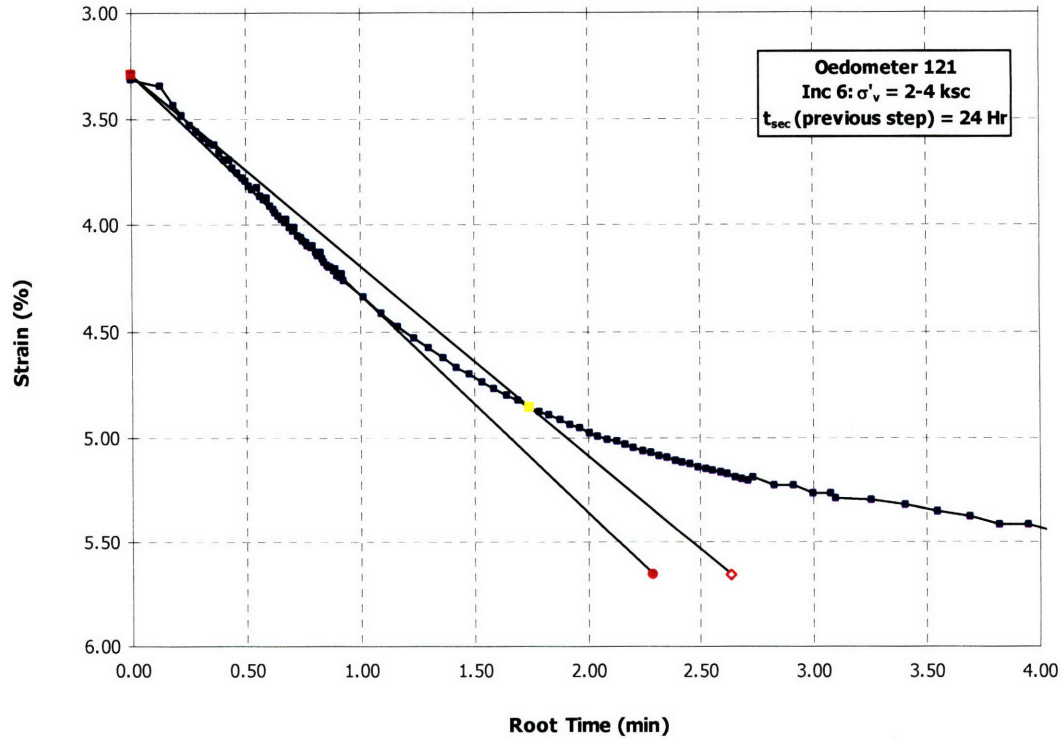

Figure A.135 Consolidation curve in $\sqrt{t}$ space for Oed121 Load Increment 6

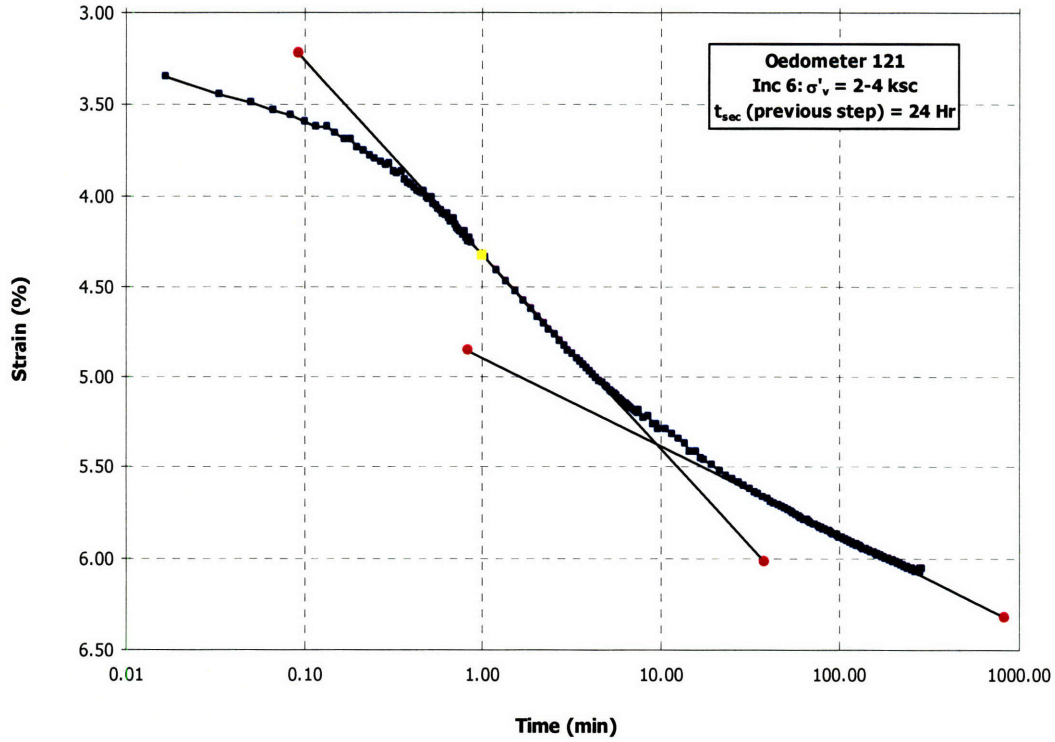

Figure A.136 Consolidation curve in Log time space for Oed121 Load Increment 6

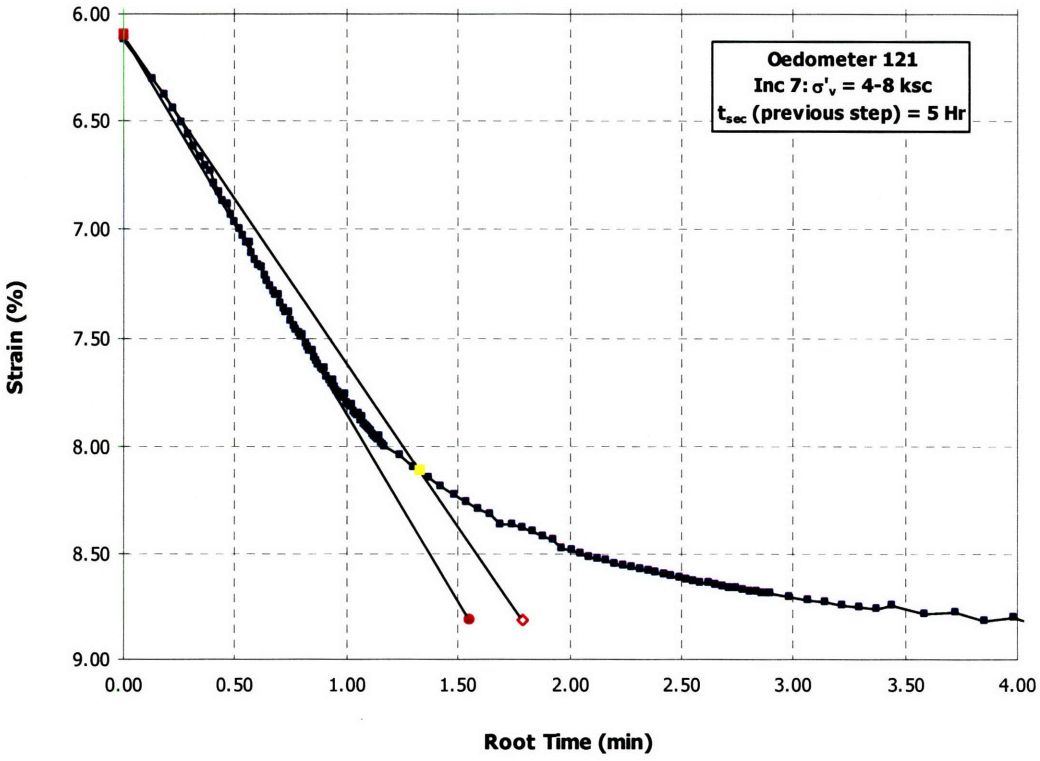

Figure A.137 Consolidation curve in $\sqrt{t}$ space for Oed121 Load Increment 7

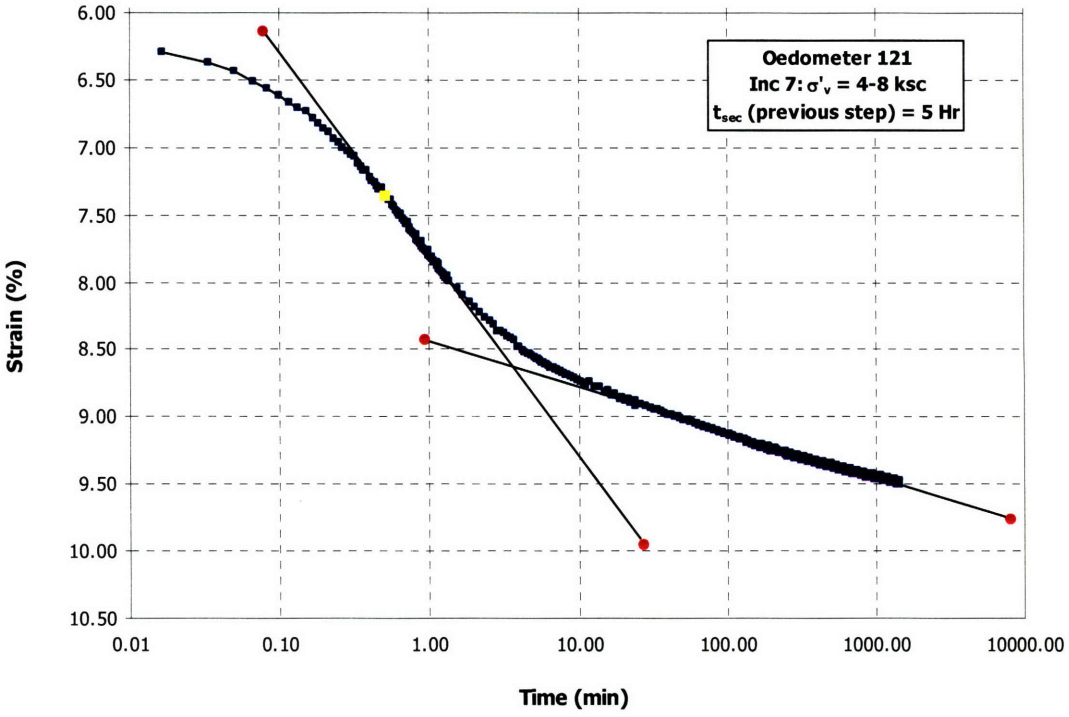

Figure A.138 Consolidation curve in Log time space for Oed121 Load Increment 7

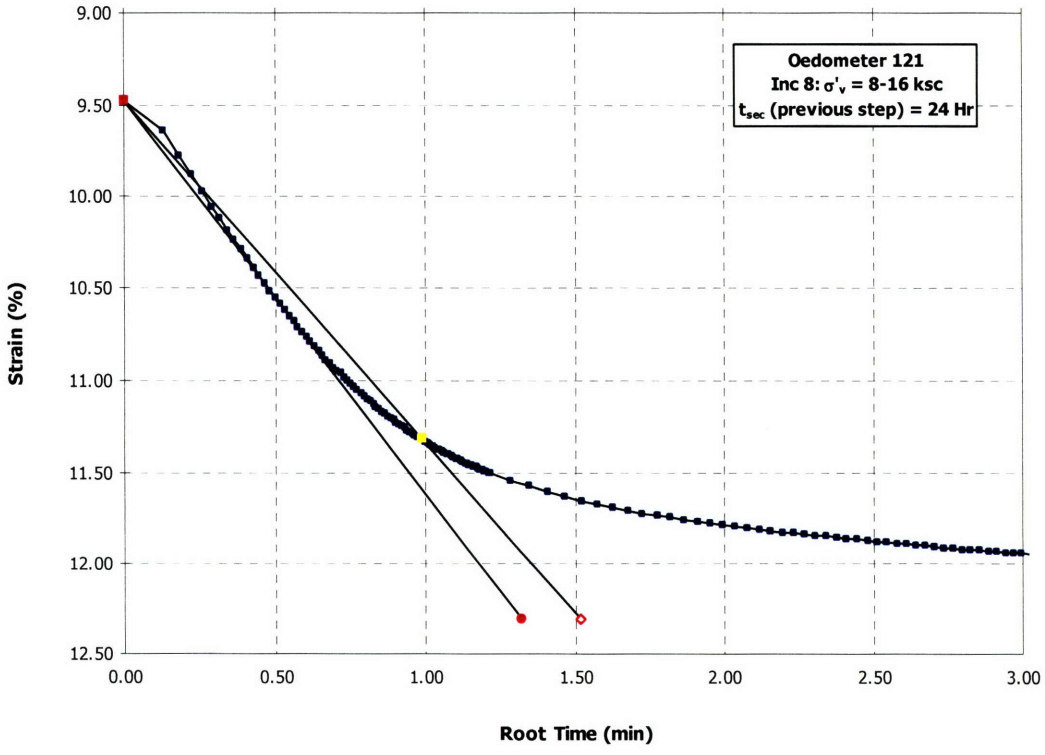

Figure A.139 Consolidation curve in $\sqrt{t}$ space for Oed121 Load Increment 8

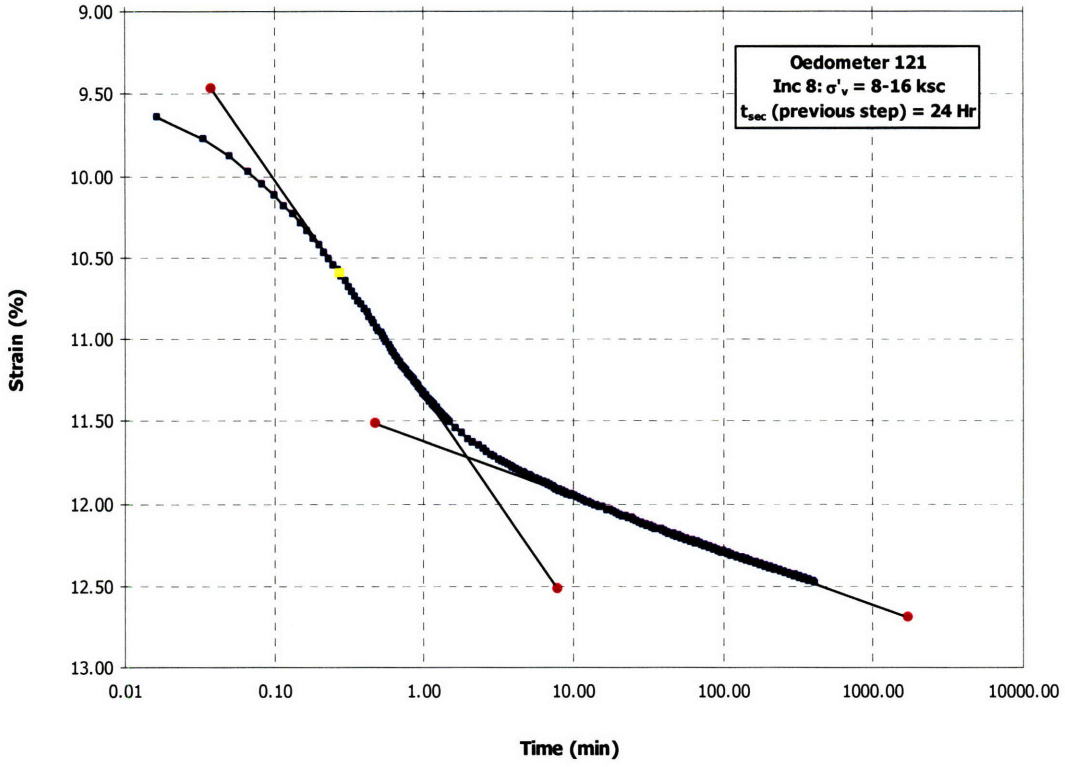

Figure A.140 Consolidation curve in Log time space for Oed121 Load Increment 8

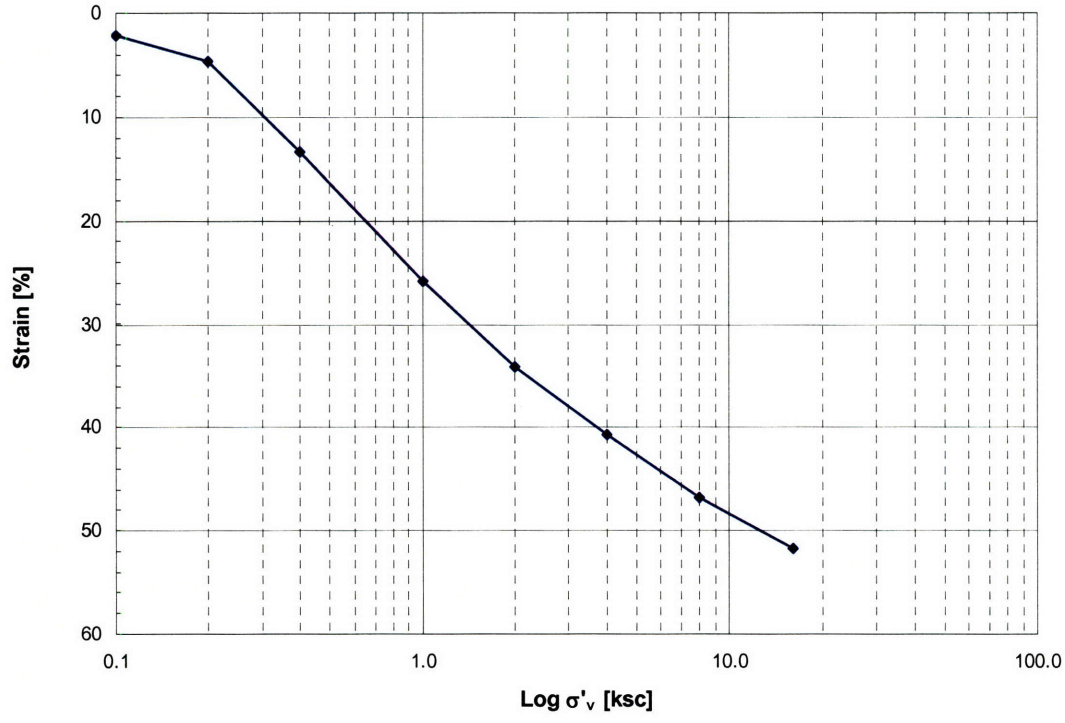

Figure A.141 Compression Curve for Oed122

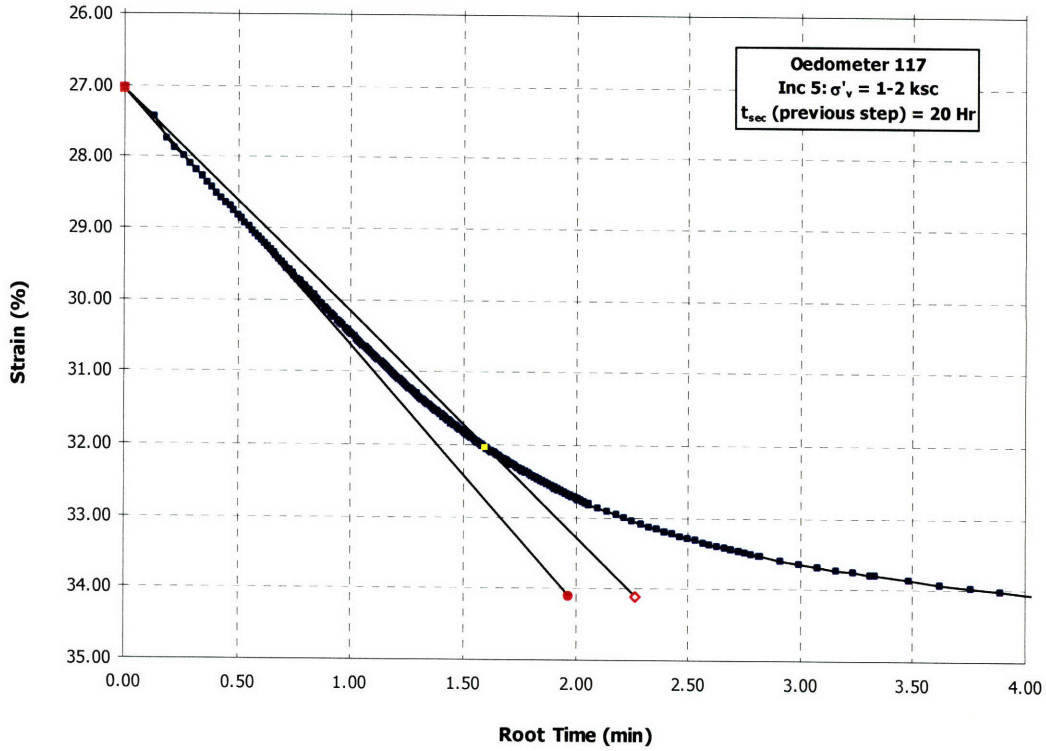

Figure A.142 Consolidation curve in $\sqrt{t}$ space for Oed122 Load Increment 5

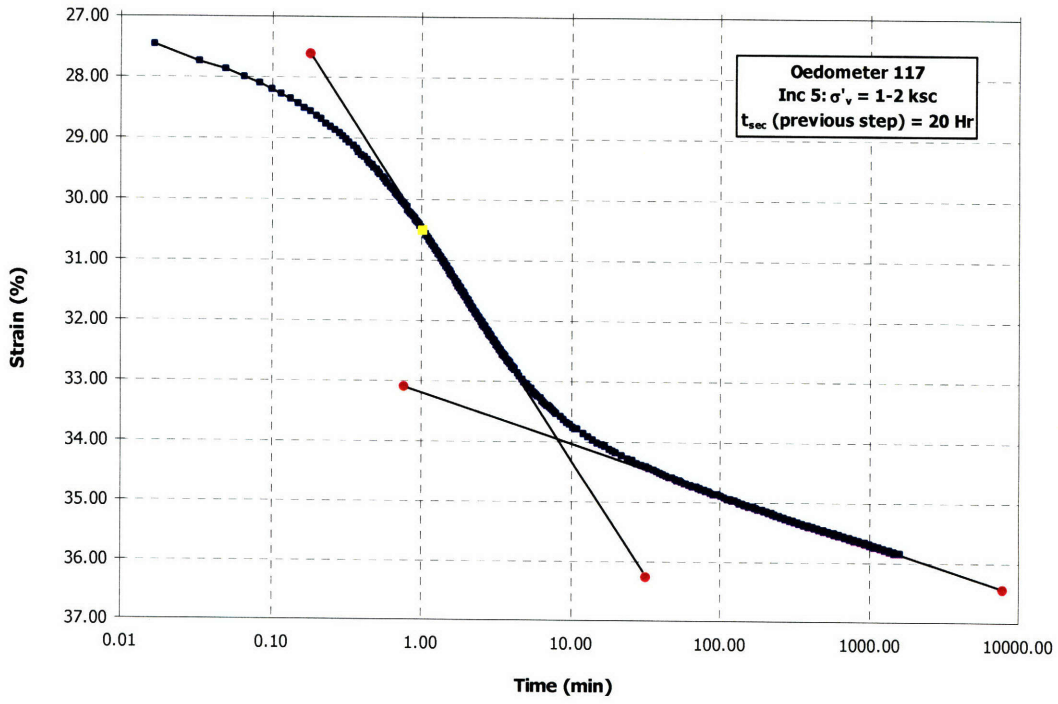

Figure A.143 Consolidation curve in Log time space for Oed122 Load Increment 5

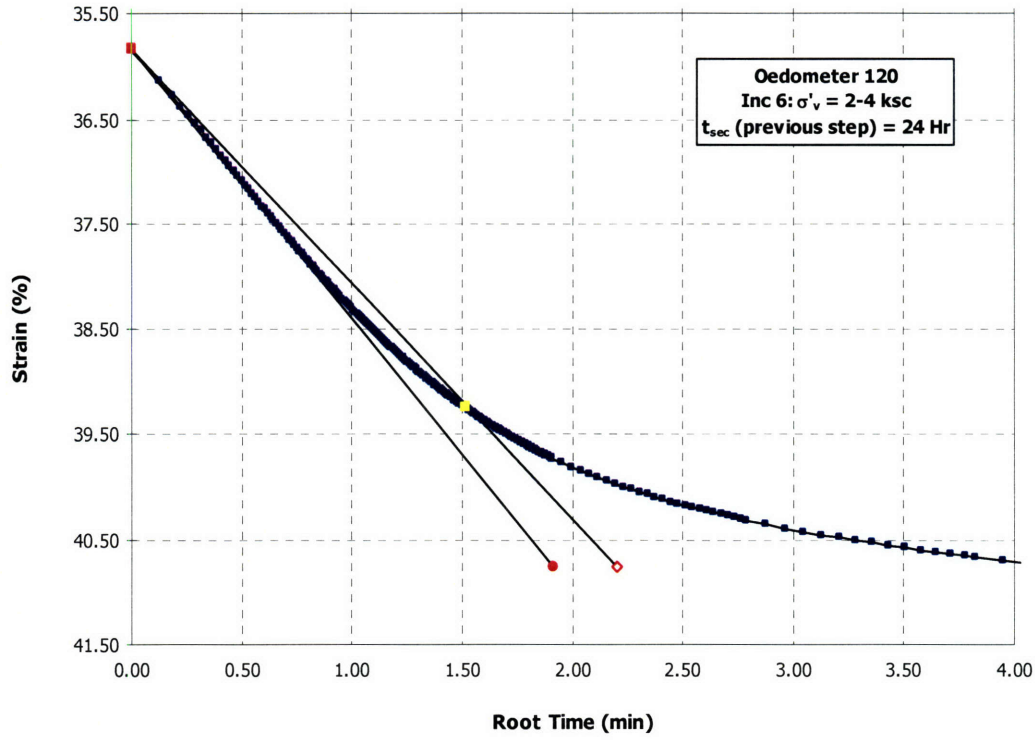

Figure A.144 Consolidation curve in $\sqrt{t}$ space for Oed122 Load Increment 6

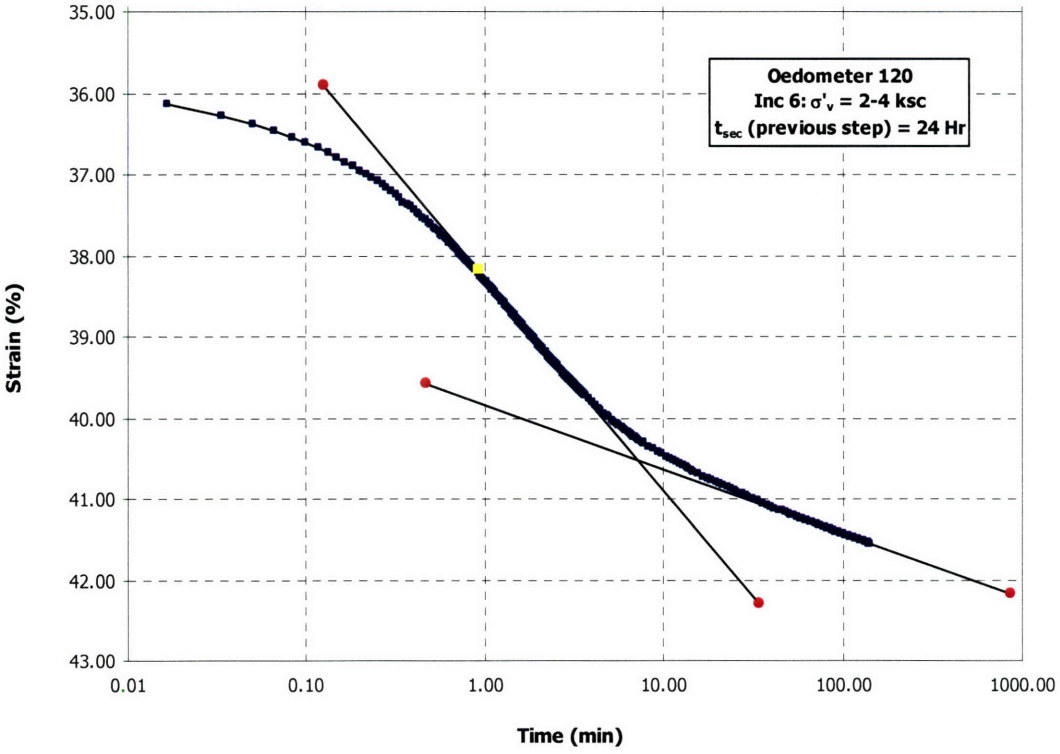

Figure A.145 Consolidation curve in Log time space for Oed122 Load Increment 6

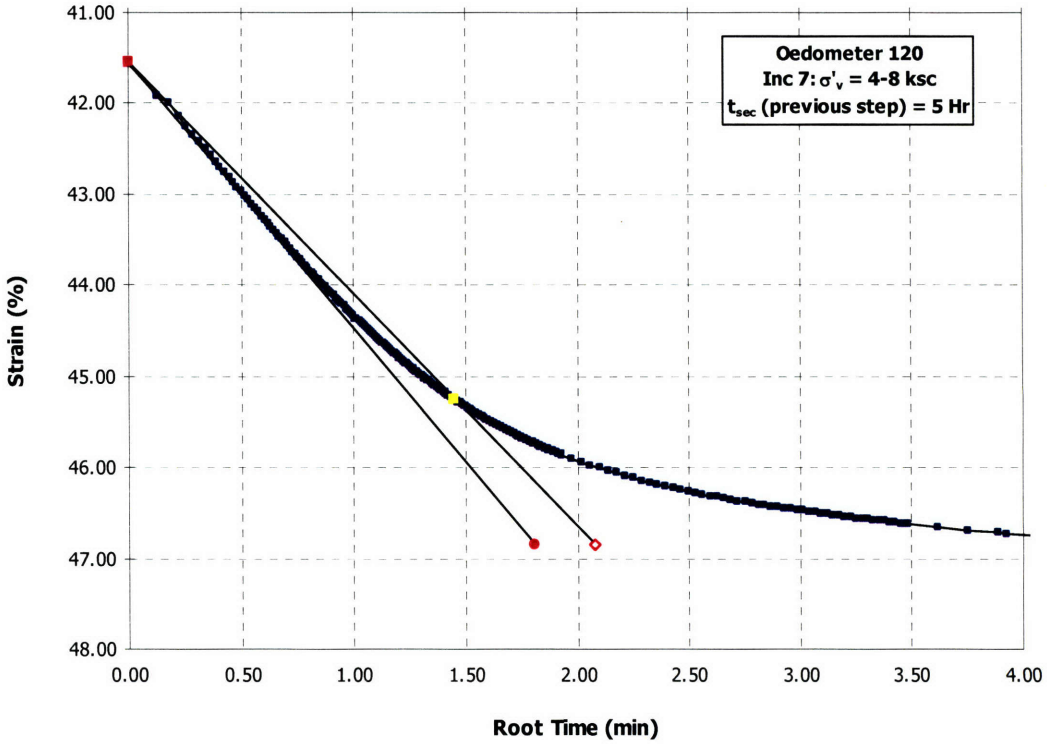

Figure A.146 Consolidation curve in $\sqrt{t}$ space for Oed122 Load Increment 7

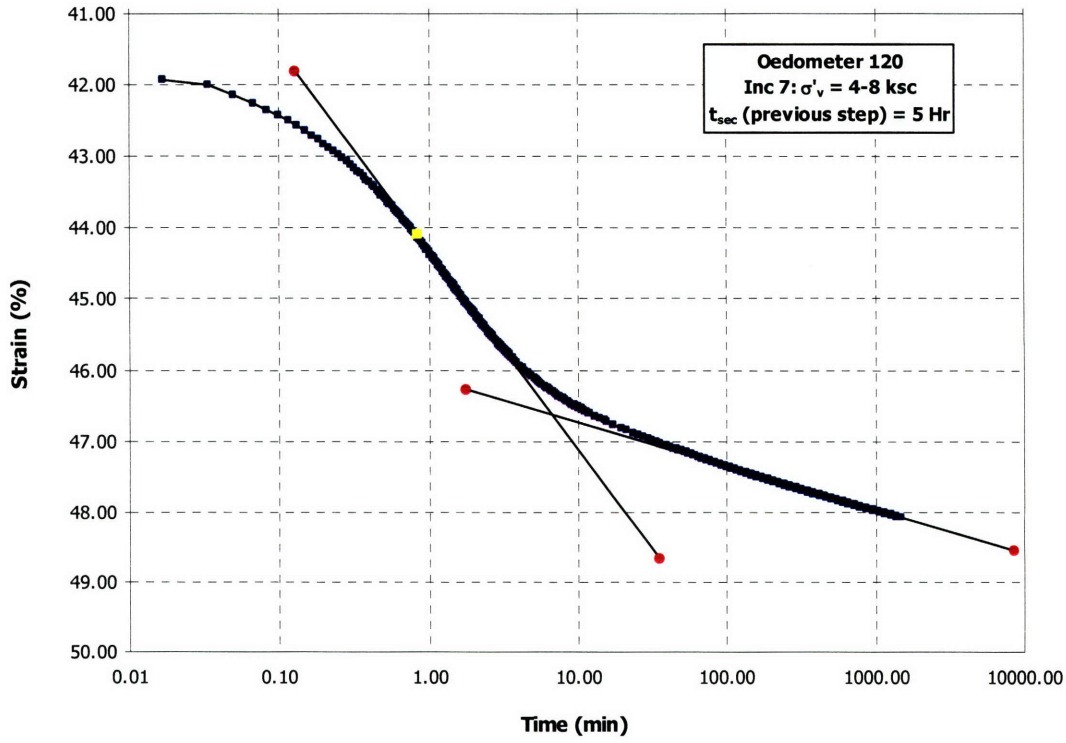

Figure A.147 Consolidation curve in Log time space for Oed122 Load Increment 7

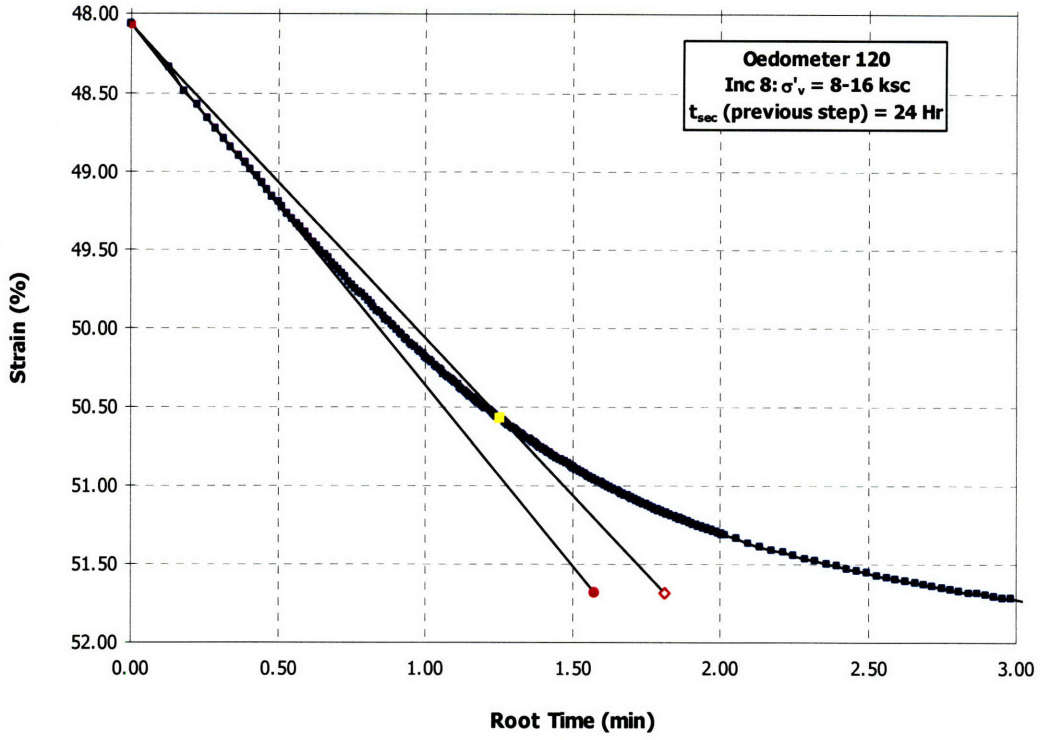

Figure A.148 Consolidation curve in $\sqrt{t}$ space for Oed122 Load Increment 8

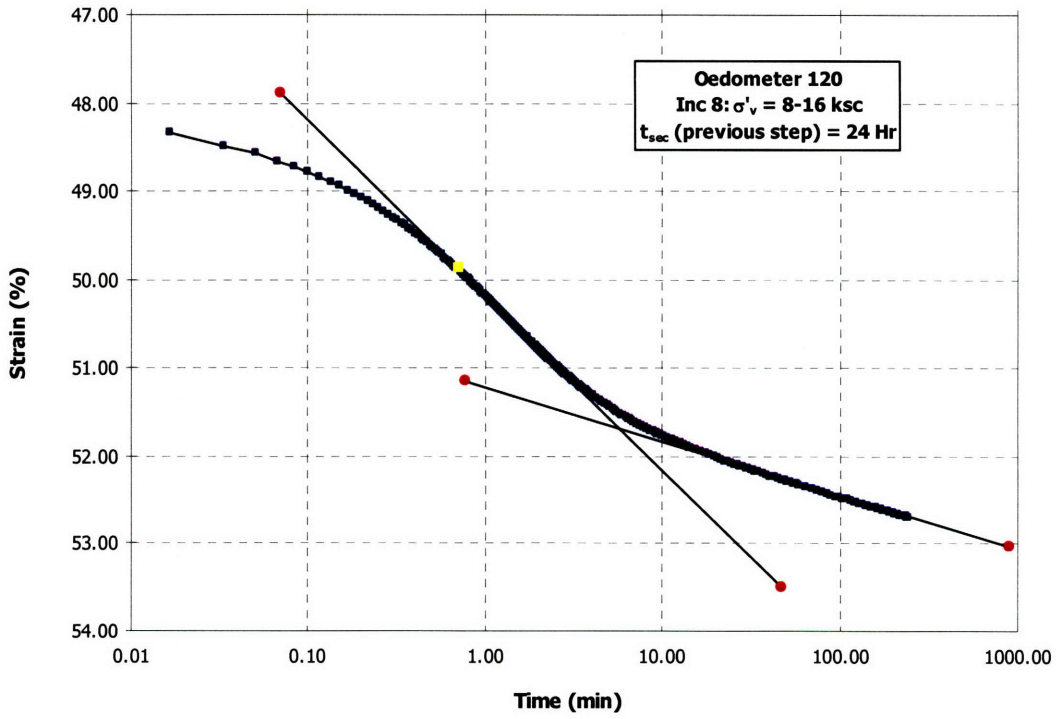

Figure A.149 Consolidation curve in Log time space for Oed122 Load Increment 8

Appendix B

The following sections include source code for the GCRS and oedometer simulation programs. The programs are written in C++ programming language for Microsoft Windows ® operating systems including Microsoft Windows ® 98, ME, 2000, and XP. Depending on the version of Microsoft Windows ® operating systems, additional C++ runtime files may be necessary to run the program. These C++ runtime files, if required, can be obtained from the official Microsoft web site (http://www.microsoft.com).

There are many versions of programs available for different modeling scenarios (for example, constant c_v simulation, constant C_c simulation, constant m_v simulation, etc.). The source code presented in this Appendix is only a single version of each simulation. Some modifications to the source code are necessary if the program will be used for a specific type of simulation.

B.1 GCRS Simulation Source Code

B.1.1 crsSIM.h (Header File)

```
#include <iostream>
#include <iomanip>
#include <cmath>
#include <fstream>
#include <cstdlib>
#include <string>

using namespace std;

class crs
{
public:
	crs();
	crs(double inputTotalOriginalHt, double inputCv, double
inputStrainR, double inputTimeIncr, double inputStartE, double
inputStartK, double inputMK, double inputCC, double inputTopDU, double
inputStartTS);
	~crs();
	void setHS();
	void setLayerHt();
	void calSpcHt();
	void setupE();
	void calDU(double topOrBottom, double inputTotalOriginalHt);
	void calTS();
	void calE();
```

```
      void calDiffRatio(double totalAfterHt, double
inputTotalOriginalHt);
      void updateVoidRatio();
      double getDiffRatio();
      double getTolerance();
      double getExcessPP(int location);
      double getNewSpcHt(int location);
      double getDarcyV(int location);
      double getTotalDef(int location);
      double getNewE(int location);
      double getUpdateE(int location);
      double getNewSecondLayerThk(int location);
      double getHS();
      double getNewLayerThk(int location);
      double getChgLayerThk(int location);
      double getStrLayerThk(int location);
      double getTotalVStress();
      double getAvgEffectiveStress(int location);
      void setStrLayerThk();
      void setInitialNALocation(double inputTotalOriginalHt);
      void setNALocation(double inputTotalOriginalHt, double
excessPPTop, double excessPPBottom, double bottomDarcyV);
      void setTopSectionHt(double inputTotalOriginalHt);
      void setBottomSectionHt(double inputTotalOriginalHt);
      void setTotalOriginalHt(double sectionHt);
      double getTopSectionHt();
      double getBottomSectionHt();
      double getNALocation();
      void setNALocationFromValue(double inputNALocation);
      double getTotalAfterHt();
      void setTolerance();
      double getSumTotalDef();
      void calGradient(double inputTotalOriginalHt,double
bottomExcessPP);
      void calExcessPPGradient(double bottomExcessPP, double
bottomSectionHt, double bottomGradient);
      double getBottomExcessPP();
      double getGradient();
      double getPPFromGradient(int location);
      void setGradient(double gradient);
      void updateTopHs(double inputTotalOriginalHt, double
bottomSectionHt);
      void updateBottomHs(double inputTotalOriginalHt, double
bottomSectionHt);

      //double diffRatio;

private:

      const double PI;
      const double E;
      //const int noLayer = 20;
      double spcHt[21];
      double strLayerThk[20];
      double assumedE[20];
      double newLayerThk[20];
      double chgLayerThk[20];
```

```
        double totalDef[21];
        double normDef[21];
        double HydC[20];
        double DarcyV[20];
        double ExcessPP[21];
        double revisedDarcyV[20];
        double revisedExcessPP[21];
        double avgPP[20];
        double totalVStress;
        double effectiveVStress[21];
        double avgVStress[20];
        double newE[20];
        double newSecondLayerThk[20];
        double newSpcHt[21];
        double errorDH[20];
        double diffRatio;
        double normExcessPP[21];
        double updateE[20];
        double startE;
        double startK;
        double maxExcessPP;
        double avgEffectiveVStress;
        double avgE;
      double avgK;
        double layerHt;
        double totalOriginalHt;
        double totalEndHt;
        double cv;
        double strainR;
        double totalStrain;
        double sumTotalDef;
        double timeIncr;
        double gammaWater;
        double hS;
        double tempDef;
        double tempDef2;
        double mK;
        double cc;
        double topDU;
        double startTS;
        double temp;
        double tolerance;
        double naLocation;
        double totalSpcHt;
        double topSectionHt;
        double bottomSectionHt;
        double diffExcessPP;
        double totalBothSectionDef;
        double gradient;
        double excessPPGradient;
        double PPGradient[21];
        double originalHs;


};
```

B.1.2 crsSIM.cpp

```
#include <iostream>
#include <iomanip>
#include <cmath>
#include <fstream>
#include <cstdlib>
#include <string>
#include "crsSIM.h"

using namespace std;

crs::crs():PI(3.1415927), E(2.7182818), totalOriginalHt(2.54)//,
noLayer(20)
{
	this->layerHt = totalOriginalHt / 20;
	this->cv = 0.002;
	//[cm^2/sec] unit
	this->strainR = 0.2;                                    //[%/hr]
unit
	this->timeIncr = 120;                                   //120 sec
as default
	this->startE = 0.1000;
	this->hS = this->totalOriginalHt / (1 + this->startE) / 20;
	this->mK = 0.4478;
	this->cc = -0.4478;
	this->startK = 6e-7;
	this->topDU = 0;
	this->startTS = 1.000;
	this->totalStrain = this->strainR * this->timeIncr / 3600;
	this->sumTotalDef = this->totalStrain * this->totalOriginalHt
/100;
	this->diffRatio = 2;
	this->gammaWater = 0.001;
	this->tolerance = 1;
	this->originalHs = this->hS;

}

crs::crs(double inputTotalOriginalHt, double inputCv, double
inputStrainR, double inputTimeIncr, double inputStartE, double
inputStartK, double inputMK, double inputCC, double inputTopDU, double
inputStartTS):PI(3.1415927), E(2.7182818)//, noLayer(20)
{

	this->totalOriginalHt = inputTotalOriginalHt;
	this->cv = inputCv;
	this->timeIncr = inputTimeIncr;
	this->strainR = inputStrainR;
	this->layerHt = totalOriginalHt / 20;
	this->startE = inputStartE;
	//this->hS = this->totalOriginalHt / (1 + this->startE) /20;

	this->hS = 1.259 / 2;                  //1.259 is for crs640 MBC
	//this->hS = 0.71126 / 2;              //0.71126 is for crs662 SBM
	//this->hS = 0.05425 / 2;
```

```
	//this->hS = 0.05425;
	this->mK = inputMK;
	this->cc = inputCC;
	this->startK = inputStartK;
	this->topDU = inputTopDU;
	this->startTS = inputStartTS;
	this->totalStrain = this->strainR * this->timeIncr / 3600;
	this->sumTotalDef = this->totalStrain * this->totalOriginalHt
/100;
	this->diffRatio = 2;
	this->gammaWater = 0.001;
	this->tolerance = 1;
	this->originalHs = this->hS;

	cout << this->hS;
	cout << endl;


}

crs::~crs()
{

}


void crs::setHS()
{

	this->hS = this->totalOriginalHt / (1 + this->startE) /20;
}

void crs::setLayerHt()
{
	this->layerHt = this->totalOriginalHt / 20;
}

void crs::calSpcHt()
{
	for(int i = 0; i < 21; i++)
	{
		this->spcHt[i] = this->totalOriginalHt - ((i) * this-
>layerHt);

	}

}

void crs::setupE()
{
	for(int i = 0; i <20; i++)
	{
		this->assumedE[i] = 0.67;

	}
```

```
}


void crs::calDU(double topOrBottom, double inputTotalOriginalHt)
{

	for(int i=0; i<21; i++)
	{
		this->spcHt[i] = this->totalOriginalHt - (this->layerHt *
i);

	}

	for(int j=0; j<20; j++)
	{
		this->strLayerThk[j] = this->spcHt[j] - this->spcHt[j+1];

	}

	for(int k=0; k<20; k++)
	{
		this->newLayerThk[k] = this->strLayerThk[k] - ((this-
>strLayerThk[k] - this->hS)/this->hS - this->assumedE[k]) * this->hS;

	}

	for(int l=0; l<20; l++)
	{
		this->chgLayerThk[l] = this->strLayerThk[l] - this-
>newLayerThk[l];

	}

	for(int m=0; m<21; m++)
	{
		this->tempDef = 0;
		for (int n=m; n<20; n++)
		{
			this->tempDef = this->tempDef + this->chgLayerThk[n];
		}

		this->totalDef[m] = this->tempDef;

	}
	this->tempDef = 0;

	for(int p=0; p<20; p++)
	{
		this->HydC[p] = pow(10.0,((this->assumedE[p] - this->startE
+ (this->mK * log(this->startK)/log(10.0)))/this->mK));
	}



	if(topOrBottom == 0)
	{
```

```
            this->PPGradient[0] = 0;
            for(int z=1; z<21; z++)
            {

                  this->PPGradient[z] = (this->strLayerThk[z-1] * z) *
this->gradient / 1000;

            }
      }

      if(topOrBottom == 1)
      {
            this->PPGradient[0] = 0;
            for(int z=1; z<21; z++)
            {

                  this->PPGradient[z] = (inputTotalOriginalHt - this-
>strLayerThk[z-1] * z) * this->gradient / 1000;

            }

      }


      for(int q=0; q<20; q++)
      {
                  this->DarcyV[q] = (this->totalDef[q+1] + (this-
>chgLayerThk[q] / 2))/this->timeIncr;// + (this->HydC[q] * this-
      }


      this->ExcessPP[0] = this->topDU;
      for(int r=1; r<21; r++)
      {
            if(topOrBottom == 0) //top section
            {
                  this->ExcessPP[r] = (this->newLayerThk[r-1] * this-
>gammaWater * this->DarcyV[r-1]) / this->HydC[r-1] + this->ExcessPP[r-
1] + this->PPGradient[r] - this->PPGradient[r-1];

            }
            if(topOrBottom == 1) //bottom section
            {

                  //This is the correct equation for the GCRS
simulation
                  this->ExcessPP[r] = (this->newLayerThk[r-1] * this-
>gammaWater * this->DarcyV[r-1]) / this->HydC[r-1] + this->ExcessPP[r-
1];// + this->PPGradient[r] - this->topDU;

            }
      }

      if(topOrBottom == 1)
      {
            this->PPGradient[0] = this->topDU;
            //this->ExcessPP[0] += this->PPGradient[0];
```

```
            for(int w=1; w<21; w++)
            {
                  this->ExcessPP[w] += this->PPGradient[w] - this-
>topDU;
            }
      }

      for(int s=0; s<20; s++)
      {
            this->avgPP[s] = (this->ExcessPP[s] + this->ExcessPP[s+1])
/ 2;

      }

}

void crs::calTS()
{
      this->totalVStress = pow(10.0, ((this->assumedE[19] - this-
>startE + this->cc * log(this->startTS)/log(10.0))/this->cc)) + this-
>ExcessPP[20];
}

void crs::calE()
{
      for(int i=0; i<21; i++)
      {
            this->effectiveVStress[i] = this->totalVStress - this-
>ExcessPP[i];

      }

      for(int j=0; j<20; j++)
      {
            this->avgVStress[j] = (this->effectiveVStress[j] + this-
>effectiveVStress[j+1]) / 2;
      }

      for(int k=0; k<20; k++)
      {
            this->newE[k] = this->cc * (log(this-
>avgVStress[k])/log(10.0) - log(this->startTS)/log(10.0)) + this-
>startE;
      }

      for(int l=0; l<20; l++)
      {
            this->newSecondLayerThk[l] = this->strLayerThk[l] -
(((this->strLayerThk[l] - this->hS)/this->hS - this->newE[l]) * this-
>hS);

      }

      for(int m=0; m<21; m++)
      {
            this->tempDef2 = 0;
            for(int n=m; n<20; n++)
```

```
            {
                  this->tempDef2 = this->tempDef2 + this-
>newSecondLayerThk[n];
            }

            this->newSpcHt[m] = this->tempDef2;

      }



}

//Criteria for the convergence of the Finite Difference
void crs::calDiffRatio(double totalAfterHt, double
inputTotalOriginalHt)
{
      this->diffRatio = totalAfterHt/(inputTotalOriginalHt - this-
>sumTotalDef);
      if(this->diffRatio <= 0)
      {
            this->diffRatio = 1;
      }


      for(int q=0; q<20; q++)
      {
            this->updateE[q] = this->newE[q]/(this->newE[q]/this-
>assumedE[q])/this->diffRatio;
      }

      this->tolerance = fabs(this->updateE[0] - this->assumedE[0]);
//    cout << "  De = " << this->tolerance;
//    cout << endl;

}


void crs::updateVoidRatio()
{


      for(int i=0; i<20; i++)
      {
            this->assumedE[i] = this->updateE[i];
      }

}

double crs::getDiffRatio()
{
      return this->diffRatio;

}

double crs::getTolerance()
{
```

```
	return this->tolerance;

}

double crs::getExcessPP(int location)
{
	return this->ExcessPP[location];

}

double crs::getNewSpcHt(int location)
{
	return this->newSpcHt[location];

}

double crs::getDarcyV(int location)
{
	return this->DarcyV[location];

}

double crs::getTotalDef(int location)
{
	return this->totalDef[location];

}


double crs::getNewE(int location)
{
	return this->newE[location];
}

double crs::getUpdateE(int location)
{
	return this->updateE[location];
}

double crs::getNewSecondLayerThk(int location)
{
	return this->newSecondLayerThk[location];
}

double crs::getHS()
{
	return this->hS;

}

double crs::getNewLayerThk(int location)
{
	return this->newLayerThk[location];
}

double crs::getChgLayerThk(int location)
{
```

```
	return this->chgLayerThk[location];
}

double crs::getStrLayerThk(int location)
{
	return this->strLayerThk[location];
}

double crs::getTotalVStress()
{
	return this->totalVStress;
}

double crs::getAvgEffectiveStress(int location)
{
	return this->avgVStress[location];
}

void crs::setStrLayerThk()
{

}

void crs::setInitialNALocation(double inputTotalOriginalHt)
{
	this->naLocation = inputTotalOriginalHt / 2;

}

void crs::setNALocation(double inputTotalOriginalHt, double
excessPPTop, double excessPPBottom, double bottomDarcyV)
{

	if(excessPPTop < excessPPBottom)// && bottomDarcyV > 0)
	{
		this->naLocation = this->naLocation - (inputTotalOriginalHt
/ 12000);

	}
	if(excessPPTop >= excessPPBottom)
	{
		this->naLocation = this->naLocation + (inputTotalOriginalHt
/ 12000);

	}

	if(this->naLocation <= 0.01)
	{
		this->naLocation = 0.01;
	}

}

void crs::setTopSectionHt(double inputTotalOriginalHt)
{
	this->topSectionHt = inputTotalOriginalHt - this->naLocation;
```

```
}

void crs::setBottomSectionHt(double inputTotalOriginalHt)
{
	this->bottomSectionHt = this->naLocation;
}

void crs::setTotalOriginalHt(double sectionHt)
{
	this->totalOriginalHt = sectionHt;
}

double crs::getTopSectionHt()
{
	return this->topSectionHt;
}

double crs::getBottomSectionHt()
{
	return this->bottomSectionHt;
}

double crs::getNALocation()
{
	return this->naLocation;
}

void crs::setNALocationFromValue(double inputNALocation)
{
	this->naLocation = inputNALocation;
	//return this->naLocation;
}

double crs::getTotalAfterHt()
{
	return this->newSpcHt[0];
}

void crs::setTolerance()
{
	this->tolerance = 1;
}

double crs::getSumTotalDef()
{
	return this->sumTotalDef;
}

void crs::calGradient(double inputTotalOriginalHt, double
bottomExcessPP)
{
	this->gradient = bottomExcessPP / inputTotalOriginalHt / 0.001;
	//cout << endl;
	//cout << this->gradient;
	//cout << endl;

}
```

```
void crs::calExcessPPGradient(double bottomExcessPP, double
bottomSectionHt, double bottomGradient)
{
	this->excessPPGradient = bottomExcessPP - bottomGradient *
bottomSectionHt / 1000;
	/*cout << endl;
	cout << " Gradient  |" << " " << "Excess PP |" << " " << "Section
Ht |" << " " << "Excess PP (G)";
	cout << endl;
	cout << "-----------------------------------------------------";
	cout << endl;
	cout << "  " << bottomGradient << "  |     " << bottomExcessPP <<
"   |    " << bottomSectionHt << "  |    " << this->excessPPGradient;
	cout << endl;
*/
}

double crs::getBottomExcessPP()
{
	return this->topDU;

}

double crs::getGradient()
{
	return this->gradient;

}

double crs::getPPFromGradient(int location)
{
	return this->PPGradient[location];
}

void crs::setGradient(double gradient)
{
	this->gradient = gradient;
}

void crs::updateTopHs(double inputTotalOriginalHt, double
bottomSectionHt)
{
	this->hS = this->originalHs * 2 * (1 - bottomSectionHt /
inputTotalOriginalHt);
}

void crs::updateBottomHs(double inputTotalOriginalHt, double
bottomSectionHt)
{
	this->hS = this->originalHs * 2 * (bottomSectionHt /
inputTotalOriginalHt);
}
```

B.1.3 crsMAIN.cpp

```
#include <windows.h>
#include <cstdlib>
#include <string>
#include <fstream>
#include "crsSIM.h"

#define BUFFER_SIZE 256

using namespace std;

int main()
{
	double inputTotalOriginalHt;
	double inputCv;
	double inputStrainR;
	double inputTimeIncr;
	double inputStartE;
	double inputStartK;
	double inputMK;
	double inputCC;
	double inputTopDU;
	double inputStartTS;
	int loopCount = 0;
	int mainLoopCount = 0;
	double temp;
	double tSectionHt;
	double bSectionHt;
	double excessPPTolerance = 2;
	double currentNALocation;
	double topAfterHt = 0;
	double bottomAfterHt = 0;
	double totalAfterHt = 0;
	double mainBottomDarcyV = 0;
	double bottomEPP = 0;
	double bottomGradient = 0;
	int flag1 = 0;


	cout << "-------------------------------------------------------
----------------------";
	cout << endl;
	cout << "This program is designed to simulate CRS consolidation
with imposed gradient.";
	cout << endl;
	cout << "The program bases on Darcy's Law of flow and Finite
Difference Analysis.";
	cout << endl;
	cout << endl;
	cout << "       Written by Attasit Korchaiyapruk.";
	cout << endl;
	cout << "       Copyright 2005 Attasit Korchaiyapruk.";
	cout << endl;
	cout << "-------------------------------------------------------
----------------------";
```

```
        cout << endl;
        cout << endl;

        cout << "Open input file..... ";
        cout << endl;
        ifstream infile("gcrs.dat");

        infile >> inputTotalOriginalHt;
        infile >> inputCv;
        infile >> inputStrainR;
        infile >> inputTimeIncr;
        infile >> inputStartE;
        infile >> inputStartK;
        infile >> inputMK;
        infile >> inputCC;
        infile >> inputTopDU;
        infile >> inputStartTS;

        cout << "Reading complete.";
        cout << endl;
        cout << endl;

        cout << "Input Data from the file.";
        cout << endl;
        cout << "-----------------------------------------------";
        cout << endl;
        cout << "  Original Height = " << inputTotalOriginalHt;
        cout << endl;
        cout << "  Cv = " << inputCv;
        cout << endl;
        cout << "  Strain Rate = " << inputStrainR;
             cout << endl;
        cout << "  Time Increment = " << inputTimeIncr;
             cout << endl;
        cout << "  Void Ratio at Start = " << inputStartE;
             cout << endl;
        cout << "  Hydraulic Conductivity at Start = " << inputStartK;
             cout << endl;
        cout << "  Slope of Log k vs e = " << inputMK;
             cout << endl;
        cout << "  Slope of Log s'v vs e = " << inputCC;
             cout << endl;
        cout << "  Excess PP at the top of the specimen = " <<
inputTopDU;
             cout << endl;
        cout << "  Total vertical stress at start = " << inputStartTS;
             cout << endl;
        cout << "-----------------------------------------------";
        cout << endl;

        //Create two CRS objects representing top and bottom section of
the specimen
        crs myCRST =
crs(inputTotalOriginalHt,inputCv,inputStrainR,inputTimeIncr,inputStartE
,inputStartK,inputMK,inputCC,inputTopDU,inputStartTS);
```

```
	crs myCRSB =
crs(inputTotalOriginalHt,inputCv,inputStrainR,inputTimeIncr,inputStartE
,inputStartK,inputMK,inputCC,1.25,inputStartTS);


	myCRST.setInitialNALocation(inputTotalOriginalHt);
	myCRST.setTopSectionHt(inputTotalOriginalHt);
	tSectionHt = myCRST.getTopSectionHt();
	myCRST.setTotalOriginalHt(tSectionHt);

	myCRSB.setInitialNALocation(inputTotalOriginalHt);
	myCRSB.setBottomSectionHt(inputTotalOriginalHt);
	bSectionHt = myCRSB.getBottomSectionHt();
	myCRSB.setTotalOriginalHt(bSectionHt);


	cout << endl;
	while(excessPPTolerance > 0.000001 && mainLoopCount < 5500)
	{

		myCRST.setHS();
		myCRST.setLayerHt();
		myCRST.calSpcHt();
		if(flag1 == 0)
		{
			myCRST.setupE();
			//flag1 = 1;
		}

		myCRSB.setHS();
		myCRSB.setLayerHt();
		myCRSB.calSpcHt();
		if(flag1 == 0)
		{
			myCRSB.setupE();
			flag1 = 1;
		}

		loopCount = 0;
		totalAfterHt = inputTotalOriginalHt;
		while(myCRST.getTolerance() > 1e-10 &&
myCRSB.getTolerance() > 1e-10 && loopCount < 1000)
		{
			bottomEPP = myCRSB.getBottomExcessPP();
			myCRST.calGradient(inputTotalOriginalHt, bottomEPP);
			myCRSB.setGradient(myCRST.getGradient());

			myCRST.calDU(0, totalAfterHt);
			myCRST.calTS();
			myCRST.calE();

			myCRSB.calDU(1, totalAfterHt);
			myCRSB.calTS();
			myCRSB.calE();

			topAfterHt = myCRST.getTotalAfterHt();
			bottomAfterHt = myCRSB.getTotalAfterHt();
```

```
                totalAfterHt = topAfterHt + bottomAfterHt;
                myCRST.calDiffRatio(totalAfterHt,
inputTotalOriginalHt);
                myCRSB.calDiffRatio(totalAfterHt,
inputTotalOriginalHt);
                myCRST.updateVoidRatio();
                myCRSB.updateVoidRatio();


                loopCount++;


            }


            excessPPTolerance = fabs(myCRSB.getExcessPP(20) -
myCRST.getExcessPP(20));




            mainBottomDarcyV = myCRSB.getDarcyV(1);
            myCRST.setNALocation(inputTotalOriginalHt,
myCRST.getExcessPP(20), myCRSB.getExcessPP(20), mainBottomDarcyV);
            currentNALocation = myCRST.getNALocation();
            myCRSB.setNALocationFromValue(currentNALocation);

            myCRST.setTopSectionHt(inputTotalOriginalHt);
            tSectionHt = myCRST.getTopSectionHt();

            myCRST.setTotalOriginalHt(tSectionHt);

            myCRSB.setBottomSectionHt(inputTotalOriginalHt);
            bSectionHt = myCRSB.getBottomSectionHt();
            myCRSB.setTotalOriginalHt(bSectionHt);

            myCRST.updateTopHs(inputTotalOriginalHt, bSectionHt);
            myCRSB.updateBottomHs(inputTotalOriginalHt, bSectionHt);

            myCRST.setTolerance();
            myCRSB.setTolerance();


            mainLoopCount++;


      }


            cout << myCRSB.getExcessPP(20);
            cout << endl;

            cout << myCRST.getExcessPP(20);
            cout << endl;

            cout << endl;
            cout << "Diff Ratio: " << myCRST.getDiffRatio();
```

```
            cout << endl;

      cout << endl;
      cout << endl;
      cout << "ExcessPPTolerance = " << excessPPTolerance;
      cout << endl;

      cout << endl;
      cout << "Total loop count = " << loopCount;
      cout << endl;

      cout << endl;
      cout << "Total main loop count = " << mainLoopCount;
      cout << endl;

      cout << endl;
      cout << "Generating an output file..... ";
      cout << endl;

      ofstream outputFile("result.dat");


      outputFile << "1st Step";
      outputFile << endl;
      outputFile << setiosflags(ios::fixed) << setprecision(4) <<
setw(20) << "Start Layer Thk" << " ";
      outputFile << setiosflags(ios::fixed) << setprecision(4) <<
setw(20) << "New Layer Thk" << " ";
      outputFile << setiosflags(ios::fixed) << setprecision(4) <<
setw(20) << "Change in Layer Thk" << " ";
      outputFile << setiosflags(ios::fixed) << setprecision(4) <<
setw(20) << "Excess PP" << " ";
      outputFile << setiosflags(ios::fixed) << setprecision(4) <<
setw(20) << "New Specimen Ht" << " ";
      outputFile << setiosflags(ios::fixed) << setprecision(4) <<
setw(20) << "Darcy Velocity" << " ";
      outputFile << setiosflags(ios::fixed) << setprecision(4) <<
setw(20) << "Total Def" << " ";
      outputFile << setiosflags(ios::fixed) << setprecision(4) <<
setw(20) << "Effective Stress" << " ";
      outputFile << setiosflags(ios::fixed) << setprecision(4) <<
setw(20) << "New E" << " ";
      outputFile << setiosflags(ios::fixed) << setprecision(4) <<
setw(20) << "Update E" << " ";
      outputFile << setiosflags(ios::fixed) << setprecision(4) <<
setw(20) << "New 2nd Layer Thk" << " ";
      outputFile << setiosflags(ios::fixed) << setprecision(4) <<
setw(20) << "PP From Gradient" << " ";
      outputFile << endl;

      for(int i=0; i<21; i++)
      {
            outputFile << setiosflags(ios::fixed) << setprecision(7) <<
setw(20) << myCRST.getStrLayerThk(i) << " ";
            outputFile << setiosflags(ios::fixed) << setprecision(7) <<
setw(20) << myCRST.getNewLayerThk(i) << " ";
```

```
            outputFile << setiosflags(ios::fixed) << setprecision(7) <<
setw(20) << myCRST.getChgLayerThk(i) << " ";
            outputFile << setiosflags(ios::fixed) << setprecision(4) <<
setw(20) << myCRST.getExcessPP(i) << " ";
            outputFile << setiosflags(ios::fixed) << setprecision(4) <<
setw(20) << myCRST.getNewSpcHt(i) << " ";
            outputFile << setiosflags(ios::fixed) << setprecision(7) <<
setw(20) << myCRST.getDarcyV(i) << " ";
            outputFile << setiosflags(ios::fixed) << setprecision(7) <<
setw(20) << myCRST.getTotalDef(i) << " ";
            outputFile << setiosflags(ios::fixed) << setprecision(7) <<
setw(20) << myCRST.getAvgEffectiveStress(i) << " ";
            outputFile << setiosflags(ios::fixed) << setprecision(7) <<
setw(20) << myCRST.getNewE(i) << " ";
            outputFile << setiosflags(ios::fixed) << setprecision(7) <<
setw(20) << myCRST.getUpdateE(i) << " ";
            outputFile << setiosflags(ios::fixed) << setprecision(7) <<
setw(20) << myCRST.getNewSecondLayerThk(i) << " ";
            outputFile << setiosflags(ios::fixed) << setprecision(7) <<
setw(20) << myCRST.getPPFromGradient(i) << " ";
            outputFile << setiosflags(ios::fixed) << setprecision(7) <<
setw(20) << myCRST.getGradient() << " ";
            outputFile << endl;

      }

      outputFile << endl;

      temp = 0;
      for(int j=19; j>=0; j--)
      {
            outputFile << setiosflags(ios::fixed) << setprecision(7) <<
setw(20) << myCRSB.getStrLayerThk(j) << " ";
            outputFile << setiosflags(ios::fixed) << setprecision(7) <<
setw(20) << myCRSB.getNewLayerThk(j) << " ";
            outputFile << setiosflags(ios::fixed) << setprecision(7) <<
setw(20) << myCRSB.getChgLayerThk(j) << " ";
            outputFile << setiosflags(ios::fixed) << setprecision(4) <<
setw(20) << myCRSB.getExcessPP(j) << " ";
            outputFile << setiosflags(ios::fixed) << setprecision(4) <<
setw(20) << myCRSB.getNewSpcHt(temp) << " ";
            outputFile << setiosflags(ios::fixed) << setprecision(7) <<
setw(20) << myCRSB.getDarcyV(j) << " ";
            outputFile << setiosflags(ios::fixed) << setprecision(7) <<
setw(20) << myCRSB.getTotalDef(j) << " ";
            outputFile << setiosflags(ios::fixed) << setprecision(7) <<
setw(20) << myCRSB.getAvgEffectiveStress(j) << " ";
            outputFile << setiosflags(ios::fixed) << setprecision(7) <<
setw(20) << myCRSB.getNewE(j) << " ";
            outputFile << setiosflags(ios::fixed) << setprecision(7) <<
setw(20) << myCRSB.getUpdateE(j) << " ";
            outputFile << setiosflags(ios::fixed) << setprecision(7) <<
setw(20) << myCRSB.getNewSecondLayerThk(j) << " ";
            outputFile << setiosflags(ios::fixed) << setprecision(7) <<
setw(20) << myCRSB.getPPFromGradient(j) << " ";
            outputFile << endl;
```

```
            temp++;
        }

        cout << "Output file generation complete.";
        cout << endl;

        return 0;

}
```

B.2 Oedometer Simulation Source Code

B.2.1 OedometerSIM.cpp

```
//Version 1.1
//Constant Cv Simulation
//Last Update May 25, 2006

#include <iostream>
#include <iomanip>
#include <fstream>
#include <cmath>
using std::ofstream;
using std::cout;
using std::cin;
using std::endl;
using std::ios;

int main()
{
      const int L = 50;       //number of layers in single drainage
(original = 50)
      const int T = 200;      //number of time steps
      const double tol = 0.000001;  //acceptable error for one time
step in effective stress
      double delt[T+1];
      double e[L+2][T+1];
      double sigma[L+2][T+1];
      double dele[L+2];
      double k[L+1];
      double q[L+1];
      double stn[L];
      double er[L+2];
      double delH[L+2];
      double H[L+1];
      double delpres[L+2];
      double HF[T+1];
      double mv[L+2];
      double avM[L+2];
      double step[6];
      double kf[T+1];   //kf is used for printing the final k at the
middle of the specimen
      double sumKf = 0.0;

      //Default input parameters (for program testing)
      /*
      double e0 = 1.00;
      double sigma0 = 1.00;
      double K0 = 1 * 0.0000001;
      double av = 0.029;
      double Ck = 0.1;
      double delsigma = 1.00;
      double H0 = 1;
      double sigmaN = 0.00;
      double cv = 0.00025;
```

```
      double mvi = 0.01;
      double avM0 = 0.05;
      */

      //For BBC from OED126 from 8-16 ksc effective stress
      /*
      double e0 = 0.862;  //1.6 is the original values
      double sigma0 = 8.00;
      double K0 = 4.12 * 0.00000001;    //4.43x10-8 is for SBM
      double av = 0.0101;  //SBM = 0.04072
      double Ck = 0.268;      //Ck = 0.18 is the interpreted value
      double delsigma = 8.00;
      double H0 = 0.0467;
      double sigmaN = 0.00;
      double cv = 0.0033;    //0.0005 for SBM
      double mvi = 0.132;    //SBM = 0.044
      double avM0 = 0.0746;
      double Cc = 0.268;
    */

      //For SBM from OED112 from 2-4 ksc effective stress

      double e0 = 1.6;  //1.6 is the original values
      double sigma0 = 4.00;
      double K0 = 4 * 0.00000001;    //1.28x10-7 is for best fit
      double av = 0.0101;  //SBM = 0.04072
      double Ck = 0.188;      //Ck = 0.148 is for the best fit
      double delsigma = 4.00;
      double H0 = 0.047;   //H0=0.03102
      double sigmaN = 0.00;
      double cv = 0.033;    //0.0005 for SBM
      double mvi = 0.132;    //SBM = 0.044
      double avM0 = 0.0746;
      double Cc = 0.468; //Cc = 0.468 is the best fit

      /*
      //For cv(rep) calculation
      double e0 = 1.6;  //1.6 is the original values
      double sigma0 = 4.00;
      double K0 = 5.5 * 0.00000001;    //1.28x10-7 is for best fit
      double av = 0.0101;  //SBM = 0.04072
      double Ck = 0.188;      //Ck = 0.148 is for the best fit
      double delsigma = 4.00;
      double H0 = 2;   //Best fit = 0.0467
      double sigmaN = 0.00;
      double cv = 0.0015;    //0.0005 for SBM
      double mvi = 0.132;    //SBM = 0.044
      double avM0 = 0.0746;
      double Cc = 0.468; //Cc = 0.468 is the best fit
*/


      int check = 0;
      double temp;
      double nL = 0;
      double totalTime = 0;
```

```
	//Set up initial condition.
	for(int i=1; i<=(L+1); i++)
	{
		sigma[i][0] = sigma0;
		e[i][0] = e0;
	}
	sigma[1][0] = sigma0 + delsigma;
	for(int i=1; i<=T; i++)
	{
		delt[i] = 1;
	}

	//mvi = cv / 1000 / K0;
	mvi = K0 / cv * 1000;
	avM0 = mvi * (1+e0);
	for(int i=1; i<=(L+1); i++)
	{
		mv[i] = mvi;
		avM[i] = mv[i] * (1+ e0);
		cout << "av[" << i << "]: " << avM[i] << endl;
	}

	cin >> temp;


	step[0] = delt[1];

	er[0] = 0.00;
	er[1] = 0.00;


	//Open file for output.
	ofstream outputFile("result.dat", ios::out);
	//Check to see if the file can be opened. If the file cannot be
opened, then exit the program.
	if (!outputFile)
	{
		cout << "File cannot be opened. Exit application." << endl;
		return 10;
	}
	else
	{
		cout << "Oedometer Simulation" << endl;
		cout << "-----------------------------------------------
-------------" << endl;
		cout << "This program perform simulation of oedometer test
under various" << endl;
		cout << "boundary conditions and specimen dimensions." <<
endl;
		cout << endl;
		cout << "    Developed by John T.Germaine and Attasit
Korchaiyapruk" << endl;
		cout << "    Department of Civil and Environmental
Engineering     " << endl;
		cout << "    Massachusetts Institute of Technology
" << endl;
```

```
            cout << "    Last update: May 18, 2006
" << endl;
            cout << endl;
            cout << "-------------------------------------------------
-------------" << endl;
            cout << "Output file name is result.dat. Start
Calculation." << endl;
      }

      //Start the main calculation loop.
      for(int i=1; i <= T; i++)
      {

            for(int j = 1; j <= (L+1); j++)
            {
                  sigma[j][i] = sigma[j][i-1];  //Set stress for the
first iteration.
                  avM[j] = avM0;    //reset avM matrix;

            }

            //Entry point for iteration.
            start:
            for(int j = 1; j <= (L+1); j++)
            {
                  //Calculate void ratio using av converted from mv
                  e[j][i] = e0 - (log10(sigma[j][i]/sigma0)) * Cc;

                  dele[j] = e[j][i-1] - e[j][i];
            }

            for(int j = L; j >= 1; j--)
            {
                  k[j] = pow(10,(log10(K0) - ((e0 - (e[j+1][i] +
e[j][i]) / 2) / Ck)));

                  delH[j] = (e0 - (e[j+1][i] + e[j][i]) / 2) / (1+e0) *
H0;    //Original formula

                  dele[j] = (dele[j] + dele[j+1]) / 2;
                  q[j] = dele[j] / (1+e0) * H0;    //Original Formula

                  if(j < L)
                  {
                        q[j] = q[j] + q[j+1];
                  }
                  H[j] = H0 - delH[j];



                  if(i == 5)
                  {
                        for(int k=1; k <= T; k++)
                        {
                              delt[k] = 1;
                        }
                        step[1] = delt[1];
```

```
                }


                if(i == 10)
                {
                        for(int k=1; k <= T; k++)
                        {
                                delt[k] = 2;
                        }
                        step[2] = delt[1];
                }

                if(i == 20)
                {
                        for(int k=1; k <= T; k++)
                        {
                                delt[k] = 20;
                        }
                        step[3] = delt[1];
                }

                if(i == 50)
                {
                        for(int k=1; k <= T; k++)
                        {
                                delt[k] = 50;
                        }
                        step[4] = delt[1];
                }


                if(i == 150)
                {
                        for(int k=1; k <= T; k++)
                        {
                                delt[k] = 400;
                        }
                        step[5] = delt[1];
                }




                //This is the original equation (the correct one)
                delpres[j] = q[j] / delt[i] / k[j] * (H[j] / 1000);



        }

        //Loop over the interfaces.
        for(int j = 2; j <= (L+1); j++)
        {
                sigmaN = sigma[j-1][i] - delpres[j-1];
                //cout << "sigmaN = " << sigmaN << endl;
                //cout << "delpres[ " << j << "-1] = " << delpres[j-
1] << endl;
```

```
                er[j] = sigma[j][i] - sigmaN;
                //cout << "er[" << j << "] = " << er[j] << endl;


        }

        //error function dampening.
        for(int j = 2; j <= (L+1); j++)
        {
                sigma[j][i] = sigma[j][i] - er[j] / 30;    //
originally er is divided by 30
                //cout << "sigma[" << j << "][" << i << "] = " <<
sigma[j][i] << endl;

        }


        int j = 1;
        cont:
        if(abs(er[j]) > tol) goto start;
        j = j+1;
        if(j == (L+2))
        {
                for(int j = 1; j<=(L+1); j++)
                {
                        //mv[j] = cv / 1000 / k[j];

                        mv[j] = k[j] / cv * 1000;
                        avM[j] = mv[j] * (1+ e0);
                }

                goto cont2;
        }
        else
        {
                goto cont;
        }

        cont2:
        cout << "time step: " << i << " is complete." << endl;
        //cout << "cv: " << cv << endl;
        //cout << "k[i]: " << k[i] << endl;
        //cout << "mv: " << mv[1] << endl;
        //cout << "avM: "  << avM[1] << endl;

        HF[i] = 0;
        for(int j = 1; j <= L; j++)
        {
                HF[i] = HF[i] + H[j];
        }
        check = 0;

        for(int m = 1; m <= L; m++)
        {
                sumKf += k[m];
        }
```

```
            kf[i] = sumKf/L;
            sumKf = 0.0;

      }
      //Complete the computation.

      //Start printing the result to the output file.

      //Output Header for the file
      outputFile << "Oedometer Simulation: Constant Cv Simulation" <<
endl;
      outputFile << "Coefficient of Consolidation, cv: " << cv << "
cm2/s" << endl;
      outputFile << "Reference Void Ratio, e0: " << e0 << endl;
      outputFile << "Reference hydraulic Conductivity, k0: " << K0 << "
cm/s" << endl;
      outputFile << "Stress Increment: " << delsigma << " ksc" << endl;

      for(int i = 0; i <= T; i++)
      {
            outputFile << i << " ";
      }

      outputFile << endl;
      outputFile << L * H0 << " ";

      for(int i = 1; i <= T; i++)
      {
            outputFile << HF[i] / L / H0 << " ";
            //outputFile << HF[i] << " ";
      }
      outputFile << endl;
      for(int j = 1; j <= (L+1); j++)
      {
            nL = L;
            outputFile << (nL + 1 - j) / nL << " ";
            //cout << (L + 1 - j) / L << endl;
            for(int i = 1; i <= T; i++)
            {
                  outputFile << (sigma[j][i] - sigma0) / delsigma << "
";

            }
            outputFile << endl;
      }

      //Print the time increment to the output file.
      outputFile << "tIncrement ";
      for(int i = 1; i <= T; i++)
      {
            if(i >= 0) temp = step[0];
            if(i >= 5) temp = step[1];
            if(i >= 10) temp = step[2];
            if(i >= 20) temp = step[3];
            if(i >= 50) temp = step[4];
            if(i >= 150) temp = step[5];
```

```
            outputFile << temp << " ";
        }
        outputFile << endl;

        //Print total time to the output file for plotting.
        outputFile << "totaltime ";
        for(int i = 1; i <= T; i++)
        {
            if(i >= 0) temp = step[0];
            if(i >= 5) temp = step[1];
            if(i >= 10) temp = step[2];
            if(i >= 20) temp = step[3];
            if(i >= 50) temp = step[4];
            if(i >= 150) temp = step[5];

            totalTime = totalTime + temp;
            outputFile << totalTime << " ";
        }
        outputFile << endl;
        outputFile << "HydraulicConductivity ";
        for(int i = 1; i <= T; i++)
        {

            outputFile << kf[i] << " ";
        }



        return 0;

}
```